8-2018

Plutonium in the Presence of Natural Organic Ligands: Sorption Kinetics, Surface Complex Stability, and Subsurface Transport

Jennifer Christine Wong
Clemson University, jcwong10@gmail.com

Recommended Citation
Wong, Jennifer Christine, "Plutonium in the Presence of Natural Organic Ligands: Sorption Kinetics, Surface Complex Stability, and Subsurface Transport" (2018). *All Dissertations*. 2175.
https://tigerprints.clemson.edu/all_dissertations/2175

PLUTONIUM IN THE PRESENCE OF NATURAL ORGANIC LIGANDS: SORPTION KINETICS, SURFACE COMPLEX STABILITY, AND SUBSURFACE TRANSPORT

A Dissertation
Presented to
the Graduate School of
Clemson University

In Partial Fulfillment
of the Requirements for the Degree
Doctor of Philosophy
Environmental Engineering and Earth Sciences

---

by
Jennifer Christine Wong
August 2018

Accepted by:
Brian A. Powell, Committee Chair
Mavrik Zavarin
Mark A. Schlautman
Elizabeth Carraway
Timothy A. DeVol

ABSTRACT

This work investigated aging of plutonium (Pu) on the surface of goethite, the effect of natural organic ligands on the enhancement of Pu desorption and mobility, and Pu transport in a natural soil. Because adsorption of Pu is frequently observed to be initially rapid followed by slower adsorption over days to weeks, Pu may undergo aging, where a surface process following initial adsorption causes a change in Pu state over time. Pu uptake which exhibits fast and slow sorption phases has been successfully modeled using a multisite model where sorbed Pu is represented as two compartments with different rates of exchange with solution, and I propose in this work that it may be modeled using consecutive compartments representing Pu states with different accessibility to the solution. Additionally, the fate and transport of Pu can be affected by the presence of natural organic ligands which may diminish Pu sorption to mineral surfaces by forming Pu–aqueous complexes or enhance Pu sorption by forming ternary surface complexes. Numerous previous studies have examined the extent of Pu sorption to pure minerals in batch experiments. However, the effect of natural organic ligands on Pu sorption kinetics and transport in natural soils requires further investigation.

The aging of Pu on goethite was observed by using batch experiments with adsorption times of 1–116 days. To assess the stability of Pu(IV) on the goethite surface, desorption was performed in the presence of desferrioxamine B (DFOB) which acted as a competing complexant and also thermodynamically drove aqueous Pu(V) to form Pu(IV)–DFOB aqueous complexes. Thus, the surface stability of Pu(IV) was measured in a system with pure oxidation state. Pu was observed to become less desorbable with increasing

adsorption times, and the effect of Pu aging was greater at lower pH values. The results were not consistent with surface mediated reduction as a process of aging, but demonstrated that Pu aging could be sensitive to pH.

The kinetics of Pu (de)sorption from goethite in the presence of DFOB, fulvic acid (Suwanee River I), and citric acid were investigated using a flow-cell design which minimized readsorption of Pu by constant dilution. Additional kinetic information was obtained by conducting stop events to vary the fluid residence time. Pu became less desorbable over three days, indicating Pu underwent aging on goethite. The Pu data was modeled using a kinetic sorption model which considered two consecutive linear sorption components. In this theoretical conceptual model, the transition to a second surface state represented aging, but the specific process was unknown. The presence of DFOB had a greater effect on Pu desorption than either citric acid or fulvic acid. Although further study is required to determine Pu–(fulvic acid) stability constants, the results are consistent with the relative stability constants for Pu–ligand aqueous complexes.

The effect of DFOB and citrate on Pu mobility was examined in column transport experiments with natural soil from the Savannah River Site. Pu was loaded onto the columns in organic-free solution, followed by a continuous input of organic ligand solution to mobilize the Pu. Due to the strong sorption of DFOB and citrate to the soil, their presence was estimated to be limited to the first 1.32 and 0.68 cm of the columns, respectively. The formation of aqueous Pu–ligand complexes did not appear to affect the Pu soil distribution, However, in each of the columns, including the ligand-free control, 9–20 % of Pu was observed to elute with retardation factors of 24–29, suggesting that Pu was mobilized by a process the columns had in common. Multiple working hypotheses to explain these data are (1) oxidation of Pu(IV) to Pu(V) within the loading solution during pH adjustment, (2) mobilization by of Pu–ligand complexes with native soil organic matter, and (3) colloid-facilitated transport.

With increased aging, Pu mobility in the subsurface may decrease if Pu is sorbed to an immobile matrix, or Pu mobility may increase if Pu is sorbed to mobile colloids. Because this work used indirect measurements of aqueous Pu to observe the effects of aging, further research is required to determine the process behind Pu aging. Flow-cell experiments demonstrated that the presence of natural organic ligands has the potential to mobilize Pu in the subsurface; however, in natural soils, further research is required to understand the enhancement of Pu mobility in the presence of natural organic ligands. Pu mobility in the subsurface environment depends on many complex interactions potentially involving contact time, soil composition, Pu redox reactions, ligand sorption, soil organic matter, and mineral colloids.

DEDICATION

I dedicate this dissertation to my mother, Carolyn, and my father, Patrick, who shaped my interest in science and puzzle solving, and who always encouraged me to strive for excellence.

I also dedicate this dissertation to Michael Epstein who has been with me in heart and spirit every step of this degree program. I am grateful for his patience and devotion. He has been my sounding board, my drill sergeant, my rock.

ACKNOWLEDGMENTS

I am thankful for the support and mentorship of my advisor, Dr. Brian A. Powell, who has made this long and challenging endeavor possible. I would also like to thank the wonderful and patient collaborators I worked with at Lawrence Livermore National Laboratory, including Drs. Annie B. Kersting, Mavrik Zavarin, James D. Begg, Pihong Zhao, Claudia Joseph, and Mark A. Boggs for use of laboratory space, materials, and advice. I also thank members past and present of the laboratory group at Clemson University for their kind support and spirit of collaboration which facilitated sharing laboratory space, equipment, and materials. I especially thank those who helped me to use instruments such as the ICP-MS and the TOC analyzer.

Additionally, I acknowledge Dr. Mavrik Zavarin for providing the compiled code used for modeling multi-site sorption kinetics, and I acknowledge Dr. Adam R. Mangel for the MATLAB code which assisted with transport modeling. I acknowledge Dr. Jirka Šimůnek for personally answering my questions about the details of C-Ride.

I acknowledge countless unnamed librarians who scanned obscure articles to electronic format at my request. I also acknowledge the kind employee at the hardware store who helped invent the column sectioning device.

This work was supported by the Subsurface Biogeochemical Research program of the U.S. Department of Energy’s Office of Biological and Environmental Research through the Science Focus Area program on Subsurface Transport of the Actinides led by Lawrence Livermore National Laboratory.

TABLE OF CONTENTS

Page

CHAPTERS

Table of Contents (Continued)

LIST OF FIGURES

List of Figures (Continued)

Figure Page

List of Figures (Continued)

List of Figures (Continued)

List of Figures (Continued)

List of Figures (Continued)

Figure Page

List of Figures (Continued)

Figure Page

List of Figures (Continued)

LIST OF TABLES

List of Tables (Continued)

Table Page

LIST OF EQUATIONS

List of Equations (Continued)

Equation Page

List of Equations (Continued)

CHAPTER ONE

INTRODUCTION

The goals of this project are to both quantify and develop a model for plutonium (Pu) aging on goethite, and to validate reactive Pu transport models which incorporate sorption in the presence of natural organic ligands (NOL). Although Pu is expected to be relatively immobile in the environment (Triay et al., 1996) due to the high sorption affinity and low solubility of Pu(IV) (Choppin, 2003; Knopp et al., 1999; Neck and Kim, 2001; Nitsche and Edelstein, 1985), long-distance transport of Pu has been observed in association with colloids (Kersting et al., 1999; Novikov et al., 2006; Santschi et al., 2002) suggesting formation of highly stable Pu surface complexes. Measurements of adsorption on mineral colloid suspensions demonstrate that Pu sorption is initially rapid (hours to a day) followed by slower sorption (10 or more days) (Lu et al., 2000; Painter et al., 2002). It has been suggested that Pu sorption can be described by fast and slow rate components (Painter et al., 2002; Romanchuk et al., 2011) and that sorption may be irreversible (i.e. not reversible on examined timescales) (Kersting et al., 1999; Novikov et al., 2006). In order to accurately capture behavior of Pu in reactive transport models, there is a need to study Pu sorption kinetics and develop rate laws to describe the observed kinetic sorption behavior.

I propose that Pu sorption kinetics on goethite are composed of fast and slow rate components which can be described by a two-site kinetic sorption model with fast and slow sorption rates corresponding to different Pu states at the mineral–water interface. The presence of a slow rate component to sorption could explain Pu which remains unrecovered after months of desorption (Lu et al., 1998a), but also suggests that prolonged slow adsorption of Pu continues after initial rapid adsorption. Pu may undergo *aging* where a surface process occurring after initial adsorption causes a change in Pu state on a surface over time. For instance, Pu may initially adsorb rapidly to weakly sorbing sites because of their higher surface density on a surface, and then slowly transfer to strongly sorbing sites with lower surface density. The expected result would be an increase in overall surface stability with contact time. In this conceptual model, the two sites are defined operationally based on differences in observed kinetic rates of uptake and release. The sites, which may be consecutive or in parallel (Fig. 1.1), may also be referred to as states or compartments. The aging model is not unique to transfer between sorption sites. There are multiple processes which could constitute aging including redox transformations, diffusion into micropores, incorporation into a solid by mineral recrystallization, and surface precipitation of the sorbate. It should be noted that this discussion is highly speculative. The exact mechanism of the proposed slow transfer reaction is unknown, as are the identities of the theoretical initial surface state and second surface state.

Pu mobility is additionally influenced by the presence of natural organic ligands by the formation of aqueous Pu–ligand complexes or ternary Pu surface complexes. Although the effect of NOL on Pu sorption to pure minerals has been studied in batch experiments (Conroy et al., 2017; Powell et al., 2011; Simpkins, 2011; Zhao et al., 2011; Zimmerman et al., 2014), their effect on Pu (de)sorption kinetics and Pu transport in natural soils requires more study. The mobility of Pu in the presence of three types of surrogates for natural organic matter (desferrioxamine B (DFOB), fulvic acid, and citric acid) in natural soils is expected to follow trends similar to those of batch sorption experiments on the basis of the strength of aqueous Pu–ligand complexes and the affinity of the ligands for mineral surfaces. Pu sorption kinetics on goethite and Pu mobility in the presence of NOL was investigated using batch sorption, flow-cell, and column experiments.

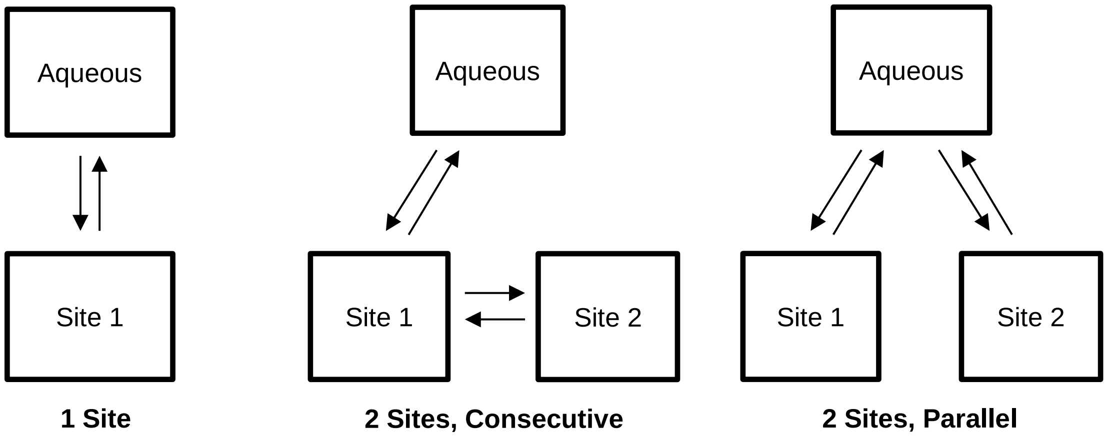

Figure 1.1. Schematic of compartment models: one-site, two-site consecutive, two-site parallel.

Aging was tested by measuring Pu distribution ratios as a function of adsorption time and pH in adsorption–desorption batch experiments on goethite suspensions in the presence of DFOB, a chelating siderophore. DFOB was used as a complexant to compete with proposed strong Pu–goethite surface complexes. Additionally, the presence of DFOB thermodynamically drove aqueous Pu(V) to form Pu(IV)–DFOB aqueous complexes, maintaining Pu in the tetravalent state.

A two-site kinetic sorption model for Pu was developed using aqueous Pu desorption measurements from flow-cell experiments in the presence of DFOB, fulvic acid, and citric acid. In flow-cells, constant dilution minimizes readsorption of Pu to goethite suspensions so that fast and slow rate components of desorption in the presence of NOL can be observed.

The effect of different types of NOL on Pu mobility was evaluated in column experiments with natural soil from the Savannah River Site (SRS). Pu soil profiles and Pu elution profiles were compared to reactive transport models incorporating surface mediated reduction, colloid-facilitated transport, and transport facilitated by organic matter in order to assess the plausibility of these processes.

To my knowledge, this is the first study to investigate aging of Pu sorbed on goethite, and the first to use flow-cells in the measurement of Pu desorption kinetics from goethite in the presence of NOL. The two-site kinetic sorption model provides a useful method of parameterizing aging. The column transport experiments with Pu in the presence of NOL offer a comparison of Pu behavior in the presence of natural soil and pure minerals.

CHAPTER TWO

BACKGROUND

At U.S. Department of Energy sites, the production and testing of nuclear weapons have resulted in a legacy of plutonium contamination in the environment. Underground nuclear testing has resulted in the release of 8.9×10^{15} Bq (240,000 Ci), equivalent to 2,800 kg, of $^{238\text{-}240}$Pu at the Nevada Test Site (Smith et al., 2003). At the Hanford Reservation, 4.37×10^{14} Bq (11,800 Ci) or 190 kg of ^{239}Pu was released as liquid waste in the near-surface environment (Cantrell, 2009; Felmy et al., 2010). A total of 5.85×10^{11} Bq (15.8 Ci), equivalent to 178 g, of $^{238+239}$Pu waste was released to the environment at the Savannah River Site in seepage basins, streams, and air (Carlton et al., 1992; Hetrick and Martin, 1990). All isotopes of Pu are radioactive and many are long-lived. For instance, ^{239}Pu has a half-life of 240,000 years. Hence, the mobility of Pu in the environment, including the subsurface, is of great concern. Factors influencing Pu subsurface mobility include redox reactions, kinetic limitations of reactions, aging, the presence of colloids, and complexation during transport (Choppin, 2007, 2006; Choppin and Stout, 1989; Silva and Nitsche, 1995). The following background review discusses observations at the laboratory and field scales which suggest further study of Pu sorption kinetics and mobility in the presence of natural organic ligands is required.

Pu Redox Behavior and Typical Sorption

Plutonium can exist in the +III, +IV, +V and +VI valence states simultaneously under natural conditions (Choppin et al., 1997; Silva and Nitsche, 1995). In oxic waters, Pu(III) is not expected to be present (Cleveland, 1979). At moderate pH and E_h, Pu(IV) and Pu(V) are the dominant oxidation states. In the absence of a sorbate, Pu(V) is the dominant oxidation state in seawater and dilute salt solutions (Morse and Choppin, 1986; Orlandini et al., 1986). Generally, in natural systems, soluble Pu is dominated by Pu(V), and Pu associated with soils and organic particles is dominated by Pu(IV) (Keeney-Kennicutt and Morse, 1985; Sanchez et al., 1985). The distribution of Pu oxidation states is supported by their different hydrolytic tendency. The sorption edges of Pu(IV) and Pu(V) follow their tendency to form hydroxide complexes. Pu(IV), which begins to hydrolyze to $Pu(OH)_x^{4-x}$ species even at pH 1 (Choppin, 2003; Knopp et al., 1999; Neck and Kim, 2001; Nitsche and Edelstein, 1985), has a sorption edge in the pH range 3 to 5, whereas Pu(V) has a sorption edge in the pH range 5 to 7 (Sanchez et al., 1985). In dissolution studies with suspensions of $PuO_{2(am)}$, the aqueous phase is dominated by Pu(V) (Rai, 1984; Rai et al., 2001, 1980). The solubility of the Pu is controlled by oxidative dissolution of $PuO_{2+x(am,hyd)}$ (Neck et al., 2007; Rai, 1984; Rai et al., 2001, 1980), where x represents the fraction of Pu(V) impurity ($0 \leq x \leq 0.5$) present in the predominantly Pu(IV) amorphous hydroxide. The solubility of Pu is limited and is dependent on Pu(IV)/Pu(V) redox couple (Choppin, 2003; Neck et al., 2007). Neck et al. (2007) determined a solubility product for the mixed-valent $PuO_{2.5(am,hyd)}$ fraction of $PuO_{2+x(am,hyd)}$ (Eqn. 2.1) where $x = 0.003$ for this solid.

$$PuO_{2.5(am,hyd)} + H^+ \leftrightarrow PuO_2^+ + \tfrac{1}{2} H_2O$$
$$K^\circ_{sp} = 10^{-14.3 \pm 0.6} \tag{2.1}$$

Due to differences in hydrolytic tendency and solubility, Pu(IV) is the most important oxidation state affecting Pu surface chemistry in the subsurface environment. Pu(V) undergoes surface mediated reduction to Pu(IV) creating a distribution wherein

Pu(V) is the dominant aqueous oxidation state and Pu(IV) is the dominant sorbed oxidation state (Keeney-Kennicutt and Morse, 1985; Penrose et al., 1987; Powell et al., 2005, 2004; Sanchez et al., 1985). In batch experiments which compared sorption of Pu added as Pu(IV) and Pu(V) to goethite suspensions, Sanchez et al. (1985) observed the sorption edge for Pu(IV) stabilized in one hour, whereas the sorption edge for Pu(V) did not stabilize, but moved to lower pH. Oxidation state analysis revealed that Pu(V) reduced to Pu(IV) at or near the surface of goethite, but remained the stable aqueous oxidation state. Keeney-Kennicutt and Morse (1985) performed batch sorption experiments with Pu(V) and goethite at pH 8. After observing more than 99% sorption in one day, the oxidation state of sorbed Pu was examined by leaching goethite with 0.03 M $HClO_3$, a concentration chosen to remove oxidized Pu and presumably leave Pu(IV) in the unleached fraction. The observed decrease in leachable Pu over a 30 day period was ascribed to reduction of Pu(V) and formation of stable Pu(IV) surface complexes. Similar decreases in the leachable Pu fraction over time using dilute $HClO_4$ were reported for goethite, hematite, and magnetite (Powell et al., 2005, 2004). These experiments demonstrate that under environmentally relevant conditions, Pu undergoes redox transformations which result in mixed oxidation states and may affect sorption behavior. Measurements of surface stability taken without knowledge of the Pu oxidation state may be inaccurate (Powell et al., 2011). If a mixed oxidation state system is assumed to be Pu(IV) during assessment of surface stability, sorption of Pu(IV) may be underestimated (Powell et al., 2011), which will impact the accuracy of transport models.

Field-Scale Transport

Although it has been generally assumed that Pu is relatively immobile in the subsurface due to the low solubility and strong sorption of Pu to mineral surfaces (Choppin, 2003; Knopp et al., 1999; Neck and Kim, 2001; Nitsche and Edelstein, 1985; Triay et al., 1996), field studies have observed kilometer-scale transport of Pu (Kersting et al., 1999; Marty et al., 1997; Novikov et al., 2006; Penrose et al., 1990). Pu distribution coefficients measured in batch experiments with Yucca Mountain tuff and J-13 well water (Triay et al., 1996) suggest significant retardation of Pu transport should occur under these geochemical conditions. However, at the nearby Nevada Nuclear Security Site (formerly Nevada Test Site), Kersting et al. (1999) identified Pu in groundwater which was transported from a detonation site 1.3 km away over a period of 30 years, in comparison to groundwater which was estimated to have a velocity of 1 to 80 $m \cdot yr^{-1}$. More than 99% of Pu was associated with the colloidal fraction of groundwater, indicating that mobile colloids could be a mechanism of long-distance, relatively rapid Pu transport. Similarly, Pu transported 4 km within 55 years at the Mayak Production Association was found associated with colloids comprised of amorphous iron oxide (Novikov et al., 2006).

Although field studies suggest that rapid Pu transport could be facilitated by sorption to mobile colloids, models for colloid-facilitated transport still under-predict Pu transport (Cvetkovic et al., 2004). They predict that over the course of transport, Pu would have the opportunity to desorb from the colloids and sorb to stationary soil particles. For Pu to travel kilometers and remain sorbed to colloids, Pu must exchange less freely than previously believed among the colloidal, aqueous, and stationary mineral phases. It has been proposed that Pu complexes with mobile colloids are very stable and that desorption is kinetically limited relative to fluid contact times (Kersting et al., 1999; Novikov et al., 2006; Penrose et al., 1990). In groundwater down-gradient of the Pu-contaminated Lake Karachai, Novikov et al. (2006) observed that the ratio of colloid-associated Pu to soluble Pu increased beyond 2.5 km from the Pu-contaminated lake. It was hypothesized that Pu underwent equilibrium partitioning within 2.5 km of the lake, and then, as colloids were transported down-gradient, Pu was either irreversibly incorporated into colloids or sorption disequilibrium developed due the kinetically limited nature of Pu desorption. If, as suggested, Pu uptake is kinetically limited relative to fluid contact times, more accurate transport models may require knowledge of kinetic rate constants for Pu uptake and release.

Sorption Kinetics

Observations of Pu Sorption Kinetics

Kilometer-scale colloid-associated transport in groundwater (Kersting et al., 1999; Novikov et al., 2006) suggests that Pu sorption reactions may be irreversible or slowly reversible. Slow desorption rates are demonstrated in batch sorption experiments with iron oxide colloids and Pu(V), which presumably undergoes surface mediated reduction to Pu(IV). In sorption experiments with goethite colloids, 81% of Pu adsorbs in one hour, but less than 1% of Pu desorbs from goethite over 150 days (Lu et al., 1998a). Slow adsorption rates for Pu on iron oxides and other mineral colloid suspensions are also observed by Lu et al. (2000). In batch experiments, Pu sorption to hematite, silica and smectite is observed to be initially rapid (hours to a day), followed by slower sorption for at least 10 days. The Lu et al. (2000) data is analyzed by comparing the performance of a one-site kinetic model and a two-site kinetic model (Painter et al., 2002). The one-site model considers first-order adsorption and desorption on a single type of sorption site. The two-site model considers two types of sorption sites with different first-order rates of adsorption and desorption. In the two-site model by Painter et al. (2002), the sorption to the sites acts in parallel, meaning that Pu exchanges between the aqueous phase and a surface site, but does not transfer directly between surface sites (Fig. 1.1). This is similar to an equilibrium speciation model that is traditionally used for sorption to iron oxides where "weak" and "strong" sorption sites are considered (Dzombak and Morel, 1990). Painter et al. (2002) concludes that the two-site model more accurately fits the data in the silica and smectite colloid suspensions, and that the one-site and two-site models perform equally well for the hematite colloid suspension. Therefore, in some cases, Pu exhibits fast and slow sorption phases, and this kinetic behavior may be modeled using uptake models which include multiple sites.

It is worth noting that the sites described in the one-site and two-site models are defined by observations of kinetic rates for uptake and release. Therefore, the sites do not necessarily represent particular surface complex species, but may more generally be considered model compartments.

Fast Sorption Followed by Slow Sorption Kinetics: Other Sorbates on Iron Oxides

As described above, Pu sorption to minerals has been observed to be initially rapid (hours to a day), followed by slower sorption (Lu et al., 2000; Painter et al., 2002). Kinetically limited sorption with fast and slow uptake/release phases has also been examined in sorption studies with divalent cations and iron oxide surfaces (Ainsworth et al., 1994; Bruemmer et al., 1988; Eick et al., 1999; Garman et al., 2007; Glover et al., 2002;

Lehmann and Harter, 1984; Sparks, 1998), and these studies suggest several possible mechanisms to explain the kinetics of metal uptake on iron oxides (Sparks, 2000, 1998). In adsorption–desorption experiments the stability of Cu^{2+} on soil is observed to increase (Lehmann and Harter, 1984). The authors speculate that Cu binds to a set of strong and weak sorption sites and transfers from weak to strong sites over contact times of hours to days, with Cu uptake into newly vacated weak sites continuing for four or more days. Since the exact speciation of the sorbate cannot be determined, it would be more appropriate to refer to weak and strong sorbate states. A surface process occurring after initial sorption which causes a change in sorbate state over time is defined as ***aging*** (Tinnacher et al., 2011). Possible processes which may be responsible for aging include:

1. Redox transformations
2. Diffusion into micropores of solids followed by sorption to interior surfaces
3. Incorporation into a solid by mineral recrystallization
4. Surface precipitation of the sorbate
5. Sorption to sites of lower reactivity

As discussed above, aqueous Pu(V) initially undergoes rapid sorption to iron oxides followed by slower surface mediated reduction resulting in sorbed Pu(IV) (Keeney-Kennicutt and Morse, 1985; Penrose et al., 1987; Powell et al., 2005, 2004; Sanchez et al., 1985). Thus, surface-mediated reduction of Pu may constitute an aging process.

Diffusion is commonly cited as a mechanism for slow metal uptake in soils, due to their heterogeneity, and due to the presence of an interlayer in some clay minerals. Diffusion is also a reasonable mechanism for slow metal uptake in goethite due to the presence of micropores between crystallite domains in goethite particles (Fischer et al., 1996; Schwertmann, 1984). In batch adsorption studies with Ni^{2+}, Zn^{2+}, and Cd^{2+} in a goethite suspension at pH 6, Bruemmer et al. (1988) accurately fits solute concentrations for contact times of 2 hours to 42 days with a Fickian diffusion model. They conclude that initial metal sorption to external surface sites is followed by aqueous diffusion into goethite micropores and fixation at interior sites. Diffusion at domain boundaries, defects, or dislocations is the rate-limiting step. After diffusion into a micropore, a metal ion sorbed on an interior surface might be more stable due to interactions with multiple surrounding surfaces, or the surface complex formed could be identical. Although the surface speciation may not change, an apparent increase in surface stability would result from the adsorbed metal ion becoming less accessible to the solution.

Adsorbed metal ions may also be sequestered to internal sites by mineral recrystallization. In adsorption–desorption experiments with Co^{2+}, Cd^{2+}, and Pb^{2+}, Ainsworth et al. (1994) observes hysteretic sorption isotherms for Co^{2+} and Cd^{2+} adsorbed to hydrous ferric oxide for 86 weeks, but not for Pb^{2+}. Dissolution of amorphous hydrous ferric oxide and reprecipitation of iron as goethite and hematite is concluded to incorporate sorbate ions into isomorphic substitution sites within the solid. For experimental systems which begin with crystalline goethite, iron may dissolve and re-precipitate as goethite resulting in no net change in the mineral. This mechanism depends on mineral dissolution rates in the system. For a mineral at dissolution equilibrium, the rate of precipitation will be the same as that of dissolution. For minerals with greater crystallinity, such as goethite, lower dissolution rates (Stumm and Morgan, 1996) will result in less reprecipitation.

Although proton-promoted goethite dissolution rates are relatively slow, the presence of organic ligands may increase dissolution rates and potentially increase the rate of sorbate incorporation.

Precipitation of $PuO_{2+x(am,hyd)}$ on the surface of goethite would lead to apparent higher surface stability as Pu atoms are incorporated into the interior of the precipitate. Over time, the Pu amorphous hydrous oxide would increase in crystallinity which would also result in decreasing Pu lability (Choppin, 2003; Stumm and Morgan, 1996). Pu solubility is controlled by the redox potential (0.70 V at pH 8) of the Pu(IV)/Pu(V) couple and the formation of $PuO_{2+x(am,hyd)}$ which is very insoluble (Neck et al., 2007). Neck et al. (2007) estimates the solubility of Pu(IV) to be 4×10^{-10} to 10^{-8} M. Below the solubility limit, Pu atoms may aggregate on the surface of goethite. However, the extremely dilute concentrations (10^{-10} M) used for this study were selected so that this would be unlikely.

The fourth process listed above, sorption to sites of lower reactivity, means that the transfer from the initial weak site to the strong site involves a change in surface chemical speciation. This could be due to either physical transfer of the ion to a less reactive site or formation of shorter, stronger bonds with the surface. Increased bond strength at the surface over time is hypothesized to be due to: dehydration of the sorbed metal ion and the mineral surface; relaxation of surface atoms to facilitate shorter and stronger bonds with the sorbed metal ion, such as a change in denticity of the sorbed complex; or incorporation/exchange of the metal ion into the mineral lattice. This type of solid-state diffusion resulting in structural incorporation/substitution is different from aqueous diffusion into micropores. Solid state diffusion of a sorbed metal ion into the mineral lattice is more likely to happen at the site of a defect or dislocation. Before undergoing bond dehydration, outer-sphere complexes are less stable than inner-sphere complexes because outer-sphere complexes involve electrostatic interactions, and a layer of water molecules separates the adsorbed metal ion from the surface. During bond dehydration to form an inner-sphere complex, the sorbed metal ion loses water molecules from its primary hydration sphere. A more stable surface complex forms because the coordinated metal ion draws electron density away from the $\equiv FeO^-$ surface group(s), resulting in bonding which has covalent as well as ionic character (Stumm and Morgan, 1996).

The processes described above each involve the transition of a sorbate over time from an initial state to another state which is either less reactive or less accessible to the solution. These states can be represented as sites or compartments in multisite or compartment models, with the change in sorbate state over time represented as the transfer from one site or compartment to another. For instance, the physical transfer of a sorbate ion to a less reactive site could be represented by the model with two parallel sites which was used by Painter et al. (2002). This mechanism may also be represented by a model with two consecutive sites, where the transfer of an ion from the aqueous phase, to the first site, and to the next site occurs successively (Fig. 1.1). It is important to recognize that although uptake kinetics may reflect a sequence of model steps, it does not necessarily correspond to a sequence of mechanistic steps. Additionally, multiple reaction scenarios may arrive at the same mathematical solution.

Macroscopic sorption studies, like those described above, are incapable of directly distinguishing different surface states. For some processes proposed, the stoichiometry is identical. In some of the processes described, such as diffusion into micropores and incorporation into the mineral lattice, sorbed metal ions are no longer on the surface of the mineral. Although spectroscopic techniques might indicate whether sorption is inner- or outer-sphere, formation of new precipitates, as well as denticity and coordination number of surface complexes, such investigation is beyond the scope of this work. Instead of treating sorption microscopically (i.e. with precisely defined surface species), sorption was treated macroscopically. Modeling efforts considered operationally defined surface states distinguished on the basis of observed kinetic behavior.

Kinetically Limited Sorption vs. Sorption Hysteresis

Observations of field-scale transport as well as laboratory adsorption–desorption studies suggest that Pu sorption may be slowly reversible or partly irreversible. For general sorption systems, irreversible sorption is often cited to explain adsorption–desorption batch experiments where the adsorption isotherm and desorption isotherm curves do not coincide (Fig. 2.1). The non-coincidence of adsorption and desorption isotherm curves can be defined *sorption hysteresis* (Adamson and Gast, 1997; Sing et al., 1985). In theoretical terms, phenomena which exhibit hysteresis have a forward mechanism which differs from the reverse mechanism. However, the occurrence of hysteresis loops might depend on the rate of change of the system inputs (e.g. solute concentration) (Visintin, 2006). Therefore, the observation of disagreement between sorption and desorption isotherms is insufficient to conclude either hysteretic mechanisms or irreversible sorption. Apparent hysteresis loops can arise in isotherm plots if contact times are too brief for a slow sorption mechanism to reach equilibrium. According to the strict definition of hysteresis, hysteresis loops would remain for infinite contact times (Visintin, 2006). Hence, disagreement in adsorption and desorption isotherm curves cannot be used to determine that mechanisms are hysteretic, but rather reflect reaction rates which are slow relative to the experiment time scale. For purposes of modeling sorption rates, sorption which is actually slowly reversible can be simplified by applying an irreversible sorption model, if sorption appears irreversible over laboratory time scales (Painter et al., 2002).

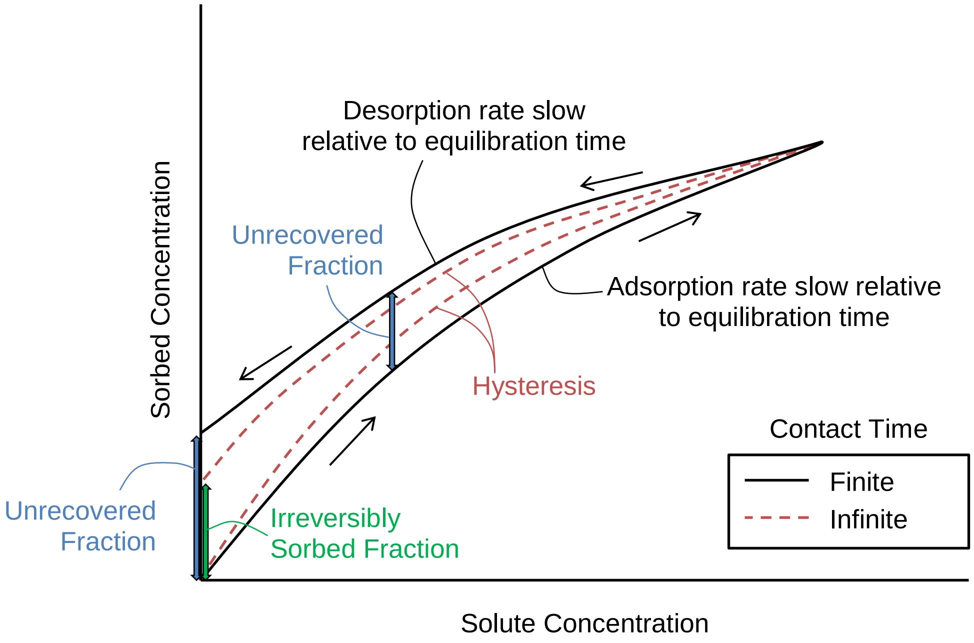

Figure 2.1. Qualitative illustration comparing true sorption hysteresis with general case of disagreement between adsorption and desorption isotherms.

I propose that Pu undergoes aging, a surface process occurring after initial sorption which causes a change in sorbate state over time (Tinnacher et al., 2011). During aging of Pu, a slow surface transfer reaction would not only kinetically limit desorption of the sorbate, but also, during adsorption, increases the overall surface stability of the sorbate with increasing contact time. The effect could be observed in adsorption–desorption batch experiments where samples receiving identical desorption treatments show different apparent distribution coefficients depending on contact time. It is unknown how long might be required for the proposed slow transfer reaction to reach equilibrium in the case of Pu. Aging may explain the high stability of Pu on soils with which it has had a decades-long association (Emerson, 2014). In adsorption–desorption batch experiments with divalent metal cations on iron oxide suspensions, changes in sorption stability have been observed over weeks to months (Ainsworth et al., 1994; Eick et al., 1999; Garman et al., 2007; Glover et al., 2002).

Terminology Side Notes

- The term *aging* should not be confused with aging of minerals, which some authors use to describe crystallization of amorphous minerals, such as hydrous iron oxide (Ainsworth et al., 1994; Stumm and Morgan, 1996; Waychunas et al., 1993).
- In some papers, the term *residence time effect* is used to describe sorbate aging (Eick et al., 1999; Garman et al., 2007; Glover et al., 2002; O’Reilly et al., 2001).

Background on Developing a Kinetic Sorption Model

As described above, Pu sorption may have fast and slow rate components and this kinetic behavior may be modeled using multisite or compartment models. For simplicity, further discussion is limited to two solid phase sites or compartments.

Previous studies modeled reactive transport for flow-through systems by coupling equations for advective transport and sorption reactions (Bar-Tal, 1990; Seyfried et al., 1989; Skopp and McCallister, 1986; Tinnacher et al., 2011). The general procedure begins with a mass balance equation (Eq. 2.2):

$$\frac{dC}{dt} = \frac{Q}{V}[C_{in} - C] - \frac{M}{V}\frac{dS}{dt} \tag{2.2}$$

where C represents the concentration of aqueous Pu in the reactor (mol·L^{-1}), C_{in} represents the concentration of Pu in the influent solution (mol·L^{-1}), S is the concentration of sorbed Pu (mol·g^{-1}), Q is the flow rate (L·min^{-1}), V is the cell volume (L), M is the total mass of sorbent (g), and t is time (min). The mathematical model can be modified to describe different types of sorption isotherms by substituting dS/dt with different rate laws (shown in Table 2.1) in Eq. 2.2. Additionally, the mass balance equations can be extended to consider multi-site models (Braithwaite et al., 2000; Selim and Amacher, 2001) which may consider combinations of sorption site types (see Appendix B for more detail). Sorption reactions at multiple sites could be considered to be parallel or consecutive. In a model with parallel sites, a solute may sorb to two different sites simultaneously. In a model with consecutive sites, a solute must sorb to one type of site before it can access a second site.

Table 2.1. Rate laws and equilibrium equations for use in kinetic modeling (Tinnacher et al., 2011).

Sorption	Rate Law	Equilibrium Equation
Linear Isotherm (1st order)	$\frac{dS}{dt} = k_f C - k_b S$	$S = K_d C$
Langmuir Isotherm	$\frac{dS}{dt} = k_f C(S_{max} - S) - k_b S$	$S = \frac{K_L S_{max} C}{1 + K_L C}$
Freundlich Isotherm	$\frac{dS}{dt} = k_f C^n - k_b S$	$S = K_F C^n$
Irreversible	$k_b = 0$	
Instantaneous Equilibrium	$\frac{dS}{dt} = 0$ Use the appropriate equilibrium equation (shown)	

C = solution concentration (mol·L^{-1}); *S* = sorbed concentration (mol·kg^{-1}); k_f = forward rate constant (min^{-1}), k_b = reverse rate constant (min^{-1}); *n*, *a*, *b* = sorption coefficients (-); K_d = distribution coefficient (L·kg^{-1}); K_L = Langmuir constant (L·mol^{-1}); K_F = Freundlich constant (dm^{3n}·kg^{-1})

Influence of Natural Organic Ligands

The presence of organic ligands can have a profound effect on Pu mobility, sorption, and oxidation state. Although Pu(V) is generally considered the stable aqueous oxidation state of Pu (Keeney-Kennicutt and Morse, 1985; Morse and Choppin, 1986; Orlandini et al., 1986), in field studies, mobile Pu(IV) has been observed associated with organic ligands. In trench leachates from the Maxey Flat Low Level Radioactive Waste facility, Pu(IV) was found complexed with dissolved organic carbon suspected of being EDTA (Cleveland and Rees, 1981). In surface waters at Rocky Flats Environmental Technology Site, mobile Pu was found in the colloidal fraction associated with organic macromolecules (Santschi et al., 2002).

Natural organic matter and the organic ligand surrogates used in this study contain carboxyl, phenol, and hydroxamic functional groups which can bind to Pu. Humic substances, which are derived from decomposing plant detritus, are complex in structure and can contain many carboxyl, phenol and aromatic groups. The soluble fraction of humic substances is defined as fulvic acid; the insoluble fraction is defined as humin. Humic acid is soluble at neutral and basic pH, but insoluble below pH 2. Humic acid is relatively hydrophobic and can aggregate into colloidal-size particles at pH values somewhat above pH 2. Fulvic acid has been observed to enhance Pu sorption to goethite at low pH (Conroy et al., 2017; Tinnacher et al., 2015), and diminish Pu sorption to mineral surfaces by forming stable aqueous complexes which compete with binary Pu surface complexes at pH 5–9 (Conroy et al., 2017; Simpkins, 2011).

Siderophores are released by plants, bacteria, and fungi in order to solubilize Fe(III) and other metals for nutrient uptake. Because Pu(IV) and Fe(III) have similar ratios of electric charge to ionic radius, siderophores also solubilize Pu(IV). Citric acid is a siderophore produced by plants, and it contains three carboxyl groups. Hydroxamate siderophores have been found in soil extracts at concentrations of 10^{-7}–10^{-8} M (soil moisture corrected to 10% w/w) (Powell et al., 1980). The hydroxamate siderophore desferrioxamine B (DFOB) is a linear molecule with three hydroxamate groups which enables it to chelate metal ions in solution. However, DFOB has shown limited ability to bond to Fe(III) sites on the surface of goethite since only one of its three hydroxamic groups is available to bond (Cheah et al., 2003; Cocozza et al., 2002; Conroy et al., 2017; Kraemer et al., 1999). DFOB is commonly used in studies of hydroxamic acids because it can be produced commercially from the actinobacteria *Streptomyces pilosus*. Citric acid and DFOB are known to form highly stable Pu–ligand aqueous complexes with log stability constants of 29 and 62 (Boukhalfa et al., 2007; Clark et al., 2010) for the formation of $Pu(Cit)_2^{2-}$ and $PuH_2(DFOB)_2^{2+}$, respectively (Figs. B.1 and B.2). In the presence of natural organic ligands, the high stability of aqueous Pu(IV)–NOL complexes thermodynamically drives Pu(V) to become Pu(IV)–NOL complexes (André and Choppin, 2000; Blinova et al., 2007), resulting in a single aqueous oxidation state.

Batch sorption experiments with Pu and NOL on pure minerals (Conroy et al., 2017; Powell et al., 2011; Simpkins, 2011; Zhao et al., 2011; Zimmerman et al., 2014) have resulted in a conceptual model in which Pu–ligand aqueous complexes compete with ternary surface complexes, and Pu–mineral complexes. The effect a particular type of NOL has on Pu sorption depends on pH. For a batch system containing 10^{-11} M Pu and 1.0 g L^{-1} goethite (Fig.2.2), the ability of NOL to maintain Pu in solution in the pH range 5 to 9 is ranked roughly DFOB > fulvic acid (Suwanee River II standard) > citric acid (Conroy et al., 2017). Citric acid is most effective at solubilizing Pu at pH 7, and fulvic acid is most effective at pH 5. However, at pH 3, these ligands enhance the sorption of Pu to goethite. Below the pH_{pzc} of goethite (7–9) (Appel et al., 2003; Atkinson et al., 1967; Schwertmann and Taylor, 1989), the goethite surface has a net positive charge, and the charge becomes more positive with decreasing solution pH values. The increased electrostatic attraction between the mineral surface and negatively charged ligands at pH 3 allows ternary surface complexes to form. Above pH 7, humic, fulvic, and citric acid are less effective at solubilizing Pu because goethite's surface charge becomes less positive, and surface hydrolysis products begin to compete with organic ligands for Pu. DFOB interacts weakly with the surface of goethite due to cation repulsion and steric hindrance (Cheah et al., 2003; Cocozza et al., 2002; Conroy et al., 2017; Kraemer et al., 1999). Therefore, DFOB does not form ternary surface complexes on goethite, and DFOB decreases Pu sorption by >80% across the pH range 3 to 8. Pu distributions measured in batch sorption experiments on pure minerals in the presence of NOL suggest that the mobility of Pu in natural soils is controlled in part by the strength of aqueous Pu–ligand complexes and the affinity of the ligand for mineral surfaces.

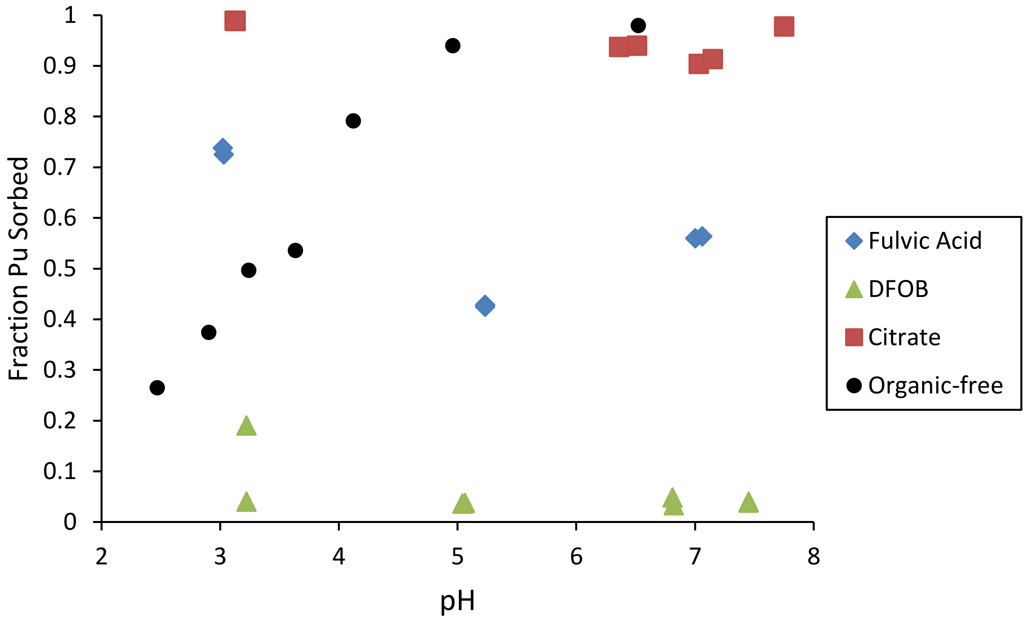

Figure 2.2. Fractional Pu sorption for 14 days equilibration in a goethite system in the presence of 5 $mg_c \cdot L^{-1}$ citric acid, fulvic acid (Suwanee River II standard), and Desferroxamine B (DFOB). Goethite suspension concentration was 1.0 $g \cdot L^{-1}$, total Pu(IV) concentration is 10^{-11} M, and ionic strength was controlled with 10 mM NaCl (Conroy et al., 2017). Ligand-free data is for 10^{-11} M Pu(IV) equilibrated 1 hour in a 28.5 $m^2 \cdot L^{-1}$ goethite suspension with 0.10 M $NaNO_3$ (Sanchez et al., 1985).

CHAPTER THREE

OBJECTIVES

Knowledge Gaps and Hypotheses

The above discussion reveals these knowledge gaps to be addressed in this study.

Knowledge Gap 1:	Previously reported measures of Pu(IV) surface stability (e.g. distribution coefficients and surface complexation constants) may be underestimated because experimental measurements are made in systems with mixed oxidation states, resulting from surface mediated reduction and oxidative leaching.
Hypothesis 1:	The surface stability of Pu(IV) on a goethite surface can be quantified for a pure Pu(IV) system by using DFOB as a competing complexant to control Pu oxidation state.
Knowledge Gap 2:	After initial fast (e.g. hours to a day) sorption on goethite, Pu sorption kinetics have an additional slow (e.g. 10 or more days) rate component. Observations of Pu strongly associated with mobile colloids in the field and unrecovered Pu in batch desorption experiments with iron oxide colloids suggest that Pu(IV) sorption to iron oxides may exhibit an aging process manifested by irreversible sorption or slow desorption. A kinetic model, possibly consisting of multiple sorption sites with fast and slow reaction rates, is needed to describe and predict Pu sorption to iron oxides (and other minerals).
Hypothesis 2:	Pu sorption kinetics for a goethite system may be described with a two-site model consisting of consecutive fast and slow uptake steps. Pu undergoes aging, a surface process occurring after initial sorption which causes a change in sorbate state over time. The change in sorbate state over time results in increased Pu surface stability or Pu becomes less accessible to the solution. Possible Aging Processes: 2a. Surface mediated reduction 2b. Aqueous diffusion of Pu from external sorption sites into goethite micropores and sorption to interior surfaces. 2c. Sorption to sites of lower reactivity by physical transfer of the ion to a less reactive site 2d. Sorption to sites of lower reactivity by formation of shorter, stronger bonds with the surface.

        i. Dehydration of the sorbed metal ion and the mineral surface
        ii. Relaxation of surface atoms to facilitate shorter and stronger bonds with the sorbed metal ion (e.g. a change in denticity of the sorbed complex)

    2e. Incorporation into solid by mineral recrystallization

    2f. Surface precipitation of sorbate

    2g. Lattice incorporation

Knowledge Gap 3:	Natural organic ligands are known to enhance Pu mobility in the field, and batch studies demonstrate the ability of NOL to enhance or diminish Pu sorption to pure minerals, depending on chemical conditions. Although Pu distribution coefficients have been measured for pure synthetic minerals in the presence of NOL, laboratory transport experiments are needed to evaluate Pu mobility in natural soils in the presence of NOL.
Hypothesis 3:	DFOB, fulvic acid, and citric acid are expected to mobilize Pu on the basis of the strength of aqueous Pu–ligand complexes and the affinity of the ligand for the mineral surface. At pH 5 to 7, Pu mobility is expected to follow the trend DFOB > fulvic acid (Suwanee River, standard I) > citric acid.

3a. DFOB is expected to result in the greatest Pu mobility due to chelation of Pu(IV) and low affinity for goethite surfaces.

3b. Fulvic acid is expected to result in moderate Pu mobility at pH 4 to 8 with fulvic acid having the greatest effect at pH 5. The formation of ternary surface complexes at lower pH will reduce mobility.

3c. Citric acid is expected to result in the least Pu mobility relative to the other ligands, and have the greatest mobilizing effect at pH 7. The formation of ternary surface complexes at lower pH will reduce mobility.

Project Objectives and General Task Descriptions

1. Quantify the surface stability of Pu(IV) on goethite for a pure oxidation state system by using DFOB as a competing complexant. (Chapter 4)
2. Obtain an experimental data set which may demonstrate Pu aging on goethite in the presence of NOL. (Chapters 4 and 5)
3. Using Pu–goethite kinetic (de)sorption data, develop a kinetic sorption model for (de)sorption in the presence of NOL by evaluating the performance of one-site and two-site models. (Chapter 5)
4. Using an appropriate kinetic sorption model, determine apparent sorption rate constants for Pu(IV) sorption on goethite in the presence of NOL. (Chapter 5)
5. Evaluate the effects of DFOB, citric acid, and fulvic acid (Suwanee River, standard I) on Pu desorption in a flow-cell system with synthetic goethite. (Chapter 5)
6. Determine the mobility of Pu on natural SRS soil in the presence of NOL by performing column experiments. Using parameters previously measured in batch experiments with pure minerals, perform predictive reactive transport modeling, and compare to experimental measurements in order to judge the performance of the models and parameters. (Chapter 6)

The above objectives meet both the project goal of quantifying and developing a model for Pu aging, and the goal of validating reactive transport models for Pu in the presence of NOL. Experimental and modeling work to complete the objectives was divided into three tasks, summarized in Table 3.1, each of which is the basis for a paper for publication. Task 1 consisted of a batch experiment which, over three months, quantified Pu aging in the presence of DFOB. DFOB was added to compete with proposed strong surface complexes, and to control aqueous oxidation state. In Task 2, slow desorption of Pu from goethite was examined with flow-cell experiments, and a kinetic sorption model was developed to describe sorption behavior in conjunction with a flow-cell transport model. Enhanced removal of Pu from the flow-cell in the presence of DFOB, fulvic acid, and citrate was compared with the relative affinities for the formation of aqueous complexes and ternary surface complexes. Task 3 used column experiments to examine mobility of Pu in natural SRS soil in the presence of DFOB and citric acid. Reactive transport models including the processes of surface mediated reduction, colloid-facilitated transport, and Pu mobilization by soil organic matter were compared to the column measurements in order to determine the plausibility of these processes. The result of these efforts was an improved understanding of Pu (de)sorption kinetics, a model describing the kinetics of Pu aging, and a demonstration of the effect of NOL on Pu transport in a natural soil.

Synthetic goethite was selected for sorption experiments because goethite is one of the most common (oxyhydr)oxides under oxidizing conditions and because iron oxides are ubiquitous in the environment (Schwertmann and Cornell, 1991; Schwertmann and Taylor, 1989), including at the Savannah River Site (Denham et al., 1999). At pH 3 to 8, a large fraction of Pu sorbs to goethite rapidly (Keeney-Kennicutt and Morse, 1985; Sanchez et al., 1985). Hence, in the natural environment, goethite is influential in controlling Pu mobility. Column experiments in this work were performed on a well-characterized soil from the Savannah River Site that is being used as part of a larger ongoing research effort.

Organic ligands were selected to represent diverse types of natural organic matter present in the environment. Fulvic acid (Suwanee River, standard I) was selected as a common soluble type of organic ligand composed of an assortment of functional groups. As siderophores, citric acid and DFOB, were selected for their known ability to form complexes with Fe(III) and other metal ions. Although not present in high concentrations in the environment (Powell et al., 1980), DFOB was selected for its properties as a chelating agent. Additionally, DFOB is not known to form ternary surface complexes due to its low affinity for goethite surfaces (Cheah et al., 2003; Cocozza et al., 2002; Kraemer et al., 1999), and so it may be added to Pu sorption systems to prevent oxidation of Pu(IV) to Pu(V) in solution, without confounding sorption measurements by formation of additional surface species.

Table 3.1. Task summaries, deliverables, and target objectives

Task/Paper Title	Summary	Deliverables	Target Objective
1. Batch Experiments "Effect of Equilibration Time on Pu Desorption from Goethite"	Batch experiments were performed to examine the stability of ^{238}Pu(IV)–goethite surface complexes with pH values ranging from 4 to 7 and adsorption equilibration times of 1, 6, 15, 34 and 116 days. During desorption, DFOB acted as a competing complexant for Pu and controlled aqueous oxidation state. Pu in supernatant was measured by liquid scintillation counting.	• Sorption data were collected in a pure oxidation state system for the quantification of Pu(IV) surface stability. • Increasing surface stability of Pu(IV) with adsorption equilibration time was an indicator of Pu aging.	1, 2
2. Flow-cell Experiments "Desorption Behavior of Plutonium from Goethite in a Flow-cell Reactor in the Presence of Natural Organic Ligands"	Flow-cells utilized constant dilution and continuous sampling to examine the desorption reaction rates of ^{238}Pu(IV) in the presence of DFOB, fulvic acid (Suwanee River, standard I), and citric acid at pH 6 for a goethite system. Periodic stop and flow events were conducted to manipulate the fluid residence time. Pu in effluent fractions was measured by liquid scintillation counting. One-site and two-site kinetic sorption models were evaluated by globally fitting effluent concentrations. Apparent sorption rate constants for Pu in the presence of NOL were obtained.	• Constant dilution was used to minimize readsorption of Pu to goethite, allowing desorption rates to be examined. • Varying equilibration time using stop and flow events allowed Pu sorption kinetics to be examined while the system moved towards sorption equilibrium or steady-state (chemical disequilibrium). • By considering multiple sorption sites in development of kinetic sorption models for Pu, a range of possible relationships between sites was explored. • Pu desorption over time in the presence of DFOB, fulvic acid (Suwanee River, standard I), and citrate was compared.	2, 3, 4, 5
3. Column Experiments "Transport of Plutonium in Soil from the Savannah River Site in the Presence of Citrate and Desferrioxamine B"	The mobilization of Pu by DFOB and citrate was examined in columns packed with SRS soil. After effluent collection, soil columns were sectioned and acid leached. Tritium and ^{238}Pu and were measured in effluent fractions and leached soil using liquid scintillation counting. Reactive transport models were compared with measurements to determine the plausibility of several processes affecting Pu mobility.	• Observations of mobile and soil-bound Pu revealed the complex nature of natural soils. • Sorption isotherms for DFOB and citrate were obtained for the SRS soil. • TOC and elemental analysis of effluent from a blank soil column indicated the possible influence of soil organic matter and mobile colloid formation. • The processes of surface mediated reduction, colloid-facilitated transport, and Pu mobilization by soil organic matter were included in predictive reactive transport modeling to determine the plausibility of these processes.	6

CHAPTER FOUR

EFFECT OF EQUILIBRATION TIME ON Pu DESORPTION FROM GOETHITE

Paper Status

This chapter has been previously published in *Radiochimica Acta* as Wong et al., (2015). It is reproduced here and modified for consistency of formatting.

Authors

Jennifer C. Wong, Mavrik Zavarin, James D. Begg, Annie B. Kersting, Brian A. Powell

Abstract

It has been suggested that strongly sorbing ions such as plutonium may become irreversibly bound to mineral surfaces over time which has implications for near- and far-field transport of Pu. Batch adsorption–desorption data were collected as a function of time and pH to study the surface stability of Pu on goethite. Pu(IV) was adsorbed to goethite over the pH range 4.2 to 6.6 for different periods of time (1, 6, 15, 34 and 116 d). Following adsorption, Pu was leached from the mineral surface with desferrioxamine B (DFOB), a complexant capable of effectively competing with the goethite surface for Pu. The amount of Pu desorbed from the goethite was found to vary as a function of the adsorption equilibration time, with less Pu removed from the goethite following longer adsorption periods. This effect was most pronounced at low pH. Logarithmic desorption distribution ratios for each adsorption equilibration time were fit to a pH-dependent model. Model slopes decreased between 1 and 116 d adsorption time, indicating that overall Pu(IV) surface stability on goethite surfaces becomes less dependent on pH with greater adsorption

equilibration time. The combination of adsorption and desorption kinetic data suggest that non-redox aging processes affect Pu sorption behavior on goethite.

Introduction

The production and testing of nuclear weapons have resulted in a legacy of plutonium (Pu) contamination in the environment (Cantrell, 2009; Carlton et al., 1992; Felmy et al., 2010; Smith et al., 2003). The mobility of Pu in the subsurface is of particular concern due to the long half-life of Pu (24,000 years for ^{239}Pu) and its radiotoxicity. Pu sorption to minerals is the main mechanism controlling its subsurface mobility. Sorption of Pu to iron oxides, of which goethite (α–FeOOH) is one of the most common, is of key interest because iron oxides are ubiquitous in the environment (Cornell and Schwertmann, 2003; Schwertmann and Taylor, 1989) and Pu exhibits a very high affinity for iron oxide surfaces. Although it is generally assumed that Pu is relatively immobile due to its low solubility (Choppin, 2003; Knopp et al., 1999; Neck and Kim, 2001; Nitsche and Edelstein, 1985) and strong sorption of Pu(IV) to mineral surfaces (Triay et al., 1996), long-distance transport of Pu has been observed in association with colloids (Kersting et al., 1999; Novikov et al., 2006; Santschi et al., 2002), suggesting formation of highly stable Pu surface complexes on colloids. At the Mayak site, colloid-facilitated transport appeared to be driven by Pu association with iron oxide colloids (Novikov et al., 2006). In sorption experiments with soluble Pu(V) and goethite colloids in natural groundwater, it was concluded that Pu desorption rates are much slower than adsorption rates (Lu et al., 1998a, 1998b). In acid leaching experiments, stabilization of sorbed nanocrystalline Pu on hematite was observed with increasing contact time (Romanchuk et al., 2013). Thus, it is hypothesized that observations of colloid-facilitated transport are due to irreversible sorption to colloids or rate-limited desorption of Pu from colloids (Cvetkovic et al., 2004; Painter et al., 2002). This hypothesis is supported by field studies in which long distance, colloid-facilitated transport of Pu has been observed (Kersting et al., 1999; Novikov et al., 2006; Penrose et al., 1990).

An irreversible reaction is an “exothermic reaction in which the activation energy for the reverse reaction is sufficiently large that the reaction proceeds only in the forward direction under practical conditions” (Fox and Whitesell, 2004). When used in the context of sorption reactions, irreversibility is characterized by an inequality between adsorption and desorption distribution coefficients. However, sorption reactions which appear irreversible on short timescales (hours to days) may actually be reversible and simply have very slow rates of adsorption or desorption. In this case, as adsorption or desorption times are increased beyond typical laboratory timescales, the inequality between adsorption and desorption distribution coefficients may vanish.

Aging is a “surface chemical process that follows the initial sorption reaction and causes changes in contaminant surface speciation over time” (Tinnacher et al., 2011). These changes in surface speciation could make the contaminant more stable on the surface. Aging is manifested by distribution coefficients which increase with contact time. As a result, the amount of contaminant which can be desorbed decreases with increasing contact time. Depending on the timescales of adsorption/desorption, aging can give the appearance of irreversible sorption. Thus, the irreversible adsorption attributed to colloid facilitated Pu transport at the Mayak Site (Novikov et al., 2006) and the slow desorption rates observed in batch Pu goethite sorption experiments (Lu et al., 1998a, 1998b) could be attributed to aging.

Though several hypotheses regarding the underlying mechanisms of aging (or irreversible sorption) have been proposed, few have been explicitly proven. The sorbate may undergo a change in surface speciation over time, either by the formation of shorter and stronger bonds with the surface or by the physical transfer of the sorbate to sites of higher reactivity (Backes et al., 1995; Lehmann and Harter, 1984; Sparks, 2000, 1998). As goethite is a microporous mineral (Fischer et al., 1996; Schwertmann, 1984), aging on goethite may also occur by aqueous diffusion into micropores followed by sorption to interior sites (Backes et al., 1995; Bruemmer et al., 1988; Eick et al., 1999; Kim et al., 2007; Lehmann and Harter, 1984; Romanchuk et al., 2013; Sparks, 2000, 1998). Surface precipitation of the sorbate has been suggested as an aging process (Kim et al., 2007; Lehmann and Harter, 1984; Sparks, 2000). Another proposed aging process is surface exchange, where a sorbate atom exchanges with an iron atom in the mineral lattice and becomes structurally incorporated (Barrow et al., 2012). Incorporation of the sorbate as a result of mineral recrystallization has also been identified as an aging process (Ainsworth et al., 1994; Kim et al., 2007; Sparks, 1998). Surface mediated reduction of Pu(V) to Pu(IV), which has been observed on iron oxide and other mineral surfaces (Keeney-Kennicutt and Morse, 1985; Penrose et al., 1987; Powell et al., 2005, 2004; Sanchez et al., 1985) may also exhibit the characteristics of an aging process. In cases where researchers have observed a rapid sorption step followed by a second, slow sorption step, the second reaction has been attributed to diffusion of Pu into micropores or surface mediated reduction of Pu(V) (Romanchuk et al., 2011; Sanchez et al., 1985).

Regardless of the proposed aging mechanisms discussed above, numerical descriptions of aging are typically parameterized as two consecutive reactions: an initial sorption reaction followed by a second aging reaction. This consideration of multiple kinetic sites is necessary to evaluate aging processes. Since sorption of ions to the initial sites appears to be rapid, the rate of the second reaction should be the rate limiting step. Thus, the rate of slow uptake commonly observed in the second phase of a kinetic sorption experiment could be a proxy of the aging process on the surface.

Pu Redox Behavior and Sorption on Iron Oxides

Plutonium can exist in the +III, +IV, +V and +VI valence states simultaneously under natural conditions (Choppin et al., 1997; Silva and Nitsche, 1995). At moderate pH and E_h, Pu(IV) and Pu(V) are the dominant oxidation states, whereas Pu(III) and Pu(VI) are generally only stable under anoxic or oxic conditions, respectively (Cleveland, 1979). Due to the profound insolubility of Pu(IV), it is commonly found in ligand-free solutions as a precipitate or sorbed to solid phases. Conversely, Pu(V) is more soluble and the stable oxidation state of aqueous Pu in dilute salt solutions and seawater (Morse and Choppin, 1986; Orlandini et al., 1986). Therefore, a common observation is that Pu(V) is the dominant aqueous phase oxidation state and Pu(IV) is the dominant oxidation state in solid phases. This is illustrated by the solubility of $PuO_{2(s)}$ phases under oxic conditions where the solubility limit is approximately 10^{-8} to 10^{-6} M with the aqueous phase dominated by Pu(V) (Choppin, 2003; Rai, 1984; Rai et al., 2001, 1980).

The distribution of Pu(IV) and Pu(V) oxidation states primarily between solid and aqueous phases, respectively, has also been observed in sorption experiments (Banik et al., 2007; Buda et al., 2008; Keeney-Kennicutt and Morse, 1985; Powell et al., 2006, 2005, 2004; Romanchuk et al., 2011; Sanchez et al., 1985). The sorption edges of Pu(IV) and Pu(V) correlate with the hydrolysis of Pu in these oxidation states (Choppin, 2003; Keeney-Kennicutt and Morse, 1985; Knopp et al., 1999; Neck and Kim, 2001; Nitsche and Edelstein, 1985; Sanchez et al., 1985). On goethite, the sorption edge for Pu(IV), which begins to hydrolyze (Choppin, 2003; Guillaumont et al., 2003; Knopp et al., 1999; Neck and Kim, 2001; Nitsche and Edelstein, 1985) to $Pu(OH)_x^{4-x}$ species at pH 1, is in the pH range 3 to 5 (Guillaumont et al., 2003; Sanchez et al., 1985). After 24 h, the sorption edge for Pu(V) is in the pH range 6 to 8, which is consistent with the expected hydrolysis of Pu(V) at pH <9.7 (Guillaumont et al., 2003; Sanchez et al., 1985). However, Pu(V) undergoes surface mediated reduction to Pu(IV) on iron oxides, leading to a shift in the sorption edge to a lower pH over time (Keeney-Kennicutt and Morse, 1985; Penrose et al., 1987; Powell et al., 2005, 2004; Sanchez et al., 1985). Thus, if Pu(V) is present in the pH range 3 to 8 the fraction of sorbed Pu is observed to increase over time (Keeney-Kennicutt and Morse, 1985; Penrose et al., 1987; Powell et al., 2005, 2004; Sanchez et al., 1985). The dominance of aqueous Pu(V) and its reduction implies that reduction of Pu(V) to Pu(IV) is a surface mediated process. Few desorption studies have been performed which monitor the aqueous oxidation state of desorbed Pu. Thus, it is unclear if desorption is coupled with a surface mediated oxidation step. Using $PuO_{2(s)}$ solubility studies as a proxy for desorption studies, similar dominance of aqueous Pu(V) has been observed (Rai, 1984; Rai et al., 2001, 1980).

Because multiple Pu oxidation states may be present simultaneously, it is necessary to know the distribution of sorbed and aqueous oxidation states in sorption experiments (Powell et al., 2011). One method to simplify the system is to add an organic ligand which can stabilize aqueous Pu(IV) and avoid the formation of Pu(V). In this case, the amount of Pu which can be desorbed from the mineral surface can be related to the relative stability of the Pu(IV)–surface and the Pu(IV)–ligand complexes without needing to address the additional complexity of Pu(IV) oxidation.

Desferrioxamine B (DFOB) can be used to stabilize Pu(IV) as the dominant aqueous oxidation state across a wide range of experimental conditions (pH, concentration, atmospheric conditions; Fig. A.1) (Boukhalfa et al., 2007; Keberle, 1964). In addition, the aqueous Pu(IV)–DFOB complex can effectively promote Pu(IV) desorption from goethite. Equilibrium speciation calculations under atmospheric conditions show that Pu(IV)–DFOB complexes dominate over $Pu(OH)_x^{4-x}$ species between pH 4 and 8 at concentrations of 10^{-10} M Pu(IV) and 1.7 µM DFOB (Fig. A.2). Under these conditions, the high stability of Pu(IV)–DFOB complexes are expected to thermodynamically maintain the dominance of the aqueous Pu(IV)–DFOB complexes and minimize Pu(IV) oxidation to Pu(V) under atmospheric conditions (Fig. A.1).

In this work, an alternative approach to examining aging has been utilized wherein desorption of Pu is monitored using a strong aqueous complexant (i.e. DFOB) that promotes Pu desorption and controls the Pu oxidation state. Adsorption equilibration periods as long as 4 months were examined to test the existence of very slow aging processes. Desorption was carried out after a 34 d equilibration period for the same reasons. The overall surface stability of Pu as a function of adsorption equilibration time was quantified by examining the linear relationship between logarithmic distributions ratios ($log\ R_d$) and pH values.

Materials and Methods

Acids and bases used were Aristar Plus grade. Cyclohexane (Alpha Aesar) and sodium chloride used were ACS reagent grade. All water used was distilled and deionized with resistivity >18 MΩ·cm. A DFOB stock solution was prepared at a concentration of 1.7 mM by dissolving desferrioxamine mesylate salt (Sigma Aldrich) in deionized water.

The goethite was prepared as described previously (Tinnacher et al., 2011) and had a BET surface area of 42 $m^2 \cdot g^{-1}$. A goethite stock suspension of 8.0 $g \cdot L^{-1}$ was prepared by suspending goethite in 100 mL deionized water, centrifuging to a particle size cutoff of 100 nm, and replacing supernatant with fresh deionized water. This washing step was performed three times to remove <100 nm goethite fines. The final goethite stock was suspended in 100 mL 10 mM NaCl.

Concentrations of ^{238}Pu were measured by liquid scintillation counting. Samples were prepared for alpha spectroscopic analysis with Optiphase Hisafe 3 scintillation cocktail (Perkin Elmer) and counted with alpha/beta discrimination using a Wallac model 1415, Hidex 300SL, or Perkin Elmer Tri-Carb 2910 TR liquid scintillation counter. For each instrument, Pu stock solutions were measured so that aqueous Pu concentrations could be calculated as a fraction of Pu added to samples.

Pu Stock Solutions and Oxidation State Analysis

A stock solution of 6.6 × 10^{-8} M ^{238}Pu(IV) was prepared by evaporating ^{238}Pu(V) (Isotope Products) in 1 M HNO_3 and redissolving in 0.1 M HCl. A Pu–DFOB stock solution was prepared by adding DFOB to 1 mL Pu(IV) stock solution to yield 3.3 × 10^{-5} M DFOB and 5.9 × 10^{-8} M Pu. Because the Pu concentrations in stock solutions and samples were too low to use direct observation techniques (e.g. UV-Vis spectroscopy), well-established co-precipitation and solvent extraction techniques were used to determine Pu oxidation state. The oxidation state of the DFOB-free Pu(IV) stock solution was verified to be 91.9 ± 0.6 % Pu(IV) by lanthanum fluoride co-precipitation (Foti and Freiling, 1964; Nitsche et al., 1988). The oxidation state of some DFOB-free samples was measured by organic solvent extraction with 0.025 M 1-phenyl-3-methyl-4-benzoyl-pyrazole-5-one (PMBP; Tokyo Chemistry Industry Co., Ltd.) in cyclohexane, which extracts Pu(IV) into the organic phase, leaving oxidized Pu in the aqueous phase (Neu et al., 1994; Nitsche and Edelstein, 1985). Aqueous and organic fractions of Pu were measured by liquid scintillation counting with alpha/beta discrimination. The Pu oxidation state of the solutions containing DFOB could not be verified due to interference of DFOB with the co-precipitation reaction and solvent extraction. The oxidation state of Pu in the Pu–DFOB stock solution is assumed to be Pu(IV) based on the initial Pu(IV) state of the stock solution and the strong complexation of DFOB with Pu(IV) (Boukhalfa et al., 2007).

Pu Batch Adsorption–Desorption in the Presence and Absence of DFOB

An adsorption–desorption batch experiment with Pu was performed on goethite suspensions as a function of pH to establish that the presence of DFOB will limit Pu adsorption and enhance Pu desorption compared to a DFOB-free solution. Solutions of 10 mM NaCl and 0.075 $g \cdot L^{-1}$ goethite were prepared in 15 mL polyethylene tubes. After addition of Pu from Pu(IV) or Pu–DFOB stock solutions, the final Pu concentration of samples was $\approx 1.7 \times 10^{-10}$ M for DFOB-containing samples and $\approx 1.9 \times 10^{-10}$ M for DFOB-free samples. The total Pu added to each sample from stock solutions was determined gravimetrically. Additional DFOB was added to DFOB-containing samples from the DFOB stock solution to yield 1.7 μM DFOB. Sample pH values were adjusted to 6 and 8 with dilute HCl and NaOH. During adsorption, aqueous Pu was measured at 2 h, 5 h, 1, 3, 10, and 25 d. Then, the supernatant was replaced with either 1.7 μM DFOB or DFOB-free solution, and aqueous Pu was monitored during desorption (see Supplementary Material). Sampling consisted of transferring a 1.4 mL homogenous aliquot to a microcentrifuge tube, centrifugation at 8000 rpm for 20 minutes (Beckman and Coulter Allegra 22R centrifuge with F2402 rotor) which is calculated to remove particles >100 nm based on Stoke's Law, and measuring the Pu concentration in the supernatant. First-order adsorption rate constants were estimated by fitting measurements spanning 2 h–25 d.

Effect of Adsorption Equilibrium Time on Pu(IV) Surface Stability

Preliminary experiments suggested that Pu(IV) desorption behavior was dependent on adsorption time. To test the effect of adsorption time on desorption behavior, DFOB-free solutions of 10 mM NaCl and 0.10 $g \cdot L^{-1}$ goethite were prepared in 1.5 mL microcentrifuge tubes in duplicate. The Pu(IV) stock solution was spiked into each sample to yield $\approx 1.2 \times 10^{-10}$ M Pu. The total Pu added to each sample from stock solutions was determined gravimetrically. The samples were initially adjusted to pH 4, 5, 6, 7 and 8 using dilute HCl and NaOH, but allowed to drift during the adsorption period. Most of the pH drift occurred in the first day. The final pH range spanned 4.2 to 6.6.

Samples were allowed to equilibrate for 1, 6, 15, 34 and 116 d. Following the adsorption step, samples were centrifuged to remove particles >100 nm from the supernatant and the Pu concentration in the supernatant was measured. Then, the supernatant was quantitatively replaced with a 1.7 µM DFOB solution adjusted to pH 4, 5, 6, 7, and 8 using dilute HCl and NaOH. Desorption of Pu from each sample was allowed to occur for 34 d for all samples, regardless of the initial equilibration time. Finally, samples were centrifuged to remove particles >100 nm from the supernatant and the Pu concentration in the supernatant was measured.

Use of DFOB in Pu–Goethite Sorption Experiments

DFOB was used to enhance desorption of Pu and to stabilize Pu(IV) as the dominant aqueous oxidation state. Although DFOB strongly complexes Fe(III) in aqueous solution, DFOB has been shown to interact weakly with the goethite surface at pH 3 to 9 due to electrostatic repulsion of the cationic DFOB and also to steric hindrance (Cheah et al., 2003; Cocozza et al., 2002; Kraemer et al., 1999). Based on previous DFOB–goethite sorption isotherms (Cheah et al., 2003; Kraemer et al., 1999) at pH 5 and 6.6, it is estimated that for 1.7 µM total DFOB and 0.1 $g \cdot L^{-1}$ goethite only 2–6 % of DFOB sorbs (see Supplementary Material; Fig. A.3). Furthermore, despite the formation of strong Fe(III)–DFOB complexes, low dissolution rates of 0.01 to 0.02 $\mu mol \cdot g^{-1} \cdot h^{-1}$ are observed for goethite in the presence of DFOB (Kraemer et al., 1999; Wateau and Berthelin, 1994). Therefore, as will be discussed below, Pu–ligand complexation rather than goethite dissolution is the driving mechanism for release of sorbed Pu. The dissolution of goethite was tested by measuring aqueous iron concentrations in the presence of DFOB by Inductively Coupled Plasma Mass Spectrometry, (ICP-MS, Thermo Scientific XSeries 2).

Because DFOB interacts weakly with goethite surfaces, formation of ternary goethite–DFOB–Pu surface complexes is expected to be minimal. As a result, DFOB is expected to have little effect on Pu surface speciation and only facilitate desorption of Pu. For the experimental conditions of this work, our conceptual model is that Pu sorption to goethite may be treated as a binary system of ≡FeOH–Pu(IV) surface complexes and aqueous Pu(IV)–DFOB complexes. Thus, differences in measured distribution ratios can be attributed directly to changes in the binding energy of the ≡FeOH–Pu(IV) surface complex.

Calculations

All data are presented as percent sorbed, percent desorbed, or a distribution ratio. Distribution ratios, R_d ($\mathrm{mL \cdot g^{-1}}$), were calculated from the aqueous Pu concentration, $C_{\mathrm{Pu,aq}}$ (M), and the total Pu added to each sample, $C_{\mathrm{Pu,total}}$ (M), according to Eq. 4.1, where SS ($\mathrm{g \cdot L^{-1}}$) represents the suspended solids concentration.

Distribution ratios are not equivalent to the more traditional distribution coefficient, K_d, because in the former case, an equilibrium condition is not assumed. For adsorption measurements, the percent sorbed was calculated based on the total Pu added at the beginning of the experiment. For desorption measurements, the percent (de)sorbed was calculated based on the estimated total Pu remaining in samples after the supernatant was exchanged.

Least-squares regression fitting was used to estimate the first-order adsorption rate constants, k_f (s^{-1}), according to Eq.4.2, where t is adsorption time in seconds. During fitting, the aqueous Pu concentration at time zero, $C_{Pu,aq}(0)$, and k_f were treated as adjustable parameters.

$$R_d = \frac{C_{Pu,total} - C_{Pu,aq}}{C_{Pu,aq}} \cdot \frac{1000}{SS} \tag{4.1}$$

$$C_{Pu,aq}(t) = C_{Pu,aq}(0)e^{-k_f t} \tag{4.2}$$

Results and Discussion

Pu Batch Adsorption–Desorption in the Presence and Absence of DFOB

In all samples, there is a rapid Pu adsorption step that occurs within the first 2 h (Fig. 4.1). After 2 h, the extent of Pu sorption tends to increase slowly for at least 25 d in DFOB and DFOB-free solutions. Thus, it appears that adsorption aging effects exist both in the presence and absence of DFOB.

Between 2 h and 25 d, the percent Pu sorbed in DFOB-containing samples increases from 9.7 ± 0.5 % to 27.7 ± 0.8 % and from 22.6 ± 0.4 % to 43.9 ± 0.6 % at pH 6 and 8, respectively. As a result of DFOB stabilizing Pu(IV) in solution, surface mediated reduction of Pu(V) should not be a relevant aging mechanism in these samples. Thus, we attribute the increase in sorption to non-redox aging effects.

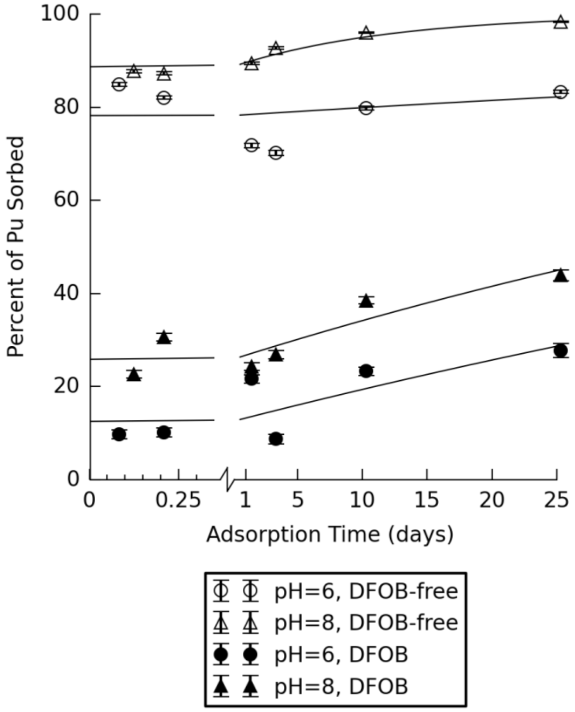

Figure 4.1. Adsorption of Pu on a 0.075 g·L^{-1} goethite suspension with 10 mM NaCl for ionic strength control. Pu was initially added as Pu(IV). Solutions contained 1.7 µM DFOB or were DFOB-free. Lines indicate first-order rate models fit to the data. Error bars represent two standard deviations of measurement uncertainty derived from counting statistics. The first data point was collected after a 2 h adsorption time period.

The percent Pu sorbed for the DFOB-free sample increases between 2 h and 25 d from 87.74 ± 0.16 % to 98.40 ± 0.07 % at pH 8. It is noteworthy that in the absence of DFOB, Pu(IV)/Pu(V) redox transformations may influence the partitioning of Pu. Oxidation state analysis of aqueous Pu in DFOB-free samples with solvent extraction confirms that Pu(V/VI) is the stable aqueous form of Pu in these samples. In samples adsorbed for 25 d at pH 6 and 8, 97 ± 7 % and 100 ± 12 % of supernatant Pu is in the V/VI oxidation state, respectively. However, the surface area normalized adsorption rate constant observed at pH 8 (1.08 ± 0.10 × 10^{-3} L·m^{-2}·h^{-1}) is much lower than the published rate of surface mediated reduction of Pu(V) (2.3 ± 0.7 × 10^{-2} L·m^{-2}·h^{-1}) (Powell et al., 2005). Thus, despite the likely occurrence of redox transformations at early time (days), some process other than surface mediated reduction of Pu(V) is responsible for observed aging behavior in the presence and absence of DFOB over the long term.

The presence of DFOB causes a marked decrease in the percent of sorbed Pu (Fig. 4.1), and greater sorption is observed at pH 8 relative to pH 6. Aqueous equilibrium speciation modeling indicates Pu speciation in 1.7 μM DFOB at pH 6 and 8 under atmospheric conditions is dominated by $PuH_2(DFOB)_2^{2+}$ rather than $Pu(OH)_x^{4-x}$ species (Figs. A.1 and A.2). Because ternary goethite–DFOB–Pu complexes are not expected to form, the slightly greater sorption at pH 8 relative to pH 6 is likely due to the increased stability of Pu(IV)–goethite surface complexes with increasing pH.

Dissolved iron measurements in the presence of DFOB were below the ICP-MS detection limit of 2.8 μM. However, given that the DFOB concentration is only 1.7 μM, competition between Fe and Pu for DFOB may have occurred in these samples. Nevertheless, the enhanced aqueous concentration of Pu in the presence of DFOB indicates that the Pu–DFOB complexes can form despite a portion of DFOB forming Fe–DFOB complexes. Some Pu desorption as a result of goethite dissolution may have occurred. However, the amount of goethite surface area available for Pu sorption did not decrease over the course of these experiments. Thus, we can conclude that formation of soluble Pu–DFOB complexes is the dominant mechanism responsible for the higher aqueous Pu concentrations in the presence of DFOB.

After 25 days of adsorption, the samples were phase separated and supernatants exchanged for fresh Pu-free solutions of the same pH and DFOB concentration as in the initial adsorption step. In less than 3 h, desorption was greater in DFOB samples than DFOB-free samples (Fig. A.4). At 3 h, the percent of Pu remaining sorbed in DFOB solutions was 74.8 ± 0.4 % and 85.2 ± 0.3 % at pH 6 and 8, respectively. In contrast, the percent of Pu remaining sorbed in DFOB-free solutions was 96.44 ± 0.11 % and 97.3 ± 0.09 % at pH 6 and 8, respectively. Importantly, in the presence of DFOB, Pu desorption experiments appear to have reached equilibrium after 18 h. In the DFOB-free samples, the pH 8 Pu desorption experiment neared equilibrium by 3 d while the pH 6 experiment approached equilibrium much more slowly. Thus, it is apparent that DFOB can effectively facilitate and accelerate Pu desorption from goethite and that desorption equilibrium is achieved on the timescale of days.

Results of Varying Adsorption Equilibrium Time

In order to test the effect of adsorption equilibration time (in the absence of DFOB) on Pu surface stability, a batch adsorption–desorption experiment was conducted on goethite suspensions with varying adsorption times in DFOB-free solution and a constant desorption time of 34 d in 1.7 µM DFOB solution. The DFOB-free adsorption data (Fig. 4.2) support the conceptual model of Pu aging on the goethite surface. This aging is seen as a steady shift in the sorption edge towards lower pH values for up to 116 d. This is in contrast to previously observed rates of surface mediated reduction, where greater than 90% of Pu(V) reduction was observed within 24 h (Powell et al., 2005). Thus, the observed aging is likely the result of a mechanism other than surface mediated reduction occurring on the goethite surface.

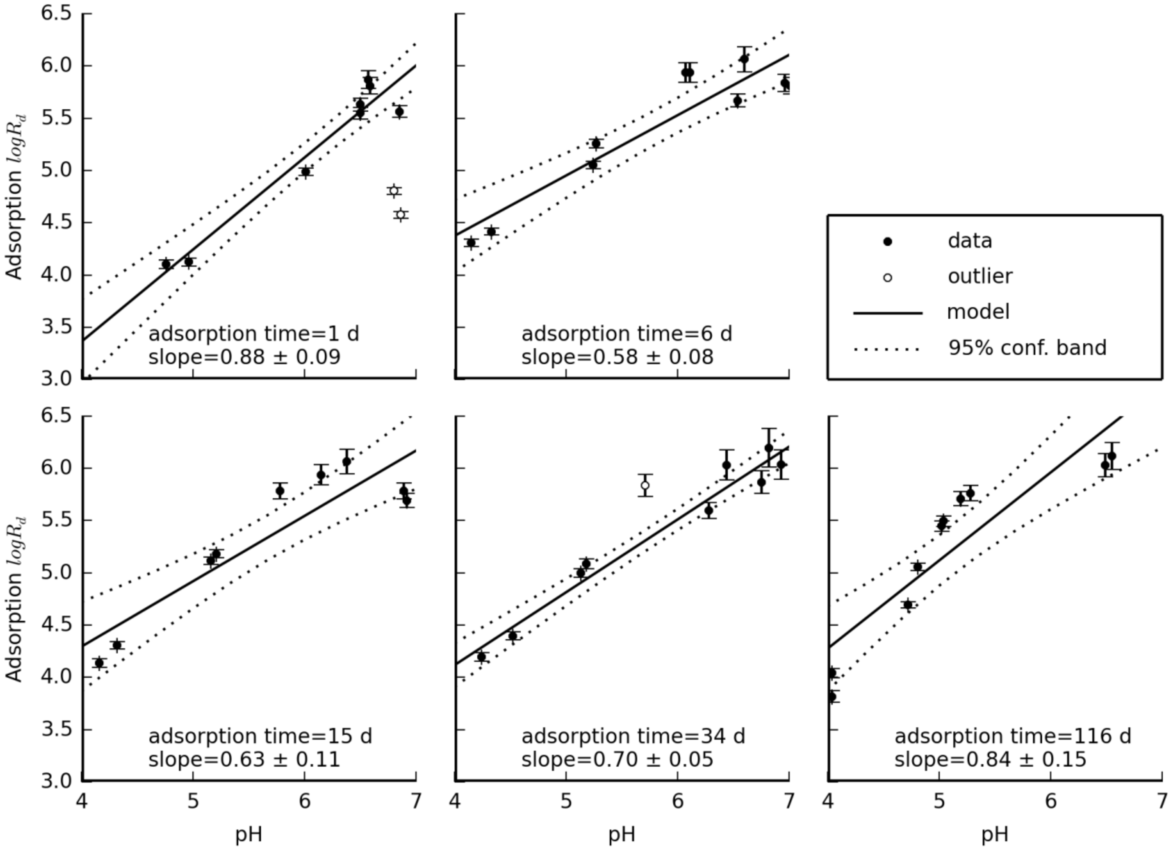

Figure 4.2. Logarithmic adsorption distribution ratios (R_d) for Pu on 0.10 g·L^{-1} goethite suspensions as a function of pH and time. Total Pu concentration is 1.2 × 10^{-10} M, and ionic strength was controlled with 10 mM NaCl. Error bars indicate two standard deviations of measurement uncertainty derived from counting statistics.

The effect of aging on Pu desorption was tested by performing a 34 d desorption in 1.7 µM DFOB solution on each of the adsorption samples. The 34 days provided ample time for samples to reach equilibrium (Fig. A.4). The decrease in percent DFOB-desorbable Pu with increasing adsorption time is indicative of Pu stabilization on the goethite surface (Fig. 4.3). During DFOB-free adsorption at pH 4, we can expect only trace amounts of Pu(V) to be sorbed to the goethite surface (Sanchez et al., 1985). Thus, aging behavior at pH 4 must be the result of Pu(IV) stabilization on the goethite surface and not Pu(IV)/(V) redox transformations.

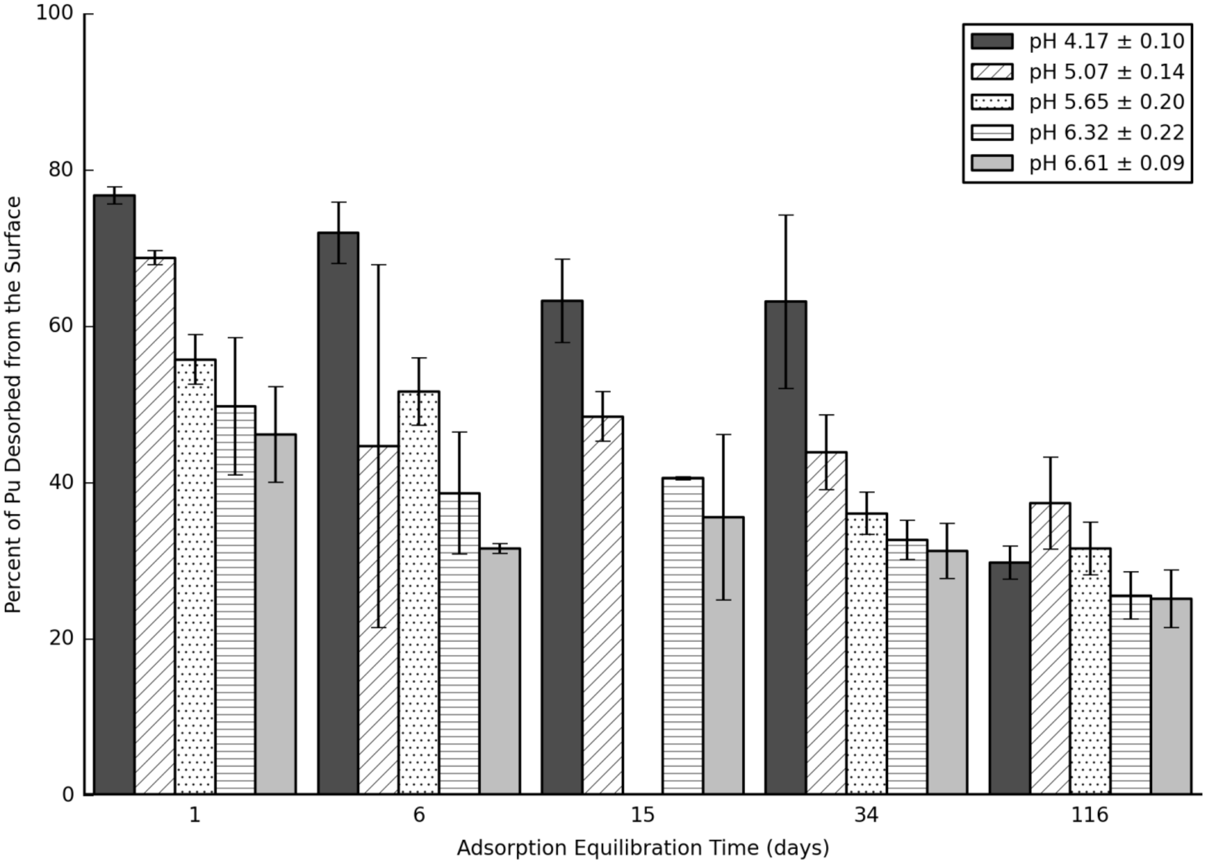

Figure 4.3. The percent of Pu desorbed is plotted against adsorption equilibration time. Samples initially contained 1.2×10^{-10} M total Pu before supernatant replacement and desorption with 1.7 µM DFOB for 34 d. The mean pH values of each sample group are shown in the legend. Goethite suspension concentration was 0.10 $g \cdot L^{-1}$, and ionic strength was controlled with 10 mM NaCl. Error bars indicate the standard deviation of duplicates.

The aging behavior observed in the desorption data is more pronounced at lower pH values. At pH 4.2, the percent Pu desorbed decreases from 76.8 ± 1.1 % to 29.8 ± 2.1 % between 1 and 116 d of adsorption equilibration, and, at pH 6.6, the percent of Pu desorbed decreases from 46 ± 6 % to 25 ± 4 %, for the same periods of adsorption. The greater change over time in the percent Pu desorbed suggests that aging is pH-dependent. Although the underlying reason for the pH dependence cannot be identified with these data, the pH-dependence may reflect the presence of a strongly sorbing (and less labile) form of Pu on the goethite surface at high pH values.

To further evaluate the pH- and time-dependence of desorption, logarithmic desorption R_d values for each adsorption equilibration time were plotted against pH (Fig. 4.4) and were fit with a linear model which considers a pH-dependent and a pH-independent term (Eq. 4.3).

$$\log R_d = slope \times pH + intercept \tag{4.3}$$

For samples adsorbed for 1 to 34 d, the estimated slopes range from 0.20 to 0.32, while at 116 d, the slope decreases to 0.06. These results suggest that Pu surface stability becomes less pH-dependent with increasing adsorption equilibration time. It also suggests that a pH-independent R_d value may describe the Pu desorption from goethite at longer, environmentally relevant timescales.

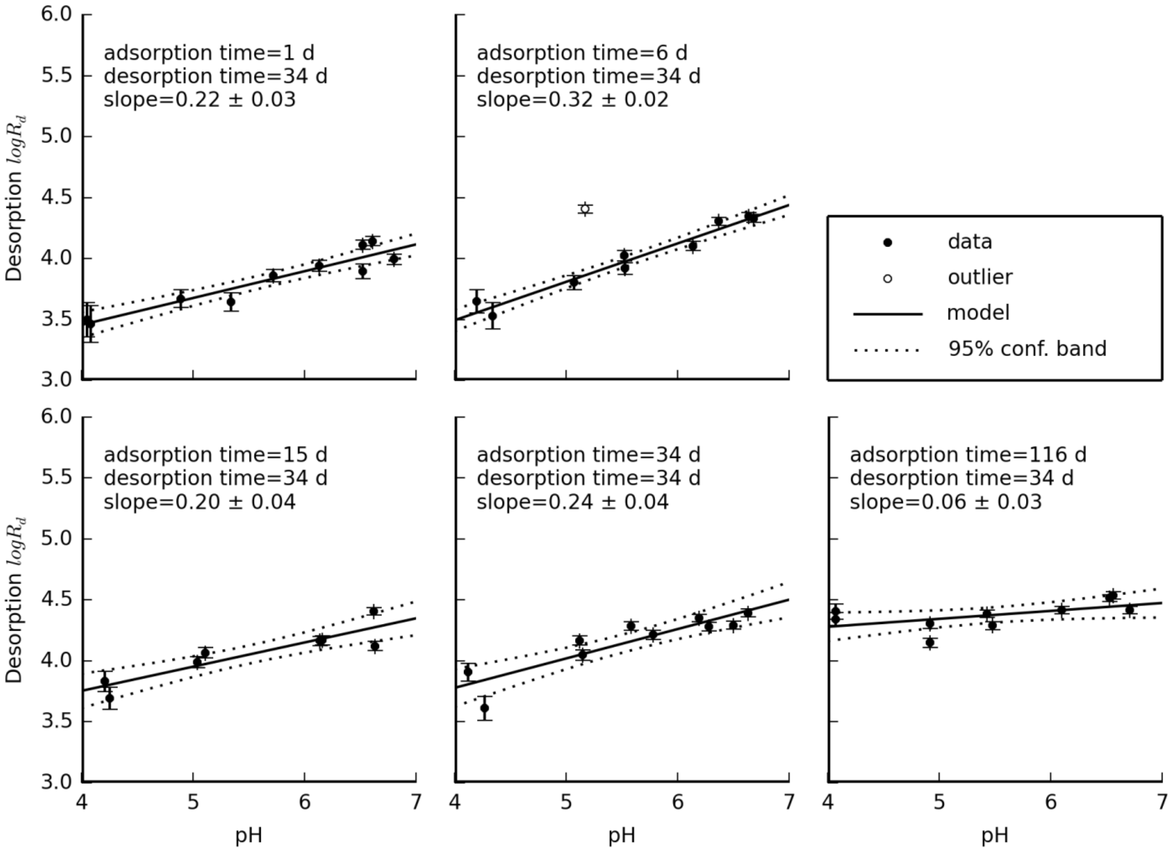

Figure 4.4. Logarithmic desorption distribution ratios (R_d) for Pu resulting from adsorption in DFOB-free solution for various equilibration times (indicated), supernatant replacement, and desorption in 1.7 μM DFOB solution for 34 d. Total Pu was originally 1.2×10^{-10} M before supernatant replacement. Goethite suspension concentration was 0.10 $g \cdot L^{-1}$, and ionic strength was controlled with 10 mM NaCl. Error bars indicate two standard deviations of measurement uncertainty derived from counting statistics. Shown are linear models which consider a pH-dependent and a pH-independent term.

The pH-dependent aging and time-dependent desorption behavior in the presence and absence of DFOB can be used to identify the aging processes that may play a role in Pu sorption behavior. Pu adsorption data in the presence of DFOB suggest that a non-redox, aging mechanism plays a role in stabilizing Pu(IV) on the goethite surface. In the absence of DFOB, the pH- and time-dependent adsorption rates are slower than previously reported rates of surface mediated Pu(V) reduction on goethite. The initial Pu(IV) stock solution contained ≈10% Pu(V). Thus, while redox transformations likely played a role in Pu adsorption rates at early times (days), the observed aging on a timescale of weeks is not consistent with surface mediated reduction processes. The decrease in Pu desorption as a function of equilibration time, particularly at pH 4, provides clear evidence that Pu(IV) sorbed to goethite becomes more stable with time. At higher pH values, the effect is less pronounced, suggesting a pH-dependence to this aging process.

Implications of Aging on Pu Subsurface Migration

The aging phenomena observed in this work may impact the fate and transport of Pu in the environment. As natural soils contaminated with Pu age, the strength of Pu sorption to bulk soil will increase and make Pu less labile. Importantly, the aging process has been shown to include non-redox mechanisms. Furthermore, R_d values based on short term adsorption or desorption experiments will underestimate long term equilibrium K_d values, and lead to overestimated *aqueous* Pu transport distances. Conversely, if Pu is sorbed to mobile colloids, aging may result in formation of stronger Pu–colloid associations and, thus, lead to greater colloid-facilitated Pu transport distances. These aging phenomena support the frequent observations of colloid-facilitated Pu transport (Kersting et al., 1999; Novikov et al., 2006) wherein Pu can be transported significant distances adsorbed to the colloid on a timescale of years. Furthermore, the pH dependency of aging implies that the magnitude of this effect will be dependent on the geochemical conditions but will occur regardless of whether Pu redox transformation is prevalent.

CHAPTER FIVE

DESORPTION BEHAVIOR OF PLUTONIUM FROM GOETHITE IN A FLOW-CELL REACTOR IN THE PRESENCE OF NATURAL ORGANIC LIGANDS

Paper Status

This chapter consists of a manuscript which has been prepared for submission to a scientific journal.

Authors

Jennifer C. Wong, Mavrik Zavarin, Annie B. Kersting, Brian A. Powell

Abstract

The desorption behavior of Pu, and its implications for near- and far-field transport are of concern. It has been suggested that Pu desorption may be kinetically limited, or irreversibly bound to mineral surfaces over time. Furthermore, the presence of natural organic ligands may alter mineral surfaces or drive desorption by the formation of aqueous Pu complexes. To overcome the difficulty of studying the desorption behavior of Pu, a strongly sorbing ion, a flow-cell experimental design was used. The desorption of ^{238}Pu(IV) from a goethite suspension was examined at pH 6 in the presence of natural organic matter surrogates (desferrioxamine B, Suwanee River I fulvic acid, and citric acid). Constant dilution in the continuously stirred flow-cell minimized Pu readsorption. Pu desorption was enhanced in the presence of the organic ligands, but the fraction of Pu which could be desorbed decreased over time. Two conceptual kinetic sorption models were compared: (1) one linear sorption site and (2) two consecutive linear sorption sites. The two-site model

better approximated the data suggesting that Pu sorption may be affected by a transition to a less desorbable form.

Introduction

In this study, the (de)sorption kinetics of plutonium (Pu) on goethite in the presence of natural organic ligands (NOL) is investigated. Plutonium is present in the environment due to legacy waste from nuclear weapons production and nuclear weapons testing, and Pu is of key concern because of its long half-life and high radiotoxicity. The mobility of Pu in the environment is primarily controlled by sorption to minerals and other particulate matter. The sorption of Pu to goethite (α–FeOOH) is of interest because of its ubiquity in the environment (Cornell and Schwertmann, 2003; Schwertmann and Taylor, 1989) and its potential to form from the corrosion of waste drums in repositories (Neff et al., 2005; Philippini et al., 2006).

Under oxic environmental conditions, Pu primarily occurs as Pu(IV) and Pu(V) (Choppin et al., 1997; Cleveland, 1979; Silva and Nitsche, 1995). Pu(IV) is highly insoluble, as illustrated by the solubility limit of $PuO_{2(s)}$ which is approximately 10^{-8} M at circumneutral pH values which limit aqueous Pu(IV) concentrations (Choppin, 2003; Rai, 1984; Rai et al., 2001, 1980). Aqueous Pu(IV) may also oxidize to Pu(V) which has been observed to be the stable oxidation state in seawater and dilute salt solutions (Morse and Choppin, 1986; Orlandini et al., 1986). Additionally, surface mediated reduction of aqueous Pu(V) to form sorbed Pu(IV) has been observed on several iron oxide phases (Keeney-Kennicutt and Morse, 1985; Penrose et al., 1987; Powell et al., 2005, 2004; Sanchez et al., 1985).

Although desorption is less commonly studied than adsorption, it plays an important role in controlling Pu fate and transport. In batch sorption studies with goethite colloids, 81% of Pu adsorbed in 1 hour, but less than 1% of Pu was desorbed from goethite colloids over 150 days (Lu et al., 1998a, 1998b). In desorption experiments with estuary sediment, only 5% of sorbed Pu, predominantly in the Pu(IV/III) oxidation state, was determined to be "exchangeable" (Hamilton-Taylor et al., 1987). Due to the duration of Pu–colloid associations, it has been proposed that Pu desorption from colloids is rate-limited (Cvetkovic et al., 2004; Painter et al., 2002). Furthermore, recent studies with iron oxides have shown that the desorbability of Pu decreases with increasing contact time (Romanchuk et al., 2013; Wong et al., 2015), suggesting that an aging component should be included in kinetic models of Pu sorption to iron oxides.

The sorption of Pu to mineral surfaces and limited solubility of Pu (Choppin, 2003; Rai, 1984; Rai et al., 2001, 1980; Sanchez et al., 1985) suggests Pu should be immobile in the subsurface (Triay et al., 1996). However, long-distance transport of Pu associated with colloids (Kersting et al., 1999; Novikov et al., 2006; Penrose et al., 1990; Santschi et al., 2002) also suggests that Pu mobility may be enhanced by the formation of highly stable surface complexes on mobile colloids. At the Mayak Production Association, it was concluded that the transport of Pu was facilitated by the association of Pu with iron oxide colloids (Novikov et al., 2006). However, rates commonly observed in laboratory-based desorption experiments indicate that desorption of Pu from mobile colloids would occur before transport over these long distances (Begg et al., 2014; Lu et al., 2003, 2000). Thus, there appears to be an aging process or some other process occurring which enables far-field colloid facilitated transport.

The presence of natural organic ligands can alter the extent of Pu sorption by the formation of aqueous Pu–ligand complexes and/or ternary surface complexes. Thus, the effect of an organic ligand on Pu sorption is dependent on both the affinity of the ligand for the mineral surface and for the Pu ion. Carboxylic, phenolic, and hydroxamic functional groups (Sposito, 2008) may allow organic ligands to bind to Pu forming aqueous complexes, or, additionally, bind to mineral surfaces forming ternary surface complexes. Desferrioxamine B (DFOB) is a chelating ligand which forms strong aqueous Pu(IV) complexes and enhances Pu desorption (Boukhalfa et al., 2007; Conroy et al., 2017; Simpkins, 2011), but exhibits weak sorption to goethite due to steric hindrance and cationic repulsion (Cheah et al., 2003; Cocozza et al., 2002; Kraemer et al., 1999). Fulvic acid is an operationally defined humic substance which is generally smaller and more soluble than humic acid. While sorption of fulvic acid and citrate to goethite may potentially alter surface properties, enhancement of Pu sorption to goethite in the presence of fulvic acid or citric acid is limited to low pH (Conroy et al., 2017; Tinnacher et al., 2015). At pH 5–9, fulvic acid and citric acid have been shown to form strong aqueous complexes with Pu which diminish Pu sorption to goethite by competing with Pu binary surface complexes (Clark et al., 2010; Conroy et al., 2017). Because these organic ligands have been demonstrated to decrease the extent of Pu sorption on metal oxides (Conroy et al., 2017; Simpkins, 2011), it is expected that the presence of organic ligands may potentially increase apparent Pu desorption rate constants, relative to an organic-free system.

In order to compare sorption reaction rate constants for Pu on goethite in the presence of different types of natural organic ligands, desorption experiments were conducted in continuously stirred flow-cell reactors (i.e. flow-cells) (Fig. 5.1). Flow-cells, have been used previously to examine the reaction kinetics of metal ions with solid phases (Begg et al., 2015; Selim and Amacher, 2001; Seyfried et al., 1989; Tinnacher et al., 2011). Flow cells have some advantages over batch experiments for studying (de)sorption kinetics because they utilize constant dilution to remove reaction products, and also allow for constant sampling. Additionally, by changing the flow rate or stopping the flow of influent solution, the contact time of a solute with a sorbent can be varied to monitor for kinetic limitations. The system can be repeatedly manipulated towards chemical equilibrium by stopping influent solution flow, or can be moved toward a steady-state condition of chemical disequilibrium by continuing solution flow. These unique aspects were used to estimate apparent sorption and desorption reaction rate constants. The effects of three organic ligands (fulvic acid, citric acid, and DFOB) with different sorption and complexation properties were investigated and analyzed using a multi-site kinetic sorption model.

Materials and Methods

Reagents

All solutions were prepared with distilled deionized water with resistivity >18 MΩ·cm. The organic ligands were obtained in the forms of desferrioxamine mesylate (Sigma Aldrich, ≥92.5%), Suwanee River fulvic acid, standard I (International Humic Substance Society), and citric acid monohydrate (J.T. Baker; ACS grade). The reported acidic functional group density (carboxylic and phenolic) for the fulvic acid is 7.5×10^{-3} eq_{sites}/g_{FA} (International Humic Substances Society). Acids, bases, and other reagents were ACS grade or higher. Adjustments to solution pH were performed with dilute HCl and NaOH.

Several liters of background solution consisting of 10 mM NaCl were prepared, and were adjusted to pH 6. Citric acid and DFOB stock solutions were prepared at concentrations of 151 $mg_c \cdot L^{-1}$ and 1000 $mg_c \cdot L^{-1}$, respectively. Organic ligand solutions were prepared by adding the organic ligand stock solutions to the background solution to reach the desired concentrations. Organic ligand solutions of DFOB (0.5 $mg_c \cdot L^{-1}$; 1.7 μM), citric acid (0.5 $mg_c \cdot L^{-1}$; 6.9 μM), and fulvic acid (30 $mg_c \cdot L^{-1}$; 230 $\mu eq_{sites} \cdot L^{-1}$) were prepared in the background 10 mM NaCl solution and then were adjusted to pH 6. Under these conditions, Pu aqueous speciation in the presence of DFOB and citrate is expected to be dominated by $PuH_2(DFOB)_2^{2+}$ and $Pu(Cit)_2^{2-}$, respectively (Figs. B.1 and B.2). Since there is no reliable formation constant for Pu–(fulvic acid) complexes, speciation calculations cannot be performed for fulvic acid. These ligand concentrations were selected based on concentrations used in previous batch sorption experiments found to facilitate desorption of Pu from metal oxide minerals (Conroy et al., 2017; Simpkins, 2011).

The preparation of goethite (α–FeOOH) has been described previously (Tinnacher et al., 2011) and the BET surface area was 42 $m^2 \cdot g^{-1}$ (Tinnacher et al., 2011). This goethite was used to prepare stock suspensions ranging from 2.3 to 7.8 $g \cdot L^{-1}$. Each suspension was washed by centrifuging sufficiently to remove <100 nm fines. Then, the supernatant was replaced with deionized water and sonicated to resuspend the particles. This washing step was repeated two times.

The aqueous concentrations of ^{238}Pu and ^{3}H in samples were determined by liquid scintillation counting (Hidex 300 SL or Perkin Elmer Tri-Carb 2900TR LSA) with alpha/beta discrimination. Samples were prepared with Optiphase Hisafe 3, Ultima Gold, or Ultima Gold LLT scintillation cocktail. Throughout each individual experiment, the same counter and scintillation cocktail were used to measure stock solutions and samples so as to maintain consistent counting efficiency. The minimum detectable concentration (MDC) of ^{238}Pu was 1.5–4 × 10^{-14} M, and the minimum detectable activity of ^{3}H was 1700 $\text{Bq}\cdot\text{L}^{-1}$.

The ^{238}Pu used in this work was purified on a BioRad AG 1 × 8, 100−200 mesh anion exchange column by loading in 8 M HNO_3, washing the column with 9 M HCl, eluting in 1 M HCl, then evaporating and redissolving in 1 M HCl to produce a 1.2 × 10^{-7} M ^{238}Pu(IV) stock solution (Bajo et al., 2007). A second 2.2 × 10^{-8} M ^{238}Pu(IV) stock solution was prepared by a similar method. Since the stock concentrations were too low to perform oxidation state analysis by traditional spectroscopic methods (e.g. UV-Vis), a well-established lanthanum fluoride co-precipitation technique was used to assess the Pu oxidation state in the stock solutions (Foti and Freiling, 1964; Kobashi et al., 1988; Nitsche et al., 1988). The method confirmed that >98 % of Pu was in the Pu(IV) oxidation state. While this technique does not discriminate between Pu(III) and Pu(IV), under the neutral pH and atmospheric conditions of these experiments, Pu(III) is expected to be unstable.

Batch Adsorption to Prepare Pu-amended Goethite Suspensions

The flow-cell experiments were performed using goethite which had been pre-equilibrated with Pu. Additionally, ^{3}H was added to this solution as a conservative tracer to verify that the flow-cell was well-mixed. To prepare the Pu-amended goethite, a 5-15 mL suspension of 0.3 $g \cdot L^{-1}$ goethite in 10 mM NaCl was prepared using the goethite stock suspension and background solution. Pu was added to the suspension from one of the $^{238}Pu(IV)$ stock solutions to obtain a total concentration of $\approx 10^{-9}$ M ^{238}Pu, and ^{3}H was added to obtain a total activity of $1.2–3.3 \times 10^{6}$ $Bq \cdot L^{-1}$. The suspension was adjusted to pH 6, and then the suspension was allowed to equilibrate for 48 hours. Aliquots of the Pu amended goethite solution were pipetted into the flow-cells, and the aqueous effluent Pu concentrations were determined as described below.

Flow-cell Design and Operation

Flow-cell reactors loaded with Pu-amended goethite were used to monitor Pu desorption from goethite (discussed below). Because the Pu concentration in the effluent is mainly driven by desorption and dilution, this allowed desorption reaction rate constants to be estimated. The flow-cell consisted of a 20 mL polytetrafluoroethylene (PTFE) chamber containing a small magnetic stir bar (Fig. 5.1). The effluent was filtered with a 100 nm pore size PTFE membrane (EMD Millipore Omnipore). Prior to use, the flow-cell was soaked in 10% HCl acid and rinsed with deionized water. The speed of the peristaltic pump (Gilson Minipuls2 or Masterflex 7518-10) was adjusted so that the fluid residence time was 50–60 min. A fraction collector (Spectra/Chrom CF-1 or Eldex) was used to collect samples at 15 min intervals in polypropylene or polystyrene tubes, and all volumes were determined gravimetrically. The ^{238}Pu and ^{3}H concentrations in effluent samples were measured using liquid scintillation counting with alpha/beta discrimination. The effluent profile of the ^{3}H tracer indicated that a displacement of 4.5 chamber volumes (CV) was sufficient to exchange 99% of the aqueous solution inside the cell (Figs. B.3, B.4, B.5, and B.6). The effluent profile demonstrated excellent agreement with the analytical solution for ideal mixing conditions.

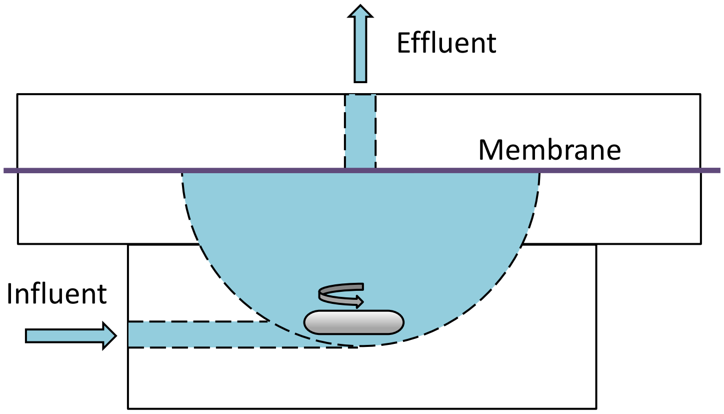

Figure 5.1. Schematic of flow-cell apparatus. A magnetic stir bar keeps the 20 mL cell well mixed. The top and bottom PTFE pieces are bolted together and sealed with an O-ring.

Flow-cell Setup and Conditioning

The flow-cell reactor was prepared by filling it with 20 mL of organic-free background solution, and the lid was attached and sealed. By pipetting through the flow-cell inlet, 2 mL of background solution was removed from the flow-cell and replaced with 2 mL of Pu-amended goethite. This resulted in 10x dilution of the Pu-amended goethite. The total Pu concentration in the system (accounting for both solid and aqueous phase Pu but expressed as a molar concentration in $\mathrm{mol_{Pu}\cdot L^{-1}}$ based on the cell volume) at this point is referred to as the total loading Pu concentration.

After loading, the flow-cell contained a small fraction of aqueous Pu which did not sorb to goethite during the batch equilibration. To remove this residual aqueous Pu from the flow-cell, the system was conditioned with organic-free background solution by pumping 6–8 chamber volumes solution through the flow-cell. Then, the flow-cell was conditioned with an organic ligand solution by pumping 6–12 chamber volumes of an organic ligand solution to allow the organic ligand concentration to reach a constant concentration. In the case of the organic-free flow-cell experiment, organic-free background solution was pumped for 12 chamber volumes. Finally, the flow of solution was stopped for 4 hours in order to be consistent with later stop events.

Flow-cell Desorption Experiments

The data used for modeling calculations was collected after the end of the conditioning step. Throughout this work, data are normalized to, $C_{Pu,0}$, the total Pu concentration in the system at the end of conditioning (accounting for both solid and aqueous phase Pu but expressed as a molar concentration in $\mathrm{mol_{Pu}} \cdot \mathrm{L}^{-1}$ based on the cell volume). Additionally, the cumulative volume of displaced fluid was normalized to the volume of the reaction chamber such that data could be plotted as the cumulative displaced chamber volumes, CV.

To monitor for sorption/desorption kinetics, stop and flow events were conducted during desorption. The flow of organic ligand solution was alternately run for 8 hours and stopped for 4 hours over the course of 3 days. During stop events, the aqueous Pu concentration builds up in the flow-cell according to the adsorption and desorption kinetics. After each stop event, the Pu effluent profile is expected to initially follow an exponential decay while Pu removal is dominated by constant dilution, and then transition to a shallower slope as Pu removal becomes limited by the rates of adsorption/desorption. Thus, the continuous flow data can be used to approximate adsorption and desorption rate constants.

Modeling

Modeling of the flow-cell breakthrough curves using multiple sorption sites was based on a similar approach used to examine Np(V) sorption to goethite (Tinnacher et al., 2011). Multi-site sorption models have been used previously to model Pu sorption to hematite colloids (Painter et al., 2002). Having two sorption sites in the model allows the model to describe previously observed behavior of Pu sorption kinetics where an initial fast sorption phase is followed by slow uptake. In this case, a “site” is purely conceptual and meant to represent any state of Pu on the surface. The slow uptake corresponds to the transition between states which might, for example, represent a physical relocation of the sorbate such as from a weakly sorbing to a strongly sorbing site on the goethite, or a chemical change such as a change in speciation of the surface complex. The model assumes two consecutive linear sorption sites (Fig. 5.2), where transfer to the second sorption site represents a pseudo-first-order aging process.

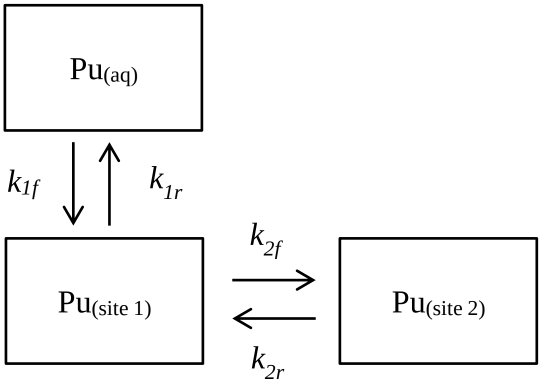

Figure 5.2. Conceptual model for sorption to two consecutive linear sorption sites.

This model can be described with a system of differential equations (Eqns. 5.1, 5.2, and 5.3), where $S_{1,Pu}$ and $S_{2,Pu}$ are the concentrations of Pu (mol·g^{-1}) sorbed to the first and second sorption sites, respectively, and C_{Pu} is the aqueous Pu concentration. The fixed parameters are the flow rate (L min^{-1}), Q; the total mass of goethite (g), M; and the volume of the reaction chamber (L), V. The adjustable parameters are apparent first-order reaction rate constants (min^{-1}): k_{1f}, k_{1r}, k_{2f}, and k_{2r}. The rate constants k_{1f} and k_{1r} represent the adsorption and desorption to site 1. The rate constant k_{2f} represents the transition from site 1 to site 2, and k_{2r} represents the back-transition. In this work, a one-site linear sorption model where $k_{2f} = k_{2r} = 0$ min^{-1} is additionally considered. The system of equations was solved by numerical approximation using a finite difference approach (Tinnacher et al., 2011). The code used to solve the equations was compiled in FORTRAN and combined with PEST (Parameter ESTimation), a non-linear parameter estimation program (Tinnacher et al., 2011). The parameter estimation performs a weighted least-squares minimization, where the inverse of the measurement uncertainty (1σ) derived from counting statistics is used as the weight.

$$\frac{dC_{Pu}}{dt} = -\frac{Q}{V}C_{Pu} - \frac{M}{V}\frac{dS_{1,Pu}}{dt} \tag{5.1}$$

$$\frac{dS_{1,Pu}}{dt} = \frac{V}{M}k_{1f}C_{Pu} - k_{1r}S_{1,Pu} - \frac{dS_{2,Pu}}{dt} \tag{5.2}$$

$$\frac{dS_{2,Pu}}{dt} = k_{2f}S_{1,Pu} - k_{2r}S_{2,Pu} \tag{5.3}$$

Results and Discussion

Flow-cell Conditioning

In order to remove residual aqueous Pu, 6, 6, 8, and 12 CV of organic-free background solution was pumped through the DFOB, fulvic acid, citric acid, and organic-free flow-cells, respectively (Table 5.1). While the first 6 CV of organic-free solution was pumped, 0.5%, 2.4%, 4.9%, and 0.1% of total loading Pu was removed from the DFOB, fulvic acid, citric acid, and organic-free flow-cells, respectively (Table 5.2). Although each flow-cell is referred to by the organic ligand to be added, at this point, organic ligands have not yet been introduced. Thus, these four experiments are essentially replicates with no organic ligands present up to this point.

Table 5.1. Pu removed from the flow-cell during conditioning as a percentage of total loading Pu, and the displaced chamber volumes (CV) of each step.

Flow-cell	Organic-Free Conditioning		Ligand Conditioning		Organic-Free and Ligand Conditioning	
	(%)	(CV)	(%)	(CV)	(%)	(CV)
DFOB	0.5	6	4.9	6	5.4	12
Fulvic acid	2.4	6	12	9	14	15
Citric acid	5.3	8	18	12	24	20
Organic-free	0.3	12	-	-	0.3	12

Table 5.2. Pu removed from the flow-cell during the first 6 CV of organic-free and ligand conditioning as a percentage of total loading Pu.

Flow-cell	6 CV of Organic-Free Conditioning (%)	6 CV of Ligand Conditioning (%)
DFOB	0.5	4.9
Fulvic acid	2.4	9.6
Citric acid	4.9	16
Organic-free	0.1	-

A possible explanation for the different amounts of Pu removed during organic-free conditioning may be oxidation of different amounts of Pu(IV) to Pu(V) during the preparation of the Pu–goethite working suspension. The Pu(IV) stock solutions are kept at a low pH to keep Pu in the tetravalent state and prevent precipitation of $PuO_2(s)$. As the pH is increased, oxidation to Pu(V) becomes favorable at trace concentrations in the 10 mM NaCl used in these experiments. Precipitation of colloidal PuO_2 can also occur in higher concentrations ($>10^{-8}$ M) though in the 10^{-9} M Pu concentrations used in these experiments, such precipitation is not expected (Neck et al., 2007; Neck and Kim, 2001). Although Pu was added as an acidic Pu(IV) stock, changes in pH during pH adjustment and differences in the time required for the pH adjustment may have allowed a fraction of Pu(IV) to oxidize to Pu(V) (Powell et al., 2011; Fig. C.4). Because Pu(V) is more soluble and has a lesser sorption affinity than Pu(IV), most oxidized Pu would be in the residual aqueous Pu which was removed in this step.

It was assumed that the remaining Pu was sorbed as Pu(IV). In order to bring the organic ligand concentration to a constant concentration, 6, 9, and 12 CV of organic ligand solution was pumped through the DFOB, fulvic acid, and citric acid flow-cells, respectively (Table 5.1). In this step, the organic ligand concentration in the flow-cell increased over time until it reached steady-state concentration. This step was unnecessary in the case of the organic-free flow-cell experiment—though, for comparison, 0.3% of the total loading Pu was removed from the organic-free experiment over the duration of conditioning. While the first 6 CV of organic ligand solution was pumped, 4.9%, 9.6%, and 16% of the total loading Pu was removed for the DFOB, fulvic acid, and citric acid flow-cells, respectively (Table 5.2). In every experiment with NOL, more Pu was removed during conditioning in the presence of NOL than was removed from the organic-free flow-cell. This suggests the enhancement of Pu desorption in the presence of NOL. However, the comparison must be done with caution because, in this step, the concentration of NOL is continuously increasing and the duration of conditioning is not the same. The total and sorbed concentrations of Pu before conditioning (at loading) and after conditioning are summarized in Table 5.3. The total Pu remaining in the flow-cells and the sorbed Pu were calculated based on the cumulative aqueous Pu removed from the flow-cells.

Table 5.3. Total and sorbed Pu concentrations at each step of the flow-cell experiments. Conditioning consisted of flushing each flow-cell with organic-free background solution and a volume of respective ligand solution sufficient to reach a steady-state ligand concentration. All solutions were pH 6 and contained 10 mM NaCl to maintain ionic strength.

		Start of Conditioning		End of Conditioning		Experiment End	
Flow-cell	Suspension Density ($g \cdot L^{-1}$)	Total Loading Pu ($mol \cdot L^{-1}$)	Sorbed Pu ($mol \cdot g^{-1}$)	Total Pu ($mol \cdot L^{-1}$)	Sorbed Pu ($mol \cdot g^{-1}$)	Total Pu ($mol \cdot L^{-1}$)	Sorbed Pu ($mol \cdot g^{-1}$)
DFOB	0.030	1.1E-10	3.7E-09	1.1E-10	3.5E-09	8.6E-11	2.8E-09
Fulvic acid	0.035	9.4E-11	2.5E-09	8.0E-11	2.2E-09	6.5E-11	1.7E-09
Citric acid	0.038	1.0E-10	2.1E-09	7.6E-11	1.6E-09	6.5E-11	1.4E-09
Organic-free	0.033	8.4E-11	2.5E-09	8.4E-11	2.5E-09	8.1E-11	2.5E-09

Results of Stop and Flow Events

The effectiveness of the organic ligands in desorbing Pu from goethite is discussed in terms of the total Pu concentration at the end of conditioning, $C_{Pu,0}$, and all plots have been normalized to this concentration. The cumulative percentage of total Pu removed from each flow-cell experiment (Fig. 5.3) clearly demonstrated that DFOB, fulvic acid, and citric acid were effective at enhancing Pu desorption from goethite, relative to an organic-free system. During the 3 days of stop and flow events, 19.0 %, 18.6 %, 12 %, and 2.1 % of total Pu was removed from the DFOB, fulvic acid, citric acid, and organic-free flow-cells, respectively. The citric acid flow-cell additionally underwent a 16 h stop followed by an 8 h flow, and 1.9% of total Pu was removed during these steps.

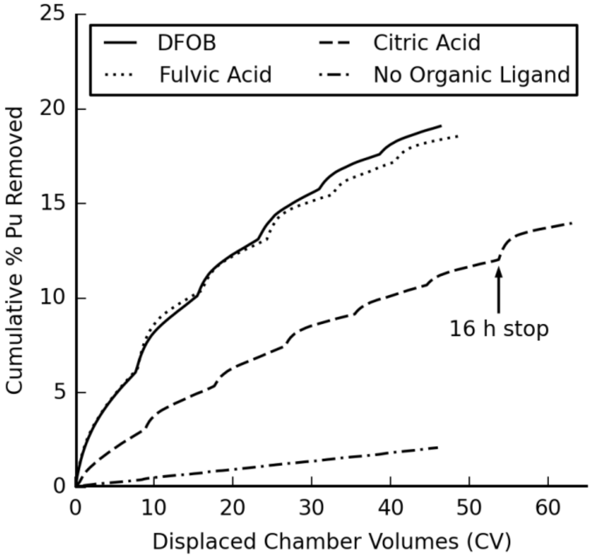

Figure 5.3. Cumulative Pu removed from each flow-cell experiment as a percentage of total Pu concentration. Each flow-cell was operated for 3 d on a stop-flow cycle of 4 and 8 hours. The citric acid flow-cell had an additional stop of 16 hours followed by an 8 hour flow period. The “dips” in the plotted lines indicate stop events. The fluid residence time was 50–60 min. The concentrations of DFOB, fulvic acid, and citric acid were 0.5, 30, and 0.5 $mg_c \cdot L^{-1}$, respectively. Ionic strength was controlled by 10 mM NaCl. The pH was ≈6, and the goethite concentration was 0.03 $g \cdot L^{-1}$.

In the DFOB and fulvic acid flow-cell experiments, similar quantities of Pu were desorbed, despite the fact that the total organic carbon in the fulvic acid flow-cell is 30 $mg_c \cdot L^{-1}$ compared to the 0.5 $mg_c \cdot L^{-1}$ in the DFOB flow-cell. This indicated that DFOB was significantly more effective at desorbing Pu from goethite than fulvic acid. Citric acid was less effective at desorbing Pu than DFOB, but still exhibited significant enhancement of Pu desorption relative to the organic-free flow-cell. This in contrast to previous observations where the extent of Pu sorption to goethite was unchanged with the addition of 5 $mg_c \cdot L^{-1}$ citric acid at pH 5–7 (Conroy et al., 2017). The difference may be due to a difference in contact times or flow condition. Previous measurements are from batch systems with a contact time of 45 days. The flow-cell experiments had contact times of 1 hour (or 4 hours when stopped), and citric acid was continuously supplied.

The relative effectiveness of the ligands at enhancing Pu desorption can be explained by the relative stability of the aqueous Pu–ligand complexes. Under the experiment conditions, the dominant Pu species in the presence of DFOB and citric acid are expected to be $PuH_2(DFOB)_2^{2+}$ and $Pu(Cit)_2^{2-}$, (Figs. B.1 and B.2) with log stability constants of 62 and 29, respectively (Boukhalfa et al., 2007; Clark et al., 2010). Pu in the form of $PuH_2(DFOB)_2^{2+}$ is expected to be be electrostatically repelled from the positively charged goethite surface, whereas $Pu(Cit)_2^{2-}$ would be electrostatically attracted. However, previously, no evidence for ternary Pu–citrate–goethite complexes has been observed at pH 5-7 (Conroy et al., 2017). In the presence of fulvic acid, the enhancement of Pu desorption observed relative to the organic-free flow-cell is consistent with previous observations where the presence of fulvic acid is observed to diminish Pu sorption at pH 5

(Conroy et al., 2017). Although Pu–fulvic stability constants are generally unavailable, Tinnacher et al. (2015) performs a calculation valid at pH 4 and 10^{-10} M total Pu to predict the fraction of Pu–fulvic acid complexes (Suwannee River Standard I). By this method, in the presence of 30 $mg_c \cdot L^{-1}$ fulvic acid, 50% of aqueous Pu is estimated to be Pu–fulvic acid complexes. Although this value cannot be applied to the fulvic acid flow-cell experiment conducted at pH 6 and containing 7.6×10^{-11} M total Pu at the end of conditioning, it can be assumed that the fraction of aqueous Pu complexed with the organic ligand was much lower than in the DFOB or citric acid flow-cell experiments where greater than 99% of aqueous Pu is expected to be $PuH_2(DFOB)_2^{2+}$ or $Pu(Cit)_2^{2-}$, respectively.

Model Results

The aqueous concentration of Pu measured in the flow-cell effluent was normalized against the total Pu concentration at the end of conditioning, $C_{Pu,0}$, and plotted in Fig. 5.4. At each stop event, there was a discontinuity in the data when no samples were collected and Pu desorption occurred over an extended contact time. These stop events were 4 h in duration, except for the final 16 h stop event in the citric acid experiment. The Pu effluent concentration decreased during each of the 8 h flow events. In the first 2–3 CV after each stop event, the Pu effluent concentration decreased exponentially as Pu desorbed during the stop event was eluted from the system, and then more slowly in the following CV demonstrating that desorption was rate limiting relative to the 1 h fluid residence time.

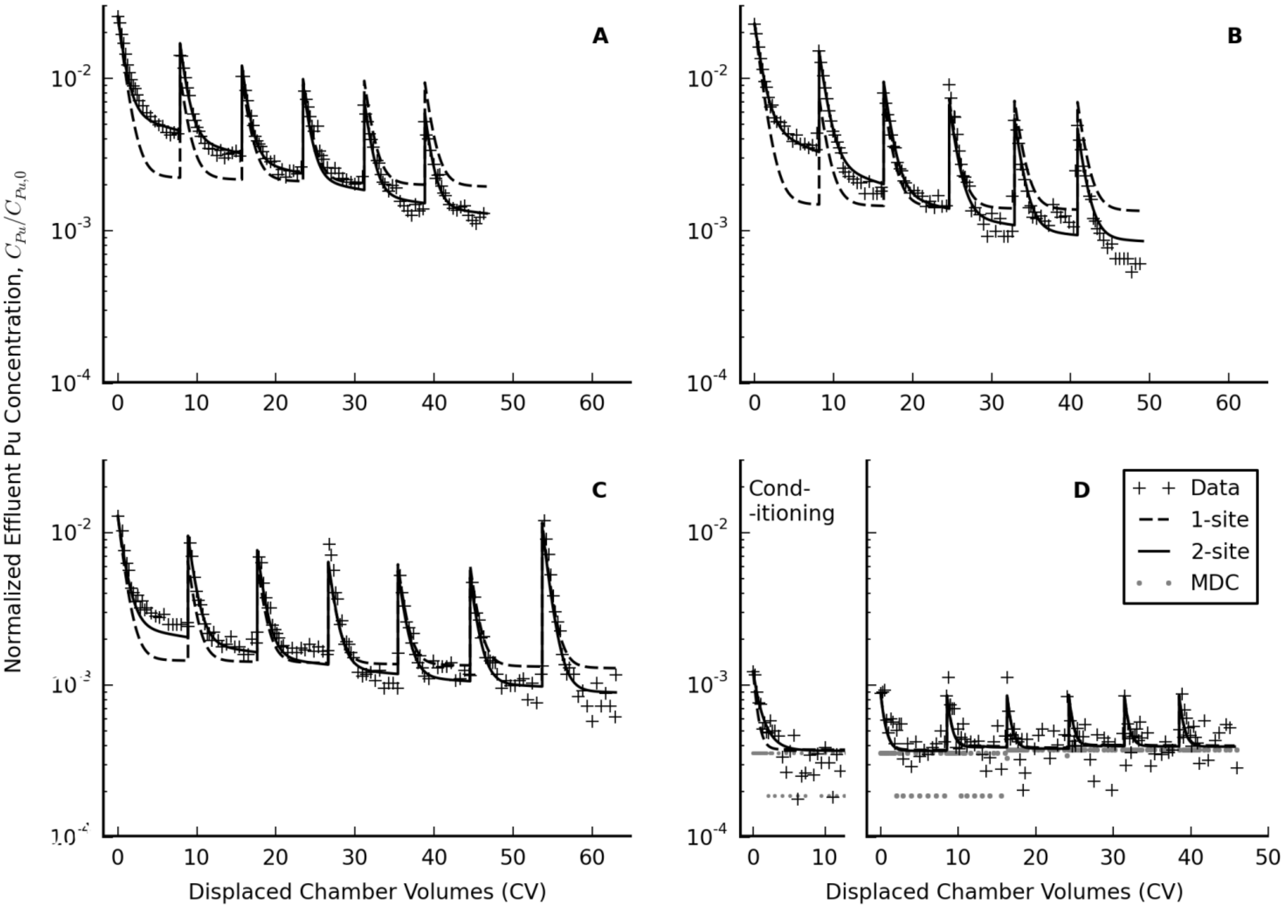

Figure 5.4. The effluent Pu concentration normalized to total Pu and plotted for the following ligands and ligand concentrations: (A) DFOB, 0.5 $mg_c \cdot L^{-1}$; (B) fulvic acid, 30 $mg_c \cdot L^{-1}$; (C) citric acid, 0.5 $mg_c \cdot L^{-1}$; (D) no organic ligand. Except for in the case of no organic ligand, measurements were above the minimum detectable concentration. The minimum detectable concentration varied depending on sample volume and counting time, but was $< 5 \times 10^{-4}$ in all cases. Ionic strength was maintained with 10 mM NaCl. The pH was ≈6, and the goethite concentration was 0.03 $g \cdot L^{-1}$.

In the presence of a ligand, the overall decrease in effluent Pu concentrations over the 3 days of stop and flow intervals indicated a decrease Pu desorbability over this time period. The overall decrease was evident as decreases in the amount of Pu which was removed from the flow-cell during each successive flow event (Fig. 5.5). Although the overall decrease in effluent Pu concentration with time may be due to decreasing Pu surface coverage, this is captured by the one-site model and is not adequate to explain the overall decrease in Pu removed over 3 days. The overall decrease in effluent Pu concentration with time is fit well by the two-site model and may be explained by the transfer of sorbed Pu to a second sorption site/state.

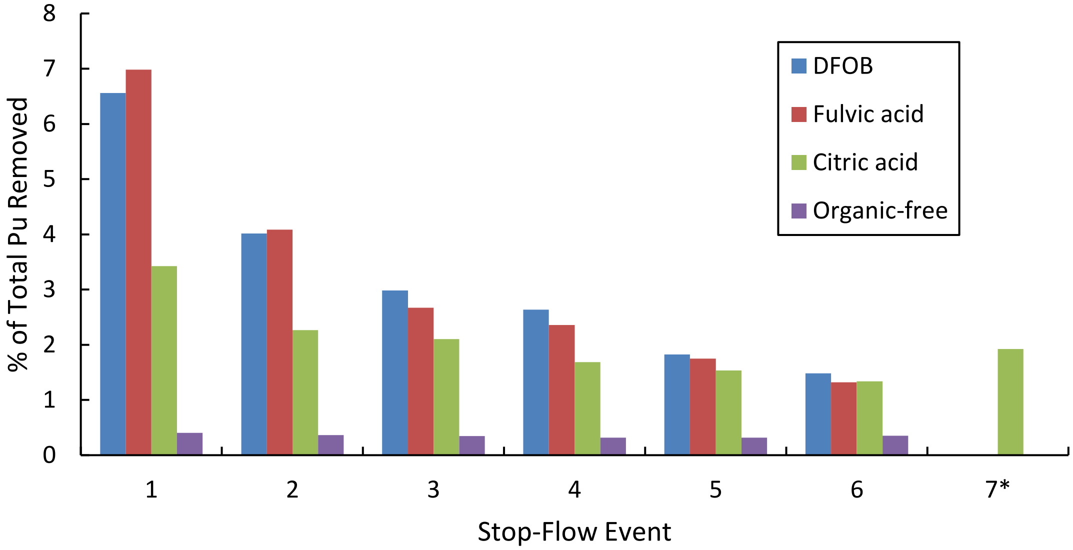

Figure 5.5. The percentage of total Pu removed in each successive stop-flow event. Stop events of 4 hours were followed by 8 hour flow events. Ligand concentrations: DFOB, 0.5 $mg_c \cdot L^{-1}$; fulvic acid, 30 $mgc \cdot L^{-1}$; and citric acid, 0.5 $mg_c \cdot L^{-1}$. Ionic strength was maintained with 10 mM NaCl. The pH was ≈6, and the goethite concentration was 0.03 $g \cdot L^{-1}$. *Event 7 had a 16 hour stop event and an 8 hour flow event.

The modeling results demonstrated that the observed decreasing desorbability of Pu over time could be described with the two-site linear sorption model. The two-site model demonstrated very good fits to the experimental data for both the ligand-containing experiments and the organic-free experiment. The one-site linear sorption model provided a poor fit to the data sets for ligand-containing experiments because it was unable to capture the overall decrease in effluent Pu concentration over time. In the cases of the DFOB, fulvic acid, and citric acid experiments, the one-site model systematically underestimated concentration values before about 15 CV and systematically overestimated concentration values after about 35 CV. The success of the two-site model suggests that the presence of a second consecutive sorption site may explain the increased difficulty of desorbing Pu at later CV.

Apparent Reaction Rate Constants

In order to compare the effect of DFOB, fulvic acid, and citric acid on the apparent (de)sorption rates, apparent first-order sorption rate constants for both the one-site (Table B.1) and two-site (Table 5.4) models were estimated. Additionally, the apparent distribution coefficient, K_d, for the two-site model was calculated (Table 5.4, Eqn. B.9). In the cases of DFOB (one-site model) and fulvic acid (both models), an estimate for the apparent rate of adsorption to the first sorption site, k_{1f}, could not be determined with any confidence. By design, the flow-cell experiments in this work minimized readsorption while solution was flowing, and the effluent could not be sampled while flow was stopped. Therefore, the experimental data sets contained little information to constrain the value of the apparent adsorption rate constant, k_{1f}. As a result, the goodness-of-fit is largely insensitive to the k_{1f} value in some cases.

Table 5.4. Parameters for two-site linear sorption model. One standard deviation of uncertainty is indicated.

Flow-cell	k_{1f} (min^{-1})	k_{1r} (min^{-1})	k_{2f} (min^{-1})	k_{2r} (min^{-1})	K_d (L·kg^{-1})[a]	WSOS/ DF[b]
DFOB	$2.23 \pm 0.3 \times 10^{-3}$	$1.08 \pm 0.04 \times 10^{-4}$	$4.6 \pm 0.4 \times 10^{-4}$	$1.4 \pm 0.3 \times 10^{-4}$	2.97×10^{3}	8.684
Fulvic acid	2.8×10^{-8} [c]	$7.94 \pm 0.25 \times 10^{-5}$	$7.3 \pm 0.5 \times 10^{-4}$	$1.96 \pm 0.20 \times 10^{-4}$	n.d.	4.959
Citric acid	$1.16 \pm 0.14 \times 10^{-3}$	$4.77 \pm 0.19 \times 10^{-5}$	$3.4 \pm 0.5 \times 10^{-4}$	$2.4 \pm 0.5 \times 10^{-4}$	1.54×10^{3}	2.547
Ligand-free	$1.32 \pm 0.16 \times 10^{-2}$	$2.2 \pm 0.7 \times 10^{-5}$	$6.16 \pm 0.13 \times 10^{-3}$	$6.7 \pm 4.9 \times 10^{-3}$	3.44×10^{4}	2.141

[a] The apparent distribution coefficients, K_d, were calculated according to Eqn. B.9.

[b] WSOS/DF is the weighted sum of squares divided by the degrees of freedom and was used as a goodness-of-fit value.

[c] This parameter value should not be considered with any real confidence because the model fit is insensitive to this parameter.

Although this is a black box model, examining the estimated apparent rate constants can reveal the driving rationale behind why the two-site model provides a good fit to the data. Apparent first-order rate constants for the two-site model have been surface-area normalized and plotted for comparison in Fig. 5.6. The apparent rate constant, k_{1r}, representing desorption from the first sorption site shows the clearest trend. The value of k_{1r} is greater in the presence of the ligands which are the most effective at enhancing Pu desorption from goethite. DFOB and fulvic acid are more effective than citric acid and no organic ligand at enhancing Pu desorption and have correspondingly greater k_{1r} values. The apparent rate constant, k_{2f}, represents the transition of Pu from the first sorption site to the second, consecutive sorption site, and k_{2r} represents the apparent rate constant for back-transition. For each of the data sets, the k_{2f} value is similar to the k_{2r} value, suggesting that Pu does not necessarily have a greater affinity for site 2 than site 1. Furthermore, the model calculations indicate that concentrations of Pu sorbed to site 1 and 2 are within an order of magnitude. Effectively, the two-site model describes the decreasing desorbability of Pu as Pu becomes less accessible over time. That is, Pu becomes less desorbable because Pu sorbed to site 2 must back-transition before desorbing from the goethite surface.

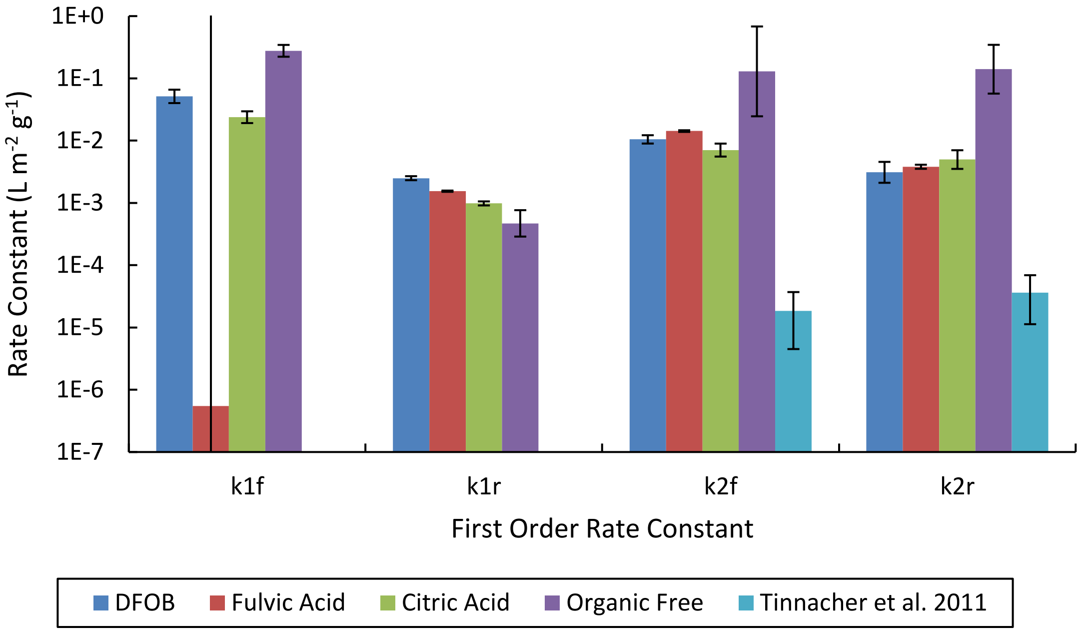

Figure 5.6. Comparison of first-order sorption rate constants for the two-site model. Error bars represent a 95% confidence interval. The Tinnacher et al. (2011) transition rates constants, k_{2f} and k_{2r}, are for Np(V) sorption to 29.6 $m^2 \cdot g^{-1}$ goethite, where a model with one Freundlich sorption site and one consecutive linear sorption site was considered.

The surface-area normalized apparent rate constants can be compared to studies with different minerals and surface area. Although there are few studies that report both adsorption and desorption rate constants for Pu, adsorption rate constants (one-site model) for 10^{-10} M Pu(V) to goethite, hematite, and magnetite have been previously summarized (Begg et al., 2013). The surface area normalized adsorption rate constants obtained from fitting the one-site model to the citric acid and organic-free data sets were $10^{-1.62}$ $L \cdot m^{-2} \cdot g^{-1}$ and $10^{-0.56}$ $L \cdot m^{-2} \cdot g^{-1}$, respectively. These are similar to reported rate constants of $10^{-1.4}$ $L \cdot m^{-2} \cdot g^{-1}$ for goethite, $10^{-0.8}$ $L \cdot m^{-2} \cdot g^{-1}$ for hematite, and $10^{-0.9}$ $L \cdot m^{-2} \cdot g^{-1}$ for magnetite (Begg et al., 2013; Powell et al., 2005, 2004).

To the author's knowledge, only one other study has applied a kinetic sorption model with two consecutive sorption sites to actinide sorption on a mineral surface (Tinnacher et al., 2011). Adsorption and desorption of 10^{-10} M Np(V) on goethite in a flow-cell was modeled using a two-site sorption model which considered a Freundlich sorption site and a second, consecutive linear sorption site. The reported first-order rate constants for the second, consecutive site have been surface-area normalized and plotted in Fig. 5.6 for comparison. Since the Np and Pu datasets were modeled with slightly different sorption assumptions, this comparison should be done with caution. It appears that, in the case of Np(V), the affinity of Np(V) for the second site is not necessarily greater than the first site similar to the observation of Pu sorption in this work. However, the k_{2f} and k_{2r} values for Np(V) are two orders of magnitude lower than in our study indicating that aging processes for Np(V) may occur more slowly than Pu(IV).

Environmental Significance

Overall it appears that organic ligands can facilitate desorption of Pu to a greater extent than ligand free systems. The greater desorption of Pu in the presence of DFOB relative to citrate is likely due to the greater complexation affinity of DFOB relative to citrate (i.e. due to higher stability constants for Pu–DFOB). Even at low concentration, citrate was effective at enhancing Pu desorption from goethite. Compared to DFOB, a higher concentration of fulvic acid based on total dissolved carbon was required to remove a similar amount of Pu, thus, it is clear that DFOB is a stronger complexant than fulvic acid. Future studies to determine the nature of Pu–fulvic acid complexes and the associated stability constants are required for a more direct comparison.

In the presence of DFOB, fulvic acid, and citric acid, Pu was observed to become less desorbable over 3 days which was consistent with aging of sorbed Pu. This has implications for subsurface transport because it means that fixed K_d values for Pu measured on shorter timescales may underestimate the stability of sorbed Pu. Thus, transport models based on these K_d values may overestimate Pu mobility, or, if Pu undergoes sorption to mobile colloids, underestimate colloid-facilitated transport. The decreasing desorbability of Pu over time was demonstrated to be consistent with a conceptual model which considered two consecutive linear sorption sites. Further studies are required to determine whether sorption of Pu or other highly charged metal ions to goethite and other mineral surfaces can be described with this two-site model.

CHAPTER SIX

TRANSPORT OF PLUTONIUM IN SOIL FROM THE SAVANNAH RIVER SITE IN THE PRESENCE OF CITRATE AND DESFERRIOXAMINE B

Paper Status

This chapter consists of a manuscript which is in preparation for submission to a scientific journal.

Authors

Jennifer C. Wong, Mavrik Zavarin, Annie B. Kersting, Brian A. Powell

Abstract

Due to legacy nuclear waste, planned nuclear fuel fabrication, and plutonium (Pu) conversion activities at the Savannah River Site (SRS), it is necessary to gain a better understanding of the fate and transport of plutonium in this subsurface environment. The mobility of Pu in soil from the Savannah River Site was examined in the presence of citrate and desferrioxamine B (DFOB) by performing column experiments. Pu(IV) was introduced to the 15 cm columns as a finite step input. Then, the column was continuously supplied with ≈100 pore volumes of citrate, DFOB, or organic-free solution. Due to sorption of citrate and DFOB to the soil, these ligands accumulated within 2 cm of the inlet. Despite this, a small enhancement of Pu mobility was observed within the columns, relative to the column supplied with organic-free solution. Fine segmentation (down to 1.5 mm) of the column allowed for detailed measurement of the soil Pu distribution. In the citrate column, elevated Pu concentrations were observed at 0.5–15 cm. In the DFOB column, elevated Pu concentrations were observed at 0.5–2 cm. Additionally, 9-20% of Pu eluted

from the columns with retardation factors of 24–29. Reactive transport modeling with Hydrus and C-Ride was performed to investigate the plausibility of Pu transport as three possible forms of eluted Pu: (1) Pu(V) which formed by oxidation of Pu(IV) in the spike solutions, (2) Pu adsorbed to mobile colloids, and (3) aqueous complexes formed with soil organic matter. The modeling exercise demonstrated the limitations of modeling a complex system with simple models, and the need for more parameter constraints when dealing with complex systems. This study highlights the dependence of Pu mobility on complex processes which may include soil composition, Pu redox reactions, ligand sorption, soil organic matter, and mineral colloids.

Introduction

In this study, plutonium (Pu) transport in a sandy clay loam soil from the Savannah River Site (SRS) in the presence of natural organic ligands was investigated. In the 1950's the SRS was constructed in South Carolina, United States to produce ^{239}Pu, ^{238}Pu, and various transuranic isotopes for nuclear weapons, medical, industrial, and scientific purposes (Carlton et al., 1992). Including releases to streams, seepage basins, and air, 5.9×10^{11} Bq (16 Ci) equivalent to 178 g of $^{238+239}$Pu was released to the environment at the SRS (Carlton et al., 1992; Hetrick and Martin, 1990). Current projects at the SRS focus on remediation of legacy waste and conversion of weapons grade Pu to nuclear reactor fuel at facilities such as the Mixed Oxide Fuel Fabrication Facility, Pit Disassembly and Conversion Facility, and the Pu Immobilization Plant. In order to assess the risks associated with legacy waste disposition and planned fuel fabrication and conversion facilities, it is imperative to better understand the fate and transport of Pu in the SRS subsurface environment. Plutonium is of key concern because of its long half-life and radiotoxicity. The mobility of Pu in the environment is governed by its oxidation state, sorption to mineral surfaces, complexation with natural organic ligands, and sorption to mobile colloids.

The Oxidation States of Pu

While Pu can exist simultaneously in four oxidation states (III, IV, V, and VI) under natural conditions, the oxidation states most relevant to subsurface transport under oxic conditions are Pu(IV) and Pu(V) (Choppin et al., 1997; Cleveland, 1979; Silva and Nitsche, 1995). The mobility of Pu is greatly dependent on oxidation state. Pu(IV) is highly insoluble and typically adsorbs more strongly to mineral surfaces than Pu(V), resulting in typical distribution coefficients, K_d, which are 2 to 3 orders of magnitude greater than K_d values for Pu(V) (Bondietti et al., 1976; Powell et al., 2002; Prout, 1958). In the absence of a sorbent, dissolved Pu(IV) is unstable at trace concentrations (i.e. $<10^{-8}$ M); within hours at pH 4–10, aqueous Pu(IV) begins to oxidize to Pu(V) (Powell et al., 2011), the dominant oxidation state in natural waters and dilute salt solutions (Choppin et al., 1997; Morse and Choppin, 1986; Orlandini et al., 1986). However, in the presence of iron and manganese (oxyhydr)oxide minerals, aqueous Pu(V) has been demonstrated to undergo surface mediated reduction to form sorbed Pu(IV) (Hu et al., 2010; Keeney-Kennicutt and Morse, 1985; Kirsch et al., 2011; Penrose et al., 1987; Powell et al., 2006, 2005, 2004; Romanchuk et al., 2011; Sanchez et al., 1985; Shaughnessy et al., 2003). Thus, Pu sorbed to mineral surfaces is typically Pu(IV), and aqueous Pu is typically Pu(V).

Natural Organic Ligands

Natural organic ligands (NOL) may influence Pu mobility in the environment by forming aqueous Pu–ligand complexes or ternary Pu–NOL–surface complexes. Both DFOB and citrate are siderophores, organic compounds exuded by bacteria, plants, and fungi to solubilize iron and other insoluble metals. Due to the similar ratios of effective charge to ionic radius of Fe(III) and Pu(IV), siderophores are generally also effective at solubilizing Pu(IV). DFOB is a linear molecule which chelates Pu with three hydroxamic functional groups and forms strong aqueous complexes with Pu (Boukhalfa et al., 2007). Citrate is a low molecular weight molecule with three carboxylic groups. Citrate can form strong 2:1 complexes with Pu (Clark et al., 2010). Equilibrium speciation calculations indicate that at pH 5 the dominant species of Pu in the presence of DFOB and citrate are $PuH_2(DFOB)_2^{2+}$ and $Pu(Cit)_2^{2-}$, respectively (Appendix C). The formation of these strong aqueous complexes suggests that DFOB and citrate might solubilize Pu by out-competing surface sites for Pu ions. However, it is also important to consider interactions between the organic ligands and mineral surfaces.

The sorption of organic ligands to mineral surfaces and possible formation of ternary surface complexes could lessen the effectiveness of organic ligands at mobilizing Pu. DFOB adsorbs significantly to smectite (Boggs et al., 2015; Haack et al., 2008; Neubauer et al., 2000; Siebner-Freibach et al., 2004), and below pH 8 its presence has been shown to enhance sorption of heavy metals to smectite. This enhanced sorption is caused by ion exchange of DFOB–metal complexes, thus, resulting in the formation of ternary surface complexes (Neubauer et al., 2000; Siebner-Freibach et al., 2006). In the case of Pu, enhanced sorption has been observed when Pu was contacted with smectite suspensions as Pu–DFOB complexes, but not when Pu was added to smectite with DFOB sorbed in the inaccessible interlayer (Boggs et al., 2015). In contrast to smectite, DFOB adsorbs weakly to goethite due to steric hindrance and cationic repulsion (Cheah et al., 2003; Cocozza et al., 2002; Conroy et al., 2017; Kraemer et al., 1999). The presence of DFOB has been observed to diminish the sorption of Pu and other heavy metals to goethite, kaolinite, and aluminum oxide minerals (Conroy et al., 2017; Kraemer et al., 2002; Neubauer et al., 2000; Simpkins, 2011). The formation of aqueous metal–DFOB complexes is expected to enhance heavy metal transport in the subsurface. However, in a soil that contains smectite, DFOB may decrease the mobility of heavy metals.

Unlike DFOB, citrate will sorb to both goethite and, to a lesser extent, clay minerals, and evidence for the formation of ternary surface complexes with Pu and goethite has been observed at pH 3 (Conroy et al., 2017; Lackovic et al., 2003). Lackovic et al. concludes that the extent of citrate sorption to goethite is greater than to kaolinite because strongly sorbing inner-sphere surface complexes dominate, whereas citrate forms weaker bidentate outer-sphere surface complexes with kaolinite. It has also been suggested that citrate is less effective at forming bonds with alumina groups at mineral surfaces, than aluminum in solution because it is more difficult for citrate to form bidentate complexes on a planar surface than in solution (Kubicki et al., 1999). At pH 5.5, goethite and illite surface sorption sites are observed to saturate below aqueous concentrations of 50 μM of citrate, whereas kaolinite surface sites do not (Lackovic et al., 2003). Batch sorption experiments demonstrate enhanced Pu sorption to goethite in the presence of citrate at pH

3, but diminished Pu sorption at pH 7–9 (Conroy et al., 2017). In a gibbsite system, diminished Pu sorption to gibbsite is observed below pH 8 (Simpkins, 2011). Thus, the effect of citrate on Pu sorption and mobility depends on soil composition and pH.

The goal of this study is to compare the effect of citrate and DFOB on the overall Pu mobility in a natural soil. Columns packed with soil from the SRS were loaded with one pore volume of Pu(IV) solution, followed by ≈100 pore volumes of citrate or DFOB solution. The effluent was measured for aqueous Pu, and the soil was finely sectioned (down to 1.5 mm) which allowed for detailed measurement of the soil Pu distribution and mobility. Batch tests consisting of Pu only, organic ligand + soil, and soil only, as well as a blank soil column test were performed to examine other processes which may influence Pu mobility, such as oxidation of Pu(IV) to Pu(V), sorption of organic ligands to the soil, dissolution of soil organic matter, and formation of mobile colloids. Reactive transport modeling was performed to examine the plausibility of three processes for the enhancement of Pu mobility: (1) the presence of Pu(V), (2) colloid-facilitated transport, and (3) mobilization by soil organic matter.

Materials and Methods

All solutions were prepared with distilled deionized water with resistivity >18 MΩ·cm. The organic ligands used were in the form of desferrioxamine mesylate (Sigma Aldrich, ≥92.5%) and citric acid monohydrate (J.T. Baker, ACS grade). All reagents were ACS grade or higher. Adjustments to solution pH were made with dilute HCl and NaOH. The concentrations of tritium and aqueous Pu were determined in Ultima Gold scintillation cocktail using liquid scintillation counting (Perkin Elmer Tri-Carb 2910 TR) with alpha/beta discrimination. The natural soil used for these experiments is from the West Borrow Pit at the Savannah River Site, South Carolina. Chemical and physical characterization of the soil has been done previously as part of a larger effort (Table 6.1).

Table 6.1. Properties of soil used for this study.

Property	Value
Sand/Silt/Clay content (%)	65.6/14.0/20.4
Composition of silt/clay-size fraction	>95% kaolinite, <5% smectite
Organic matter fraction	0.9%
Hydraulic conductivity	3.38×10^{-4} cm·s^{-1}
Total Fe as Fe_2O_3 [a]	2.64%
Soil pH	4.8

[a] Total Fe is from (Montgomery et al., 2017)

Plutonium Preparation and Oxidation State Measurement

A Pu stock solution was prepared by purifying a ^{238}Pu solution in 1 % HNO_3 on a BioRad AG 1-X8, 100–200 mesh anion exchange column. The Pu was eluted in a solution of 9 M HCl and 0.1 M HI (Bajo et al., 2007). The eluate was evaporated and redissolved in 1 mL 1 M HCl, resulting in an 8×10^{-8} M ^{238}Pu(IV) stock solution. Oxidation state was confirmed to be >99.0 % Pu(IV/III) by lanthanum fluoride co-precipitation (Foti and Freiling, 1964; Nitsche et al., 1988). Another ^{238}Pu stock solution (98.7 % ^{238}Pu, 0.3 % ^{239}Pu, and 0.01 % ^{242}Pu by activity), which was prepared using the same method and used for testing the oxidation state of simulated spike solutions, was 9.8×10^{-7} M Pu and 99.9% Pu(IV) as measured by a well-established organic extraction technique (Neu et al., 1994; Nitsche and Edelstein, 1985; Powell et al., 2004).

Preparation of Background and Spike Solutions

A 10 mM NaCl background solution was prepared. Ligand solutions of 0.278 mM were prepared by dissolving sodium citrate dihydrate and desferrioxamine mesylate, respectively, into background solution, and then adjusting the pH values to 4.8. A stock solution of tritium (^3H), which was used as a conservative tracer, was prepared by diluting NIST Standard Reference Material (4927F) to 4.9×10^9 $Bq \cdot L^{-1}$.

For each experiment, a 10 mL spike solution was freshly prepared by adding tritium stock solution, 1 M NaOH, and Pu(IV) stock solution to 10 mM NaCl background solution. The 1 M NaOH was added just before the Pu(IV) stock solution to minimize swings in pH. Then, the spike solution was adjusted to pH 4.8. Following the addition of Pu, each spike solution was used in each column experiment after approximately 1.5 hours. The concentrations, $C_{T,0}$ and $C_{Pu,0}$, of tritium and Pu in the spike solution were analyzed by liquid scintillation counting. The final spike solutions contained 5×10^{-10} M ^{238}Pu and 4.8×10^5 $Bq \cdot L^{-1}$ ^3H.

Column Experiments

The glass columns (Kontes Chromflex) were 15 cm long and 1 cm in diameter. The columns had Teflon end caps and polyethylene diffusion plates with a 20 µm pore size. The experiment set up used a peristaltic pump (Gilson Minipuls 2) with 1.02 mm inner diameter peristaltic tubing (Ismatec, Pharmed BPT), and Teflon extension tubing (Cole Parmer, 1/32” inner diameter). The length of tubing was measured so the dead volume could be estimated.

The columns were packed by pouring a single scoop of dry soil into the top of each uncapped column while continuously tapping the column. This was to minimize the formation of heterogeneous layers of silt-sized grains between individual lifts. Next, the column top cap and tubing were attached, and background solution was pumped into the bottom of the column to saturate the soil. The masses of soil and background solution within the column were measured gravimetrically in order to determine the bulk density ($g{\cdot}mL^{-1}$), ρ, and the saturated water content ($mL{\cdot}mL^{-1}$), θ. The pore water was assumed to occupy the entire column porosity ($mL{\cdot}mL^{-1}$), φ.

The soil was conditioned by pumping 12–16 pore volumes (PV) of background solution into the column. Then, the flow rate was adjusted to obtain a residence time of ≈one hour, and the spike solution was loaded as a finite step input with a total of one PV loaded. The precise volume of spike solution loaded was determined from the difference in weight of the spike solution before and after loading. Next, 2–3 PV of background solution were pumped into the column, followed by ≈100 PV of ligand solution. The ligand solution did not directly follow the Pu loading solution in order to minimize any mixing in the tubing and end cap before the solutions reached the columns. In the organic-free control experiment, additional background solution was pumped into the column instead of ligand solution.

Effluent was collected in polystyrene tubes on a fraction collector (Specta/Chrom CF-1). Some effluent fractions were reserved for pH measurements. Measurements of effluent pH confirmed that the pH was typically 4.5 to 5, presumably due to buffering in the columns. Effluent fractions were acidified to 1% HCl with concentrated HCl and measured for tritium and aqueous Pu by liquid scintillation counting. In figures, aqueous concentrations are presented normalized against the spike concentrations, $C_{T,0}$ and $C_{Pu,0}$.

At the end of the experiment, the column was sectioned by pushing a plunger into the bottom of the column (end caps were first removed), and extruding the soil out of the top of the column (Fig. 6.1). Soil sections, which varied in thickness from 1.5 to 10 mm, were collected in 50 mL centrifuge tubes, and soil residue from the lip of the column was rinsed into the tube with 2–6 mL of water. The soil samples were acidified to ≈6 M HNO_3, and allowed to leach for 4 days. After gravity settling, sample aliquots of 1 mL were centrifuged 30 min at 10k rpm (Beckman F2402H rotor), and 150 μL aliquots of the supernatant were analyzed for Pu by liquid scintillation counting. The minimum detectable concentration (MDC) varied depending on soil mass and leachate volume. The typical Pu MDC values for samples with thickness ≥2 mm were in the ranges of $0.4–2.3 \times 10^{-14}$ $mol \cdot g^{-1}$, $0.2–1.1 \times 10^{-14}$ $mol \cdot g^{-1}$, and $0.3–1.2 \times 10^{-14}$ $mol \cdot g^{-1}$ for the control, citrate, and DFOB columns, respectively. Samples containing ≤2 mm of soil had higher MDC values. However, these soil sections were mainly from the first 2 cm of the column where higher concentrations of Pu were present, and consequently, measured Pu concentrations were typically more than two standard deviations greater than MDC values (Fig. 6.6) in this region. The remainder of the supernatant in each sample was removed and weighed. The soil samples were washed by adding 8 mL of water, centrifuging 16 min at 9k rpm (Beckman C0650 rotor), and removing the supernatant. Then, they were dried in a 50˚C oven and weighed to determine the dry mass. The position of each section within the column was determined assuming a uniform dry mass distribution.

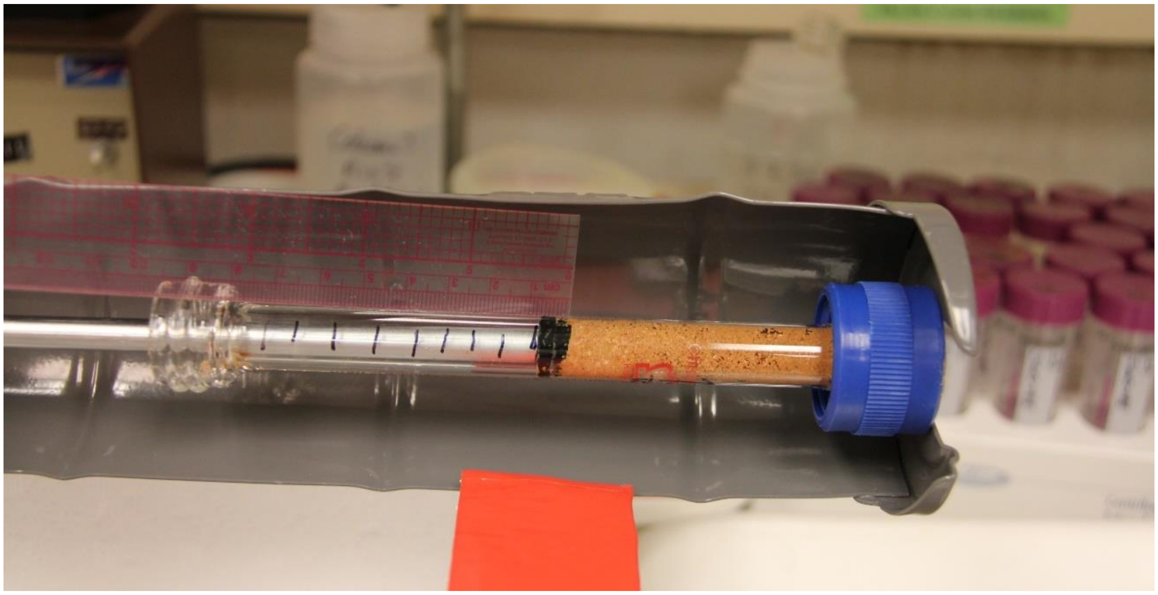

Figure 6.1. Apparatus for extruding soil columns built out of a caulking gun. The end which was the fluid outlet is to the right. The position of soil sections in the column was calculated based on the dry weight of soil and assuming a uniform mass distribution.

Blank Column

An additional, blank column experiment was performed without any Pu, citrate, or DFOB in order to estimate the amount of soil organic matter (SOM), Mg, Ca, Al, and Fe that leached from the soil (details in Appendix C). Although the blank column effluent cannot be directly compared to the effluent of the other experiments, since the presence of Pu, citrate, or DFOB may potentially perturb the organic carbon and major element chemistry, the blank column was used to establish the effluent composition in the absence of Pu, citrate, or DFOB. Dissolved soil organic matter was measured using a total organic carbon (TOC) analyzer (Shimadzu TOC-L CSH), and the other elements were measured using Inductively Coupled Plasma Mass Spectrometry, (ICP-MS, Thermo Scientific XSeries 2).

Pu Sorption to Soil

A batch test was performed to determine the distribution coefficient for Pu on the SRS soil. A 20 mL sample was prepared by adding soil, 1 M NaOH, and ^{238}Pu(IV) stock to 10 mM NaCl. The suspended solids concentration was 25 $g \cdot L^{-1}$. The 1 M NaOH was added before the Pu(IV) stock to minimize fluctuations in pH. The pH was adjusted to 4.8 ± 0.2 with dilute NaOH and HCl. After one day, the aqueous Pu was measured by removing 1.1 mL of solution for centrifugation (20 min, 10k rpm, Eppendorf MiniSpin) and 1 mL of supernatant was removed for liquid scintillation counting.

Citrate and DFOB Sorption to Soil

In order to construct isotherms for citrate and DFOB sorption to the soil, batch samples were prepared with 25 $g \cdot L^{-1}$ soil. Ligand stock solutions of 13.9 mM citrate and 13.3 mM DFOB were prepared by dissolving sodium citrate dihydrate and desferrioxamine mesylate, respectively, into water. Soil, 10 mM NaCl, and either citrate or DFOB stock solution were added to 50 mL tubes. The total ligand concentrations ranged from 0.070 to 0.700 mM. The range of ligand concentrations was selected to span a wide range of concentrations around the 0.278 mM concentration used for the column experiments. Samples were adjusted to pH 4 and 5, placed on a mixer/tumbler (≈10 rpm), and allowed to equilibrate for 2 days. The samples were centrifuged 30 min at 3k rpm (Allegra 6KR centrifuge, GH3.8 rotor) and 20 mL of supernatant was removed for TOC analysis.

The extent of the ligand front in the columns at the end of the experiments was calculated because DFOB and citrate exhibited unexpectedly strong sorption to the soil (Appendix C). The sorption isotherms were used to determine the concentration of sorbed ligand ($\mathrm{mmol\cdot g^{-1}}$) expected in soil contacted with 0.278 mM aqueous ligand. The cumulative moles of citrate or DFOB were used to calculate the volume of soil at the front of a column which reached this solid concentration.

Tracer Modeling

Transport modeling of ^{3}H used the classical one-dimensional advection-dispersion equation for reactive transport (Eqn.6.1). Using a least-squares approach, this model was optimized to fit the ^{3}H data using the longitudinal dispersion coefficient ($\mathrm{cm^2\cdot min^{-1}}$), D, and the retardation factor, R, as adjustable parameters. The retardation factor and the distribution coefficient, K_d, are related by Eqn. 6.2. The tubing dead volume was included in calculations to account for a slight delay in the arrival of the ^{3}H front.

$$\varphi R \frac{\partial C}{\partial t} = D \frac{\partial^2 C}{\partial x^2} - u \frac{\partial C}{\partial x} + g(t) \tag{6.1}$$

$$R = 1 + K_d \frac{\rho}{\varphi} \tag{6.2}$$

The variables in Eqns. 6.1 and 6.2 are defined: C, aqueous analyte concentration ($\mathrm{mol\cdot cm^{-3}}$); S, solid phase analyte concentration ($\mathrm{mol\cdot g^{-1}}$); u, mean fluid velocity ($\mathrm{cm\cdot min^{-1}}$); ρ, bulk density ($\mathrm{g\cdot cm^{-3}}$); φ, porosity (-); x, distance from the column inlet (cm); t, the coordinate (min); and $g(t)$, a source or sink function ($\mathrm{mol\cdot cm^{-3}\cdot min^{-1}}$).

Reactive Transport Modeling of Pu

The preliminary efforts to model Pu transport with K_d as the only adjustable parameter (Eqns. 6.1 and 6.2) could not successfully fit the soil and elution profiles. In order to explore other potential reactive processes affecting Pu transport, transport models which included surface mediated reduction, colloid-facilitated transport, and transport facilitated by soil organic matter were solved numerically using the software Hydrus 1D (PC-Progress). No optimization was performed with Pu data, rather parameters were systematically varied across a range of values to explore the parameter space. The goal of this modeling effort was to determine whether models for these processes could be used to describe the observed distributions of Pu in the soil and effluent profiles. Because the discussed processes are hypothetical, the modeling exercise was highly speculative and included many simplifying assumptions.

Surface Mediated Reduction of Pu

In this model, first-order reduction of Pu(V) to Pu(IV) in the solid phase was considered. Some Pu in the loading solution may have oxidized to Pu(V) during pH adjustment resulting in a portion of Pu(V). Sorption of Pu(V) and Pu(IV) to the solid phase was assumed to be linear and reach equilibrium instantaneously, and oxidation of Pu(IV) to Pu(V) in the column was not considered. This is similar to the approach of Fjeld et al. (2003). A schematic for the modeled reactions is shown in Fig. 6.2 and variables for Pu concentrations, distribution coefficients, and reduction rate constant are defined in Table 6.2. Further detail is given in Appendix D. Briefly, the classical one-dimensional advection-dispersion transport equation was used for the Pu(IV) and Pu(V) components with a source/sink term representing reduction in the solid phase. The equations were solved numerically using Hydrus 1D software. The model used the separate distribution coefficients for Pu(IV) and Pu(V), and a first-order reduction rate constant, μ'_s, as adjustable parameters. The source term is a finite-step input of loading solution composed of a mixture of Pu(IV) and Pu(V). The fraction of Pu(V) is given by $f_{Pu(V)}$ which is also an adjustable parameter.

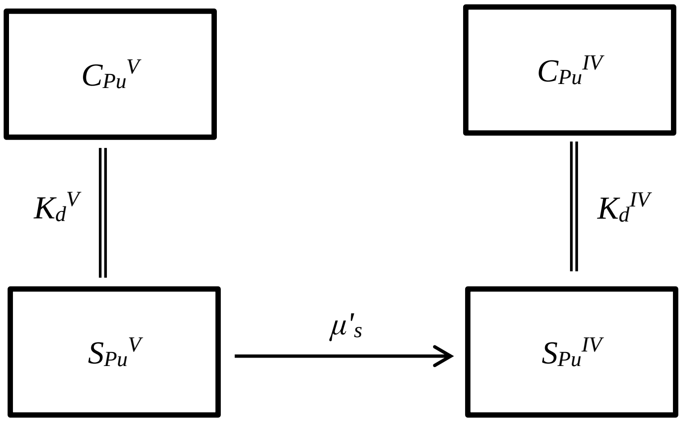

Figure 6.2. Schematic for reactions included in the surface mediated reduction model.

Table 6.2. Variable definitions for the surface mediated reduction model, where M is the solute mass unit.

Variable	Units	Description
C_{Pu}^{V}	$M \cdot cm^{-3}$	aqueous Pu(V) concentration
S_{Pu}^{V}	$M \cdot g^{-1}$	sorbed Pu(V) concentration
C_{Pu}^{IV}	$M \cdot cm^{-3}$	aqueous Pu(IV) concentration
S_{Pu}^{IV}	$M \cdot g^{-1}$	sorbed Pu(IV) concentration
K_d^{V}	$cm^3 \cdot g^{-1}$	distribution coefficient for Pu(V)
K_d^{IV}	$cm^3 \cdot g^{-1}$	distribution coefficient for Pu(IV)
μ'_s	min^{-1}	first-order reduction rate constant of sorbed Pu(V) to sorbed Pu(IV)
$f_{Pu(V)}$	-	fraction of Pu(V) in the column loading solution

Colloid-Facilitated Transport of Pu

Colloid-facilitated transport was modeled using the C-Ride module of Hydrus 1D (Šimůnek, 2017; Šimůnek et al., 2006; Šimůnek and van Genuchten, 2015) which numerically solved transport equations for three components: Pu, Pu sorbed to colloids, and colloids (see Appendix D). This model has previously been successful at modeling transport facilitated by bacteria (Pang and Šimůnek, 2006) and other types of colloids. Since each of these components may be in the mobile phase or attached to the soil, the model defines six compartments or species: C_{Pu}, S_{Pu}, S_{mc}, S_{ic}, C_c, and S_c (Table 6.3). The model for colloid-facilitated transport used an attachment/detachment model for colloid reactions with the solid phase, where "*k*" variables represented pseudo-first-order reaction rate constants which were treated as adjustable parameters. Included in the model are the processes of colloid attachment and detachment on the soil, Pu (de)sorption on colloids, and instantaneous linear sorption of Pu on the soil (Table 6.3 and Fig. 6.3).

Table 6.3. Variable definitions for the colloid-facilitated transport model, including six compartments or species and four pseudo-first-order rate constants. Solute mass units are represented by M, and n represents the unit for the amount of colloids.

Variable	Units	Species description
C_{Pu}	$M\cdot cm^{-3}$	aqueous Pu concentration
S_{Pu}	$M\cdot g^{-1}$	sorbed Pu concentration
S_{mc}	$M\cdot n^{-1}$	Pu sorbed to mobile colloids
S_{ic}	$M\cdot n^{-1}$	Pu sorbed to immobile colloids
C_c	$n\cdot cm^{-3}$	mobile colloid concentration
S_c	$n\cdot g^{-1}$	colloids attached to soil
k_{att}	min^{-1}	colloid attachment
k_{det}	min^{-1}	colloid detachment
k_{ac}	min^{-1}	Pu sorption to colloids
k_{dc}	min^{-1}	Pu desorption from colloids
K_d	$cm^3\cdot g^{-1}$	Pu distribution coefficient

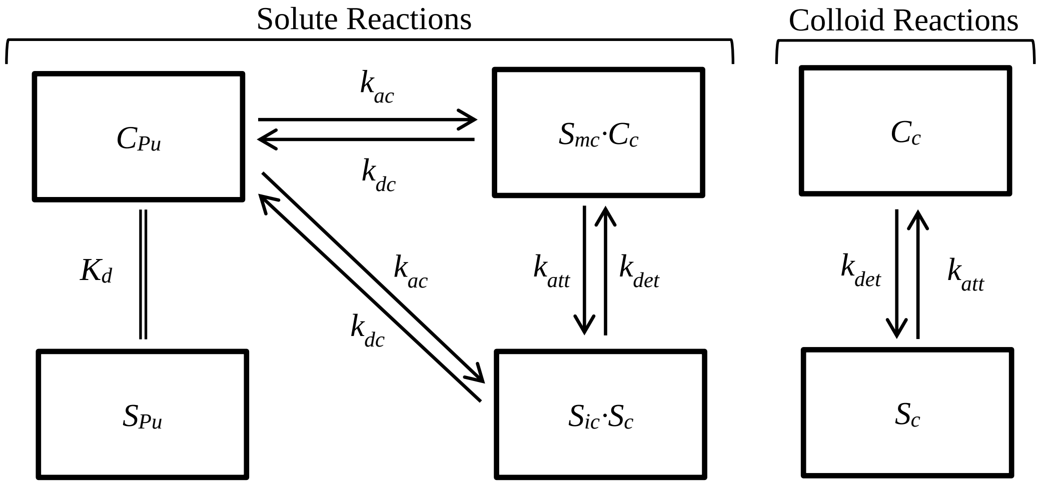

Figure 6.3. Schematic for reactions included in the colloid-facilitated transport model

The columns were treated as saturated throughout the modeling, and, thus no air interface was considered. The model was simplified by assuming no colloid straining and no colloid exclusion. Blocking, or saturation of attachment/sorption sites, was not considered. The (de)sorption rate constants of the solute on the colloids were assumed to be the same for mobile and immobile colloids. No other source or sink terms were considered.

Since the colloids in the system were generated in the soil, initial conditions specified a uniform concentration of immobile colloids in the soil, S_c^0, and no mobile colloids initially present. The equivalent mobile colloid concentration in the pore volume, if all colloids were to detach, is defined as C_c^0 according to Eqn. 6.3. The model used pseudo-first-order rate constants for Pu (de)sorption on colloids based on the assumption that the concentration of colloids in the aqueous and solid phase was much greater than the concentration of Pu. Therefore, the model is insensitive to the total concentration of colloids in the system, and colloid concentrations were reported normalized to S_c^0 or C_c^0. The source term for the transport model was a finite-step input of colloid-free loading solution containing Pu at a concentration of $C_{Pu,0}$. Aqueous Pu concentrations were reported normalized to $C_{Pu,0}$.

$$C_c^0 = \frac{\rho}{\theta} S_c^0 \tag{6.3}$$

Pu Transport Facilitated by Soil Organic Matter

Since the organic matter in this soil has not been characterized, a single organic ligand with properties representative of the dissolved soil organic matter was considered. This organic ligand was a hypothetical concept used for modeling purposes and does not represent any specifically defined organic molecule. In this conceptual model of ligand-facilitated transport, the organic ligand desorbed and re-adsorbed on the soil surfaces. The organic ligand also formed aqueous complexes and ternary surface complexes with Pu. The same variables were used for the ligand-facilitated transport model as for the colloid-facilitated transport model, but the conceptual meaning of the reactions has been changed (Table 6.4). The key difference from the colloid-facilitated transport model was that ligand sorption and complexation reactions were assumed to reach equilibrium instantaneously, with equilibrium described by a ligand distribution coefficient, K_d^{ligand}, and a conditional stability constant, K'_{PuL} (See Appendix D for model details). Throughout modeling the Pu distribution coefficient, K_d, was fixed at 1000 $mL \cdot g^{-1}$ in order to roughly capture the Pu soil distribution in the first 2 cm of the columns. Since the dissolved organic matter originates from the soil, initial conditions specified a uniform distribution of sorbed organic ligand in the soil and no aqueous organic ligand initially present.

Table 6.4. Variable definitions for the ligand-facilitated transport model, where M represents the solute mass units and n represents the ligand mass units.

Variable	Units	Species description
C_{Pu}	$M\cdot cm^{-3}$	aqueous concentration of free ionic Pu
S_{Pu}	$M\cdot g^{-1}$	Pu sorbed to the solid phase
$S_{mc}\cdot C_c$	$M\cdot cm^{-3}$	aqueous Pu-ligand complexes
$S_{ic}\cdot S_c$	$M\cdot g^{-1}$	sorbed Pu-ligand complexes (ternary complexes)
C_c	$n\cdot cm^{-3}$	dissolved ligand concentration
S_c	$n\cdot g^{-1}$	sorbed ligand concentration
K_d	$cm^3\cdot g^{-1}$	Pu distribution coefficient
K_d^{ligand}	$cm^3\cdot g^{-1}$	ligand distribution coefficient
K'_{PuL}	-	Pu–ligand complex conditional stability constant

Results and Discussion

Pu Distribution Coefficient on SRS Soil

The calculated distribution coefficient for Pu on SRS soil was 1390 $mL\cdot g^{-1}$, and was determined from a batch test with 25 $g\cdot L^{-1}$ soil. The measured K_d was lower than the previously reported values of 2100 $mL\cdot g^{-1}$ and 3000 $mL\cdot g^{-1}$ which were reported for Pu(IV) in batch tests with sandy loam soil from the SRS (Powell et al., 2002). The difference may be due to differences in soil composition, such as clay fraction minerology, iron content, or organic content.

Tracer Results

The elution profiles for ^3H, which was used as a conservative tracer to monitor for channeling, contained a single symmetric peak which was first detected after the displacement of one pore volume (Fig. 6.4). The data was fitted with the analytical solution to the one-dimensional advection-dispersion equation (Eqn. 6.1) in order to estimate retardation and longitudinal dispersion coefficients. The retardation coefficients, *R*, for tritium ranged from 1.01 to 1.04, and the dispersion coefficients, *D*, ranged from 0.015 to 0.022 $cm^2 \cdot min^{-1}$ (Table 6.5). This is similar to the previously determined value 0.046 $cm^2 \cdot min^{-1}$ determined by Haliena et al. (2016) for sandy soils from the SRS, but is much lower than the dispersion coefficient of 1.8 $cm^2 \cdot min^{-1}$ determined by Fjeld et al. (2003) for another sandy loam soil from the SRS. The model over-estimated the peak ^3H concentration in the case of the citrate and DFOB columns, and under-estimated the broadness of the ^3H elution curve for the citrate column. Overall, the ^3H data supported the use of the classical advection-dispersion model and showed excellent recovery.

Table 6.5. Column results and parameters for the tritium tracer analysis. Uncertainty is based on the 0.1 g precision of the balance used to weigh the column apparatus.

Experiment	R (-)	Disp. D [(a)] ($cm^2 \cdot min^{-1}$)	Porosity φ (-)	Bulk Dens. ρ ($g \cdot cm^{-3}$)	Pore Volume (mL) [b]	Residence Time (min)	Recovery (%)
Control	1.04 ± 0.04	0.022	0.449 ± 0.018	1.25 ± 0.04	5.3	51.5	101
Citrate	1.01 ± 0.05	0.020	0.466 ± 0.024	1.49 ± 0.03	5.5	57.0	104
DFOB	1.01 ± 0.06	0.015	0.389 ± 0.024	1.44 ± 0.03	4.6	49.3	90

[a] The longitudinal dispersion coefficient was not sensitive to 0.1 g uncertainty in water or soil masses.

[b] Uncertainty in pore volume was 0.1 g due to the precision of the balance.

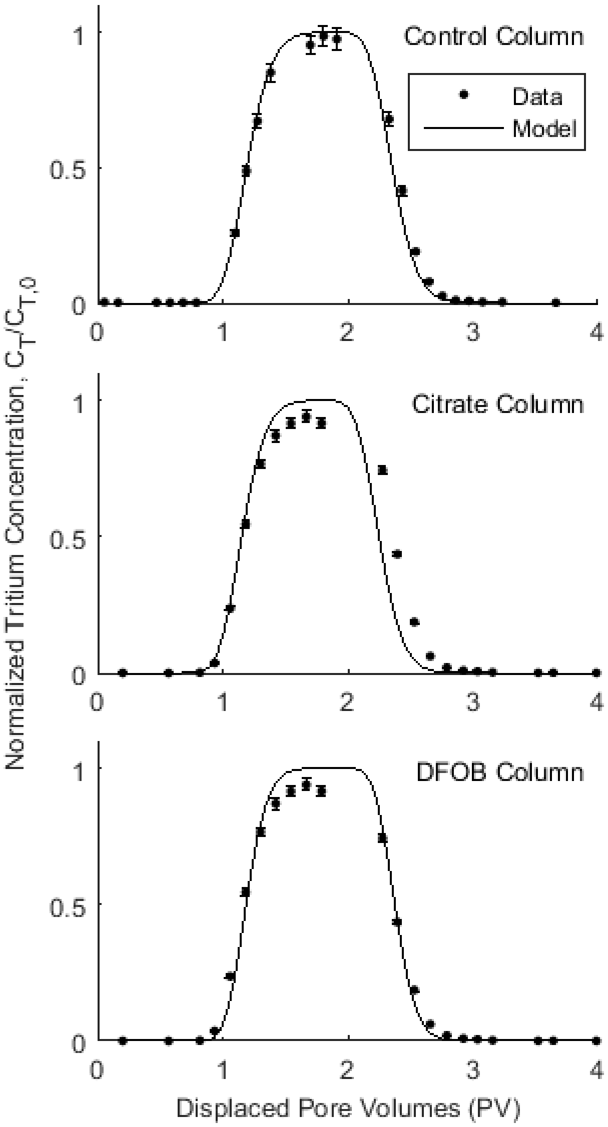

Figure 6.4. Elution profile of the tritium tracer with the one-dimensional advection-dispersion model. The concentration of ^{3}H is shown normalized against the ^{3}H concentration in the spike solution, $C_{T,0}$, which was introduced as a one PV finite step. The recoveries in the control, citrate, and DFOB column experiments were 101%, 104%, and 90%, respectively.

Pu Column Effluent Results

In the elution profiles of all three column experiments, a single well-defined Pu peak was observed (Fig. 6.5). The elution profiles of this mobile Pu were remarkably similar in timing and shape for all three experiments. The mobile Pu was first detected after the displacement of 7–8 PV, and Pu concentrations peaked at ≈17 PV. This mobile Pu comprised 9.1%, 9.3%, and 20% of the total Pu added to the control, citrate, and DFOB experiments, respectively (Table 6.6). The peaks were broad and had more tailing than could be accounted for by one-dimensional advection-dispersion equation (Eqn. 6.1). This suggested that there was some process causing a distribution of Pu arrival times. For instance, sorption of the mobile Pu may have been kinetically limited relative to the residence time of the mobile Pu. Because the peak shape was non-ideal, the centroid of each peak was used to estimate the following retardation factors for mobile Pu: 25, 29, and 24 in the control, citrate and DFOB experiments, respectively.

Table 6.6. Pu recovery as a percent of total Pu

Experiment	Total Pu Loaded (10^{-10} mol)	Aqueous Recovery (%)	Soil Recovery (%)	Total Recovery (%)	Mobile Pu Retardation Factor, *R*
Organic-free	0.025	9.08 ± 0.10	92.4 ± 0.8	101.5 ± 0.9	25
Citrate	0.033	9.29 ± 0.06	64.9 ± 0.5	74.2 ± 0.5	29
DFOB	0.023	19.99 ± 0.21	108.6 ± 0.5	128.6 ± 0.6	24

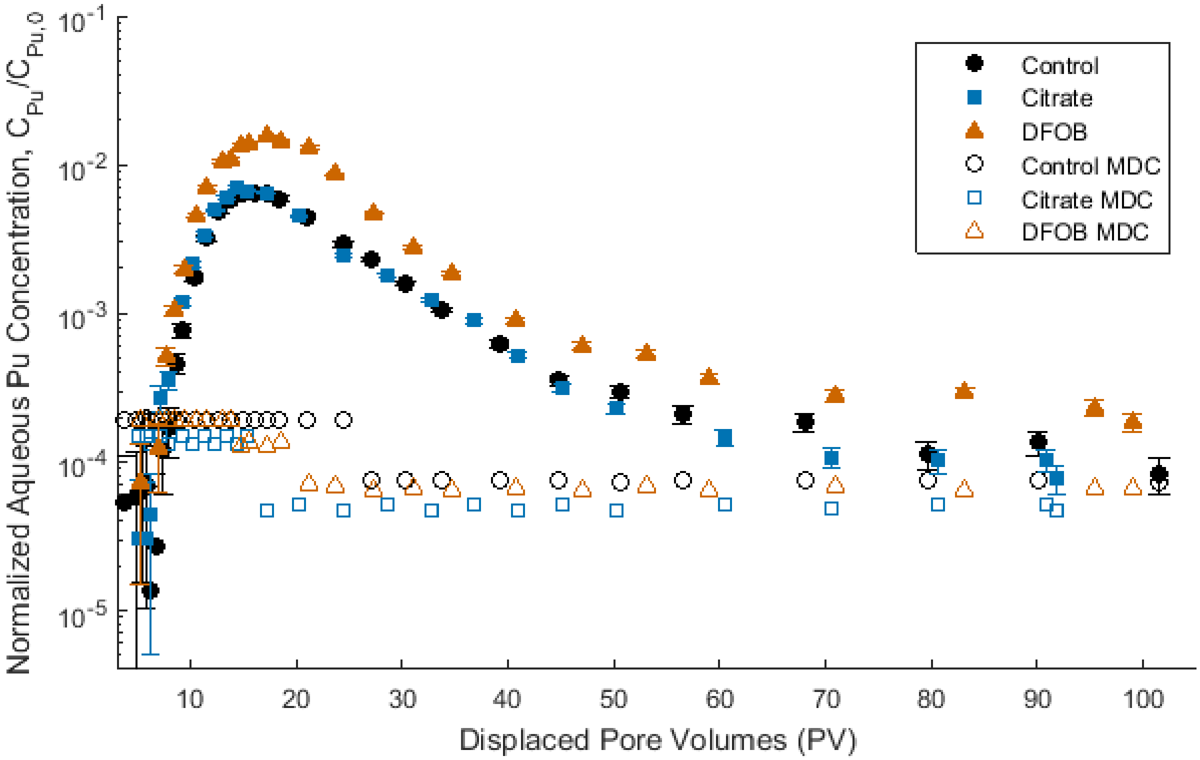

Figure 6.5. Pu elution profile for columns packed with soil from the SRS. The organic-free Pu spike solution was added as a one PV finite step followed by 2–3 PV background solution and ≈100 PV of citrate, DFOB, or organic-free solution as noted in the legend. The concentration of Pu is shown normalized against the Pu concentration of the spike solution, $C_{Pu,0}$. The minimum detectable concentration for each sample depended on sample volume. Note: Despite the experiment names including each organic ligand, the ligands were predicted to migrate no more than 1.3 cm into the column, limiting the interaction between the organic ligands and Pu. Conditions: 10 mM NaCl; pH = 4.8 ± 0.2

Because similar elution profiles were observed in all three experiments, including the organic-free column, the addition of citrate and DFOB solution appeared to have no effect on Pu mobility. This was in contrast to previous studies which demonstrated the formation of strong aqueous Pu–ligand complexes in the presence of citrate and DFOB which is expected to increase the fraction of aqueous Pu, and, thus enhance Pu mobility (Conroy et al., 2017; Simpkins, 2011; Zimmerman et al., 2014). The sorption of citrate and

DFOB to the soil was further examined to determine whether the limited transport of citrate and DFOB in the columns could explain their lack of effect on Pu mobility.

In order to better understand the distribution and transport of citrate and DFOB in the columns, sorption isotherms of DFOB and citrate were determined for this soil (Fig. C.3). Subsequent transport calculations (Appendix C) estimated that, although the citrate and DFOB reached high concentrations in the soil (88% and 48% surface coverage, respectively), citrate and DFOB traveled no further than 0.68 cm and 1.32 cm into the columns, respectively. Thus the interaction of citrate and DFOB with Pu was predicted to be limited.

The surprisingly high amount of sorption exhibited by citrate and DFOB on this soil might be due to the large clay-sized fraction. Citrate has previously been shown to adsorb to clay minerals (Lackovic et al., 2003). Although DFOB has previously been shown to adsorb to montmorillonite, a smectite clay mineral (Siebner-Freibach et al., 2004), >95% of the silt/clay-sized fraction is kaolinite to which DFOB adsorbs only slightly (Siebner-Freibach et al., 2004). It's possible that up to 5% of the silt/clay-sized fraction is montmorillonite. The apparently strong sorption of both DFOB and citrate to this soil, retaining the organic ligands at the front of the column, explains why the presence of organic ligands in the column influent solution had no effect on the breakthrough of the mobile Pu relative to the control experiment.

Possible Process Affecting Pu Mobility

It is possible that the mobile Pu consisted of Pu(V) which formed in the spike solution, aqueous Pu complexes formed with dissolved soil organic matter, or Pu adsorbed to mobile mineral or organic colloids. These three hypotheses are described below, and reactive transport modeling was performed to demonstrate these processes (presented after soil results).

First, the presence of Pu(V) is considered. The observed retardation factors (Table 6.6) are greater than those previously observed (4.4 to 4.8) for Pu(V) in a subsurface sandy SRS soil (Powell et al., 2014) which might suggest that the mobile Pu was not Pu(V). However, this difference could be due to different soil composition since the silt/clay-size fraction (34.4%) of this soil is dominated by kaolinite, and the soil used in the previous work (Powell et al., 2014) was <1% clay-sized particles with vermiculite, gibbsite, and goethite coatings as the major reactive mineral phases. Some Pu may have oxidized from Pu(IV) to Pu(V) during the ≈1.5 h that elapsed after adding Pu to the spike solutions. The rate of oxidation from Pu(IV) to Pu(V) is sensitive to solution pH and increases with increasing pH (Choppin et al., 1997; Powell et al., 2011). Increasing the pH of the solution to 4.8 is expected to have allowed some Pu(IV) to oxidize to Pu(V). In tests of simulated spike solutions prepared from a 99.9% Pu(IV) stock, 16 ± 5 % of Pu was observed to become oxidized during the timeframe of the spike preparation and pH adjustment (Appendix C). This percentage is similar to the percentage of Pu recovered in the effluent. However, the implication is that the oxidized Pu traveled through the column with little to no reduction to Pu(IV). Previous studies have observed greater than 90% of Pu(V) reduces to Pu(IV) in within 24 h in the presence of iron oxides (Powell et al., 2005, 2004; Sanchez et al., 1985). This soil contains 2.64% Fe as Fe_2O_3 but the Fe mineralogy is unknown as specific Fe oxides were not observed in XRD analysis. Thus, the Fe may be bound within phyllosilicate phases which exhibit slower reduction kinetics and, thus, allow for transport of Pu(V) through the column with the observed retardation factors of 24–29.

The mobile Pu could also represent Pu sorbed to mobile colloids. Numerous previous studies have suggested Pu may be mobilized by sorption to mobile colloids (Kersting et al., 1999; Novikov et al., 2006; Santschi et al., 2002). The large clay-sized fraction of this soil could be a source of colloids. In order to determine whether elements associated with mineral colloids were present in the effluent, the effluent from the Pu-free column was acidified and measured for Mg, Ca, Al, and, Fe using ICP-MS. A sample of background solution was also measured for comparison. The concentrations of Mg, Ca, and Al were elevated relative to the background solution (Fig. C.6), and the concentrations decreased over the first 60 PV before reaching steady-state. The ratio of the concentration in the first effluent fraction to the steady state concentration was calculated. These ratios were 310, 27, and 18 for Mg, Ca, and Al respectively. The Fe concentration was elevated relative to the background solution in one measurement representing 17–35 PV, but was otherwise at background levels (Fig. C.7). The elevated concentrations of these elements in the effluent suggest possible mineral dissolution or colloid formation in the soil column.

Another possible explanation for the presence of the mobile Pu could be the formation of aqueous complexes with dissolved soil organic matter. The column test to measure soil organic matter (Fig. C.5) suggested there may be 0.52 to 0.12 $mg_c \cdot L^{-1}$ soil organic matter present in the pore water. Previous studies have observed diminished Pu sorption to mineral surfaces in the presence of natural organic ligands caused by the formation of stable aqueous Pu–ligand complexes (Buda et al., 2008; Conroy et al., 2017; Simpkins, 2011; Zimmerman et al., 2014), but this was at higher TOC concentrations than were observed in the column test. While a DFOB concentration of 0.5 $mg_C \cdot L^{-1}$ has been demonstrated to diminish the sorption of Pu(IV) to goethite (Wong et al., 2015), it is unlikely that natural soil organic matter has Pu complexation strength similar to DFOB. In order for soil organic matter to enhance Pu mobility, the soil organic matter must be mobile in the soil and form stable complexes with Pu. However, characterizing the dissolved organic matter in this soil is beyond the scope of this work, and so the composition of the soil organic matter remains unknown.

It is important to keep in mind that these proposed processes resulting in mobile forms of Pu are speculative. While the mobile Pu had similar arrival times in all three column experiments, and, therefore, resulted from a process that each had in common, the precise form of mobile Pu cannot be determined from this data.

Measurements of Pu in Soil

After the elution of ≈100 PV, the columns were segmented (1.5 to 10 mm thick) to determine the solid phase distribution of Pu within each column. Soil recovery of Pu from leaching with 6 M HNO_3 was 93%, 65%, and 109% for the ligand-free control, citrate, and DFOB columns, respectively (Table 6.6). The low recovery of Pu within the citrate column is likely due to incomplete recovery of the soil from the front end cap of the column. In both the DFOB and ligand-free control columns, a significant amount of the total Pu was contained within the small amount of soil rinsed from the front end cap. While uncapping the columns and inserting the plunger used for sectioning, a few grains of sand and a few droplets of water containing silt and clay were lost from the front of the columns. Since Pu is concentrated at the front of the column against the end cap, the loss of a small amount of soil from this location could represent a disproportionate deficiency in the Pu mass balance.

In the columns, 49–80 % of the *soil-bound* Pu was found in the first 2 cm of the column profile with the rest distributed from 2 to 15 cm (Table 6.7; Figs. 6.6 and C.10). The average Pu concentrations measured between 2 and 15 cm were $3.1 \pm 1.3 \times 10^{-14}$ mol·g^{-1}, $7.4 \pm 3.1 \times 10^{-14}$ mol·g^{-1}, and $4.2 \pm 2.1 \times 10^{-14}$ mol·g^{-1} for the control, citrate, and DFOB columns, respectively. The Pu distributed between 2 and 15 cm may have been left by the passage of the mobile Pu through the column. The mechanism for retaining this Pu in the soil would have depended on the form of the mobile Pu. As expected, Pu(IV) mobility in the columns was limited in the ligand-free column and in columns where the citrate and the DFOB are expected to be soil-bound. This is consistent with previous studies which have determined large K_d values for Pu(IV) on soil from the SRS which are expected to limit its mobility (Powell et al., 2002; Prout, 1958), and with previous observations of Pu(IV) transport (Powell et al., 2014).

Table 6.7. Pu distribution in soil column as a percent of Pu recovered from soil acid leaching

Experiment	< 1 cm (%)	< 2 cm (%)	2 to 15 cm (%)
Control	75	80	20
Citrate	37	49	51
DFOB	65	80	20

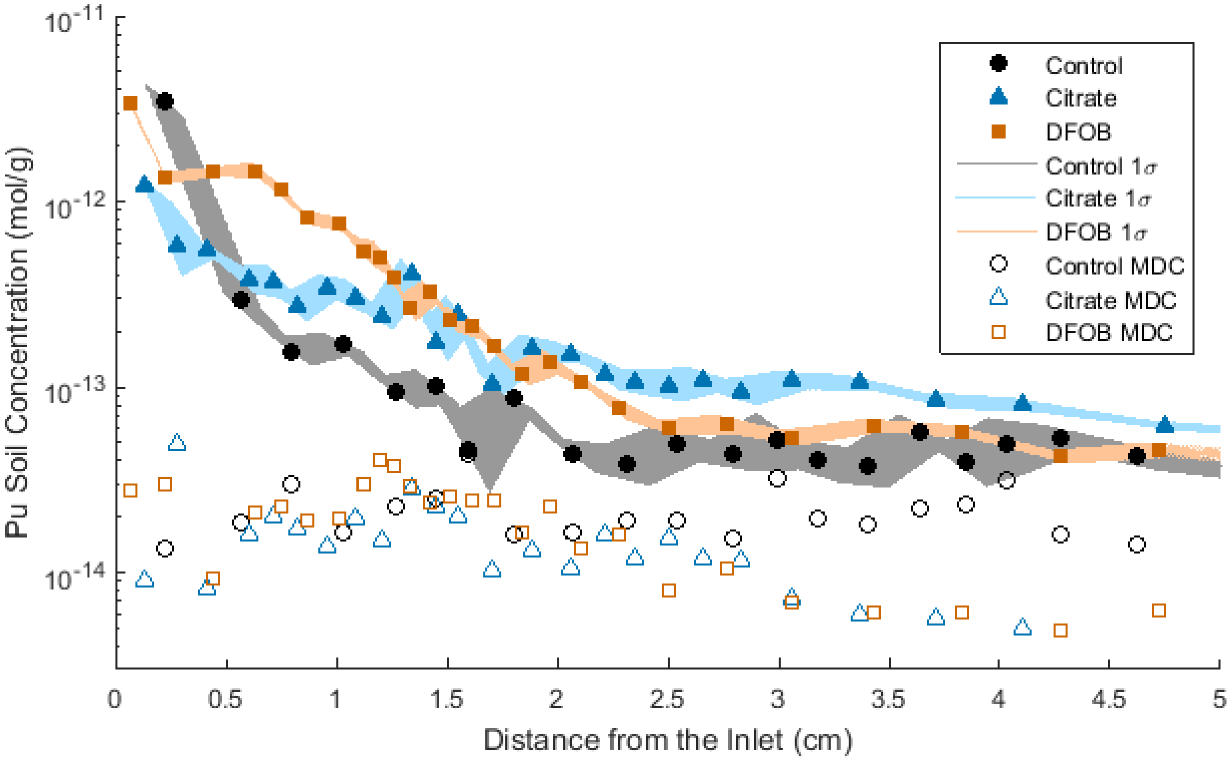

Figure 6.6. Pu soil profile in columns packed with soil from the SRS. The uncertainty in the Pu soil concentration and the distance from the inlet were derived from counting statistics and the uncertainty in the mass of soil sections. The 1σ confidence band is shown.

The original purpose of adding ≈100 PV of ligand solutions to the columns was to flood the soil with an organic ligand and to examine Pu mobilization under the conditions of uniform ligand concentration and flux. However, strong sorption of citrate and DFOB resulted in regions of concentrated ligand at the front of the columns. Despite this unintentional feature, there were subtle differences in Pu mobility in the soil profiles which may suggest that Pu mobility was enhanced in by the organic ligands, relative to the control experiment where no ligand was added. In the DFOB experiment, elevated Pu soil concentrations were observed within 2.5 cm of the inlet, with 80% of soil-bound Pu within the first 2 cm. The region of elevated Pu overlapped the DFOB front which was predicted to extended 1.3 cm into the column. Aqueous Pu–ligand complexes may have formed within the DFOB front, but the formation of aqueous Pu–ligand complexes was not expected to enhance Pu mobility beyond the DFOB front. Outside this region, any Pu which uncomplexed from DFOB would strongly adsorb to the sediment. In the citrate experiment, slightly elevated Pu soil concentrations were observed between 0.5 and 14 cm in the column. While the Pu soil concentration is consistently greater than that measured in the organic-free column in ≈20 measurements, elevated Pu soil concentration may be due to variations between experiments, such as differences in soil packing or heterogeneity of the natural soil.

Reactive Transport Modeling Results

In this work, three main hypotheses have been discussed as possible explanations for the mobile Pu eluted from the columns as well as Pu soil distributions:

1. A portion of Pu(V) which was present in the Pu loading solution did not reduce to Pu(IV) in the column and was eluted.
2. Colloids were generated in the soil during the experiment which resulted in colloid-facilitated transport of Pu.
3. Native soil organic matter dissolved into solution and formed aqueous complexes with Pu.

The purpose of this speculative modeling exercise was to determine whether transport models based on these three processes could reasonably explain the experimental data. The transport models were used to create predictive elution and soil profiles for Pu in the column experiments. Parameter values for the transport models were based on values reported in literature (Tables D.4, D.5, and D.7), but there was great uncertainty in the parameter values. The parameters were systematically varied in order to explore a range of possible model outputs. The modeling results were compared to both the Pu elution profiles and the Pu soil distributions. However, each of these models contained simplifying assumptions and may not fully describe the complexity of the experiments.

Model for Pu Transport with Surface Mediated Reduction

Previous studies have successfully modeled Pu transport, distribution, and redox state in the presence of iron oxides using models which included surface mediated reduction (Demirkanli et al., 2007; Fjeld et al., 2003; Powell et al., 2005, 2004). Parameters for Pu(IV) and Pu(V) distribution coefficients, K_d^{IV} and K_d^{V}, reduction rate constant in the solid phase, μ'_s, and fraction of Pu(V), $f_{Pu(V)}$, were systematically varied (Tables 6.8 and D.3) to determine whether the surface mediated reduction model might be a reasonable process to explain the observed soil and aqueous Pu distributions, or if surface mediated reduction should be ruled out as a primary process.

Table 6.8. Parameters for consideration in the surface mediated reduction model

Parameter	Units	Literature Range	Range Modeled	Reasonable Fit
K_d^{IV}	mL·g^{-1}	200 – 3000	200 – 3000	600 – 3000
K_d^{V}	mL·g^{-1}	6 – 2500	6 – 30	8
μ'_s	min^{-1}	6 ×10^{-6} – 0.1	(0.3 – 3.0) ×10^{-3}	(0.5 – 1.5) ×10^{-3}
$f_{Pu(V)}$	-		0.05 – 0.80	0.20 – 0.50

In the surface mediated reduction model, the K_d^{IV} parameter controlled the position of the Pu peak in the soil profile, and the K_d^{V} parameter controlled the timing of the elution of Pu. The model was sensitive to the reduction rate constant, because the passage of Pu(V) through the column and reduction of Pu(V) to Pu(IV) determine the distribution of Pu from 2 to 15 cm. Once reduced to Pu(IV), the movement of Pu in the soil was retarded. The fraction of Pu(V) in the loading solution determined the amount of Pu(V) which was available for reduction and deposition throughout the soil column.

The range of parameters modeled was selected to push the limits of fitting the data, and generally fell within the range of values provided from literature (Table D.4). The result of a base case is provided in Fig. 6.7 for consideration. The full set of model results and parameter values from previously published works are provided in Appendix D. The surface mediated reduction model provided reasonable fits to the soil profile with reduction rate constants in the range $0.5–1.5 \times 10^{-3}$ min^{-1}, which is similar to the value of 0.8×10^{-3} previously measured on soil from the Savannah River Site (Kaplan et al., 2001). The non-zero values of reduction rate constant, indicate that surface mediated reduction was significant (Figs D.4–D.8). Reasonable fits to the Pu soil profile were obtained for K_d^{IV} values of 600–3000 $\text{mL}\cdot\text{g}^{-1}$, and the K_d^{V} value of 8 $\text{mL}\cdot\text{g}^{-1}$ provided the best fit to the Pu effluent peak. These Pu distribution coefficients are consistent with previous observations of soil from the Savannah River Site (Powell et al., 2002; Prout, 1958). When the fraction of Pu(V) in the loading solution was varied, a range of 0.2–0.5 was found to provide reasonable fits to the Pu soil profile. When the surface mediated reduction model was run with a $f_{Pu(V)}$ value less than 0.2, the results underestimated the soil concentration of Pu between 2 and 15 cm. Thus, at least 20% of Pu in the loading solution would be required to oxidize to Pu(V) in order to accurately predict the Pu soil profile. This is consistent with the estimate that 16 ± 5% of Pu in the loading solution could have oxidized to Pu(V).

Although the surface mediated reduction model could be parameterized to fit the Pu soil profile excellently, the model performed poorly at predicting the Pu elution profile which exhibited a broad peak with tailing. It's possible that this tailing was due to a kinetic limitation of Pu(V) adsorption/desorption. The surface mediated reduction model otherwise demonstrated an excellent fit to the data. Therefore, surface mediated reduction cannot be ruled out a possible explanation for the Pu data.

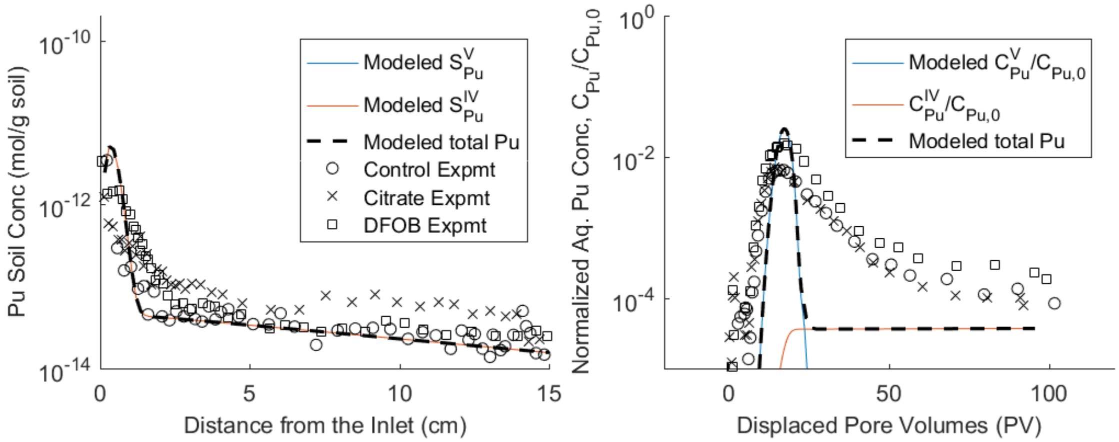

Figure 6.7. A reactive transport model which includes surface mediated reduction was used to predict concentrations of Pu(IV) and Pu(V) in the soil profile (left) and in the elution profile (right). Experimental data from the control, citrate, and DFOB column experiments is shown. $\mu's$ = 0.0008 min^{-1}; K_d^{IV} = 1000 mL·g^{-1}; K_d^{V} = 8 mL·g^{-1}; $f_{Pu(V)}$ = 0.2

Model for Colloid-Facilitated Transport

Previous studies of mineral colloids found in soils from the Savannah River Site and elsewhere on the Atlantic Coastal Plain have been characterized as ferric oxyhydroxides and kaolinite (Bunn et al., 2002; Haliena et al., 2016; Seaman et al., 2007). Under the assumption that the soil in this study contained colloidal ferric oxyhydroxides and kaolinite, published rate constants for colloid attachment, detachment, and Pu (de)sorption on these minerals were used as a starting point for choosing model parameters (Tables 6.9 and D.5).

Preliminary results using the colloid-facilitated transport model indicated that it was not possible to simultaneously fit the Pu soil profile and the Pu elution profile. A range of parameters (Table 6.9) was chosen for which it was generally possible to demonstrate Pu in the soil column at 2–15 cm as well as Pu breakthrough with similar timing to experiment observations (Figs. 6.8 and 6.9; detailed results in Appendix D). This range of parameters was used to determine the effect of each parameter on the model results. In models where Pu was predicted between 2 and 15 cm, it was in the form of Pu sorbed to colloids remaining in the column. This created a continuous supply of Pu-carrying colloids to the eluted solution which resulted in an elution profile where the Pu concentration reached a plateau, but did not exhibit a peak (Fig. 6.8). The only cases in which the model was able to predict a Pu effluent peak were ones where Pu effluent concentration declined because Pu could no longer be scavenged from the soil by colloids. This occurred when the colloid mobility (controlled by k_{att} and k_{det}) was so great that colloids were completely flushed from the column (Fig. 6.9), or when the colloids could not effectively compete with the soil for Pu (Figs. D.42 and D.43). In each of these cases, the Pu concentration of the effluent was underestimated, the effluent peak was predicted to be too broad, or no Pu was predicted in the column between 2 and 15 cm. So although the colloid-facilitated transport model can predict enhanced Pu mobility by sorption and retention on colloids, it performed poorly at simultaneously fitting soil and effluent data.

Table 6.9. Range of parameter values modeled with colloid-facilitated transport model

Parameter	Units	Literature Range	Range Presented
k_{att}	min^{-1}	0.005 – 5	0.01 – 0.15
k_{det}	min^{-1}	0.015 – 0.070	5×10^{-5} – 0.005
k_{ac}	min^{-1}	5×10^{-6} – 0.01	0.3 – 5
k_{dc}	min^{-1}	$(0.7 – 2.3) \times 10^{-4}$	1×10^{-5} – 0.002
K_d	mL·g^{-1}	200 – 3000	200 – 5000

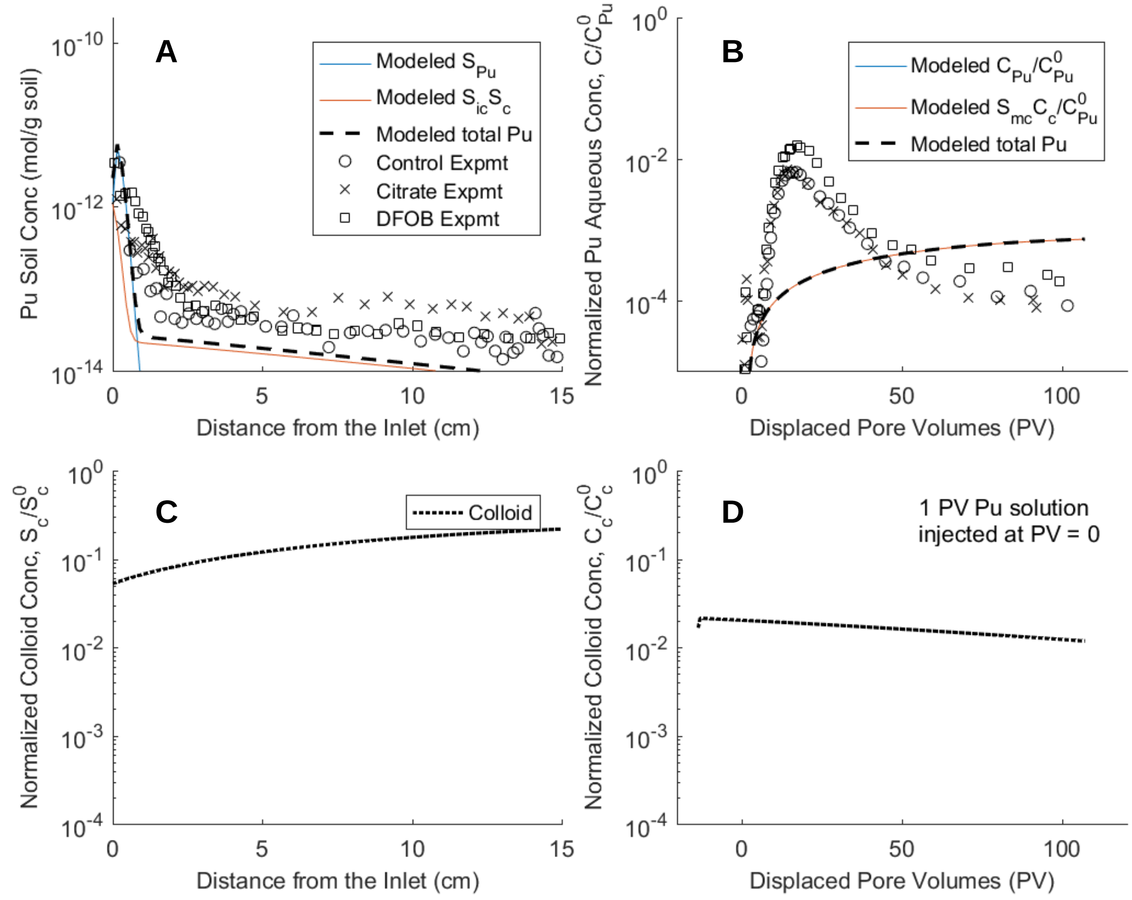

Figure 6.8. Predicted concentrations of Pu and colloids in the soil profile and elution profile. Displayed are the Pu soil concentration (A), the Pu effluent concentration (B), the colloid concentration in the column (C), and the colloid concentration in the effluent (D). Experimental data from the control, citrate, and DFOB column experiments is shown. $k_{att} = 0.04\ \text{min}^{-1}$; $k_{det} = 3 \times 10^{-4}\ \text{min}^{-1}$; $k_{ac} = 1.0\ \text{min}^{-1}$; $k_{dc} = 6.9 \times 10^{-5}\ \text{min}^{-1}$; $K_d = 2000\ \text{mL·g}^{-1}$

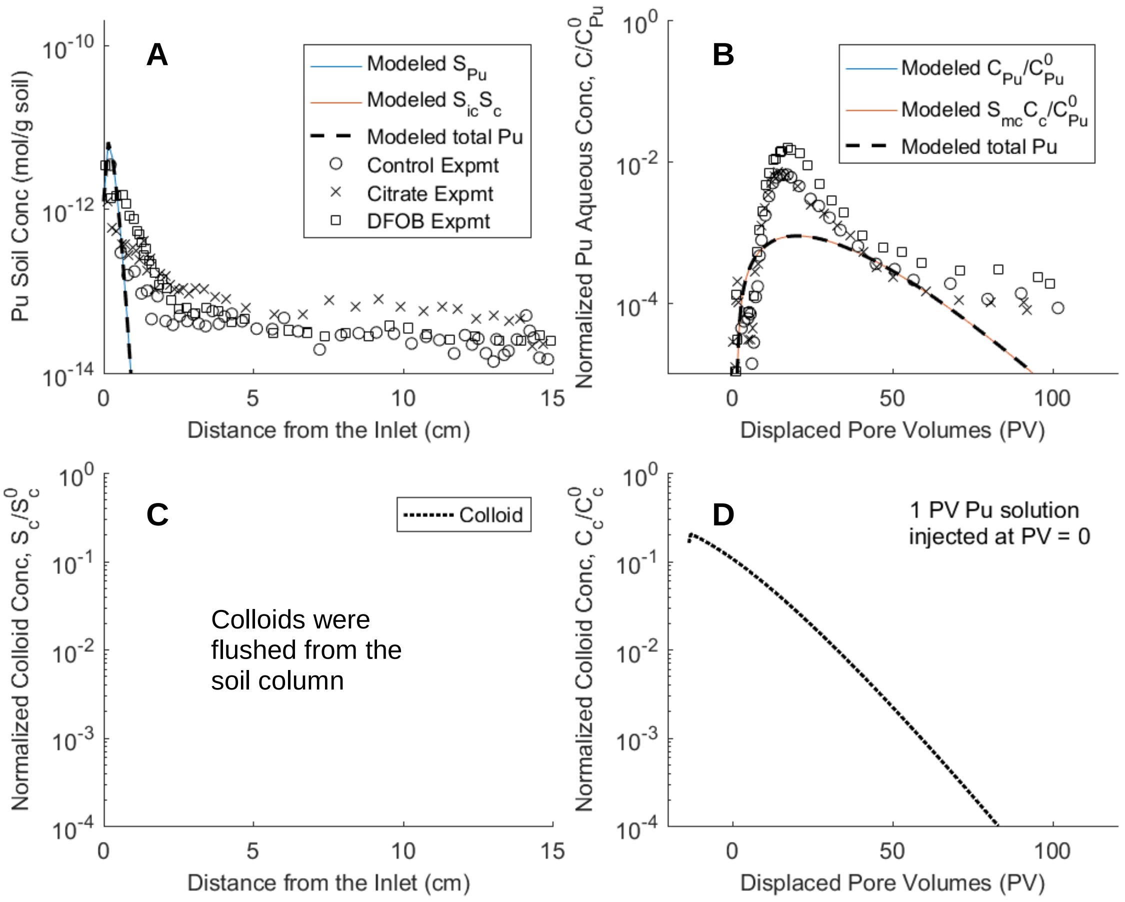

Figure 6.9. Predicted concentrations of Pu and colloids in the soil profile and elution profile. Displayed are the Pu soil concentration (A), the Pu effluent concentration (B), the colloid concentration in the column (C), and the colloid concentration in the effluent (D). Experimental data from the control, citrate, and DFOB column experiments is shown. k_{att} = 0.04 min^{-1}; k_{det} = 3 × 10^{-3} min^{-1}; k_{ac} = 5.0 min^{-1}; k_{dc} = 6.9 × 10^{-5} min^{-1}; K_d = 2000 mL·g^{-1}

The range of parameters presented (Table 6.9) roughly represents the outer bounds for which colloid-facilitated transport with a resemblance to the observed experiment results could occur. The values of k_{att} fell between the reported values for kaolinite and goethite colloid attachment to quartz (0.011 min^{-1} and 4.7 min^{-1}, respectively) which was consistent with colloids composed of a mixture of these minerals (Saiers and Hornberger, 1996; Wang et al., 2015). The values of k_{det} were lower than those determined from literature, but these studies (Bunn et al., 2002; Ryan and Gschwend, 1994a) were conducted at pH 9–11 under transient flow conditions which enhanced colloid detachment. The values of k_{ac} were higher than those previously estimated (Ohnuki et al., 2007; Painter et al., 2002; Powell et al., 2005; Romanchuk et al., 2011), and this could be due to a difference in Pu oxidation state, mineral composition, or other experimental conditions. The values of k_{dc} and K_d were similar to those determined from literature. Although literature data for reaction rate constants was sparse, the agreement of some of the model parameters suggests that the parameter values chosen for the model were not unrealistic.

Overall, this model for colloid-facilitated transport could predict the peak concentration in the solid phase, but was unable to fit the peak shape of the effluent profile. The process of colloid-facilitated transport *as it is formulated in this work* is unsuccessful at explaining the experimental data. However, a more nuanced model of colloid-facilitated transport might represent transport processes more accurately. For instance, colloid straining or filtration might retain Pu-carrying colloids in the soil even if colloids are otherwise relatively mobile. Therefore, colloid-facilitated transport cannot be ruled out as a possible transport process which occurred in the column experiments.

Model for Transport Facilitated by Soil Organic Matter

The limits of the ligand-facilitated transport model were tested across a wide range of values for K_d^{ligand} and K'_{PuL} (Table D.8), but it was unable to predict the elution profile of Pu from the column, and it predicted the Pu soil profile poorly. When the mobility of the organic ligand (controlled by K_d^{ligand}) was increased sufficiently to elute Pu from the column, the organic ligand was flushed down-gradient before it contacted any Pu. Despite varying the K'_{PuL} value over four orders of magnitude, this limitation could not be overcome. The modeling results departed from the experimental data over an extensive range of parameters. This indicated that the process of ligand-facilitated transport *as it is formulated in this model* should be ruled out as an explanation for the observed experimental data. Although the assumptions of the ligand-facilitated transport model neglected some realistic conditions—heterogeneous organic matter, kinetic effects, heterogeneous sorption sites—examining these is beyond the scope of this work.

Implications

In this study, little, if any enhancement of Pu mobility by citrate and DFOB was observed in a natural soil from the Savannah River Site. However, in each of the three columns, 9–20 % of Pu was observed to elute with retardation factors of 24–29. Due to the strong sorption of citrate and DFOB to the soil, the influence of citrate and DFOB may have been confined to a limited region near the column entrance. As a result, it is unlikely that Pu–ligand aqueous complexes influenced the transport of Pu in the soil. Importantly, sorption of citrate and DFOB was demonstrated to be sufficiently strong to this Savannah River Site soil that their impact on Pu mobility is likely to be negligible on a field scale.

Multiple working hypotheses may explain the data presented: (1) oxidation of Pu(IV) to Pu(V) within the spike solution during pH adjustment, (2) colloid-facilitated transport, and (3) mobilization by of Pu–(organic matter) complexes with native SOM. Reactive transport modeling with the hypothesized processes was unsuccessful at demonstrating either colloid-facilitated transport or Pu mobilization by soil organic matter, possibly due to simplifying assumptions. The persistence of Pu(V) in the soil was demonstrated as the most likely explanation, but there was no direct evidence to support this. Determination of the exact mechanism occurring is beyond the scope of this study (focused on examining the influence of citrate and DFOB) but will be the subject of future work. From these processes, it is clear that Pu mobility in natural soils depends on many complex interactions potentially involving soil composition, Pu redox reactions, ligand sorption, soil organic matter, and mineral colloids.

CHAPTER SEVEN

CONCLUSIONS AND FUTURE WORK

Conclusions

This work investigated aging of Pu on the surface of goethite, the effect of natural organic ligands on the enhancement of Pu desorption and mobility, and Pu transport in natural soil from the SRS. Pu aging was observed in a batch desorption experiment with goethite over 116 days (Chapter 4), and also in a flow-cell desorption experiment with stop and flow events over 3 days (Chapter 5). In Chapter 4, Pu aging was found to be pH dependent and determined to not be a redox process. However, the exact Pu aging process is unknown and cannot be determined from indirect measurements of aqueous Pu concentration as was done in this work. However, even this empirical determination of an aging process suggests that, in the environment, the magnitude of Pu aging depends on geochemical conditions, and that Pu aging will happen regardless of Pu redox transformations. In Chapter 5, a conceptual model for aging which considered two consecutive linear sorption components was used to describe the kinetics of Pu (de)sorption in the presence of DFOB, fulvic acid, and citric acid. The exact speciation or state of Pu on the surface was unknown. Therefore, for modeling purposes, each state was distinguished based on different kinetic rates of uptake and release. The model used apparent first-order rate constants to describe the sorption of Pu and the transfer from the first surface state to the second.

Organic ligands were observed to enhance Pu desorption in flow-cell experiments, relative to systems where no organic ligand was added. In flow-cell experiments, greater

Pu desorption was observed in the presence of DFOB than citrate, likely due to the greater relative stability of the Pu–DFOB aqueous complex compared to the Pu–citrate aqueous complex, and the electrostatic repulsion of the expected dominant $PuH_2(DFOB)_2^{2+}$ species from the positively charged goethite surface. Compared to DFOB, fulvic acid was less effective at enhancing Pu desorption in the flow-cell experiments. Based on these results, natural organic ligands have the potential to mobilize Pu in substrates where reactive surfaces are dominated by goethite.

In the column experiments with SRS soil (Chapter 6), the interpretation of ligand effects on Pu mobility was complex. Both DFOB and citrate adsorbed strongly to the SRS soil which limited the influence of these organic ligands despite the loading of ≈100 pore volumes of organic ligand solution. Since DFOB and citrate traveled no further than 1.5 cm into the columns, the strength of Pu–ligand aqueous complexes did not appear to affect the extent of Pu transport. Thus, the processes controlling Pu transport in the soil column were more complex than simple competition of organic ligands for Pu with surface sites. Importantly, sorption of citrate and DFOB was demonstrated to be sufficiently strong to this Savannah River Site soil that their impact on Pu mobility is likely to be negligible on a field scale. These results indicate that it is critical to understand both the ligand sorption as well as Pu sorption. Comparison of experiments using pure goethite and SRS soil indicated that differences in ligand interactions with the surface have a major impact of Pu mobility. For example, DFOB facilitated significant desorption from goethite due to the low interaction of DFOB with goethite. However, in the kaolinite clay dominated soil, DFOB exhibited much higher sorption and thus was not present in the aqueous phase to induce Pu mobility.

In Chapter 6, further analysis of the natural SRS soil determined that it contained significant amounts of soluble organic matter, and was possibly a source of mobile colloids. In the column experiments, 9–20% of Pu was observed to elute with retardation factors of 24–29. Given the complexity of the soil, multiple working hypotheses may explain these data: (1) oxidation of Pu(IV) to Pu(V) in the spike solution during pH adjustment, (2) colloid-facilitated transport, and (3) formation of aqueous Pu complexes with soil organic matter. However, based on the simple modeling of these various hypotheses, it appears most likely that the Pu elution behavior was due to the presence of Pu(V) and the strong sorption in the column was due to the high affinity of both Pu(IV) and the organic ligands.

Future Work

The research presented in this dissertation has revealed knowledge gaps in the areas of Pu sorption kinetics and subsurface environmental fate and transport. Chapters 4 and 5 treat Pu aging as a conceptual transfer of a Pu atom from an initial surface state to a second state, but indirect measurements of aqueous Pu concentration are insufficient to identify the aging process. X-ray absorption fine structure measurements could be used to determine whether Pu aged on the surface of goethite formed shorter, stronger bonds with the surface relative to freshly sorbed Pu. Pu which has migrated to the interior of goethite crystals (i.e. by diffusion into micropores, lattice incorporation, or mineral recrystallization) could be directly measured by using laser ablation inductively coupled plasma mass spectrometry (LA-ICP-MS) or nano-secondary ionization mass spectrometry (nanoSIMS) to measure Pu within the mineral matrix at different depths. The rates of Pu lattice incorporation into goethite and mineral recrystallization are expected to be very slow. Thus, an extensive aging period may be needed to observe a measurable effect. Direct measurements comparing fresh and aged Pu could shed light on the mechanism(s) involved in Pu aging, allowing for improved models of Pu kinetics and transport.

In Chapter 5, a kinetic uptake and release model for aging is developed and fit to flow-cell data describing 3 days of Pu desorption from goethite in the presence of natural organic ligands. As the author is unaware of any other studies using this model, there is a need to more broadly validate this model using varied data sets. Specifically, it would lend credence to the model to use sorption data from experiments which: spanned months to years, included both adsorption and desorption steps, or maintained a constant/no ligand concentration for the duration of the experiment. These experiments could be of a flow-cell or batch design. A timeframe of months to years would be a more realistic timeframe for Pu in the environment than 3 days. By including adsorption/desorption and a constant ligand concentration, the entire data set could be modeled with a single set of apparent reaction rate constants, without the need to exclude conditioning data. Further validation of the two-site uptake/release model is needed to demonstrate the usefulness of this model for describing Pu aging under different conditions.

Chapter 6 identified multiple working hypotheses for the mobilization of Pu in SRS soil. Further characterization of soil properties is required in order to understand the fate and transport of Pu in this soil. One of the confounding factors of the column transport experiments was the non-uniform distributions of DFOB and citrate which developed. In order to uniformly distribute an organic ligand in the soil column, the soil could be pre-equilibrated with a ligand solution system (which is exchanged several times) in a batch system before packing the column. Characterization of the native soil organic matter is needed in order to determine the nature of any Pu–SOM complexes which might form. Alternatively, column transport experiments could be conducted with soil which has been washed to remove the soluble soil organic matter. The rate of reduction of Pu(V) to Pu(IV) in the presence of the SRS soil could be determined using batch sampling with oxidation state analysis. These data could help to understand the large fraction of Pu observed in the effluent. Finally, it is important to determine whether this soil generates colloids. This could be tested by equilibrating the soil in batch samples, centrifuging the samples, and analyzing the supernatant using dynamic light scattering and asymmetric field flow field fractionation to detect and characterize colloidal-sized particles. Such experiments could be coupled with more traditional filtration experiments.

APPENDICES

Appendix A

Supplementary Material for Chapter Four

Pu Speciation in the Presence of DFOB

In the presence of DFOB, Pu(IV) species in the form of $PuDFOB^{2+}$, $PuH_2(DFOB)_2^{2+}$, and $Pu(OH)_{4(aq)}$ dominate a large range of pH and E_h conditions. The software Geochemist's Workbench Standard 8.0 was used to perform equilibrium speciation modeling. The formation constants are from Boukhalfa et al. (2007) and Guillaumont et al. (2003).

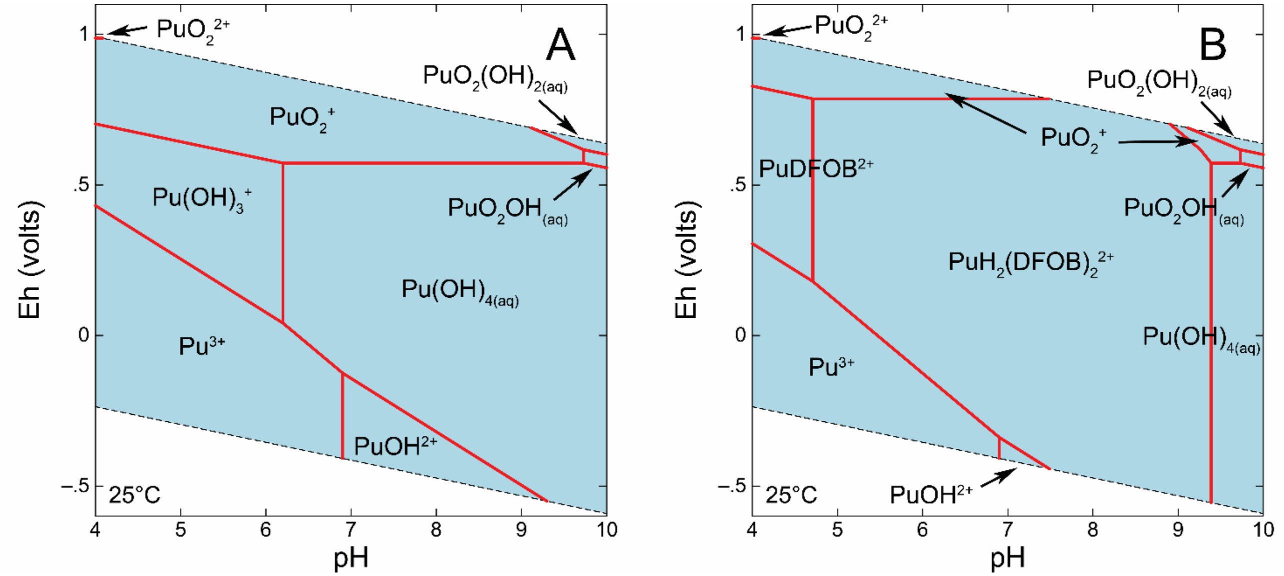

Figure A.1. Equilibrium speciation for 10^{-10} M Pu (A) in the absence of DFOB and (B) in the presence of 1.7 μM DFOB. PuO_2 minerals suppressed and 10 mM NaCl is included.

Pu Speciation in the Presence of DFOB and Fe(III)

In the presence of 1.7 μM DFOB and 1.0 μM Fe^{3+}, Pu(IV)–DFOB species in the form of $PuDFOB^{2+}$ and $PuH_2(DFOB)_2^{2+}$ dominate over $Pu(OH)_x^{4-x}$ species at experimentally relevant pH values. The formation constants are from Boukhalfa et al. (2007), Guillaumont et al. (2003), and Kraemer (2004).

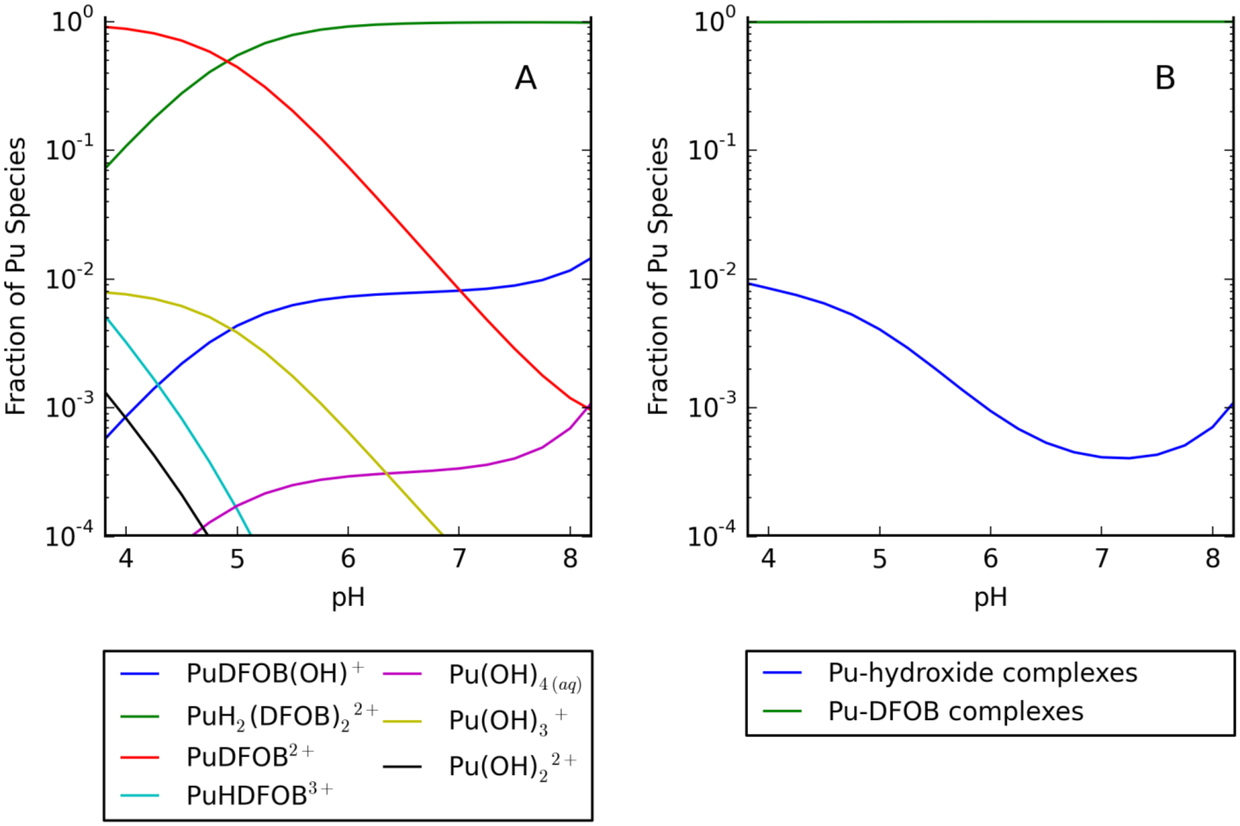

Figure A.2. Pu Speciation in the Presence of DFOB and Fe(III). (A) Equilibrium speciation of 10^{-10} M Pu(IV) in the presence of 1.7 μM DFOB, 1.0 μM Fe^{3+} and 10 mM NaCl. (B) Total fractions $Pu(OH)_x^{4-x}$ and Pu(IV)–DFOB species are shown.

Isotherms for DFOB Sorption to Goethite

The DFOB surface coverage was estimated by using published sorption isotherms for goethite with specific surface area of 35 ± 3 $m^2 \cdot g^{-1}$ as measured by the static BET method (Cheah et al., 2003; Kraemer et al., 1999) to extrapolate to 1.7 μM total DFOB and 0.10 $g \cdot L^{-1}$ goethite. Based on the Langmuir isotherm model (Eq. A.1) shown in Fig. A.3, a conservative estimate for the amount of DFOB sorbed to goethite is 1.1 $\mu mol \cdot g^{-1}$ or 6.2%. The Langmuir isotherm model indicated a maximum surface excess, n_{max}, of 1.2 ± 0.2 $\mu mol \cdot g^{-1}$ and Langmuir parameter, K_L, of 3.7 ± 2.1 μM. From linear isotherm fits to the lowest concentration measurements from Kraemer et al. and Cheah et al., the amount of DFOB sorbed to goethite is 0.7 $\mu mol \cdot g^{-1}$ and 0.3 $\mu mol \cdot g^{-1}$ or 4% and 2%, respectively.

Langmuir Equation:

$$n_{DFOB} = n_{max} \frac{K_L C}{K_L C + 1} \qquad \text{(A.1)}$$

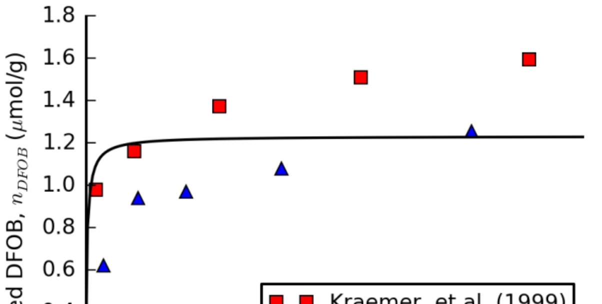

Figure A.3. Isotherms for DFOB Sorption to Goethite. The isotherm from Kraemer et al. (1999) is measured at pH 6.6 for 13 $g \cdot L^{-1}$ goethite, 10 mM $NaClO_4$, and 5 mM MOPS buffer. The isotherm from Cheah et al. (2003) is measured at pH 5 for 10 $g \cdot L^{-1}$ goethite, 10 mM $NaClO_4$, and 5 mM MOPS buffer. The Langmuir model is from Cheah et al.

Estimated Dissolved Iron in the Presence of DFOB

The iron dissolution rate was previously measured (Kraemer et al., 1999) at pH 6.5, in the presence of 0.5 $g \cdot L^{-1}$ goethite, 240 µM DFOB, 5mM MOPS buffer, and 10 mM $NaClO_4$. The surface area of the goethite used by Kraemer et al. (1999) was 35 ± 3 $m^2 \cdot g^{-1}$ as determined by the static BET method.

$$0.02\,\frac{\mu\text{mol}}{\text{g}\cdot\text{h}} \times 0.1\,\frac{\text{g}}{\text{L}}(\text{goethite}) \times 24\,\frac{\text{h}}{\text{day}} \times 25\text{ days} = 1.2\,\frac{\mu\text{mol}}{\text{L}} \qquad \text{(A.2)}$$

Batch Adsorption–Desorption Experiment in the Presence and Absence of DFOB

Solutions of 10 mM NaCl and 0.075 g·L^{-1} synthetic goethite were prepared in 15 mL polyethylene tubes. After addition of Pu from Pu(IV) or Pu–DFOB stock solutions, the final Pu concentration of samples was 1.7 × 10^{-10} M for DFOB-containing samples and 1.9 × 10^{-10} M for DFOB-free samples. Additional DFOB was added to DFOB-containing samples from the DFOB stock solution to yield 1.7 µM DFOB. Samples were adjusted to pH 6 and 8 with dilute HCl and NaOH. After 25 d adsorption, experiments were phase separated and supernatants exchanged for fresh Pu-free solutions of the same pH and DFOB concentration. During desorption, aqueous Pu was measured at 3 h, 5 h, 18 h, 3 d, and 12 d and plotted (Fig. A.4) as a percentage of total Pu remaining after supernatant exchange.

Table A.1. Percent Pu sorbed during adsorption step

DFOB Conc. (µM)	pH	2 h	5 h	1 d	3 d	10 d	25 d
0.0	6	84.9 ± 0.4	82.1 ± 0.4	71.8 ± 0.5	70.2 ± 0.5	79.8 ± 0.4	83.3 ± 0.4
0.0	8	87.74 ± 0.3	87.28 ± 0.3	89.42 ± 0.3	92.8 ± 0.3	96.04 ± 0.20	98.40 ± 0.14
1.7	6	9.7 ± 1.0	10.1 ± 1.0	21.7 ± 0.9	8.7 ± 1.0	23.3 ± 0.9	27.7 ± 1.5
1.7	8	22.6 ± 0.9	30.6 ± 0.8	24.3 ± 0.9	26.8 ± 0.9	38.5 ±0.8	43.9 ± 1.2

Table A.2. Estimated first-order adsorption rate constants (s^{-1}).

pH	DFOB-free	1.7 µM DFOB
6	$9 \pm 16 \times 10^{-8}$	$9 \pm 4 \times 10^{-8}$
8	$9.4 \pm 0.9 \times 10^{-7}$	$1.4 \pm 0.8 \times 10^{-7}$

Table A.3. Percent Pu sorbed during desorption step

DFOB Conc. (µM)	pH	3 h	5 h	18 h	3 d	12 d
0.0	6	96.44 ± 0.22	95.41 ± 0.24	88.1 ±0.4	76.9 ± 0.5	74.0 ± 0.5
0.0	8	97.32 ± 0.17	96.90 ± 0.18	94.30 ± 0.24	93.13 ± 0.25	92.1 ± 0.3
1.7	6	74.8 ± 1.0	72.6 ± 1.0	64.3 ± 1.1	61.1 ± 1.2	70.2 ± 1.0
1.7	8	85.2 ± 0.6	83.5 ± 0.6	75.7 ± 0.7	73.4 ± 0.8	75.8 ± 0.7

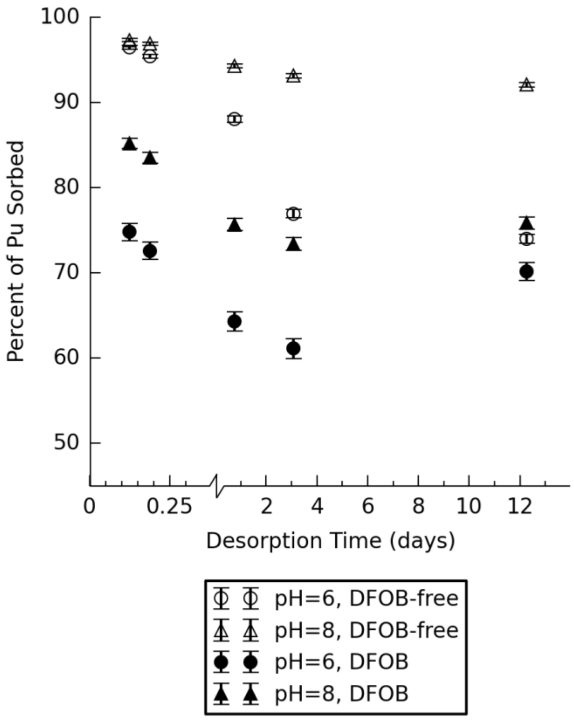

Figure A.4. The percent of Pu sorbed is plotted against time for Pu desorption from 0.075 g·L^{-1} goethite suspensions with 10 mM NaCl for ionic strength control. Pu was initially added as Pu(IV) to samples containing 1.7 μM DFOB and DFOB-free solutions. Error bars represent two standard deviations of measurement uncertainty derived from counting statistics. The first data point was collected after a 3 h desorption time period.

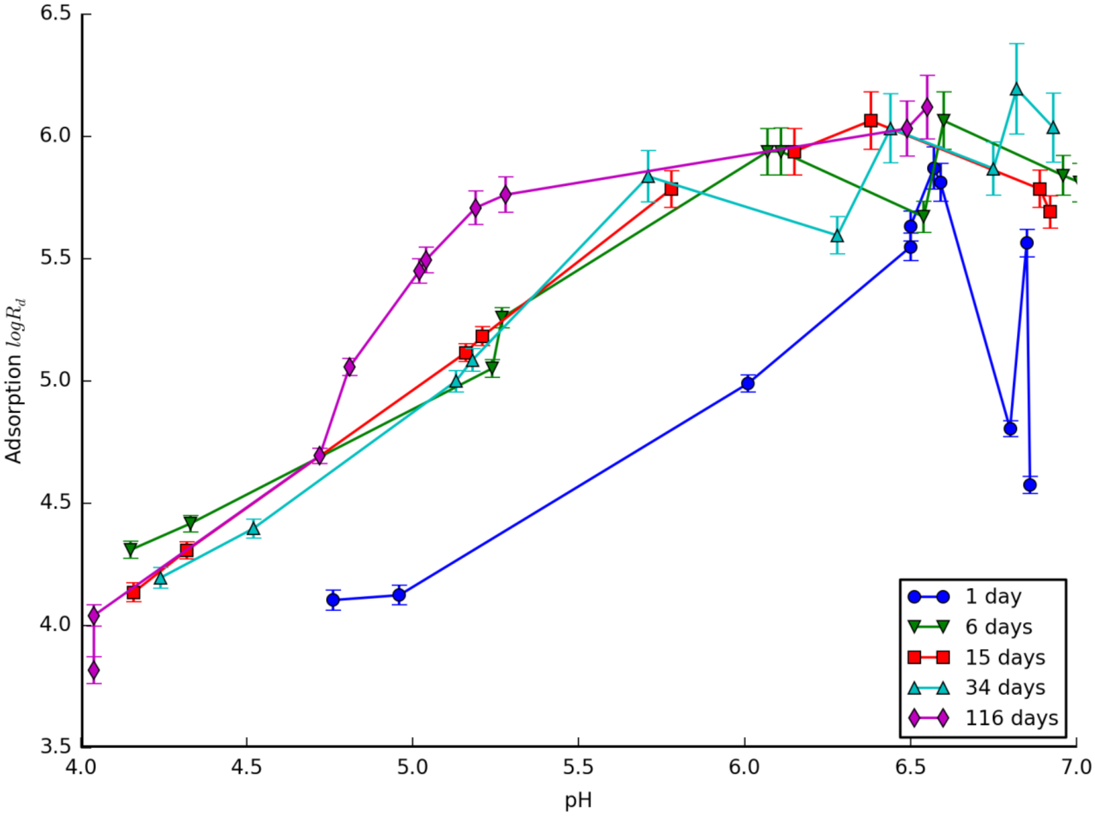

Figure A.5. Logarithmic adsorption distribution ratios (R_d) for Pu on 0.10 g·L^{-1} goethite suspensions as a function of pH and time. Total Pu concentration is 1.2 × 10^{-10} M, and ionic strength was controlled with 10 mM NaCl. Error bars indicate two standard deviations of measurement uncertainty derived from counting statistics. The lines are to guide the eye.

Appendix B

Supporting Information for Chapter Five

Plutonium Equilibrium Speciation with DFOB and Citrate

Equilibrium speciation calculations were performed using the software Geochemist's Workbench Student Edition 11.0 with formation constants from Boukhalfa et al. (2007), Clark et al. (2010), and Guillaumont et al. (2003).

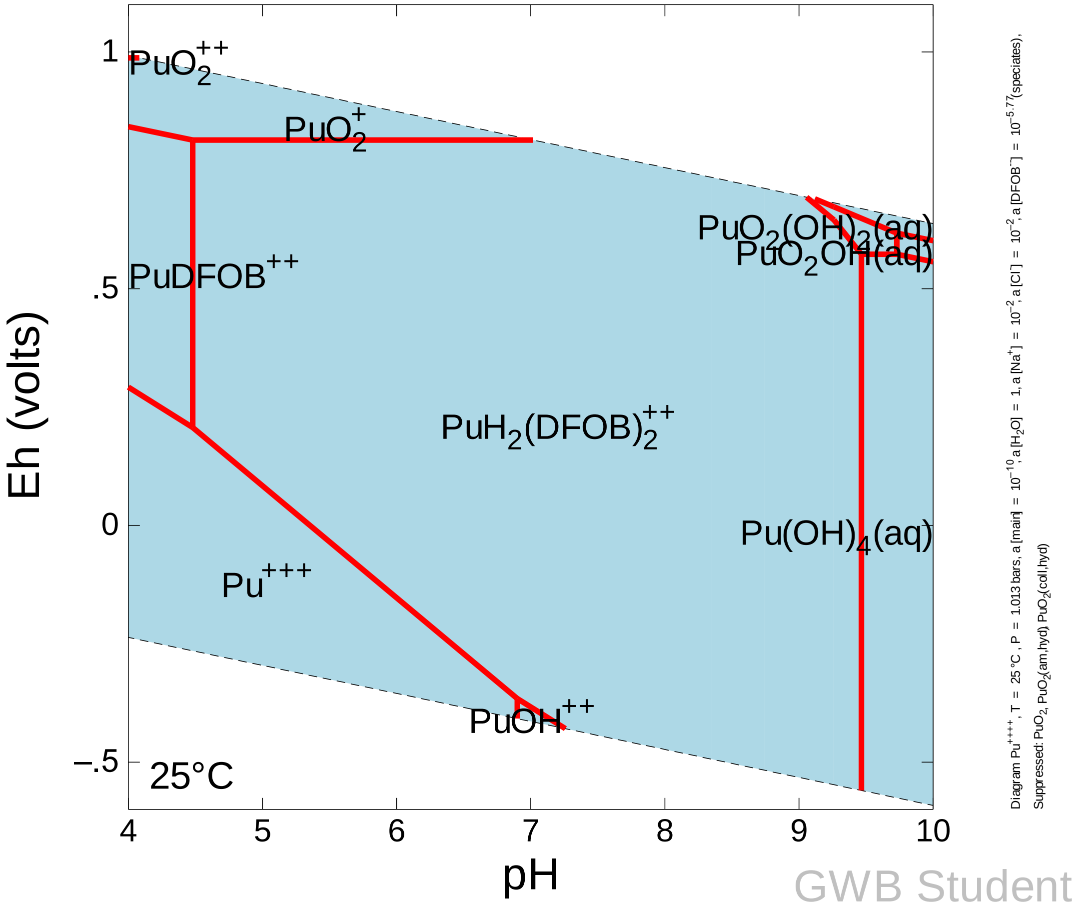

Figure B.1. Equilibrium speciation model results for 1.7 µM DFOB, 10^{-10} M Pu, and 10 mM NaCl. The minerals PuO_2, $PuO_{2(am,hyd)}$, and $PuO_{2(coll,hyd)}$ are suppressed.

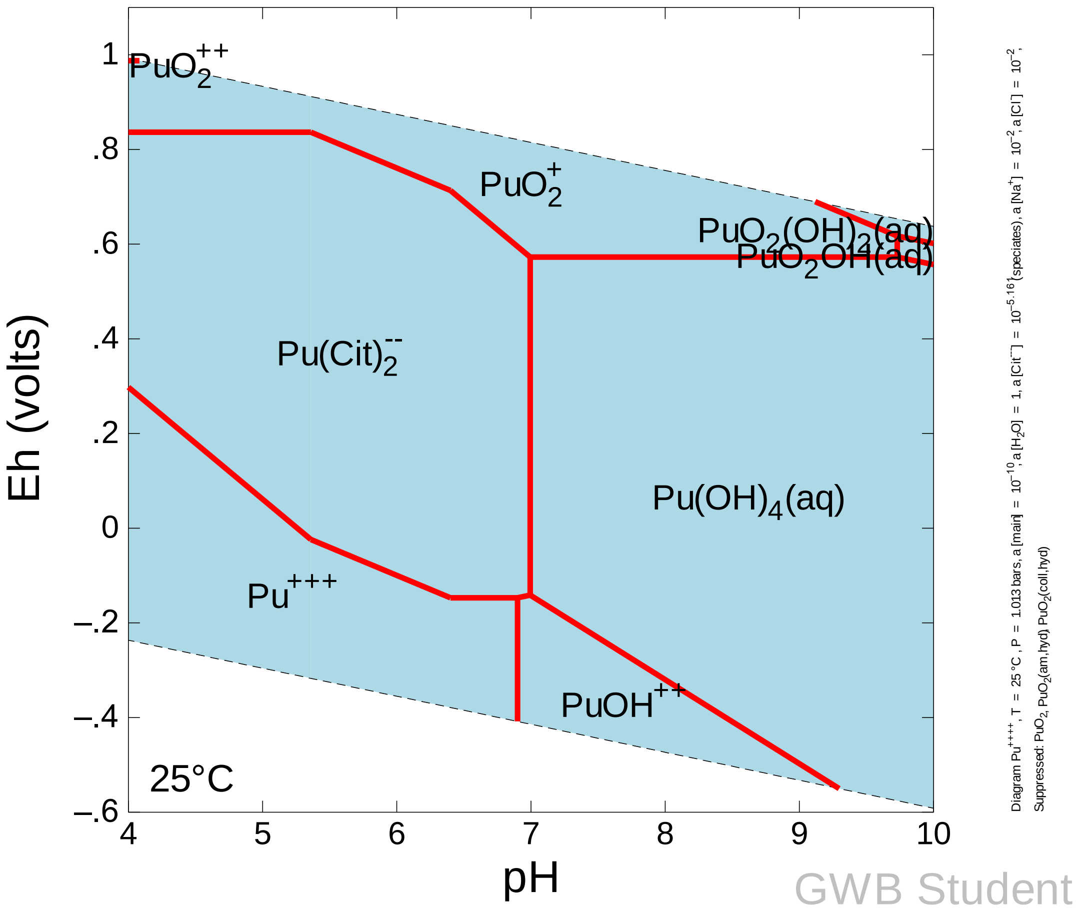

Figure B.2. Equilibrium speciation model results for 6.9 μM citrate, 10^{-10} M Pu, and 10 mM NaCl. The minerals PuO_2, $PuO_{2(am,hyd)}$, and $PuO_{2(coll,hyd)}$ are suppressed.

Tracer Results

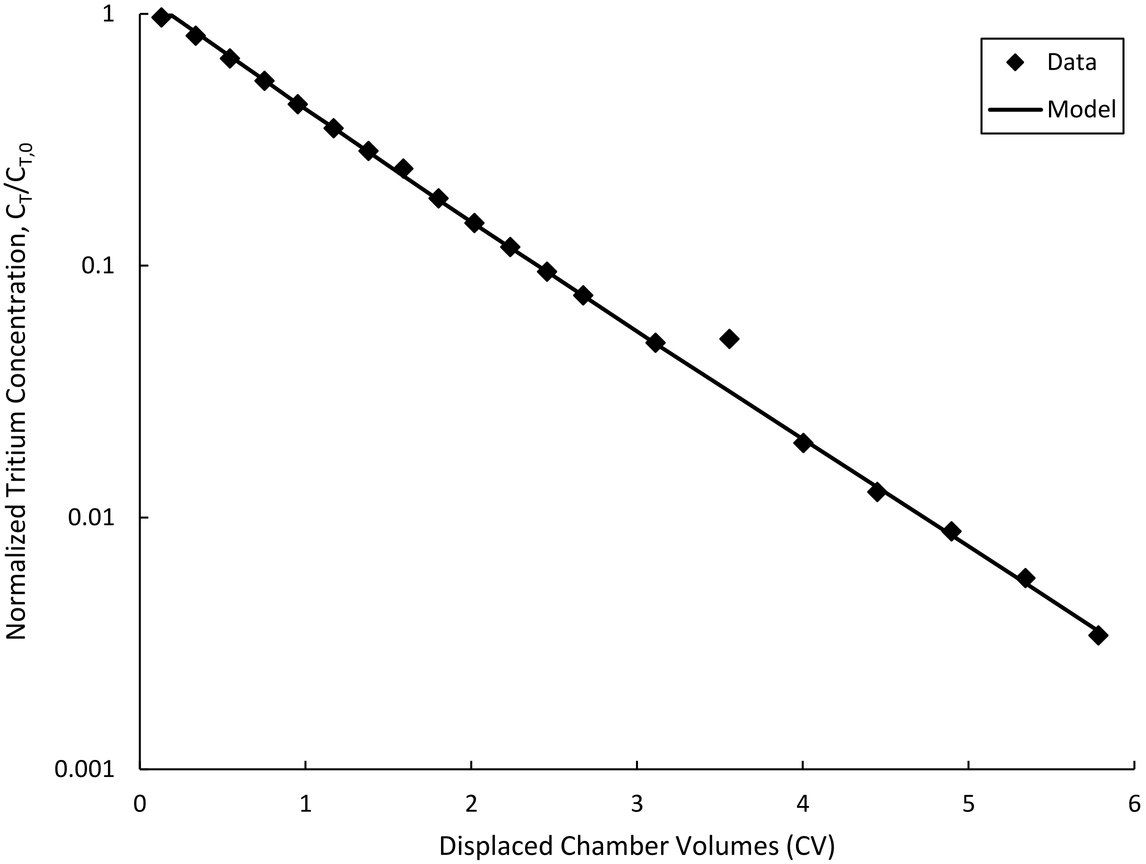

Figure B.3. Measured concentration of the ^{3}H tracer in the organic-free flow-cell efluent. Concentration is normalized against the concentration of ^{3}H in the Pu–goethite working solution, $C_{T,0}$. The flow rate was 0.37 mL·min^{-1}. The residence time and effective chamber volume were determined from the model to be 55 min and 20.1 mL, respectively.

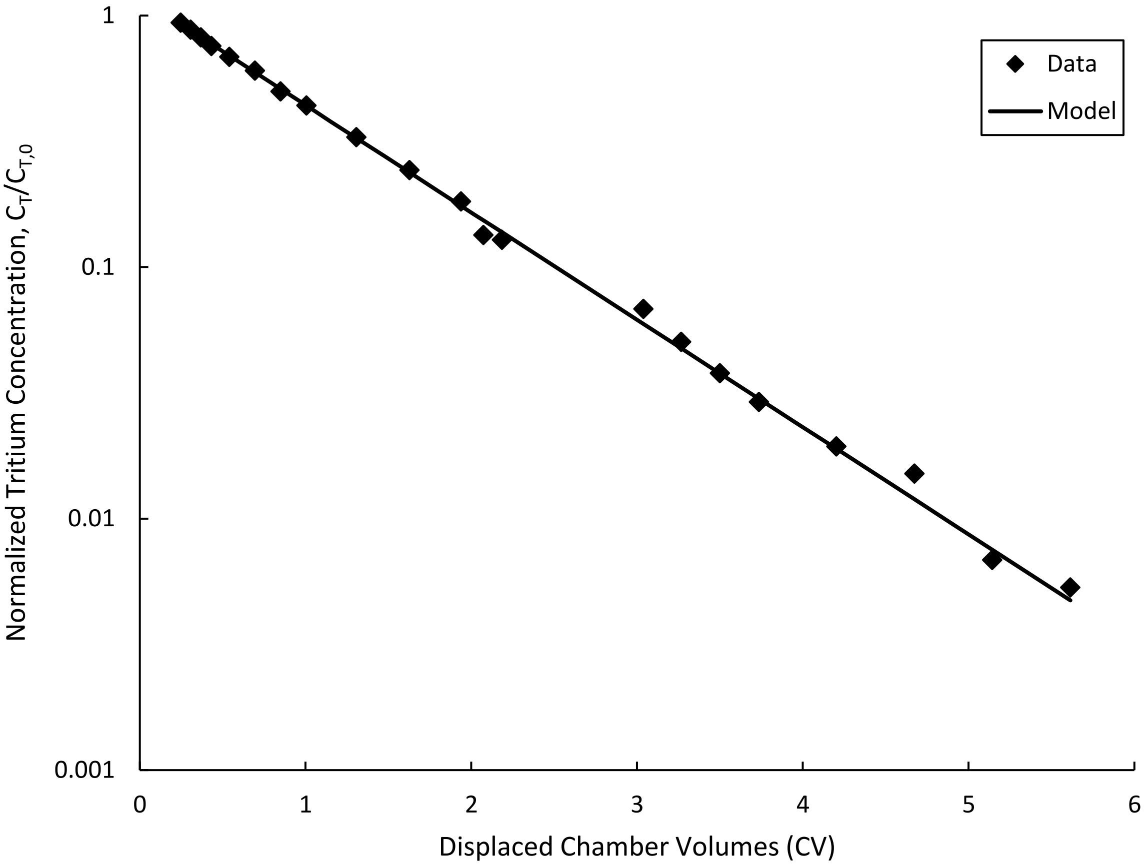

Figure B.4. Measured concentration of the ^3H tracer in the DFOB flow-cell effluent. Concentration is normalized against the concentration of ^3H in the Pu–goethite working solution, $C_{T,0}$. The flow rate was 0.34 mL·min^{-1}. The residence time and effective chamber volume were determined from the model to be 61 min and 20.5 mL, respectively.

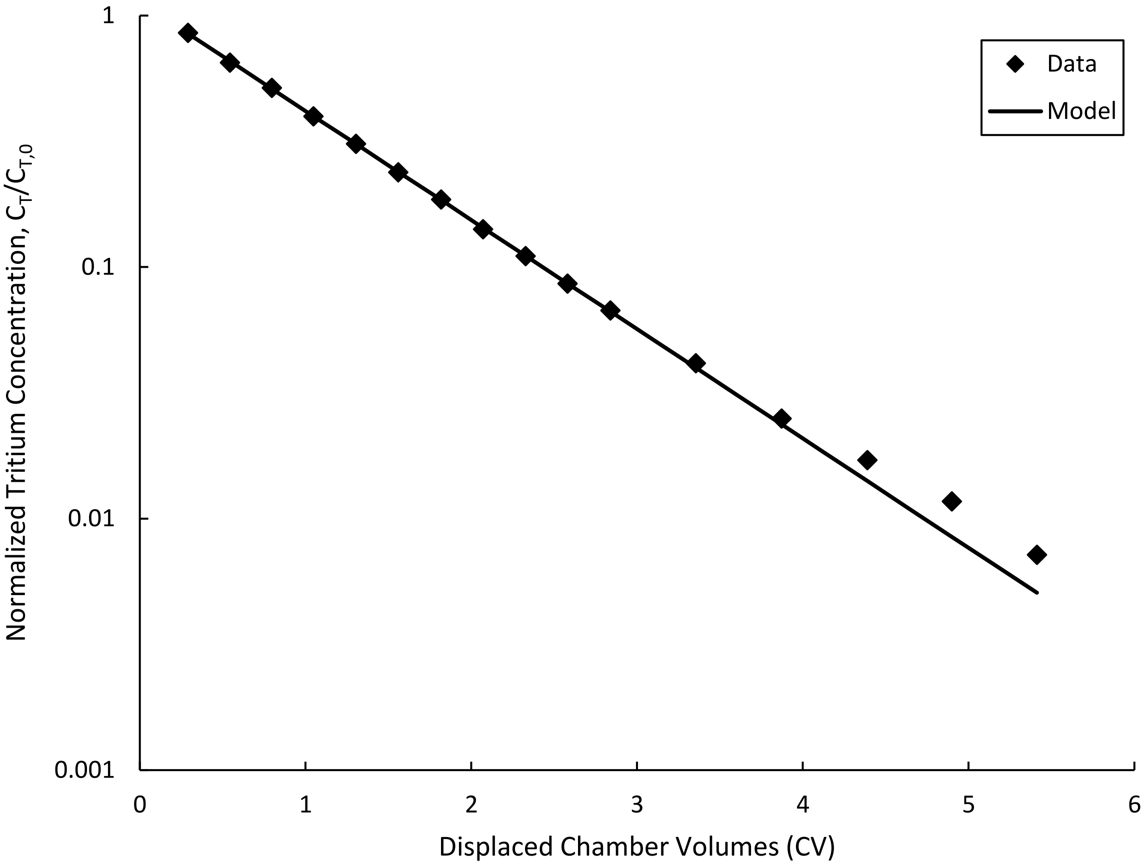

Figure B.5. Measured concentration of the ^3H tracer in the fulvic acid flow-cell effluent. Concentration is normalized against the concentration of ^3H in the Pu–goethite working solution, $C_{T,0}$. The flow rate was 0.35 mL·min^{-1}. The residence time and effective chamber volume were determined from the model to be 59 min and 20.3 mL, respectively.

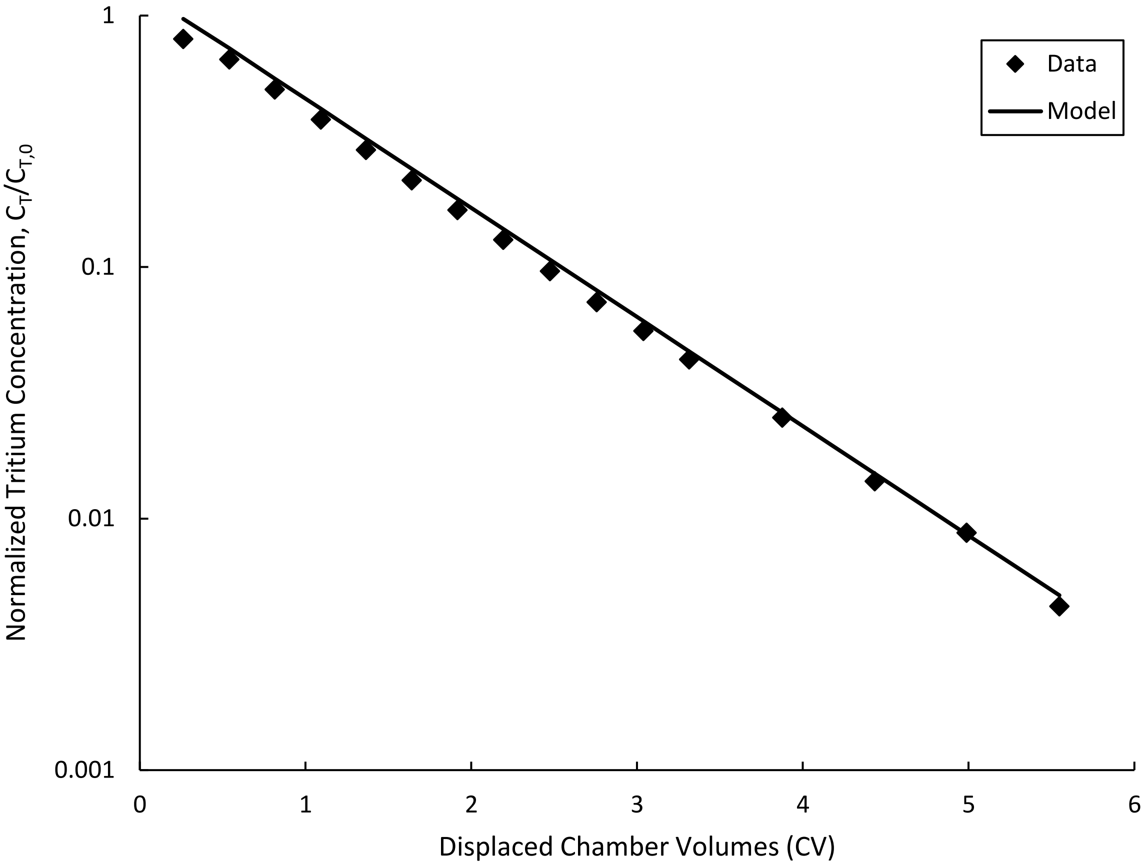

Figure B.6. Measured concentration of the ^3H tracer in the citric acid flow-cell effluent. Concentration is normalized against the concentration of ^3H in the Pu–goethite working solution, $C_{T,0}$. The flow rate was 0.33 mL·min^{-1}. The residence time and effective chamber volume were determined from the model to be 54 min and 18.1 mL, respectively.

Calculation of Distribution Coefficient in Two-Site Linear Sorption Model

The distribution coefficient ($L \cdot kg^{-1}$), K_d, is defined (Eqn. B.1) as the concentration ($mol \cdot g^{-1}$) of sorbed Pu divided by the concentration ($mol \cdot L^{-1}$) of the aqueous Pu, C, at sorption equilibrium. A conversion factor of 1000 is necessary because the chamber volume, V, is defined in liters and the total mass of goethite, M, is defined in grams. The sorbed Pu concentration consists of Pu sorbed to site 1, S_1, and Pu sorbed to site 2, S_2. At sorption equilibrium, net rates of change of S_1 and S_2 are zero (Eqns. B.2 and B.5), where k_{1f}, k_{1r}, k_{2f}, and k_{2r} represent apparent first-order reaction rate constants (min^{-1}). Equation B.2 can be manipulated to obtain an expression for S_2 (Eqn. B.4). Equation B.5 can be manipulated using Eqn. B.3 to obtain an expression for C (Eqn. B.7). Finally, Eqns. B.4 and B.7 can be substituted into Eqn. B.1, and the final expression (Eqn. B.9) is obtained for the distribution coefficient.

Definition of K_d:
$$K_d = \frac{S_1 + S_2}{C} \times 1000\,\frac{\text{g}}{\text{kg}} \tag{B.1}$$

Net rate of change of S_2:
$$\frac{dS_2}{dt} = k_{2f}S_1 - k_{2r}S_2 = 0 \tag{B.2}$$

$$k_{2f}S_1 = k_{2r}S_2 \tag{B.3}$$

$$S_2 = \frac{k_{2f}}{k_{2r}}S_1 \tag{B.4}$$

Net rate of change of S_1:
$$\frac{dS_1}{dt} = \frac{V}{M}k_{1f}C - k_{1r}S_1 - k_{2f}S_1 + k_{2r}S_2 = 0 \tag{B.5}$$

$$\frac{V}{M}k_{1f}C = k_{2f}S_1 \tag{B.6}$$

$$C = \frac{M}{V}\frac{k_{1r}}{k_{1f}}S_1 \tag{B.7}$$

$$K_d = \frac{S_1 + \frac{k_{2f}}{k_{2r}}S_1}{\frac{M}{V}\frac{k_{1r}}{k_{1f}}S_1} \times 1000\,\frac{\text{g}}{\text{kg}} \tag{B.8}$$

Final Expression for K_d:
$$K_d = \frac{V}{M}\frac{k_{1f}}{k_{1r}}\left(1 + \frac{k_{2f}}{k_{2r}}\right) \times 1000\,\frac{\text{g}}{\text{kg}} \tag{B.9}$$

Parameters from One-Site Linear Sorption Model

Table B.1. Comparison of parameters for the one-site linear sorption model. One standard deviation of uncertainty is indicated.

Flow-cell	k_{1f} (min^{-1})	k_{1r} (min^{-1})	K_d (L·kg^{-1})	WSOS/DF[a]
DFOB	4.8×10^{-4} [b]	$3.9 \pm 0.6 \times 10^{-5}$	n.d.	97.69
Fulvic acid	4.6×10^{-6} [b]	$2.6 \pm 0.4 \times 10^{-5}$	n.d.	58.73
Citric acid	$2.01 \pm 0.26 \times 10^{-3}$	$3.02 \pm 0.12 \times 10^{-5}$	1.74×10^{3}	10.06
Organic free	$1.32 \pm 0.16 \times 10^{-2}$	$1.18 \pm 0.09 \times 10^{-5}$	3.39×10^{4}	4.980

[a] WSOS/DF is the weighted sum of squares divided by the degrees of freedom.

[b] This parameter value should not be considered with any real confidence because the model fit is insensitive to this parameter.

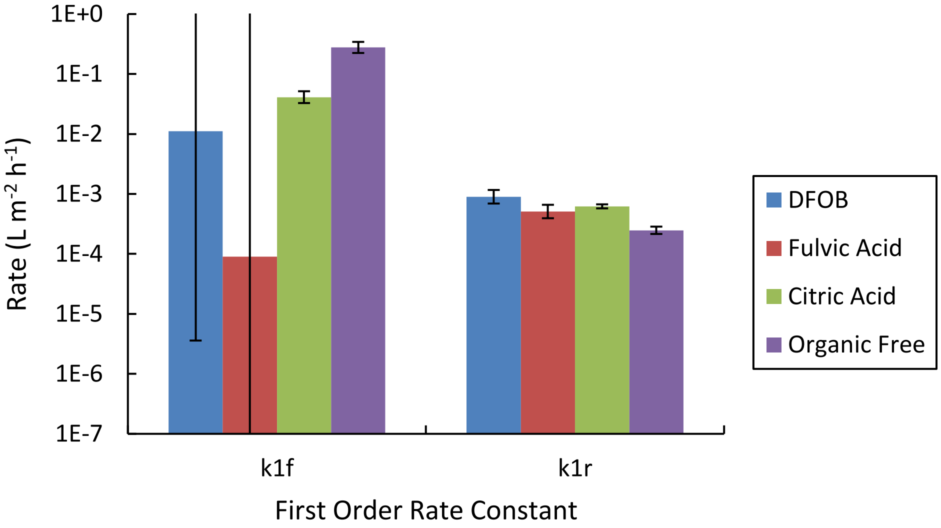

Figure B.7. First-order sorption rate constants for the one-site model. Error bars represent a 95% confidence interval.

Multi-Site Kinetic Sorption Models

For reactive transport modeling of flow-cell data, various kinetic rate laws including single-site models, multi-site models with consecutive reactions, and multi-site models with parallel reactions were considered. These rate laws were based on coupled first-order differential equations. After sorption to a single site was considered (Eqn. 2.2 and Table 2.1), modeling was extended to consider two-site kinetic models. Sorption reactions which are instantaneous or irreversible over the experiment time scale were also considered. It was preferred to simulate kinetics with multiple linear sorption sites over Langmuir or Freundlich type sites because the experiments were performed at low sorbate concentrations which can appropriately be represented by linear isotherms. Figure B.8 illustrates possible relationships between sorption sites, not all of which were considered simultaneously. The flow-cell equation for a single sorption site (Eqn. 2.2) was re-written to encompass multi-site modeling (Eqn. B.10). The applicable rate laws are given in Eqns. B.11–B.14. Several two-site models for consideration are tabulated (Table B.2) along with applicable rate constants and reaction rate equations. Although during model development, it was only necessary to consider two-site models, three-site models could also have been considered if more complexity were required to fit flow-cell data. Of the one-site and multi-site kinetic sorption models described, only the model considering one linear sorption site and the model considering two consecutive linear sorption sites provided reasonable fits to the flow-cell data.

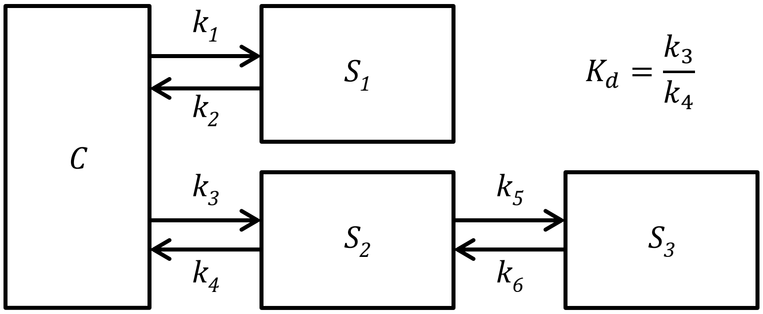

Figure B.8. Schematic of the multireaction model for Pu sorption to surfaces. S_1 and S_2 represent sites in direct contact with the solution phase, C. S_3 represents a consecutive site. Instantaneous equilibrium between C and S_2 can be considered by letting K_d be the linear distribution coefficient. Irreversible adsorption to a site can be considered by setting the corresponding desorption rate constant to zero.

$$\frac{dC}{dt} = \frac{Q}{V}C - \frac{M}{V}\frac{dS_1}{dt} - \frac{M}{V}\frac{dS_2}{dt} \tag{B.10}$$

$$S_2 = \frac{k_3}{k_4}C = K_dC \tag{B.11}$$

$$\frac{dS_1}{dt} = k_1C - k_2S_1 \tag{B.12}$$

$$\frac{dS_2}{dt} = k_3C - k_4S_2 - k_5S_2 + k_6S_3 \tag{B.13}$$

$$\frac{dS_3}{dt} = k_5S_2 - k_6S_3 \tag{B.14}$$

Table B.2. Possible two-site kinetic rate constants and equations for coupling with Eqn. B.10 in the development of a reactive transport model. Rate constants not included in a sorption model are assumed to be zero.

Kinetic Sorption Model	Rate Constants	Included Rate Eqns.
One linear site	k_1, k_2	B.12
Two consecutive sites, each linear	k_3, k_4, k_5, k_6	B.13, B.14
Two parallel sites, each linear	k_1, k_2, k_3, k_4 k_5=k_6=0	B.12, B.13
One linear site and one consecutive irreversible site	k_3, k_4, k_5 k_6=0	B.13, B.14
One linear site and one parallel irreversible site	k_1, k_2, k_3 k_4=k_5=k_6=0	B.12, B.13
One linear site and one parallel equilibrium site	K_d, k_1, k_2	B.11, B.12
One equilibrium site and one consecutive linear site	K_d, k_5, k_6	B.11, B.14
One equilibrium site and one consecutive irreversible site	K_d, k_5 k_6=0	B.11 B.14

Appendix C

Supporting Information for Chapter Six

Plutonium Equilibrium Speciation in the Presence of Citrate and DFOB

Equilibrium speciation calculations were performed using the software Geochemist's Workbench Student Edition 11.0 with formation constants from Boukhalfa et al. (2007), Clark et al. (2010), and Guillaumont et al. (2003).

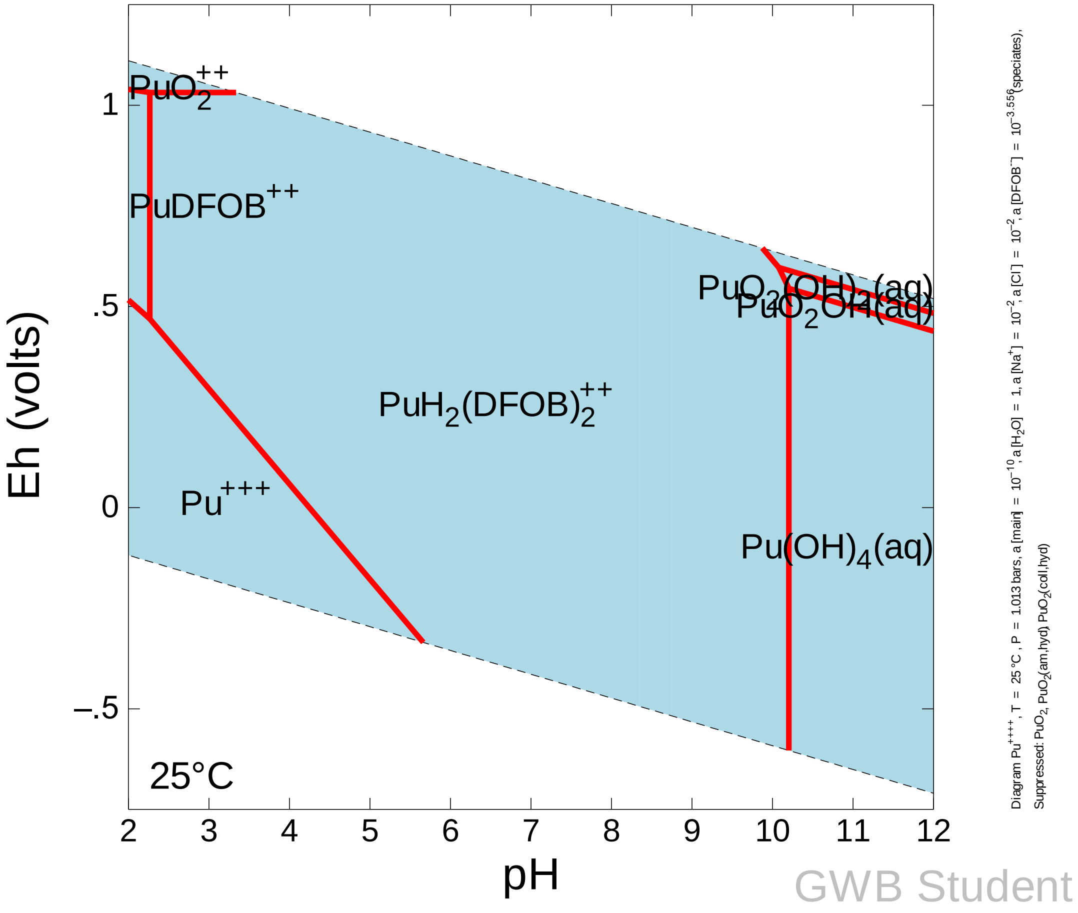

Figure C.1. Equilibrium speciation model results for 0.278 mM DFOB, 10^{-10} M Pu, and 10 mM NaCl. The minerals PuO_2, $PuO_{2(am,hyd)}$, and $PuO_{2(coll,hyd)}$ are suppressed.

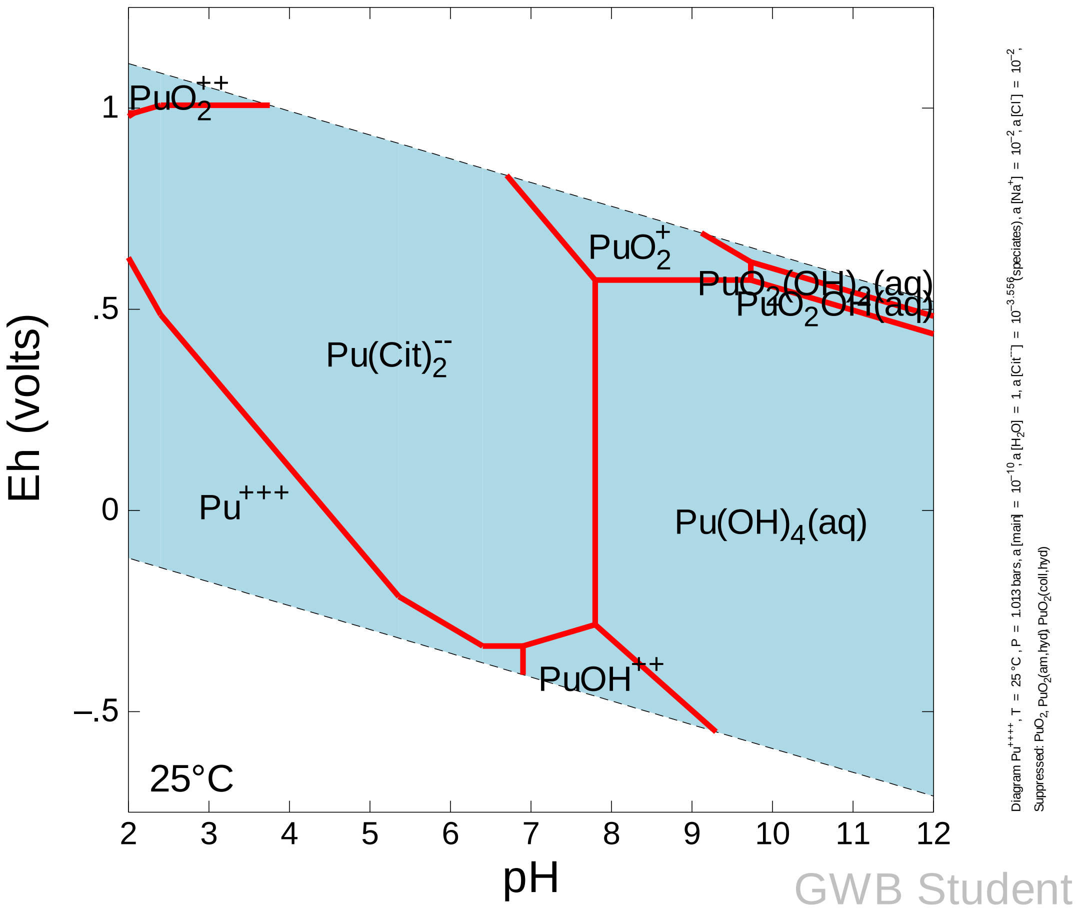

Figure C.2. Equilibrium speciation model results for 0.278 mM citrate, 10^{-10} M Pu, and 10 mM NaCl. The minerals PuO_2, $PuO_{2(am,hyd)}$, and $PuO_{2(coll,hyd)}$ are suppressed.

Calculation of Centroid

Centroid/ retardation factor: $$\bar{p} = \frac{\sum pC(p)}{\sum C(p)} - \frac{V_{pore}}{2} \tag{C.1}$$

In the equation for centroid, V_{pore} is the pore volume of the soil column and p is the number of displaced pore volumes (Fjeld et al., 2001; Jin et al., 1995).

Sorption and Transport Distance of Citrate and DFOB in SRS Soil

In order to construct isotherms for citrate and DFOB sorption to the soil, batch samples were prepared. Stock solutions of 13.9 mM citrate and 13.3 mM DFOB were prepared by dissolving sodium citrate dihydrate and desferrioxamine mesylate, respectively, into water. SRS soil, 10 mM NaCl, and either citrate or DFOB stock solution were added to 50 mL tubes. The total ligand concentrations ranged from 0.070 to 0.700 mM, and the suspended solids concentration was 25 $g \cdot L^{-1}$. The range of ligand concentrations was selected to span a wide range of concentrations around the 0.278 mM concentration used for the column experiments. Samples were adjusted to pH 4 and 5, placed on a mixer/tumbler (≈10 rpm), and allowed to equilibrate for 2 days. The samples were centrifuged 30 min at 3k rpm (Allegra 6KR centrifuge, GH3.8 rotor) and 20 mL of supernatant was removed for TOC analysis (Shimadzu TOC analyzer).

The sorption data was fit using Langmuir type sorption isotherms (Fig. C.3, Eqn. C.2, and Table C.1), where S_{max} is the saturated sorbed concentration ($\mu mol \cdot g^{-1}$), K_L is the Langmuir parameter ($mL \cdot \mu mol^{-1}$), S_{lig} is the sorbed ligand concentration ($\mu mol \cdot g^{-1}$), and C_{lig} is the aqueous ligand concentration ($\mu mol \cdot mL^{-1}$). Only the results at pH 5 are considered for analysis. The Langmuir sorption model suggested that the sorbed:aqueous concentration ratios, R_d, at pH 5 for 0.278 mM citrate and DFOB solutions equilibrated with the soil are 632 $mL \cdot g^{-1}$ and 300 $mL \cdot g^{-1}$, respectively. Both ligands sorbed strongly to the soil, and were expected to reach the steady-state concentration rapidly upon the arrival of the ligand front. Preliminary reactive transport modeling with Hydrus indicated that, in this case, the ligand soil profile would form a very abrupt front, essentially a step function, which was challenging to solve numerically with the Hydrus software.

The extent of the solute front in the column was determined by considering this steady state sorbed:aqueous concentration ratio, R_d, and the total amount of ligand added to the column. The bulk ligand concentration in the column (assuming concentrations have reached steady state) is given by (Eqns. C.3 and C.4), ρ is the bulk density ($g \cdot mL^{-1}$), φ is the porosity (-), V_{pore} is the pore volume (mL), p is the number of displaced pore volumes (-), A is the column cross-sectional area (cm^2), and x is the distance (cm) of the ligand front from the inlet. Equation C.4 was rearranged to yield Eqn. C.5 which was used to determine that citrate and DFOB accumulated within 0.68 and 1.32 cm of the column inlet. The total pore volumes of ligand solution passed through the columns were 91.5 and 97.3 PV for the citrate and DFOB columns, respectively.

For citrate and DFOB, the fraction of occupied sites (mol_{ligand}/mol_{site}) was estimated to be 0.88 and 0.48, respectively.

The Langmuir isotherms suggest that a significant amount of soil surface sites are saturated at the citrate and DFOB aqueous concentration of 0.278 mM. For citrate and DFOB, the sorbed concentrations are 97% and 41 % of their respective S_{max} values.

Langmuir Equation:

$$S_{lig} = S_{max}\frac{K_L C_{lig}}{K_L C_{lig} + 1} \qquad \text{(C.2)}$$

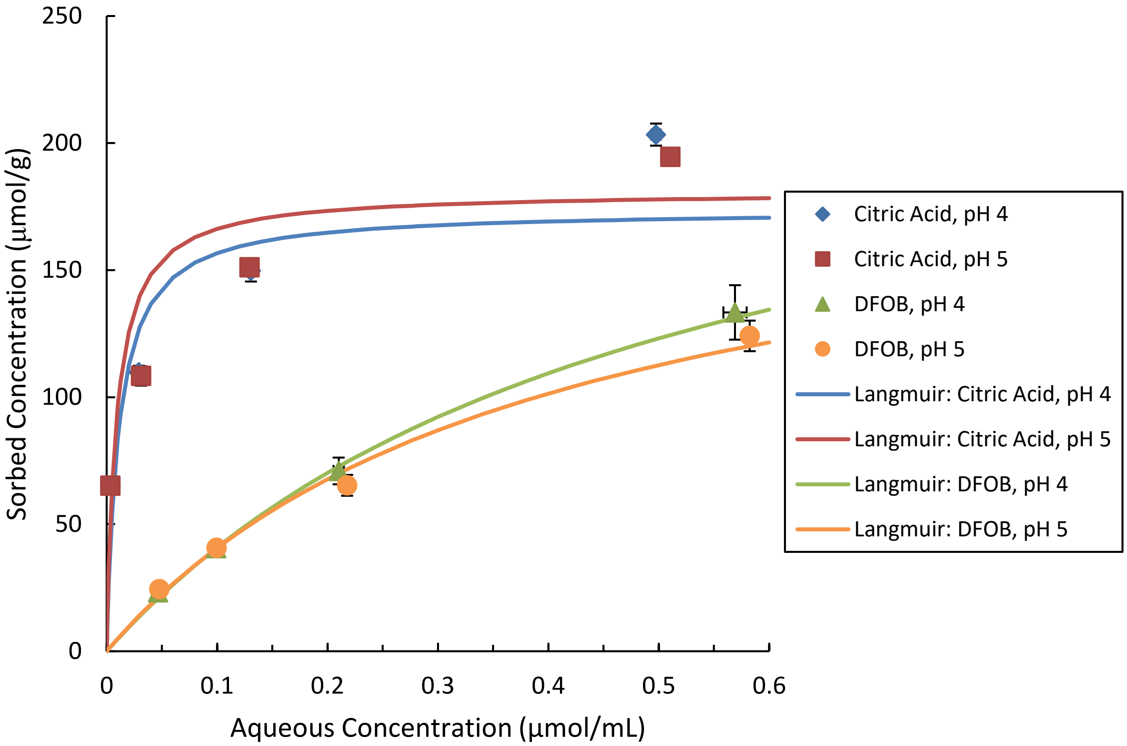

Figure C.3. Sorption isotherm for citrate and DFOB on 25 g·L^{-1} soil at pH 4 and 5. The sorption data was fit with a Langmuir model. Ionic strength was maintained with 10 mM NaCl. Confidence intervals represent 2σ measurement uncertainty.

Table C.1. Langmuir parameters for citrate and Pu sorption on soil from the Savannah River Site

Ligand	pH	S_{max} (µmol·g^{-1})	K_L (mL·µmol^{-1})
Citrate	4	174	93
Citrate	5	181	114
DFOB	4	248	2.0
DFOB	5	202	2.5

$$\text{bulk conc sorbed } + \text{bulk conc aq} = \frac{\text{total ligand added}}{\text{volume occupied by ligand}} \qquad \text{(C.3)}$$

$$C_{lig}R_d\rho + C_{lig}\varphi = \frac{C_{lig}V_{pore}p}{Ax} \qquad \text{(C.4)}$$

$$x = \frac{C_{lig}V_{pore}p}{A\left(C_{lig}R_d\rho + C_{lig}\varphi\right)} \qquad \text{(C.5)}$$

Oxidation State of Simulated Spike Solutions

A Pu stock solution was freshly prepared. The ^{238}Pu (98.7 % ^{238}Pu, 0.3 % ^{239}Pu, and 0.01 % ^{242}Pu by activity) stock solution was 9.8×10^{-7} M Pu and 99.9% Pu(IV) as measured by a well-established organic extraction technique. Triplicate solutions 45 mL in volume were prepared by first adding 1 M NaOH to 10 mM NaCl to minimize swings in pH, and then adding Pu(IV) stock solution to a concentration of 4.7×10^{-10} M. The pH of solutions was adjusted to 4.8 using dilute HCl and NaOH. The solutions were sampled between 0.6 and 25 hours to determine the distribution of Pu oxidation states. The oxidation states were determined using well-known organic extraction and lanthanum co-precipitation techniques (Foti and Freiling, 1964; Neu et al., 1994; Nitsche et al., 1988; Powell et al., 2004). The oxidation states showed no apparent trend in time (Fig. C.4). The average percentage of oxidized Pu(V+VI) from all measurements was 16 ± 5%. The average percentages of Pu(IV), Pu(V), and Pu(IV) were 84 ± 4%, 6 ± 2%, and 10 ± 4%, respectively.

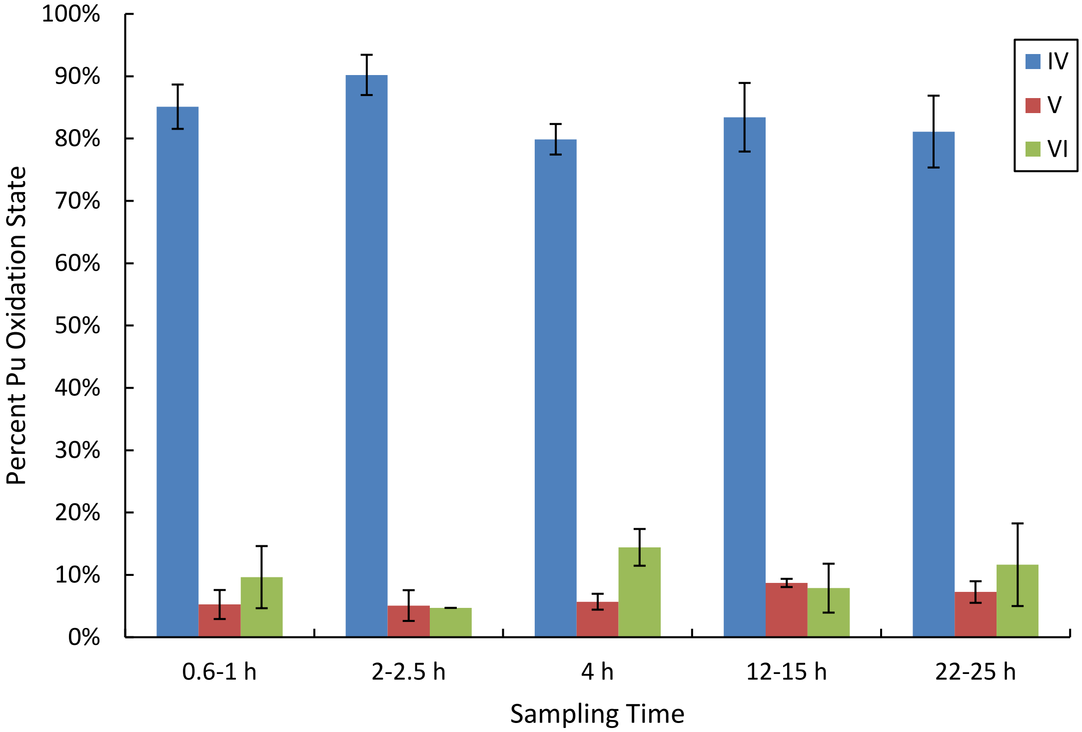

Figure C.4. Pu oxidation state distribution over time in simulated column spike solutions. The data shown is for triplicate samples initially containing 4.7 × 10^{-10} M ^{238}Pu(IV). Following Pu addition, samples were measured at five times (shown).

Blank Column Experiment

In order to investigate the concentrations of soil organic matter in the columns, a Pu-free column experiment was performed. Effluent fractions of 17–20 PV were measured for dissolved organic carbon. The column was packed and weighed as before, except that the residence time was 24 min. Then, 120 PV of background solution was pumped into the column. The column contained 16.5 g of soil and had a pore volume of 5.0 mL. Effluent fractions of 17–20 PV (≈100 mL) were collected for TOC analysis and elemental analysis by ICP-MS.

Effluent from the first 17 PV had a TOC concentration of $1.8 \pm 0.2\ \mathrm{mg_c \cdot L^{-1}}$ (Fig. C.5). Effluent measurements for 17–118 PV were approximately constant, and ranged from 0.52 to $0.12\ \mathrm{mg_c \cdot L^{-1}}$ with an average of $0.26 \pm 0.13\ \mathrm{mg_c \cdot L^{-1}}$. The dissolved SOM may differ from column experiments where Pu, citrate, or DFOB was added since these may perturb the solution and soil chemistry. However, the results suggest that the soil organic matter reaches equilibrium after 17 PV. Importantly, the results indicate that soil organic matter can be leached from the soil, meaning that soluble soil organic matter may possibly influence the transport of Pu or other contaminants in this soil without the addition of other organic ligands.

In order to determine whether elements associated with mineral colloids were present in the effluent, the effluent from the Pu-free column was acidified and measured for Mg, Ca, Al, and Fe using ICP-MS. A sample of background solution was also measured for comparison. The ICP-MS samples were monitored with a semi-quantitative approach (i.e. without using calibration standards) only to examine the presence of each ion in the effluent and compare changes in detector signal in effluent fractions. Measurements from the effluent fractions were background-subtracted. The concentrations of Mg, Ca, and Al were elevated relative to the background solution, and the concentrations decreased over the first 60 PV before reaching steady-state. The ratio of the concentration in the first effluent fraction to the steady state concentration was calculated. These ratios were 310, 27, and 18 for Mg, Ca, and Al, respectively. The Fe concentration was elevated relative to the background solution in a single measurement between 17 and 35 PV, but was otherwise lower than the concentration in the background solution.

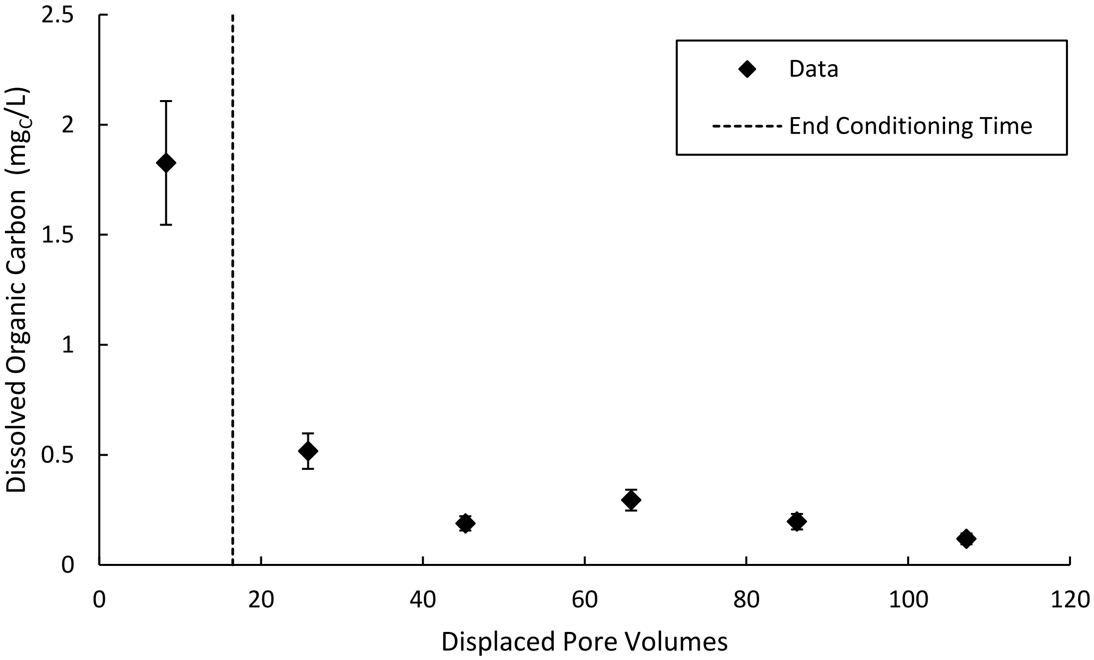

Figure C.5. Measurements of dissolved organic carbon in effluent from the blank column experiment. Confidence intervals of 1σ are derived from replicate measurements of each sample and uncertainty in the TOC calibration curve.

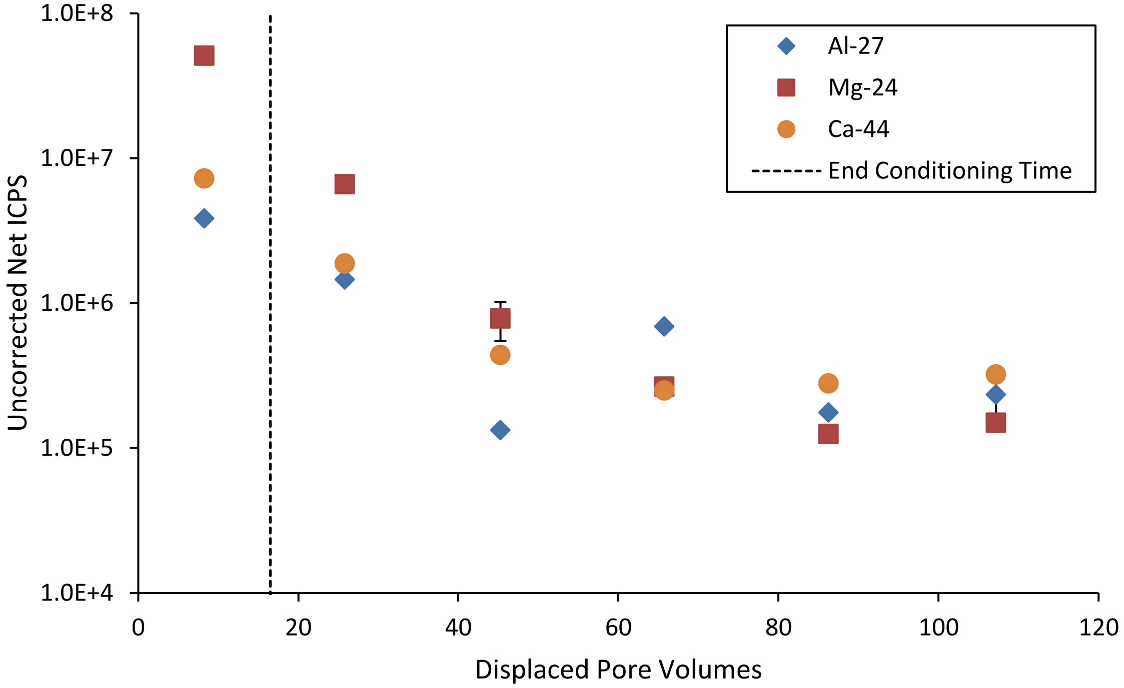

Figure C.6. Elements measured in the blank column effluent by ICP-MS on a semi-log scale. Confidence intervals of 1σ are derived from triplicate measurements of each sample.

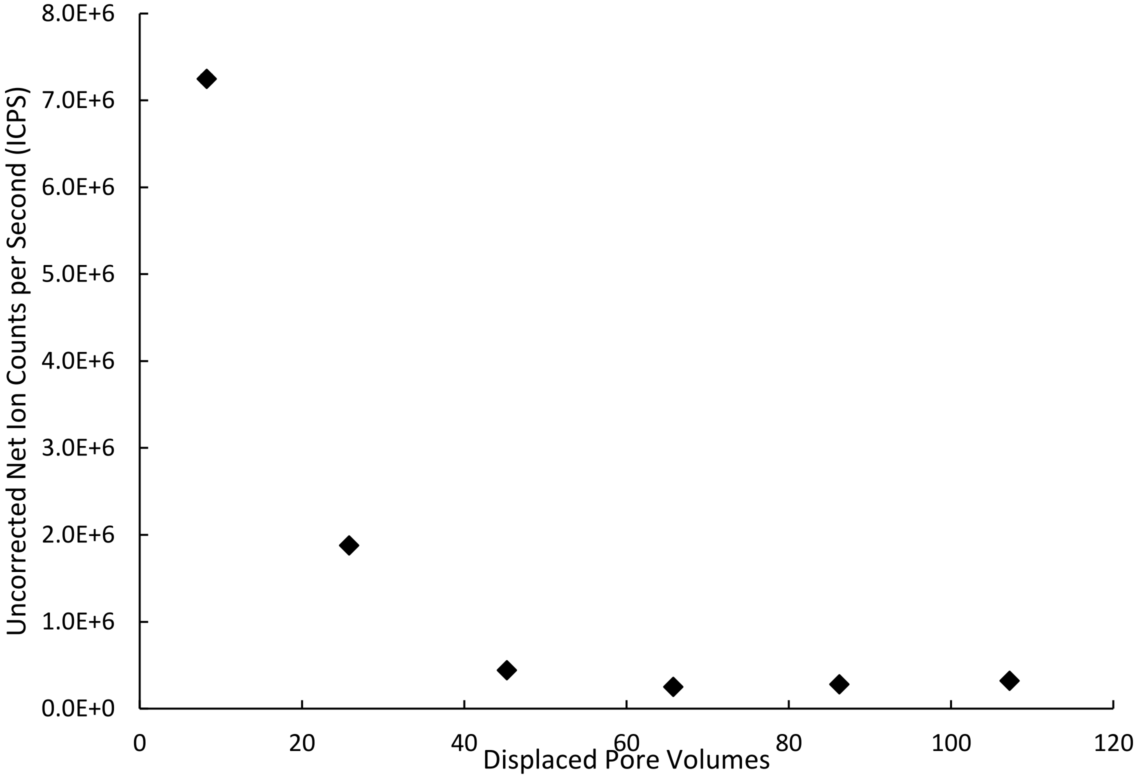

Figure C.7. Iron measured in the blank column effluent by ICP-MS on a linear scale. Confidence intervals of 1σ are derived from triplicate measurements of each sample.

Measurements of Soil Organic Matter in Batch Experiments

In order to test for the presence of soluble soil organic matter, batch samples of soil from the SRS were prepared in triplicate. Batch samples of 25 $g \cdot L^{-1}$ soil were prepared by adding 10 mM NaCl to 50 mL tubes and adjusting each sample to a pH of 4 or 5. Next, soil was added, and the pH was adjusted again. Batch samples of 114 $g \cdot L^{-1}$ soil were prepared by adding soil and water to 50 mL tubes. The solution pH was not adjusted, but buffered to pH 4.8 in contact with the soil. All samples were placed on a mixer/tumbler (≈10 rpm) for two days. At the sampling time, samples were centrifuged, and 20 mL of supernatant was removed for TOC analysis. When the 25 $g \cdot L^{-1}$ samples were centrifuged after 2 days they were centrifuged 30 min (3.2k rpm Allegra 6KR GH3.8 rotor). At all other sampling events, samples were centrifuged 16 min (9k rpm, Beckman C0650 rotor).

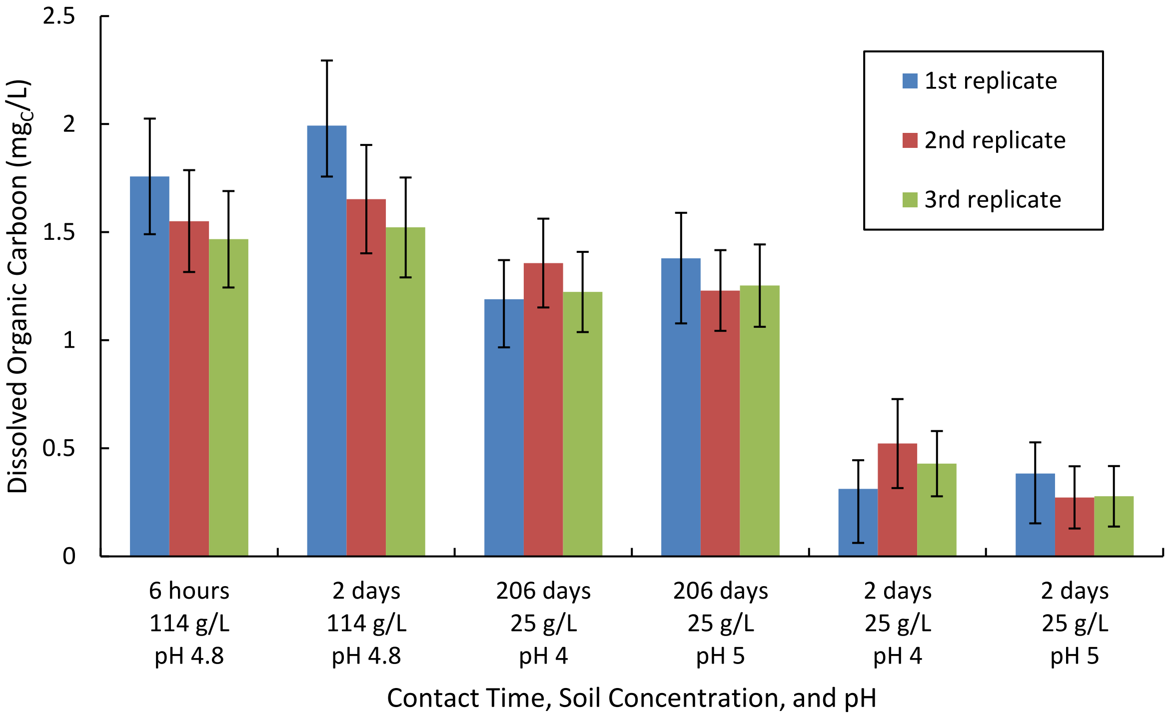

Figure C.8. Dissolved organic carbon measured in solutions contacted with soil from the Savannah River Site. The contact times, soil concentrations, and pH values are shown. Confidence intervals of 1σ are derived from replicate measurements of each sample and uncertainty in the TOC calibration curve.

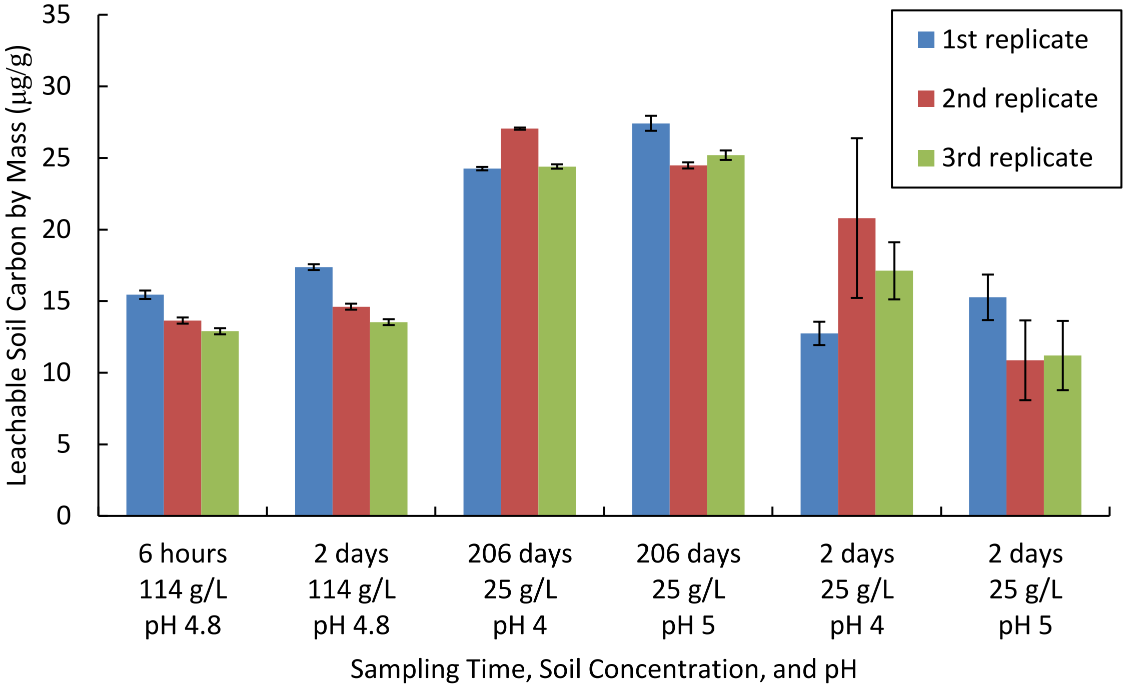

Figure C.9. Leachable soil carbon measured in solutions contacted with soil from the Savannah River Site. The contact times, soil concentrations, and pH values are shown. Confidence intervals of 1σ are derived from replicate measurements of each sample and uncertainty in the TOC calibration curve.

Mass of Organic Carbon Leached from the Soil

The mass of carbon leached from the soil was calculated for batch experiments (Fig. C.9) and can be calculated for the blank column experiment. By integrating the TOC measurements from the blank column experiment over the volume of water displaced, it was calculated that 280 ± 5 μg of carbon was eluted from the column containing 16.5 g of soil. Therefore, 17 $\mu g_c/g_{soil}$ was leached from the column. This is comparable to the 10–20 $\mu g_c/g_{soil}$ leachable organic carbon measured in batch experiments for up to 2 days.

An organic content of 0.9% was reported for the soil, and typical humic substances are approximately 50% carbon by mass (International Humic Substances Society). Therefore, the soil can be expected to contain 0.45% organic carbon, or 4500 $\mu g_c/g_{soil}$. The fraction of soil organic carbon which leached from the soil was only 0.002–0.004 in the blank column experiment and in batch experiments.

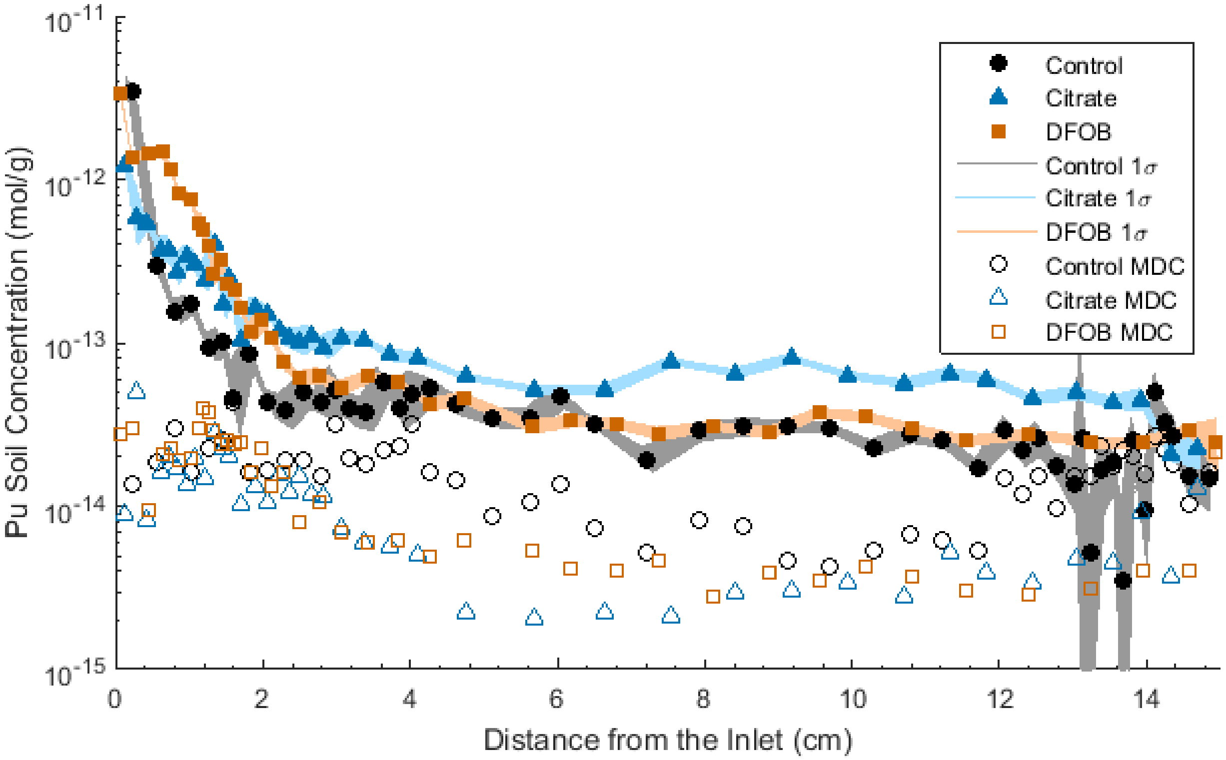

Figure C.10. Pu soil profile in columns packed with soil from the SRS. The uncertainty in the Pu soil concentration and the distance from the inlet were derived from counting statistics and the uncertainty in the mass of soil sections. The 1σ confidence band is shown. The minimum detectable concentration varied depending on soil mass and soil leachate volume.

Appendix D

Models of Pu Transport in Soil Columns

Table D.1. Variable definitions for the reactive transport models, where M represents the solute mass units and n represents the amount of colloids or ligands.

Var.	Units	Description
Q	$cm^3 \cdot min^{-1}$	flow rate
A	cm^2	cross sectional area
ρ	$g \cdot cm^{-3}$	bulk density
D	$cm^2 \cdot s^{-1}$	longitudinal dispersion coefficient, i.e. hydrodynamic dispersivity
u	$cm \cdot min^{-1}$	mean fluid velocity, i.e. Darcy velocity or volumetric water flux density
θ	-	volumetric water content
φ	-	porosity
x	cm	distance from the column inlet
t	min	time from start of spike injection
T	min	duration of spike injection
$g(t)$	$M \cdot cm^{-3} \cdot min^{-1}$	source or sink term
$h(t)$	n.a.	Heaviside function
$erfc(\ )$	n.a.	complimentary error function
V_{pore}	cm^3	pore volume
p	-	number of displaced pore volumes
C_{Pu}	$M \cdot cm^{-3}$	aqueous Pu concentration
S_{Pu}	$M \cdot g^{-1}$	sorbed Pu concentration
C_{Pu}^{IV}	$M \cdot cm^{-3}$	aqueous Pu(IV) concentration
S_{Pu}^{IV}	$M \cdot g^{-1}$	sorbed Pu(IV) concentration
C_{Pu}^{V}	$M \cdot cm^{-3}$	aqueous Pu(V) concentration
S_{Pu}^{V}	$M \cdot g^{-1}$	sorbed Pu(V) concentration
K_d	$cm^3 \cdot g^{-1}$	Pu distribution coefficient
K_d^{IV}	$cm^3 \cdot g^{-1}$	Pu(IV) distribution coefficient
K_d^{V}	$cm^3 \cdot g^{-1}$	Pu (V) distribution coefficient
R	-	Pu retardation coefficient
R^{IV}	-	Pu(IV) retardation coefficient
R^{V}	-	Pu(V) retardation coefficient

Table D.1 (Continued)

Var.	Units	Description	
μ'_s	min^{-1}	first-order reduction rate constant of sorbed Pu(V) to sorbed Pu(IV)	
$f_{Pu(V)}$	-	fraction of Pu(V) in the column loading solution	
K'_{PuL}	-	Pu–ligand complex conditional stability constant	
K_d^{ligand}	$\mathrm{cm}^3\cdot\mathrm{g}^{-1}$	ligand distribution coefficient	
$C_{Pu,0}$	$\mathrm{M}\cdot\mathrm{cm}^{-3}$	spike solution Pu concentration	
		Colloid Facilitated Transport	Ligand Facilitated Transport
$S_{mc}\cdot C_c$	$\mathrm{M}\cdot\mathrm{cm}^{-3}$	Pu sorbed to mobile colloids	aqueous Pu–ligand complexes
$S_{ic}\cdot S_c$	$\mathrm{M}\cdot\mathrm{g}^{-1}$	Pu sorbed to immobile colloids	sorbed Pu–ligand complexes
C_c	$\mathrm{n}\cdot\mathrm{cm}^{-3}$	mobile colloid concentration	dissolved ligand concentration
S_c	$\mathrm{n}\cdot\mathrm{g}^{-1}$	colloids attached to soil	sorbed ligand concentration
k_{att}	min^{-1}	colloid attachment	ligand sorption to soil
k_{det}	min^{-1}	colloid detachment	ligand desorption from soil
k_{ac}	min^{-1}	Pu sorption to colloids	formation of Pu–ligand complexes
k_{dc}	min^{-1}	Pu desorption from colloids	dissociation of Pu–ligand complexes
C_c^0	$\mathrm{n}\cdot\mathrm{cm}^{-3}$	initial concentration of colloids if they were entirely mobilized	initial concentration of ligands if they were entirely dissolved
S_c^0	$\mathrm{n}\cdot\mathrm{g}^{-1}$	initial concentration of colloids if they were entirely attached to soil	initial concentration of ligands if they were entirely sorbed

Classical Reactive Transport Model (a.k.a. K_d Model)

This classical reactive transport model considers instantaneous linear sorption equilibrium between the solute and the soil. The general one-dimensional advection-dispersion equation is given by Eqn. D.1. In Eqn. D.2, the effect of solute sorption is described by the retardation factor, R, which is related to the distribution coefficient, K_d, (Eqns. D.3 and D.4). The use of the retardation factor assumes instantaneous sorption equilibrium and a linear sorption isotherm. The source term, $g(t)$, for a finite step input is given in Eqn. D.5, and remaining variables are defined in Table D.1. The analytical solution to Eqn. D.2 with a finite step input is given in Eqn. D.6 with an auxiliary function, $a(t)$, defined in Eqn. D.7. The ^{3}H Tracer was modeled with retardation factor as an adjustable parameter so that any deviation from unity could be detected. This analytical solution was used with least-squares fitting to model the ^{3}H tracer. The general equation forms the basis of further reactive transport modeling.

$$\varphi \frac{\partial C}{\partial t} = D \frac{\partial^2 C}{\partial x^2} - u \frac{\partial C}{\partial x} + g(t) \tag{D.1}$$

$$\varphi R \frac{\partial C}{\partial t} = D \frac{\partial^2 C}{\partial x^2} - u \frac{\partial C}{\partial x} + g(t) \tag{D.2}$$

Retardation factor:

$$R = 1 + K_d \frac{\rho}{\varphi} \tag{D.3}$$

Distribution coefficient:

$$K_d = \frac{S}{C} \tag{D.4}$$

$$g(t) = C_0[h(g) - h(t - T)] \tag{D.5}$$

Analytical solution:

$$\frac{C}{C_0} = \frac{1}{2}[a(t) - h(t - T)a(t - T)] \tag{D.6}$$

$$a(t') = erfc\left(\frac{x - \frac{u}{\varphi R} t'}{\sqrt{4 \frac{D}{\varphi R} t'}}\right) + exp\left(\frac{ux}{D}\right) erfc\left(\frac{x + \frac{u}{\varphi R} t'}{\sqrt{4 \frac{D}{\varphi R} t'}}\right) \tag{D.7}$$

Determination of Apparent K_d from a Batch Experiment

A batch test was performed to determine the distribution coefficient for Pu on the SRS soil in the presence of citrate and DFOB. A ^{238}Pu(IV) stock in 1 M HCl was prepared as previously described. Stock solutions of 13.9 mM (1000 $\mathrm{mg_c \cdot L^{-1}}$) citrate and 3.3 mM (1000 $\mathrm{mg_c \cdot L^{-1}}$) DFOB were prepared by dissolving sodium citrate dihydrate and desferrioxamine mesylate, respectively, into water. Samples 20 mL in volume were prepared by adding soil, organic ligand stock solution, 1 M NaOH, and ^{238}Pu(IV) stock to 10 mM NaCl. A sample with no organic ligand added was also prepared. The suspended solids concentration was 25 $\mathrm{g \cdot L^{-1}}$. The 1 M NaOH was added before the Pu(IV) stock to minimize fluctuations in pH. The pH was adjusted to 4.8 ± 0.2 with dilute NaOH and HCl. The concentrations of citrate and DFOB were selected to range from 0.5 $\mathrm{mg_c \cdot L^{-1}}$ to 50 $\mathrm{mg_c \cdot L^{-1}}$. The molar concentrations were 0.0059–0.79 mM and 0.0016–0.17 mM for citrate and DFOB, respectively. After one day, the aqueous Pu was measured by removing 1.1 mL of solution for centrifugation (20 min, 10k rpm, Eppendorf MiniSpin) and 1 mL of supernatant was removed for liquid scintillation counting.

In the DFOB samples (Fig. D.1), the fraction of Pu sorbed was elevated compared to the sample with no added ligand and showed no trend. In the citrate samples, the fraction of Pu sorbed was increased for citrate concentrations less than 0.07 mM and diminished for citrate concentrations greater than 0.21 mM, relative to the sample with no added ligand.

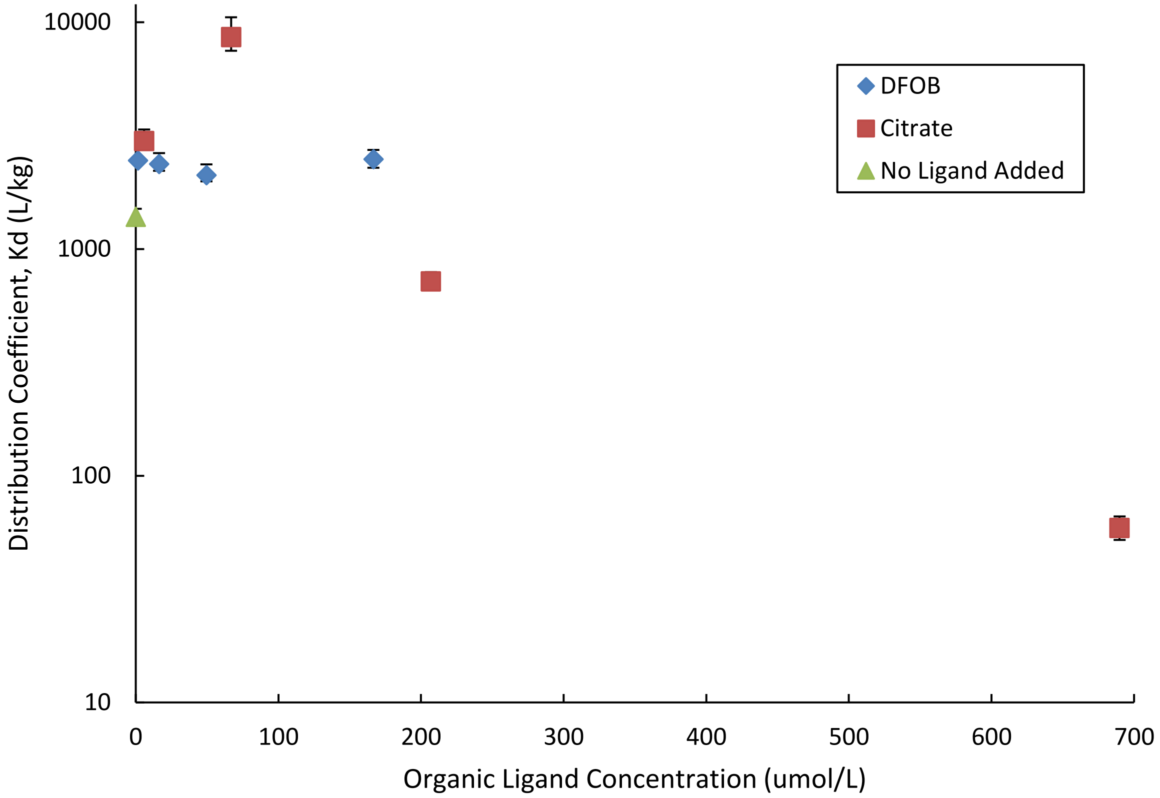

Figure D.1. Measured K_d values for Pu in the presence of citrate and DFOB. The K_d values for citrate (210 and 690 µM), DFOB (170 µM), and no organic ligand were used in reactive transport modeling to predict the Pu soil distribution in columns.

In order to test whether the mobility of the soil-bound Pu could be predicted from the measured K_d values (Table D.2), the estimated K_d values for Pu in the presence of no added ligand, 0.21 mM citrate, 0.69 mM citrate, and 0.17 mM DFOB were used to try to predict Pu mobility with a reactive transport model. These measurements were chosen because they correspond to samples which had the most similar ligand concentrations to the column experiments. The one-dimensional advection-dispersion model with a K_d model of sorption was used to model Pu with a finite-step input.

Table D.2. Summary of Pu batch sorption to soil in the presence of citrate and DFOB. The suspended solids concentration was 25 g·L^{-1}. The pH was 4.8, and the ionic strength was maintained with 10 mM NaCl. The uncertainty of 2σ was propagated from counting statistics.

Ligand	Total Ligand Concentration (mM)	Fraction Pu Sorbed	Distribution Coefficient, K_d (mL·g^{-1})
Organic-free	n.a.	0.972 ± 0.002	1390 [a]
Citrate	0.0059	0.987 ± 0.001	3000
Citrate	0.067	0.995 ± 0.001	8590
Citrate	0.21	0.948 ± 0.002	720 [a]
Citrate	0.69	0.594 ± 0.001	59 [a]
DFOB	0.0016	0.985 ± 0.001	2460
DFOB	0.016	0.984 ± 0.001	2370
DFOB	0.050	0.982 ± 0.004	2120
DFOB	0.17	0.984 ± 0.029	2490 [a]

[a] The estimated K_d values for Pu in the presence of no added ligand, 0.21 mM citrate, 0.69 mM citrate, and 0.17 mM DFOB were used to try to predict Pu mobility with a reactive transport model.

K_d Model of Pu Soil Profile Only

Batch sorption experiments were performed to gain an understanding of the potential mobility of Pu in the absence and presence of citrate and DFOB. Apparent distribution coefficients for Pu of 1390, 720, 59, and 2490 $mL \cdot g^{-1}$ were estimated from batch tests with 25 $g \cdot L^{-1}$ soil and no organic ligand, 0.21 mM total citrate, 0.69 mM total citrate, and 0.17 mM total DFOB, respectively (Table D.3). The measured ligand-free Pu K_d value of 1390 $mL \cdot g^{-1}$ was lower than previously measured K_d values on similar soils. Previously, K_d values of 2100 $mL \cdot g^{-1}$ and 3000 $mL \cdot g^{-1}$ were reported for Pu(IV) in batch tests with sandy loam soil from the SRS (Powell et al., 2002). The difference could be due to differences in soil composition, such as clay fraction minerology, iron content, or organic content.

The K_d values from the batch tests, were used to predict the Pu soil profile using the advection-dispersion reactive transport model with K_d sorption and a finite step input of Pu (Fig. D.2). This model does not account for aqueous Pu eluted from the column. The model provided an excellent fit to the soil Pu data in the control column. It correctly predicted that the Pu was highly concentrated in the first soil section of the control column. Neither K_d value measured in the presence of citrate provided a good fit to the Pu soil measurements in the citrate column. The Pu was more broadly distributed in the column than could be predicted from this model. Although the model does a poor job at predicting most of the soil Pu profile in the DFOB column, it correctly predicts a portion of Pu with very low mobility which is found in the first two soil segments within 0.3 cm of the inlet. While the resolution of the column data is not high enough to indicate whether a portion of the Pu has diminished mobility in the presence of DFOB, the greater Pu K_d value measured in the DFOB batch sample, relative to the ligand-free sample, suggests that the presence of DFOB enhanced Pu sorption to this soil. One possible explanation for increased sorption in the batch test with DFOB is that there is a small amount of smectite in the soil, and DFOB enhanced Pu sorption to this soil component (Boggs et al., 2015).

In an effort to quantify the mobility of the soil Pu, the reactive transport model was fit to the Pu soil data with K_d as an adjustable parameter (Table D.3 and Fig. D.3). Aqueous Pu eluted from the column was excluded from model optimization. The model estimated K_d values of 1200 $mL \cdot g^{-1}$ and 940 $mL \cdot g^{-1}$ for the control and citrate columns, respectively. Since two Pu peaks were observed in the DFOB column, the model was optimized separately for each peak resulting in K_d values of 1900 $mL \cdot g^{-1}$ and 300 $mL \cdot g^{-1}$. Compared to the K_d values measured in the batch experiment, the optimized K_d values for the control column and the first peak of the DFOB column were similar, and they provided similarly good fits. Thus, the K_d measurements from the batch experiment were good predictors of Pu mobility in ligand-free solution and the mobility of a portion of Pu in the presence of DFOB. Batch measurements did not predict the enhanced mobility of the Pu which comprises the second peak located 0.6 cm from the entrance of the DFOB column. This could be because DFOB was added to the column after the addition of Pu, or because the DFOB column experiment had a much greater aqueous concentration of DFOB (0.28 mM aqueous) compared to the batch experiment (0.17 mM total). In the citrate column, as disucssed above, the Pu soil data is too broad to be represented with a single K_d value. This

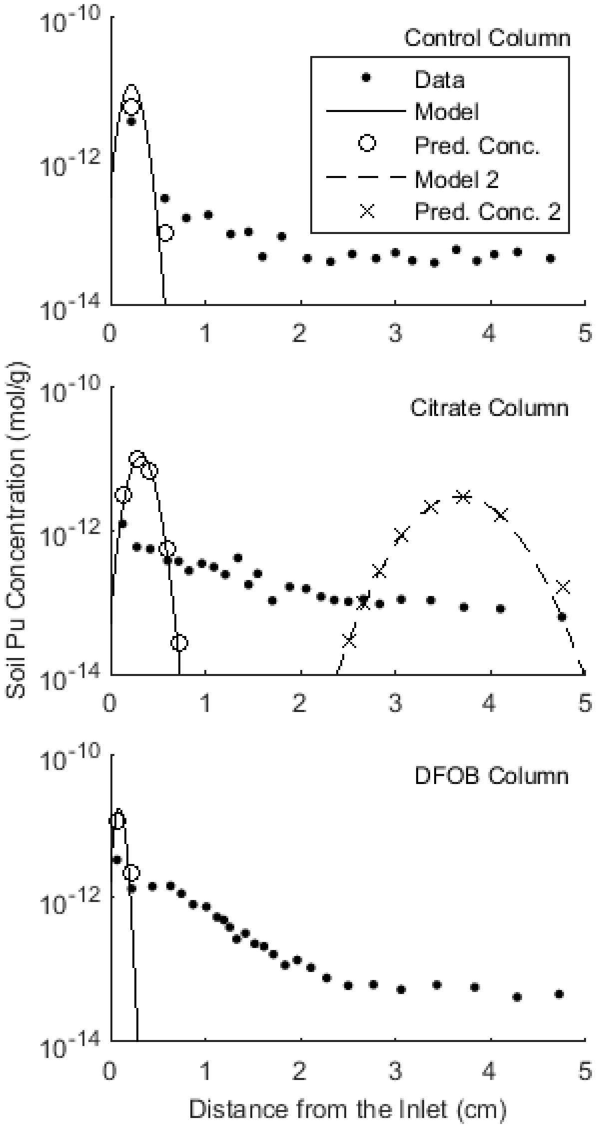

Figure D.2. Predicted transport of Pu in soil using K_d values measured in a batch experiment. The K_d values used for modeling were determined from batch experiments at pH 4.8 with added ligand concentrations as follows: control, no ligand added; citrate, 0.21 and 0.69 mM; and DFOB, 0.17 mM. The K_d values were 1390, 720, 59, and 2490 mL·g^{-1} for the control, first citrate, second citrate, and DFOB models respectively. The predicted concentration of each soil section (shown) was determined by averaging the model concentration over the width of each soil section.

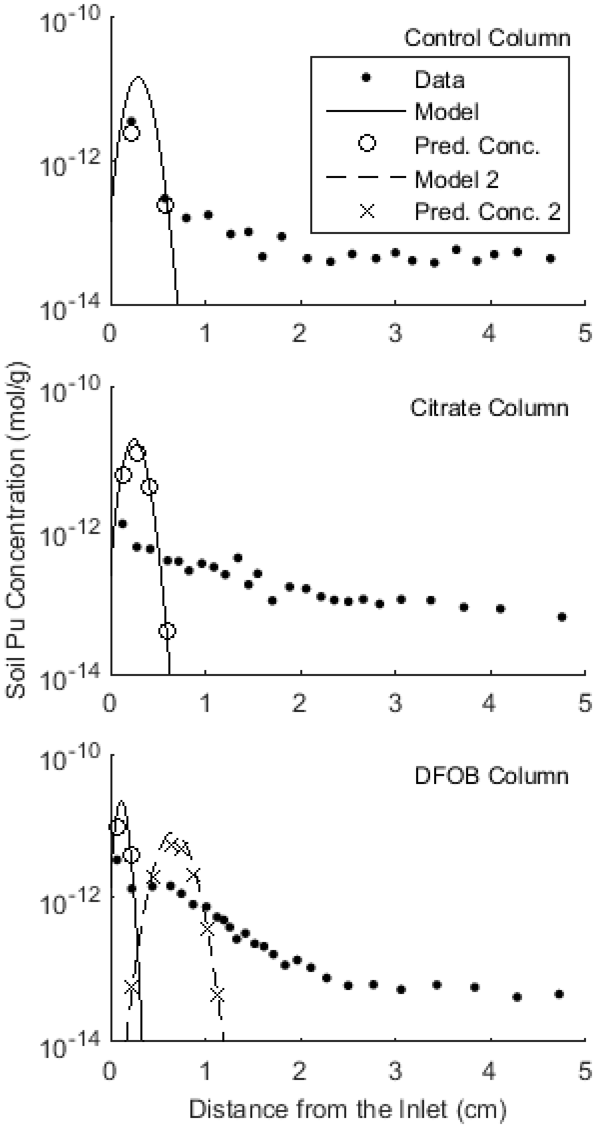

Figure D.3. Modeled transport of Pu in soil with optimized K_d values of 1200, 940, 1900, and 300 mL·g^{-1} for the control, citrate, first DFOB and second DFOB models, respectively. The predicted concentration of each soil section (shown) was determined by averaging the model concentration over the width of each soil section.

Table D.3. K_d values estimated from fitting the K_d model to the Pu soil profile

Experiment	Soil Pu K_d (L·kg^{-1})
Ligand-free Control	1200
Citrate	940
DFOB, first peak	1900
DFOB, second peak	300

could be due to kinetic limitations of sorption rates compared to theh Pu contact time with the soil.

There were some limitations to using the K_d transport model both in a predictive capacity, and also as a parameter estimation for the K_d value. The K_d model indicates no elution of Pu from the columns, but 9–20% of Pu was observed to elute from the columns. The citrate and DFOB ligands were not explicitly included in the model, but the model used an apparent K_d value which assumed a constant concentration of the ligand. Therefore, the K_d model for the citrate and DFOB columns was only valid in the small region where the ligands were present. This may explain why the model was unable to describe the observed broad Pu distributions (extending to 2.5 cm in the DFOB column and 14 cm in the citrate column). The Pu observed at 2–15 cm was likely retained in the soil after the passage of the mobile Pu. However, there also appeared to be some ligand-dependent behavior suggesting that the presence of a ligand influenced the mobility of Pu beyond the predicted range of the ligand distribution in the soil. One difference between the batch K_d measurements and the columns was the order of addition; in the column experiments, Pu adsorbed to the soil might have been less available to the ligands or desorption facilitated by the ligands could be rate limiting relative to the timeframe of these experiments.

Pu Transport with Surface Mediated Reduction

Transport of Pu(IV) and Pu(V) are each modeled according to the one-dimensional advection-dispersion transport equation (Eqn. D.2), where an additional first-order source/sink term representing reduction of sorbed Pu(V) to form sorbed Pu(IV) is included (Eqns. D.8 and D.9). The first-order reduction rate constant reduction of Pu(V) to Pu(IV) is given by μ'_s. Because K_d sorption is assumed, the sorbed Pu concentrations are given by (Eqns. D.10 and D.11). The respective retardation factors for Pu(IV) and Pu(V) are defined according to Eqn. D.3 using respective distribution coefficients.

Transport of Pu(V):

$$\varphi R^{V} \frac{\partial C_{Pu}^{V}}{\partial t} = D \frac{\partial^2 C_{Pu}^{V}}{\partial x^2} - u \frac{\partial C_{Pu}^{V}}{\partial x} - \mu'_s \frac{\rho}{\varphi} K_d^{V} C_{Pu}^{V} + g(t) \tag{D.8}$$

Transport of Pu(IV):

$$\varphi R^{IV} \frac{\partial C_{Pu}^{IV}}{\partial t} = D \frac{\partial^2 C_{Pu}^{IV}}{\partial x^2} - u \frac{\partial C_{Pu}^{IV}}{\partial x} + \mu'_s \frac{\rho}{\varphi} K_d^{V} C_{Pu}^{V} + g(t) \tag{D.9}$$

$$S_{Pu}^{V} = K_d^{V} C_{Pu}^{V} \tag{D.10}$$

$$S_{Pu}^{IV} = K_d^{IV} C_{Pu}^{IV} \tag{D.11}$$

Table D.4. Summary of parameters from literature for modeling of surface mediated reduction

K_d^{IV} ($\mathrm{mL\cdot g^{-1}}$)	K_d^{V} ($\mathrm{mL\cdot g^{-1}}$)	R^{IV}	R^{V}	μ'_s ($\mathrm{min^{-1}}$)	pH	Source	Comment
1390					4.8	This work	
				2.04E-03	5	Powell et al. (2005)	goethite
				1.12E-01	6	Kaplan et al. (2004)	loamy SRS sediment
			7.9–8.8	1.80E-03	5	Fjeld et al. (2003)	SRS sandy loam
		1500 [a]	38 [a]		4.75	Powell et al. (2002)	SRS soil
2100					4.81	Powell et al. (2002)	Subsurface Clayey
	10				4.74	Powell et al. (2002)	Subsurface Clayey
220					4.53	Powell et al. (2002)	Subsurface Sandy
390					4.75	Powell et al. (2002)	Subsurface Sandy
	6				4.75	Powell et al. (2002)	Subsurface Sandy
3000					4.63	Powell et al. (2002)	Surface Clayey
	2500				4.71	Powell et al. (2002)	Surface Clayey
620					4.18	Powell et al. (2002)	Surface Sandy
260					4.19	Powell et al. (2002)	Surface Sandy
	30				4.82	Powell et al. (2002)	Surface Sandy
180		1030 [a]	52 [a]		4.7	Prout (1958)	SRS soil
290		920 [a]	50 [a]		5.0	Prout (1958)	SRS soil
				8.40E-04	5	Kaplan et al. (2001)	SRS soil
				1.20E-03 [b]		Sanchez et al. (1985)	goethite, lower estimate
				1.20E-02 [b]		Sanchez et al. (1985)	goethite, upper estimate
				6.00E-06 [b]	8	Keeney-Kennicutt and Morse (1985)	goethite, lower estimate
				6.00E-02 [b]	8	Keeney-Kennicutt and Morse (1985)	goethite, upper estimate

[a] Calculated by Fjeld et al. (2003)

[b] Calculated by McGinnis (2000)

Effect of Varying Reduction Rate Constant, μ'_s

The model was sensitive to the reduction rate constant (Figs. D.4 – D.8). Increasing the reduction rate constant caused less Pu to be eluted from the column since Pu(V) was more rapidly reduced to Pu(IV) which remained sorbed to the soil. This affected the shape of the Pu soil profile because more Pu was deposited closer to the entrance of the column. For example, at the highest reduction rate constant modeled (Fig. D.8), 0.003 min^{-1}, the concentration of Pu in the soil declined from 2 cm to 15 cm more steeply than when lower reduction rate constants were modeled. Reduction rate constants in the range 0.0005 to 0.0015 min^{-1} demonstrated reasonable fits to the Pu soil profile. The reduction rate constant had no effect on the broadness of the effluent Pu peak.

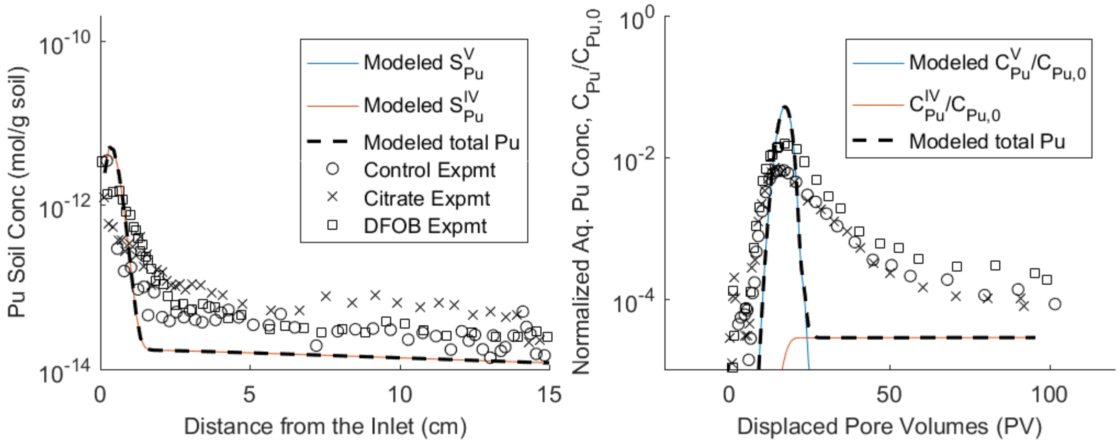

Figure D.4. A reactive transport model which includes surface mediated reduction was used to predict concentrations of Pu(IV) and Pu(V) in the soil profile (left) and in the elution profile (right). Experimental data from the control, citrate, and DFOB column experiments is shown. $\boldsymbol{\mu's}$ **= 0.0003 min^{-1}**; K_d^{IV} = 1000 mL·g^{-1}; K_d^{V} = 8 mL·g^{-1}; $f_{Pu(V)}$ = 0.2

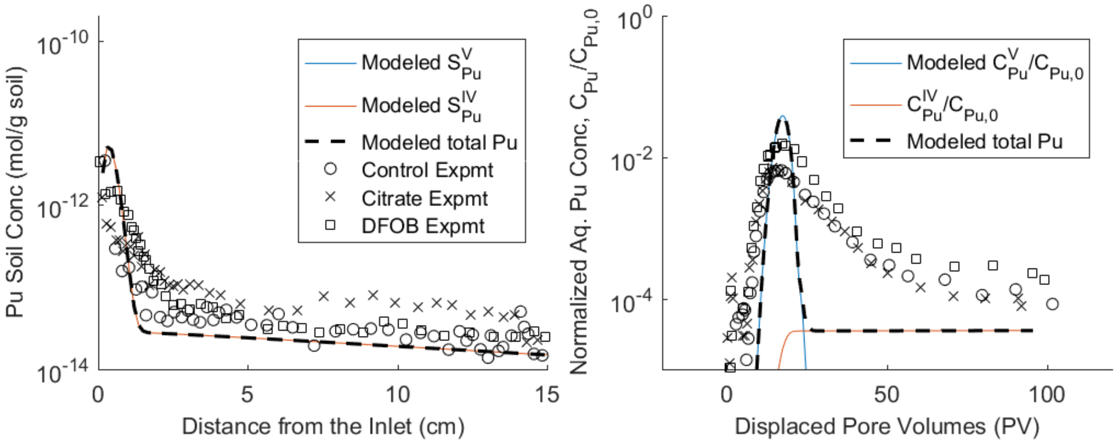

Figure D.5. A reactive transport model which includes surface mediated reduction was used to predict concentrations of Pu(IV) and Pu(V) in the soil profile (left) and in the elution profile (right). Experimental data from the control, citrate, and DFOB column experiments is shown. **μ's = 0.0005 min^{-1}**; K_d^{IV} = 1000 mL·g^{-1}; K_d^{V} = 8 mL·g^{-1}; $f_{Pu(V)}$ = 0.2

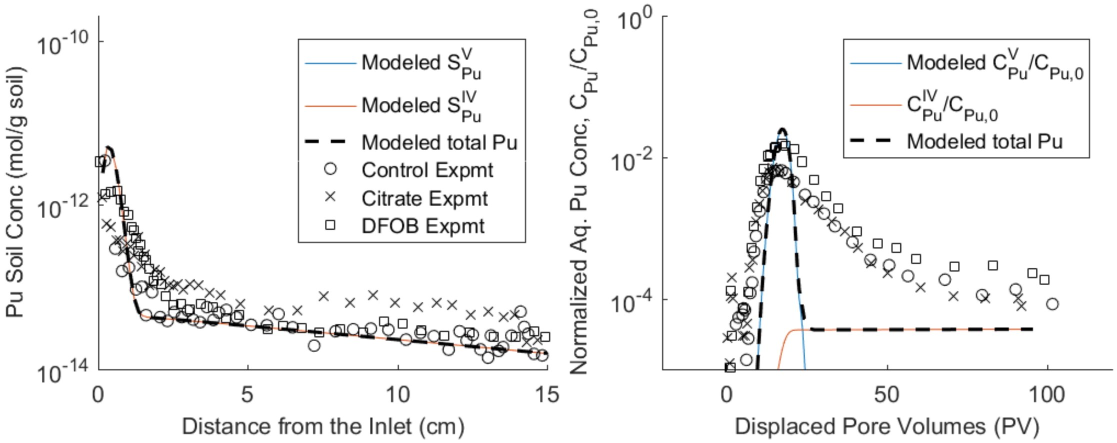

Figure D.6. A reactive transport model which includes surface mediated reduction was used to predict concentrations of Pu(IV) and Pu(V) in the soil profile (left) and in the elution profile (right). Experimental data from the control, citrate, and DFOB column experiments is shown. **μ's = 0.0008 min^{-1}**; K_d^{IV} = 1000 mL·g^{-1}; K_d^{V} = 8 mL·g^{-1}; $f_{Pu(V)}$ = 0.2

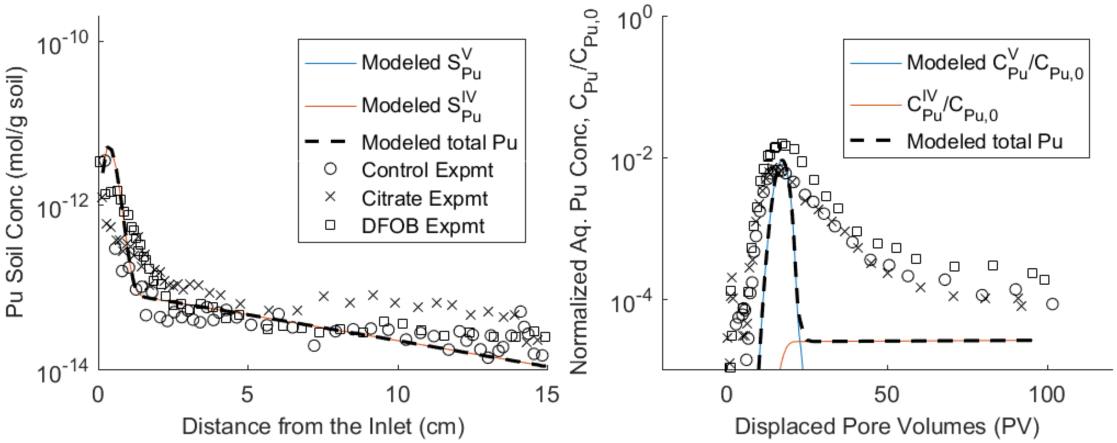

Figure D.7. A reactive transport model which includes surface mediated reduction was used to predict concentrations of Pu(IV) and Pu(V) in the soil profile (left) and in the elution profile (right). Experimental data from the control, citrate, and DFOB column experiments is shown. ***μ's* = 0.0015 min^{-1}**; K_d^{IV} = 1000 mL·g^{-1}; K_d^{V} = 8 mL·g^{-1}; $f_{Pu(V)}$ = 0.2

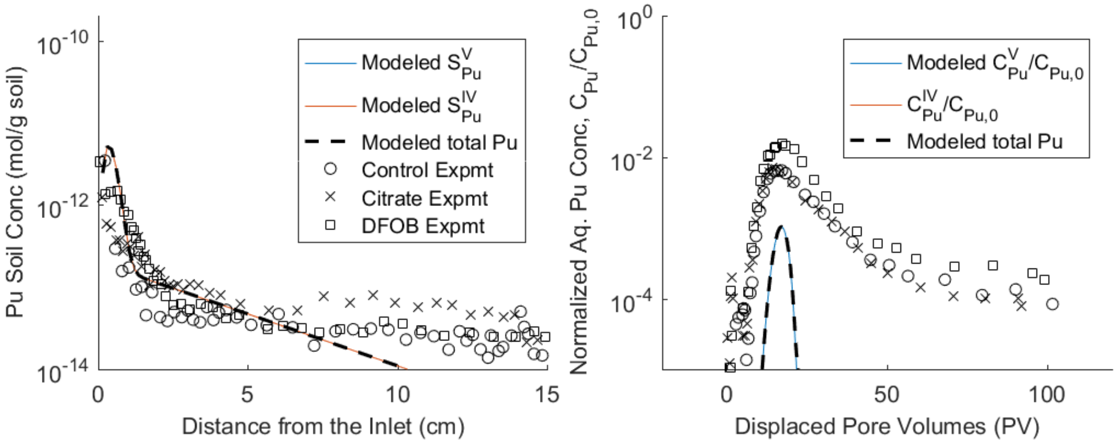

Figure D.8. A reactive transport model which includes surface mediated reduction was used to predict concentrations of Pu(IV) and Pu(V) in the soil profile (left) and in the elution profile (right). Experimental data from the control, citrate, and DFOB column experiments is shown. ***μ's* = 0.003 min^{-1}**; K_d^{IV} = 1000 mL·g^{-1}; K_d^{V} = 8 mL·g^{-1}; $f_{Pu(V)}$ = 0.2

Effect of Varying Pu(IV) Distribution Coefficient, K_d^{IV}

The Pu(IV) distribution coefficient controlled the position of the Pu peak in the soil profile and the amount of Pu(IV) which is eluted from the column (Figs. D.9–D.13). A range of K_d^{IV} values from 600 mL·g^{-1} to 3000 mL·g^{-1} was able to reasonably fit the soil profile in the first 2 cm of the column. At lower K_d^{IV} values below 600 mL·g^{-1}, too much Pu was predicted to be flushed from the first 2 cm of the column (Fig. D.9). As the value of K_d^{IV} decreased, more Pu(IV) was eluted from the column. This is because Pu(IV) was distributed throughout the column by the passage and reduction of Pu(V), and lower K_d^{IV} values allow this distributed Pu(IV) to be eluted. However, Pu(IV) is predicted to elute at nearly a constant rate, and the K_d^{IV} has no effect on the broadness of the peak predicted in the elution profile.

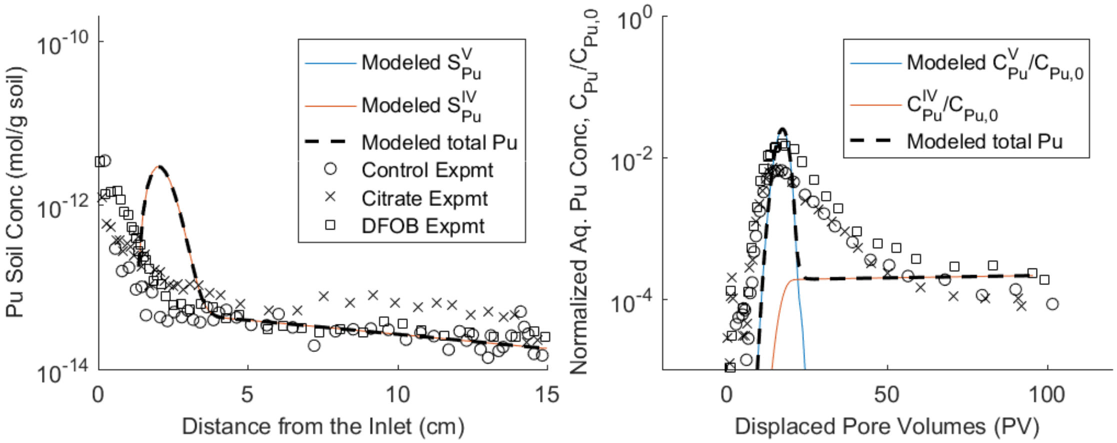

Figure D.9. A reactive transport model which includes surface mediated reduction was used to predict concentrations of Pu(IV) and Pu(V) in the soil profile (left) and in the elution profile (right). Experimental data from the control, citrate, and DFOB column experiments is shown. $\mu's$ = 0.0008 min^{-1}; **K_d^{IV} = 200 mL·g^{-1}**; K_d^{V} = 8 mL·g^{-1}; $f_{Pu(V)}$ = 0.2

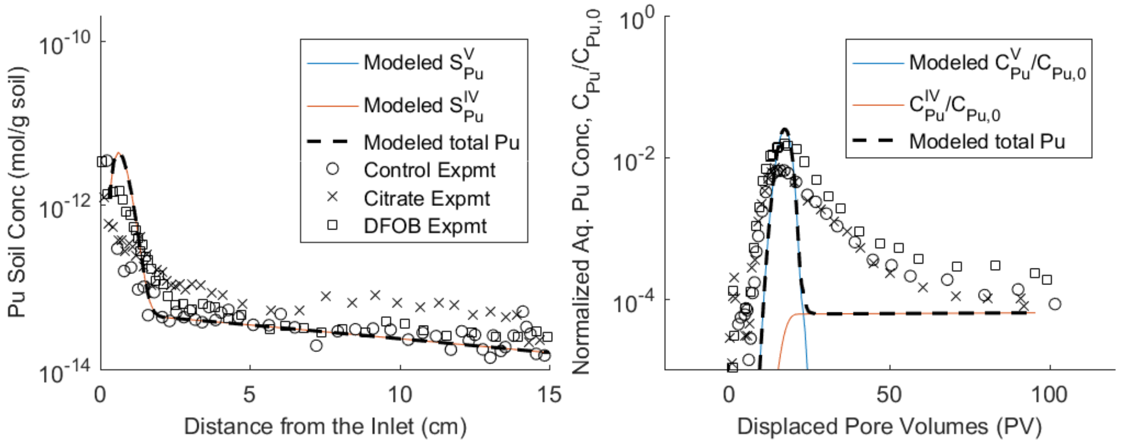

Figure D.10. A reactive transport model which includes surface mediated reduction was used to predict concentrations of Pu(IV) and Pu(V) in the soil profile (left) and in the elution profile (right). Experimental data from the control, citrate, and DFOB column experiments is shown. $\mu's$ = 0.0008 min^{-1}; $\boldsymbol{K_d^{IV}}$ **= 600 mL·g^{-1}**; K_d^{V} = 8 mL·g^{-1}; $f_{Pu(V)}$ = 0.2

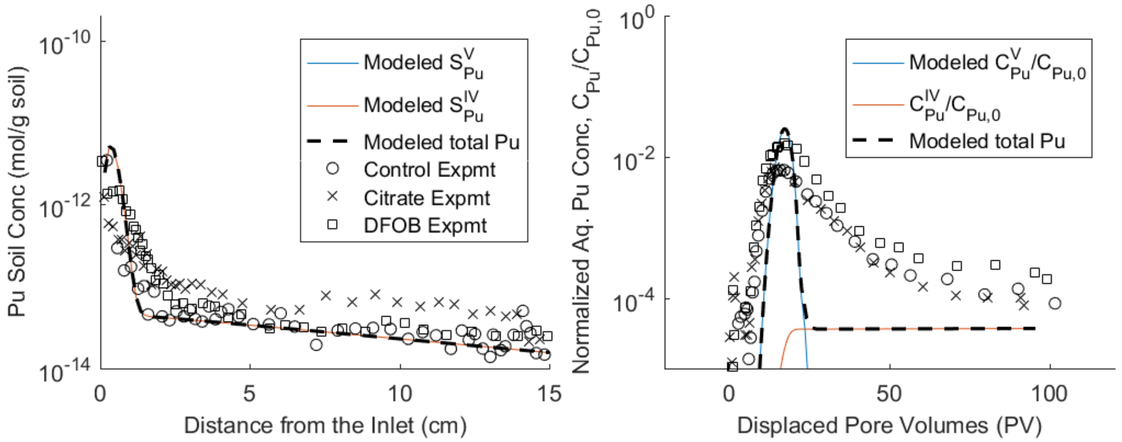

Figure D.11. A reactive transport model which includes surface mediated reduction was used to predict concentrations of Pu(IV) and Pu(V) in the soil profile (left) and in the elution profile (right). Experimental data from the control, citrate, and DFOB column experiments is shown. $\mu's$ = 0.0008 min^{-1}; $\boldsymbol{K_d^{IV}}$ **= 1000 mL·g^{-1}**; K_d^{V} = 8 mL·g^{-1}; $f_{Pu(V)}$ = 0.2

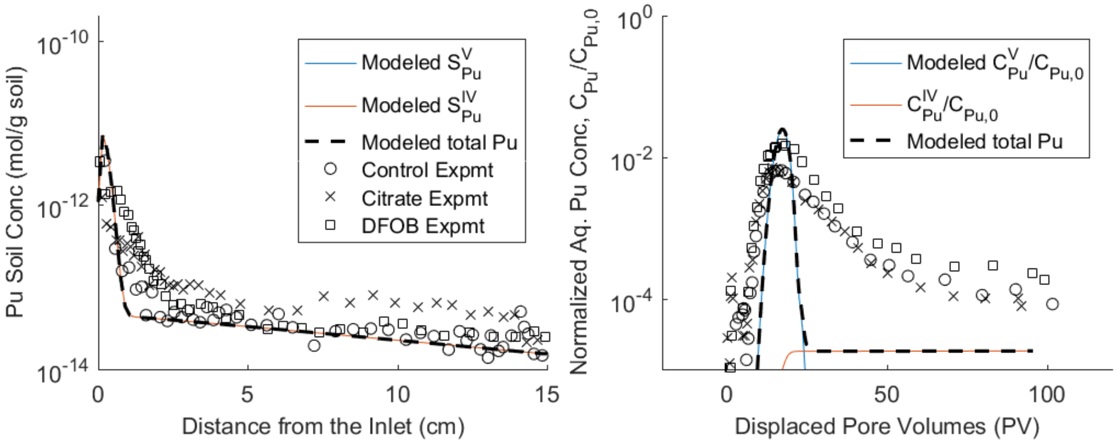

Figure D.12. A reactive transport model which includes surface mediated reduction was used to predict concentrations of Pu(IV) and Pu(V) in the soil profile (left) and in the elution profile (right). Experimental data from the control, citrate, and DFOB column experiments is shown. $\mu's$ = 0.0008 min^{-1}; $\boldsymbol{K_d^{IV} = 2000\ \mathrm{mL \cdot g^{-1}}}$; K_d^{V} = 8 $\mathrm{mL \cdot g^{-1}}$; $f_{Pu(V)}$ = 0.2

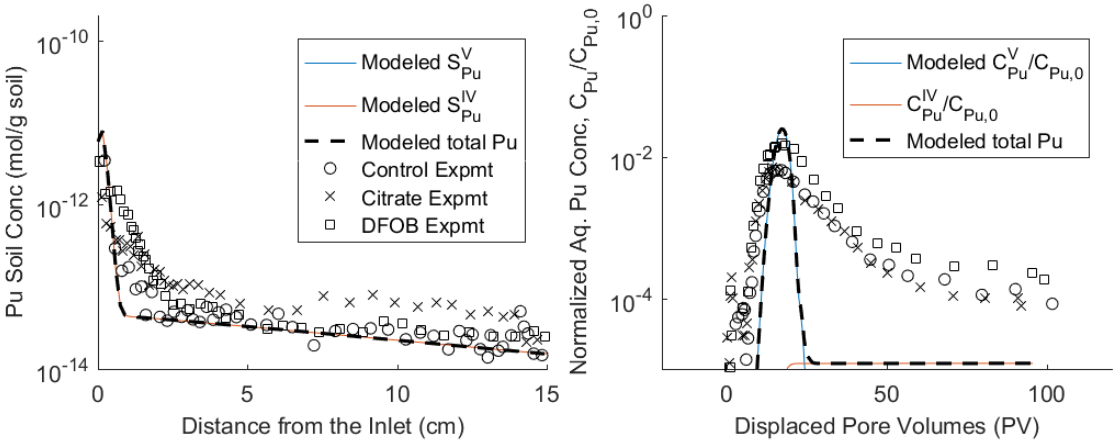

Figure D.13. A reactive transport model which includes surface mediated reduction was used to predict concentrations of Pu(IV) and Pu(V) in the soil profile (left) and in the elution profile (right). Experimental data from the control, citrate, and DFOB column experiments is shown. $\mu's$ = 0.0008 min^{-1}; $\boldsymbol{K_d^{IV} = 3000\ \mathrm{mL \cdot g^{-1}}}$; K_d^{V} = 8 $\mathrm{mL \cdot g^{-1}}$; $f_{Pu(V)}$ = 0.2

Effect of Varying Pu(V) Distribution Coefficient, K_d^V

The Pu elution profile was sensitive to the Pu(V) distribution coefficient (Figs. D.14 – D.17). A K_d^V value of 8 mL·g^{-1} demonstrated the best fit to the peak in the Pu elution profile. For K_d^V values that were too low, the peak was predicted too early (Fig. D.14), and for values that are too high the peak was predicted too late (Figs. D.16 and D.17). The K_d^V value also affected the Pu soil profile. As the K_d^V value was increased, Pu(V) moved through the column more slowly, resulting in more Pu deposited in soil closer to the column entrance as Pu(V) was reduced to Pu(IV). The best fit K_d^V value of 8 mL·g^{-1} did not predict the broadness of the Pu effluent peak observed.

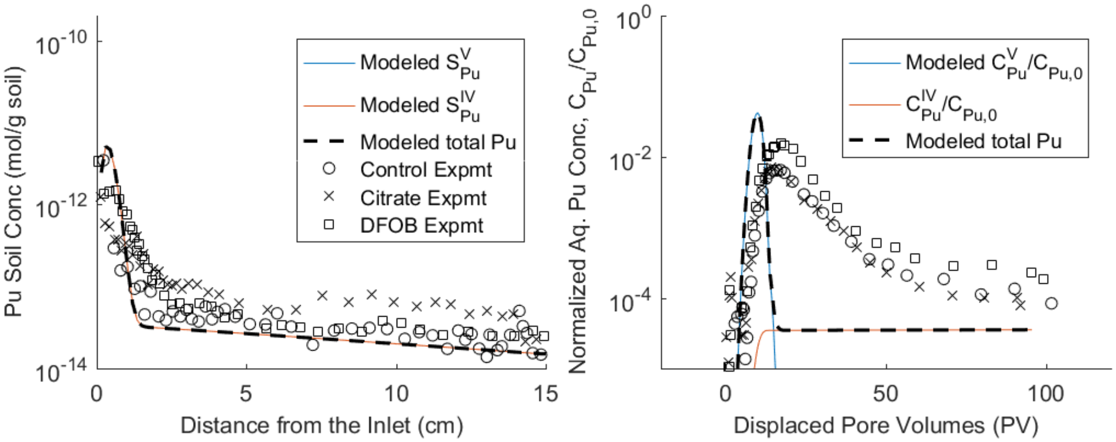

Figure D.14. A reactive transport model which includes surface mediated reduction was used to predict concentrations of Pu(IV) and Pu(V) in the soil profile (left) and in the elution profile (right). Experimental data from the control, citrate, and DFOB column experiments is shown. $\mu's$ = 0.0008 min^{-1}; K_d^{IV} = 1000 mL·g^{-1}; $\boldsymbol{K_d^V = 6}$ **mL·g^{-1}**; $f_{Pu(V)}$ = 0.2

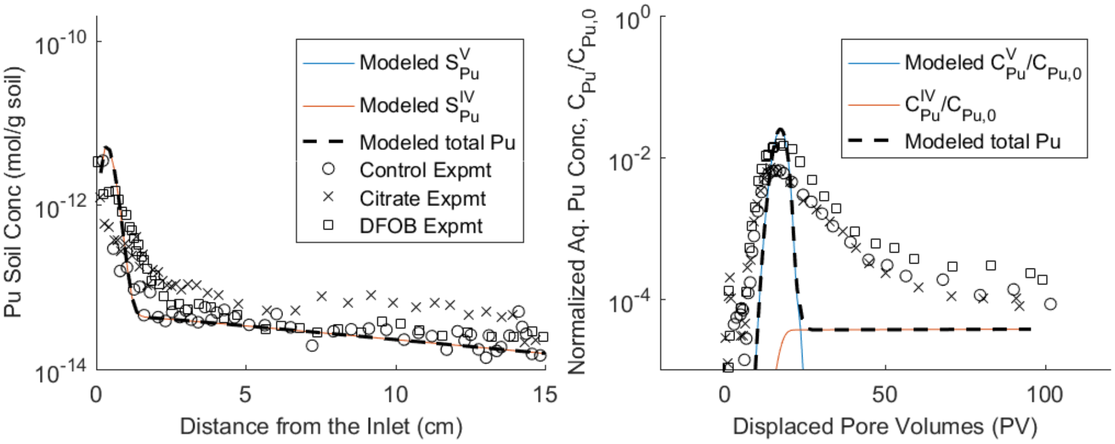

Figure D.15. A reactive transport model which includes surface mediated reduction was used to predict concentrations of Pu(IV) and Pu(V) in the soil profile (left) and in the elution profile (right). Experimental data from the control, citrate, and DFOB column experiments is shown. $\mu's$ = 0.0008 min^{-1}; K_d^{IV} = 1000 $\text{mL}\cdot\text{g}^{-1}$; $\boldsymbol{K_d^{V} = 8\ \text{mL}\cdot\text{g}^{-1}}$; $f_{Pu(V)}$ = 0.2

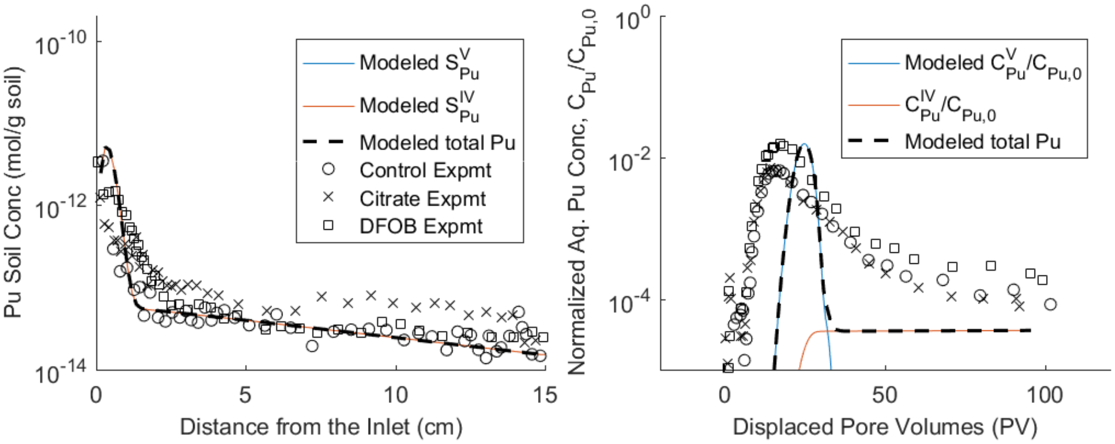

Figure D.16. A reactive transport model which includes surface mediated reduction was used to predict concentrations of Pu(IV) and Pu(V) in the soil profile (left) and in the elution profile (right). Experimental data from the control, citrate, and DFOB column experiments is shown. $\mu's$ = 0.0008 min^{-1}; K_d^{IV} = 1000 $\text{mL}\cdot\text{g}^{-1}$; $\boldsymbol{K_d^{V} = 10\ \text{mL}\cdot\text{g}^{-1}}$; $f_{Pu(V)}$ = 0.2

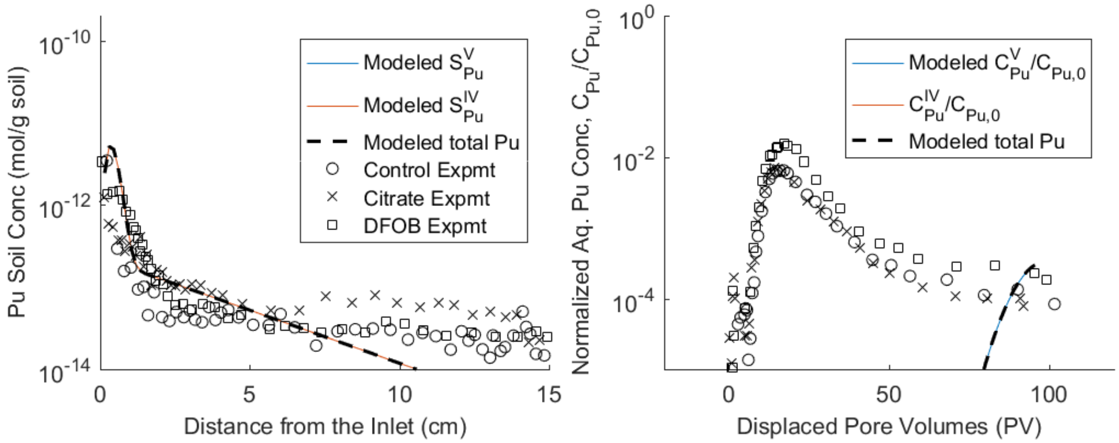

Figure D.17. A reactive transport model which includes surface mediated reduction was used to predict concentrations of Pu(IV) and Pu(V) in the soil profile (left) and in the elution profile (right). Experimental data from the control, citrate, and DFOB column experiments is shown. $\mu's$ = 0.0008 min^{-1}; K_d^{IV} = 1000 mL·g^{-1}; **K_d^{V} = 30 mL·g^{-1}**; $f_{Pu(V)}$ = 0.2

Effect of Varying the Fraction of Pu(V), $f_{Pu(V)}$, in the Loading Solution

A wide range of Pu oxidation state distributions was modeled (Figs. D.18 – D.22). The fraction of Pu(V) in the loading solution was varied from 0.05 to 0.80, with the balance composed of Pu(IV). Pu(V) fractions of 0.20–0.50 provided reasonable fits to the Pu soil profile. As the fraction of Pu(V) was increased, the concentration of Pu in the first 2 cm of the column decreased and the concentration of Pu distributed throughout the soil increased. Additionally, the concentration of Pu(V) predicted in the effluent peak increased, but the fraction of Pu(V) had no effect on the broadness of the effluent peak.

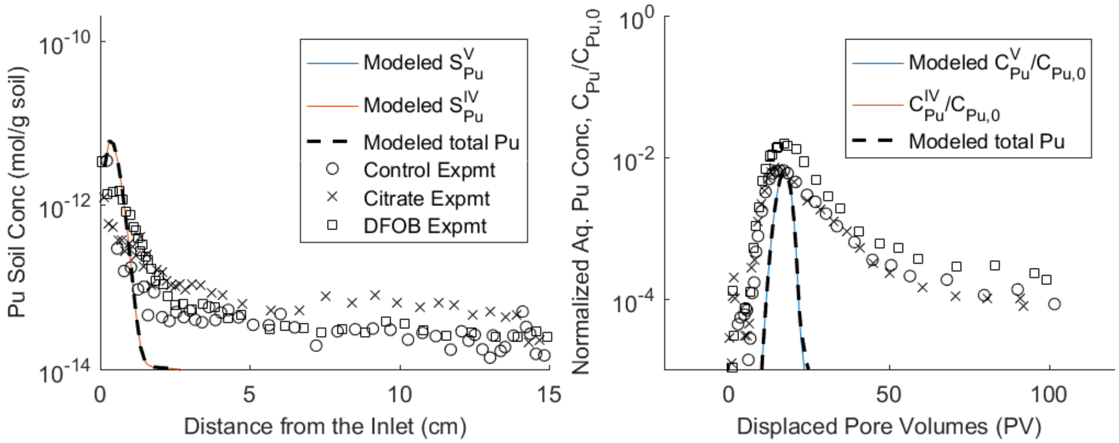

Figure D.18. A reactive transport model which includes surface mediated reduction was used to predict concentrations of Pu(IV) and Pu(V) in the soil profile (left) and in the elution profile (right). Experimental data from the control, citrate, and DFOB column experiments is shown. $\mu's = 0.0008$ min^{-1}; $K_d^{IV} = 1000$ mL·g^{-1}; $K_d^{V} = 8$ mL·g^{-1}; **$f_{Pu(V)} = 0.05$**

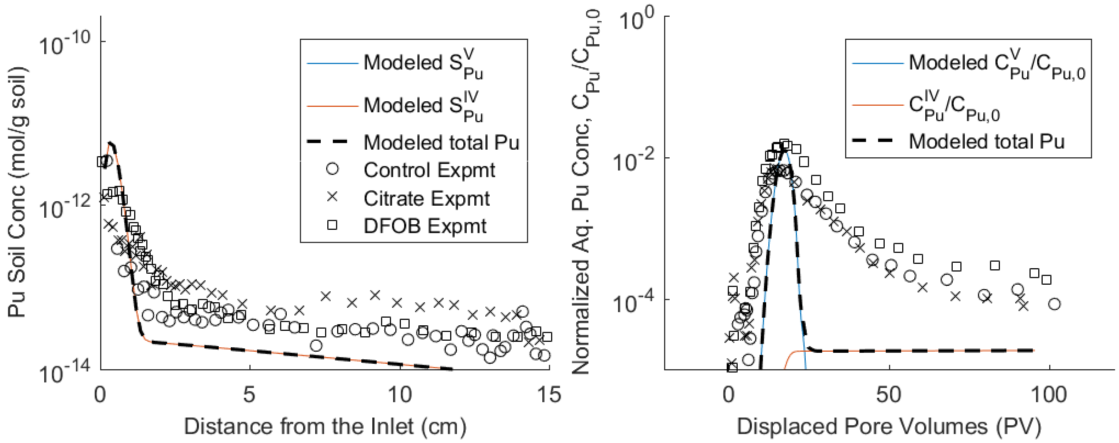

Figure D.19. A reactive transport model which includes surface mediated reduction was used to predict concentrations of Pu(IV) and Pu(V) in the soil profile (left) and in the elution profile (right). Experimental data from the control, citrate, and DFOB column experiments is shown. $\mu's$ = 0.0008 min^{-1}; K_d^{IV} = 1000 $\text{mL}\cdot\text{g}^{-1}$; K_d^{V} = 8 $\text{mL}\cdot\text{g}^{-1}$; $\boldsymbol{f_{Pu(V)}}$ **= 0.1**

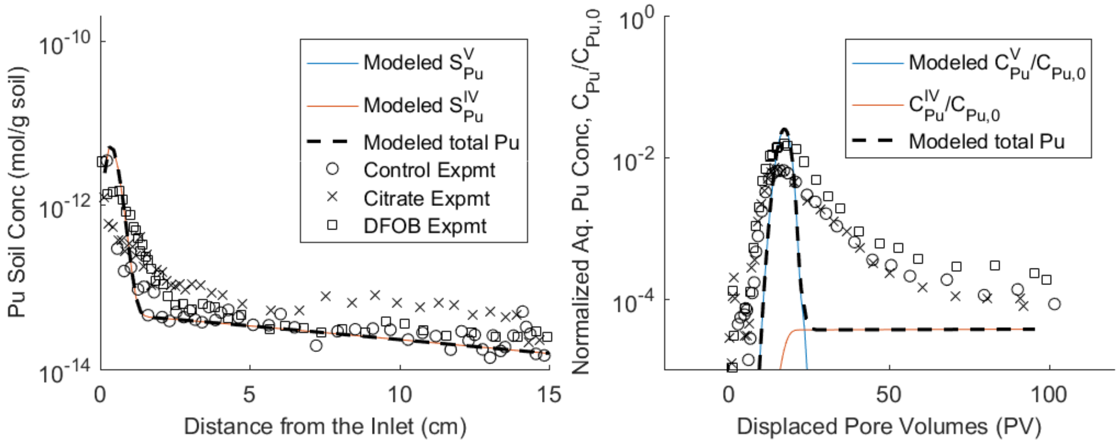

Figure D.20. A reactive transport model which includes surface mediated reduction was used to predict concentrations of Pu(IV) and Pu(V) in the soil profile (left) and in the elution profile (right). Experimental data from the control, citrate, and DFOB column experiments is shown. $\mu's$ = 0.0008 min^{-1}; K_d^{IV} = 1000 $\text{mL}\cdot\text{g}^{-1}$; K_d^{V} = 8 $\text{mL}\cdot\text{g}^{-1}$; $\boldsymbol{f_{Pu(V)}}$ **= 0.2**

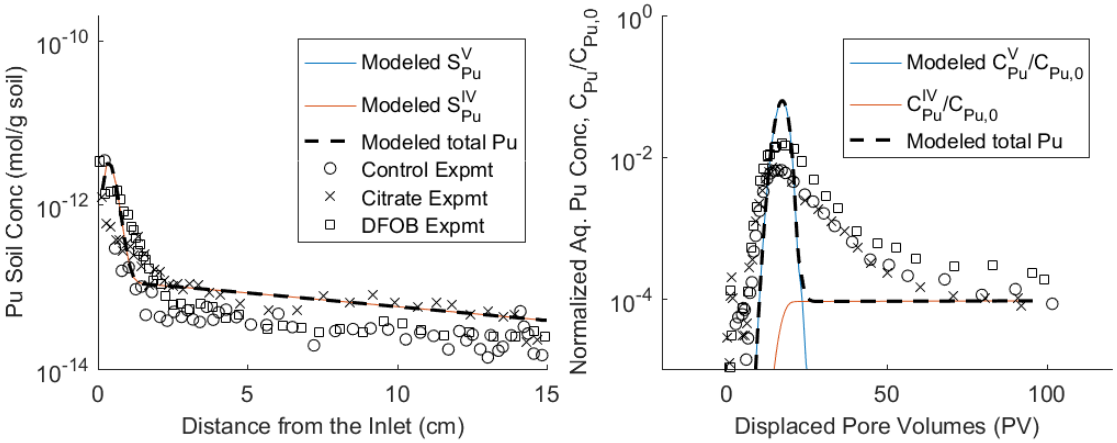

Figure D.21. A reactive transport model which includes surface mediated reduction was used to predict concentrations of Pu(IV) and Pu(V) in the soil profile (left) and in the elution profile (right). Experimental data from the control, citrate, and DFOB column experiments is shown. $\mu's$ = 0.0008 min^{-1}; K_d^{IV} = 1000 mL·g^{-1}; K_d^{V} = 8 mL·g^{-1}; $\boldsymbol{f_{Pu(V)}}$ **= 0.5**

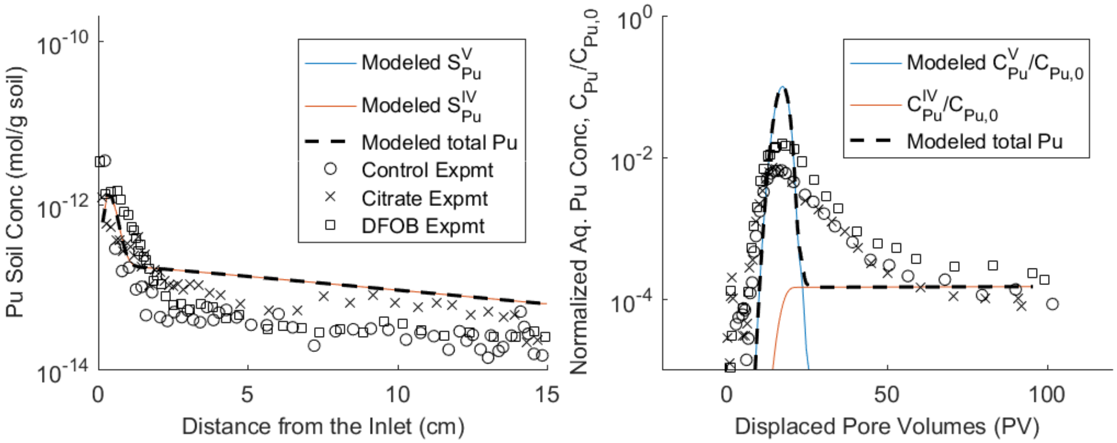

Figure D.22. A reactive transport model which includes surface mediated reduction was used to predict concentrations of Pu(IV) and Pu(V) in the soil profile (left) and in the elution profile (right). Experimental data from the control, citrate, and DFOB column experiments is shown. $\mu's$ = 0.0008 min^{-1}; K_d^{IV} = 1000 mL·g^{-1}; K_d^{V} = 8 mL·g^{-1}; $\boldsymbol{f_{Pu(V)}}$ **= 0.8**

Colloid-Facilitated Transport

Equations for mass balance (Eqns. D.12–D.17), as well as transfer to the solid phase, and transfer between components were solved numerically using the C-Ride module of Hydrus 1D.

Colloid transport equation:

$$\frac{\partial \theta C_c}{\partial t} + \rho \frac{\partial S_c}{\partial t} = \frac{\partial}{\partial x}\left(\theta D \frac{\partial C_c}{\partial x}\right) - \frac{\partial u C_c}{\partial x} \tag{D.12}$$

Colloid mass transfer term between aqueous and solid phases:

$$\rho \frac{\partial S_c}{\partial t} = \theta k_{att} C_c - \rho k_{det} S_c \tag{D.13}$$

Mass balance equation for contaminant sorbed to mobile colloids:

$$\begin{aligned}\frac{\partial \theta C_c S_{mc}}{\partial t} = \frac{\partial}{\partial x}\left(\theta S_{mc} D \frac{\partial C_c}{\partial x}\right) - \frac{\partial u C_c S_{mc}}{\partial x} + \theta k_{ac} C_{Pu} - \theta k_{dc} C_c S_{mc} \\ - \theta k_{att} C_c S_{mc} + \rho k_{det} S_c S_{ic}\end{aligned} \tag{D.14}$$

Mass balance equation for contaminant sorbed to immobile colloids:

$$\rho \frac{\partial S_c S_{ic}}{\partial t} = \theta k_{ac} C_{Pu} - \rho k_{dc} S_c S_{ic} + \theta k_{att} C_c S_{mc} - \rho k_{det} S_c S_{ic} \tag{D.15}$$

Mass balance equation for the total contaminant:

$$\begin{aligned}\frac{\partial \theta C_{Pu}}{\partial t} + \rho \frac{\partial S_{Pu}}{\partial t} + \frac{\partial \theta C_c S_{mc}}{\partial t} + \rho \frac{\partial S_c S_{ic}}{\partial t} \\ = \frac{\partial}{\partial x}\left(\theta D \frac{\partial C_{Pu}}{\partial x}\right) - \frac{\partial u C_{Pu}}{\partial x} + \frac{\partial}{\partial x}\left(\theta S_{mc} D \frac{\partial C_c}{\partial x}\right) - \frac{\partial u C_c S_{mc}}{\partial x}\end{aligned} \tag{D.16}$$

Equilibrium between sorbed contaminant and aqueous contaminant:

$$S_{Pu} = K_d C_{Pu} \tag{D.17}$$

Literature Review

Soil colloids were assumed to be composed of iron oxyhydroxides and kaolinite. Previous studies have characterized colloids found in soils from the Savannah River Site and elsewhere on the Atlantic Coastal Plain. Sandy soil from the E-Area of the Savannah River site was studied, and the soil colloids were found to be composed of goethite and kaolinite (Haliena et al., 2016). This same soil was used in some previous studies of Savannah River Site soil (Li et al., 2012; Powell et al., 2002). In well tests at the Savannah River site, colloids were composed of kaolinite, goethite, and to a lesser extent illite and quartz (Seaman et al., 2007). In laboratory and field studies of Atlantic Coastal Plain soil consisting of ferric oxyhydroxide-coated sand and gravel, colloids were observed to consist of quartz, feldspar, and kaolinite with small amounts of smectite and illite/muscovite (Bunn et al., 2002). However, no goethite or other ferric oxyhydroxides were observed. In studies comparing soils from the Atlantic Coastal Plain, it was hypothesized that under oxic conditions, ferric oxyhydroxide coatings cement colloids onto soil surfaces by electrostatic forces, but under anoxic conditions, slow reductive dissolution of ferric oxyhydroxides causes the release of these soil colloids (Ryan and Gschwend, 1994b, 1990).

Under the assumption that the soil colloids, were composed of iron oxyhydroxides and kaolinite, a literature review was conducted of kinetic sorption studies of Pu and these minerals (Table 2.1). Studies of Pu adsorption are much more common than studies of desorption, and several of these studies attributed Pu uptake kinetics to multiple reaction steps (Painter et al., 2002; Powell et al., 2005; Romanchuk et al., 2011). Estimates of Pu desorption rate constants, k_{dc}, were only available from fitting Pu measurements as adsorption approached equilibrium (Ohnuki et al., 2007; Painter et al., 2002). Experiments to measure the attachment rate constant, k_{att}, of colloidal goethite and kaolinite have been previously conducted on quartz media (Saiers and Hornberger, 1996; Wang et al., 2015). Previous studies of colloid mobilization have typically been conducted at high pH and focused on the total mass of colloids mobilized (Bunn et al., 2002; Haliena et al., 2016; Li et al., 2012; Ryan and Gschwend, 1994a; Seaman et al., 2007). The range of parameter values determined from literature served as a starting point for systematically varying the model parameters.

Additional reviews on colloid-facilitated transport have been authored by van Genuchten and Šimůnek (2004), Flury and Qiu (2008), and Ryan and Elimelech (1996).

Table D.5. Summary of parameters from literature for modeling colloid-facilitated tranport

k_{att} (min^{-1})	k_{det} (min^{-1})	k_{ac} (min^{-1})	k_{dc} (min^{-1})	K_c $^{(a)}$ ($\text{mL}\cdot\text{g}^{-1}$)	pH	Source	Comment
		5.22E-05			4.6	Powell et al. (2005)	Pu(V), 10 $\text{m}^2\cdot\text{L}^{-1}$ hematite
		1.38E-04			4.9	Powell et al. (2005)	Pu(V), 10 $\text{m}^2\cdot\text{L}^{-1}$ hematite
		5.10E-03			5.9	Powell et al. (2005)	Pu(V), 100 $\text{m}^2\cdot\text{L}^{-1}$ goethite
		4.17E-03	2.33E-04	110	8.2	Painter et al. (2002) [b]	Pu(V), 0.2 $\text{g}\cdot\text{L}^{-1}$ colloidal hematite
		2.34E-02			5.4	Romanchuk et al. (2011)	Pu(IV), hematite
		1.06E-02			6.5	Romanchuk et al. (2011)	Pu(IV), hematite, first site of two-site sorption
		2.17E-03			6.5	Romanchuk et al. (2011)	Pu(IV), hematite, second site of two-site sorption
		5.00E-03	6.90E-05	18	5	Ohnuki et al. (2007) [c]	Pu(VI), 40 $\text{g}\cdot\text{L}^{-1}$ kaolinite
				370 – 750	5	Banik et al. (2007) [c]	Pu(IV), 4 $\text{g}\cdot\text{L}^{-1}$ kaolinite
				3100 – 4000	5	Marsac et al. (2015) [d]	Th(IV), 4 $\text{g}\cdot\text{L}^{-1}$ kaolinite
				4000	4	Marsac et al. (2015) [e]	Pu(IV), kaolinite
1.07E-02					7.2 – 7.4	Saiers and Hornberger (1996)	50 $\text{mg}\cdot\text{L}^{-1}$ colloidal kaolinite, irreversible sorption to quartz
4.83E-03					7.2 – 7.4	Saiers and Hornberger (1996)	100 $\text{mg}\cdot\text{L}^{-1}$ colloidal kaolinite, irreversible sorption to quartz
5.67E-03					7.2 – 7.4	Saiers and Hornberger (1996)	200 $\text{mg}\cdot\text{L}^{-1}$ colloidal kaolinite, irreversible sorption to quartz
4.7					6.5	Wang et al. (2015)	100 $\text{mg}\cdot\text{L}^{-1}$ colloidal goethite, sorption to quartz with blocking
	1.46E-02				9.5	Bunn et al. (2002)	Atlantic Coastal Plain undisturbed soil column
	6.66E-02				11	Ryan and Gschwend (1994a)	colloidal hematite desorption from quartz, ionic strength = 0.01 M

[a] Equation: $K_c = k_{ac} / (k_{dc}\cdot C_c)$ where C_c is in units of $\text{g}\cdot\text{mL}^{-1}$

[b] Based on data from Lu et al. (Lu et al., 2000)

[c] Calculated for this work

[d] Based on data from Banik et al. (2007)

[e] Based on data from Banik (2006)

Results of Modeling Colloid-Facilitated Transport

Selected modeling results are presented below in order to demonstrate the effect of each parameter on the colloid facilitated transport model. The results were selected to show the range of parameter values which predicted Pu in the soil column at 2–15 cm as well as Pu breakthrough with similar timing to experiment observations. The colloid-facilitated transport model predicted that Pu with enhanced mobility was sorbed to colloids. However, the model was unable to simultaneously provide a reasonable fit to both the Pu soil profile and the Pu elution profile. In models where Pu was predicted between 2 and 15 cm, it was in the form of Pu sorbed to colloids remaining in the column. This created a nearly continuous supply of Pu-carrying colloids to the effluent solution which resulted in an elution profile where the Pu concentration reached a plateau, but did not exhibit a peak.

The mobility of colloids was controlled by the parameters for colloid attachment, k_{att}, and detachment, k_{det}. For greater values of k_{att} or lower values of k_{det}, colloid mobility was lower, and less colloid was eluted from the column. Accordingly, the concentration of Pu sorbed to colloids in the soil at 2–15 cm was greater, and less Pu sorbed to colloids eluted from the column (Figs. D.23–D.32). However, when colloid mobility was decreased too much (k_{att} = 0.15 min^{-1}; k_{det} = 3 × 10^{-4} min^{-1}; Fig. D.27), colloids with sorbed Pu were predicted to be deposited closer to the column entrance, and the elution of colloids with sorbed Pu was delayed. However, when the colloid mobility was increased to the condition where colloids were flushed from the column, colloids with sorbed Pu were not predicted to be distributed between 2 and 15 cm (Figs. D.31 and D.32). Under this condition, a peak was predicted in the Pu elution profile, but the predicted peak was too broad and under-estimated the effluent Pu concentration.

In the colloid-facilitated transport model, colloids competed with soil sorption sites for Pu. The partitioning of Pu between soil surfaces and colloid surfaces depended on the rate constants for Pu adsorption to colloids, k_{ac}, and Pu desorption from colloids, k_{dc}. For greater values of k_{ac} or lesser values of k_{dc}, Pu partitioning to colloids was greater. For greater partitioning to colloids, less Pu was retained in the first 2 cm of the column, more Pu was sorbed to colloids between 2 and 15 cm, and more Pu was eluted (Figs. D.33–D.43). When the soil partitioning was increased to the condition where the colloids exhausted the Pu which could be scavenged from the soil (Figs. D.42 and D.43), the model predicted a peak in the elution profile, but the peak was too broad and under-estimated the Pu concentration in the effluent.

The Pu distribution coefficient, K_d, affected the partitioning of Pu between the soil and colloids (Figs. D.44–D.48), and also controlled the mobility of Pu not associated with colloids. For greater K_d values, more Pu was sorbed to colloids between 2 and 15 cm, and the concentration of Pu in the effluent was predicted to be greater. When the K_d value was decreased to 200 $mL \cdot g^{-1}$ and 500 $mL \cdot g^{-1}$ (Figs. D.44 and D.45, respectively), colloids were able to compete with the soil for Pu in the first 2 cm of the column. Whereas scenarios with K_d values greater than 500 $mL \cdot g^{-1}$ predicted that the concentration of Pu in the soil profile decreased monotonically, lower K_d values predicted a peak in the Pu soil profile. By happenstance, a good fit to the soil profile of the DFOB experiment was obtained for a K_d

value of 500 $mL \cdot g^{-1}$ (Fig. D.44). However, the K_d value had little effect on the predicted Pu elution profile which remained a poor fit to the experiment data.

Effect of Varying Colloid Attachment Coefficient, k_{att}

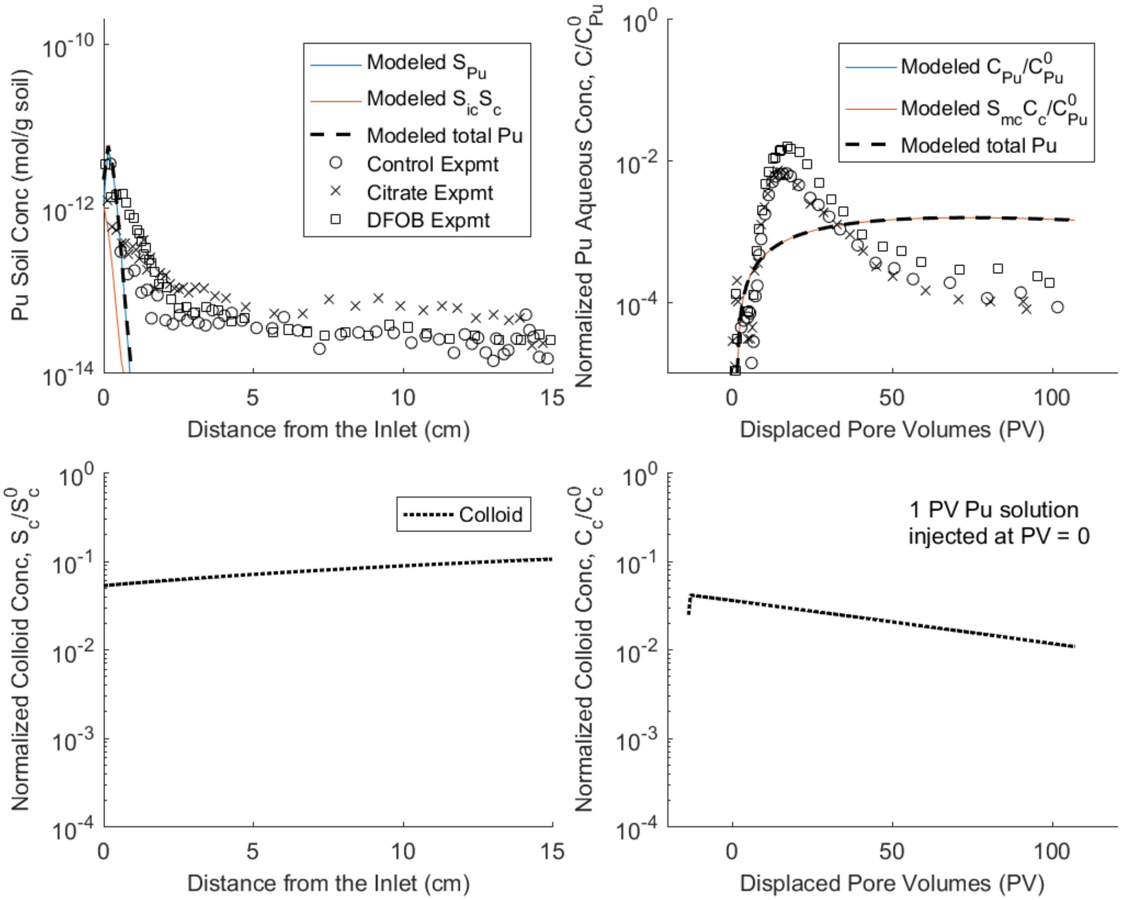

Figure D.23. Plutonium and colloid concentrations were modeled using a one-dimensional colloid-facilitated transport model in HYDRUS. Experimental data from the control, citrate, and DFOB column experiments is shown.
k_{att} = 0.01 min^{-1}; $k_{det} = 3 \times 10^{-4}$ min^{-1}; $k_{ac} = 1.0$ min^{-1}; $k_{dc} = 6.9 \times 10^{-5}$ min^{-1}; $K_d = 2000$ mL·g^{-1}.

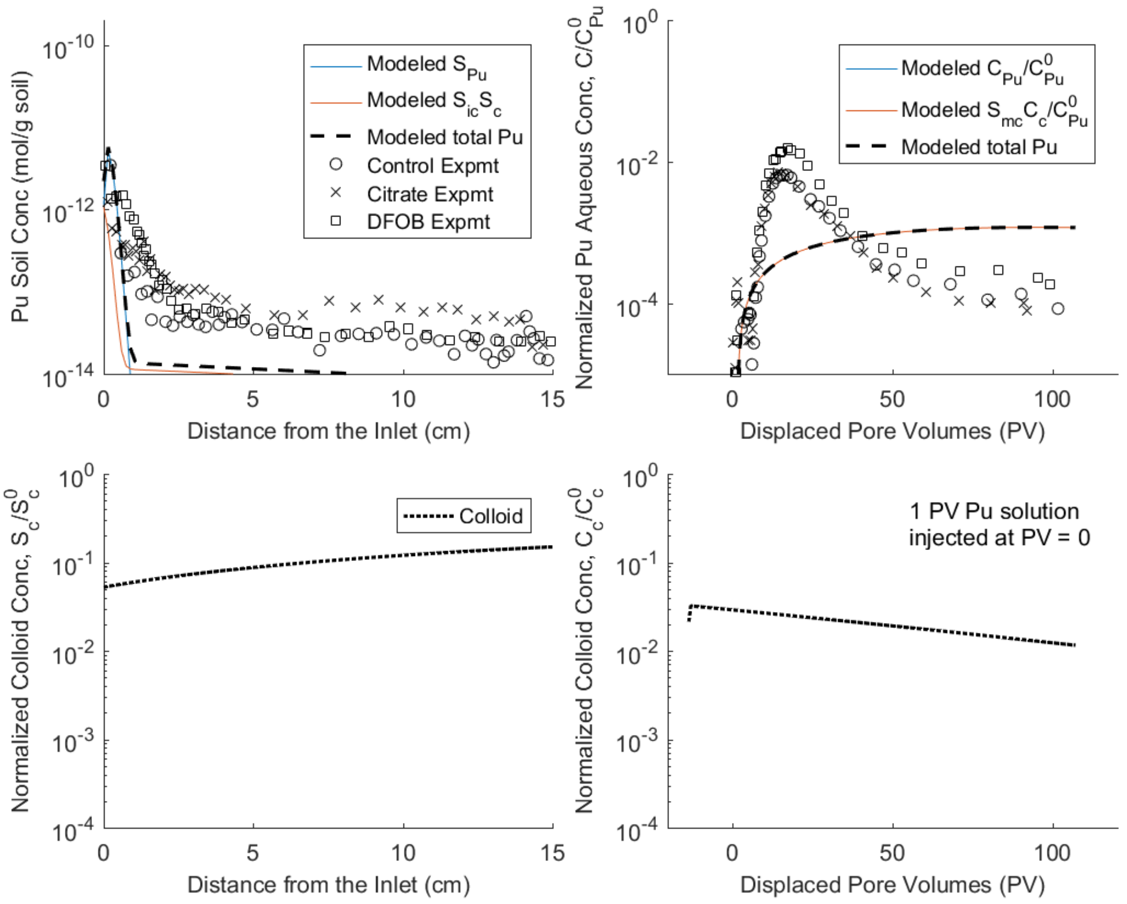

Figure D.24. Plutonium and colloid concentrations were modeled using a one-dimensional colloid-facilitated transport model in HYDRUS. Experimental data from the control, citrate, and DFOB column experiments is shown.
$\boldsymbol{k_{att}}$ **= 0.02 min^{-1}**; $k_{det} = 3 \times 10^{-4}$ min^{-1}; $k_{ac} = 1.0$ min^{-1}; $k_{dc} = 6.9 \times 10^{-5}$ min^{-1}; $K_d = 2000$ mL·g^{-1}.

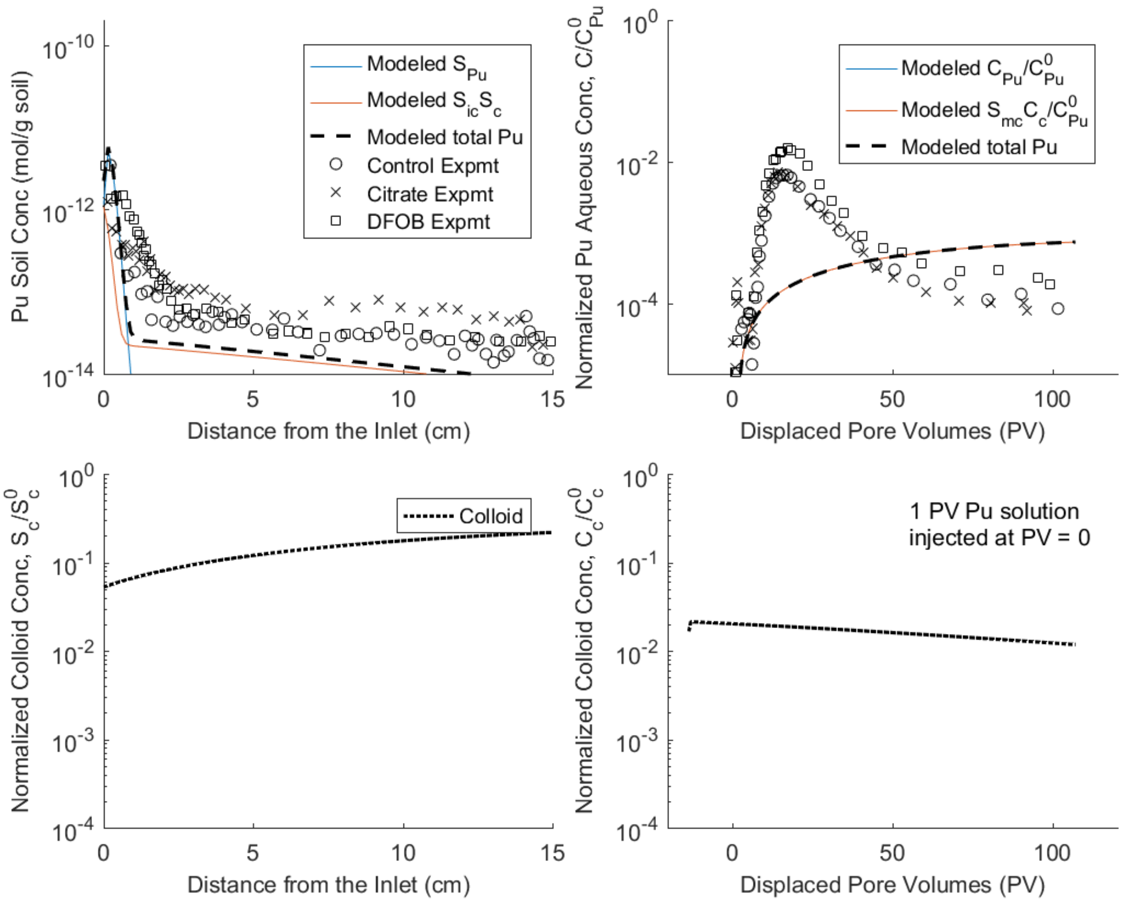

Figure D.25. Plutonium and colloid concentrations were modeled using a one-dimensional colloid-facilitated transport model in HYDRUS. Experimental data from the control, citrate, and DFOB column experiments is shown.
k_{att} = 0.04 min^{-1}; k_{det} = 3 × 10^{-4} min^{-1}; k_{ac} = 1.0 min^{-1}; k_{dc} = 6.9 × 10^{-5} min^{-1}; K_d = 2000 mL·g^{-1}.

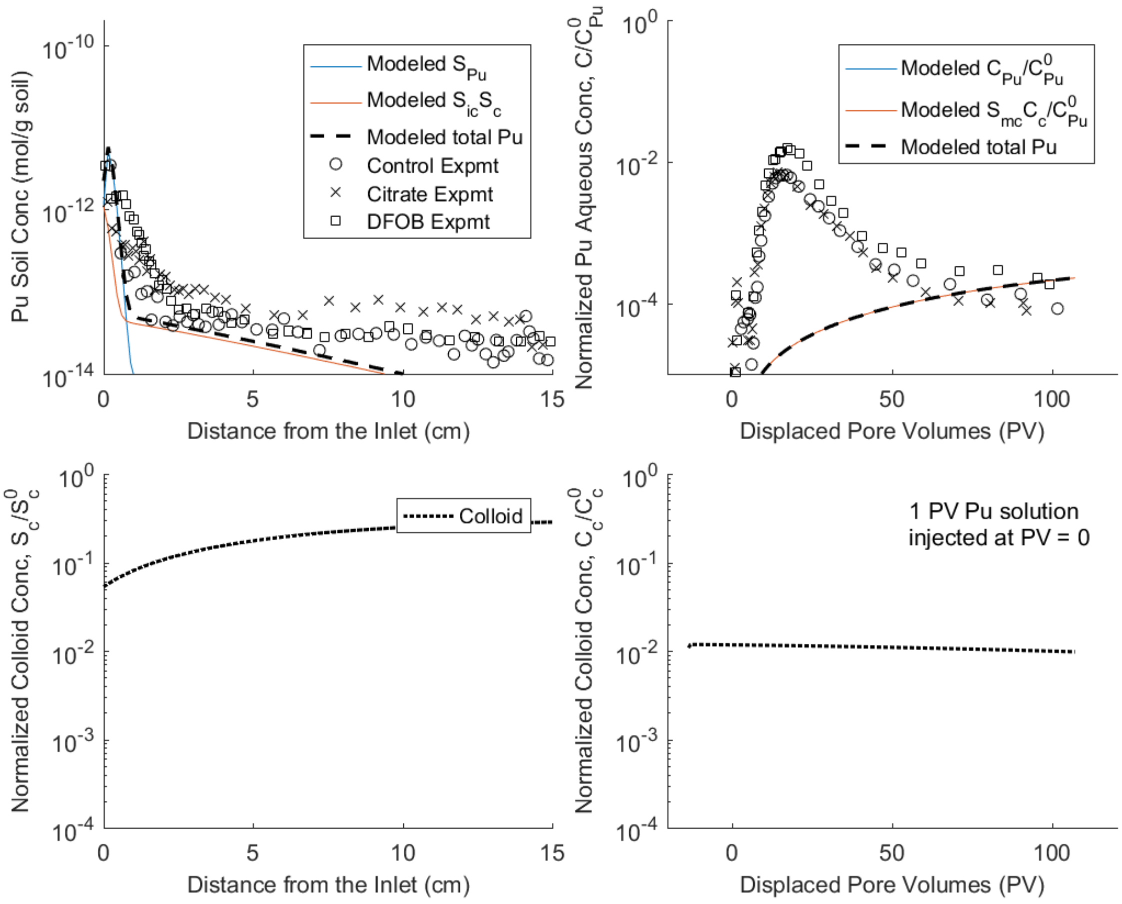

Figure D.26. Plutonium and colloid concentrations were modeled using a one-dimensional colloid-facilitated transport model in HYDRUS. Experimental data from the control, citrate, and DFOB column experiments is shown.
$\boldsymbol{k_{att}} = \mathbf{0.08\ min^{-1}}$; $k_{det} = 3 \times 10^{-4}$ min^{-1}; $k_{ac} = 1.0$ min^{-1}; $k_{dc} = 6.9 \times 10^{-5}$ min^{-1}; $K_d = 2000$ mL·g^{-1}.

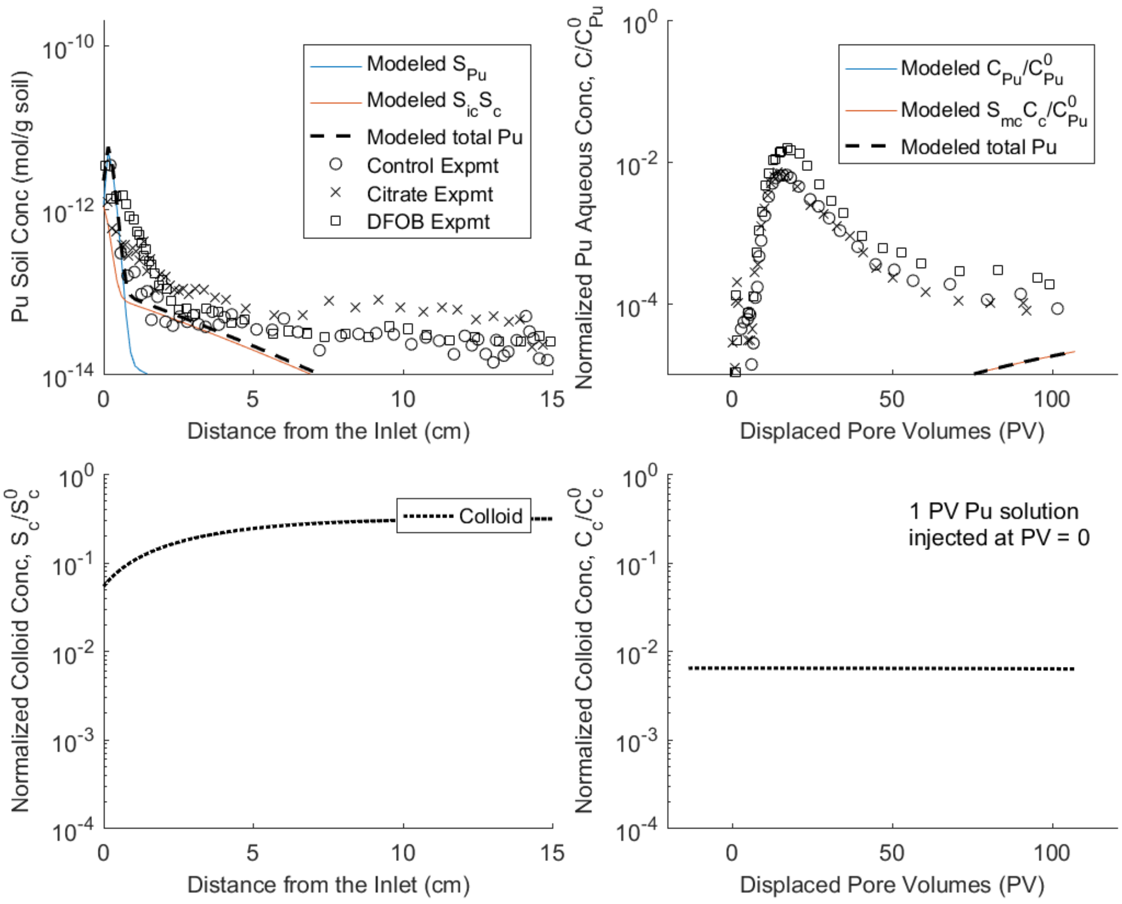

Figure D.27. Plutonium and colloid concentrations were modeled using a one-dimensional colloid-facilitated transport model in HYDRUS. Experimental data from the control, citrate, and DFOB column experiments is shown.
$\boldsymbol{k_{att}}$ **= 0.15 min**$^{\mathbf{-1}}$; $k_{det} = 3 \times 10^{-4}$ min^{-1}; $k_{ac} = 1.0$ min^{-1}; $k_{dc} = 6.9 \times 10^{-5}$ min^{-1}; $K_d = 2000$ mL·g^{-1}.

Effect of Varying Colloid Detachment Coefficient, *k_{det}*

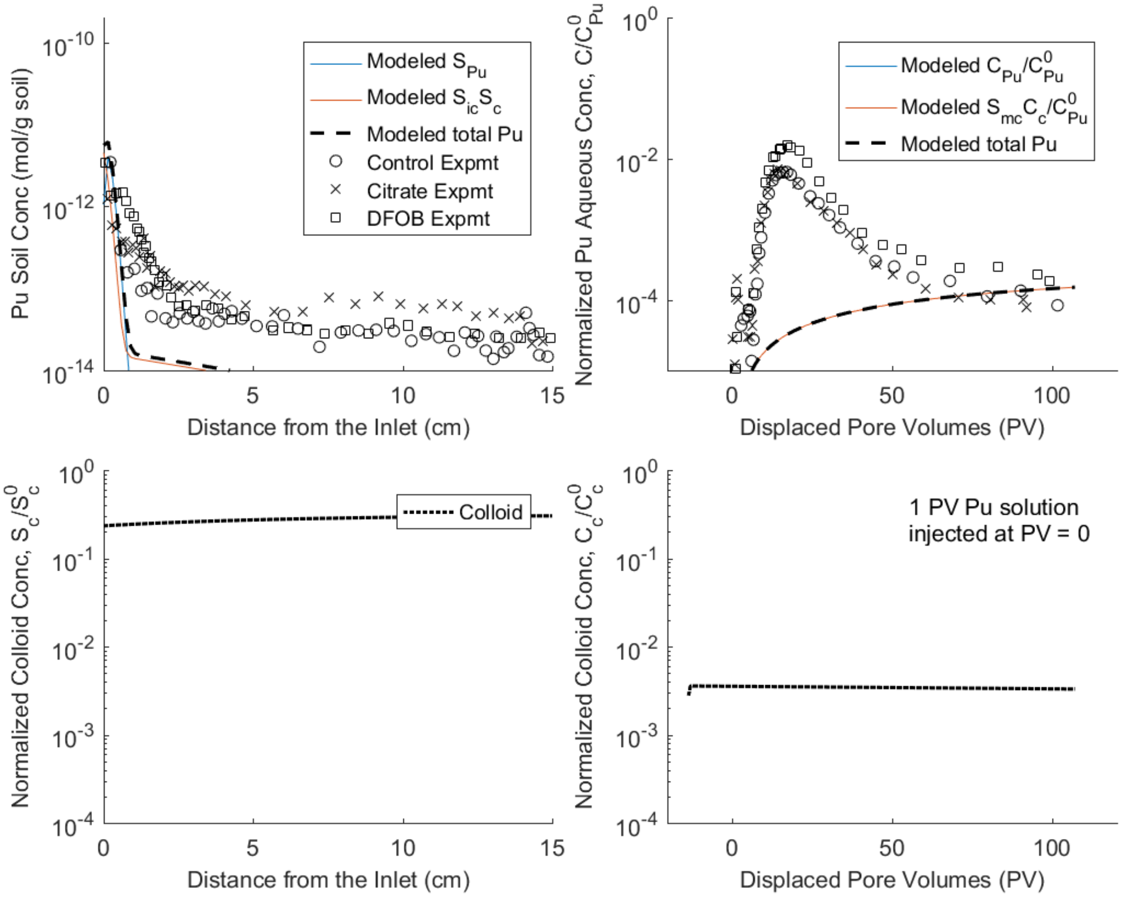

Figure D.28. Plutonium and colloid concentrations were modeled using a one-dimensional colloid-facilitated transport model in HYDRUS. Experimental data from the control, citrate, and DFOB column experiments is shown.
k_{att} = 0.04 min^{-1}; **k_{det} = 5 × 10^{-5} min^{-1}**; k_{ac} = 1.0 min^{-1}; k_{dc} = 6.9 × 10^{-5} min^{-1}; K_d = 2000 mL·g^{-1}.

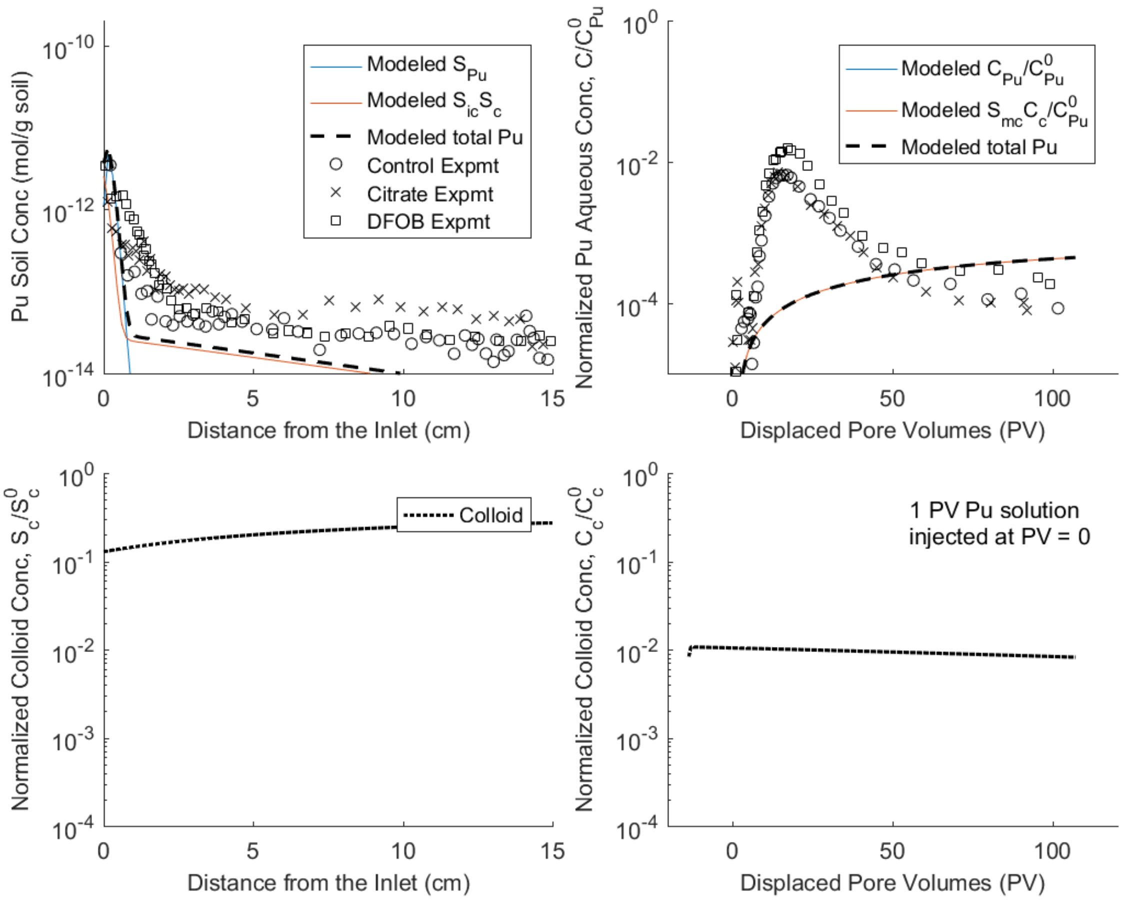

Figure D.29. Plutonium and colloid concentrations were modeled using a one-dimensional colloid-facilitated transport model in HYDRUS. Experimental data from the control, citrate, and DFOB column experiments is shown.
k_{att} = 0.04 min^{-1}; $\boldsymbol{k_{det} = 1.5 \times 10^{-4}}$ **min^{-1}**; k_{ac} = 1.0 min^{-1}; k_{dc} = 6.9 × 10^{-5} min^{-1}; K_d = 2000 mL·g^{-1}.

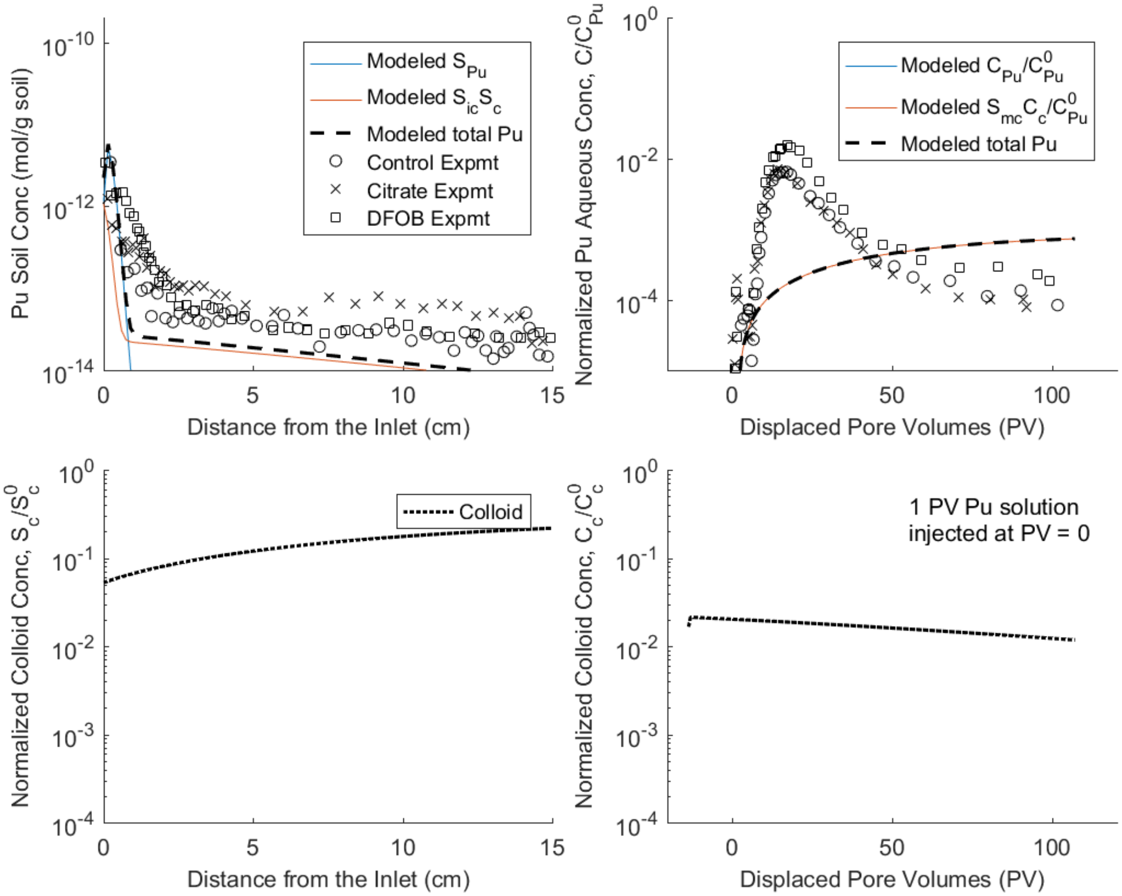

Figure D.30. Plutonium and colloid concentrations were modeled using a one-dimensional colloid-facilitated transport model in HYDRUS. Experimental data from the control, citrate, and DFOB column experiments is shown.
k_{att} = 0.04 min^{-1}; **k_{det} = 3 × 10^{-4} min^{-1}**; k_{ac} = 1.0 min^{-1}; k_{dc} = 6.9 × 10^{-5} min^{-1}; K_d = 2000 mL·g^{-1}.

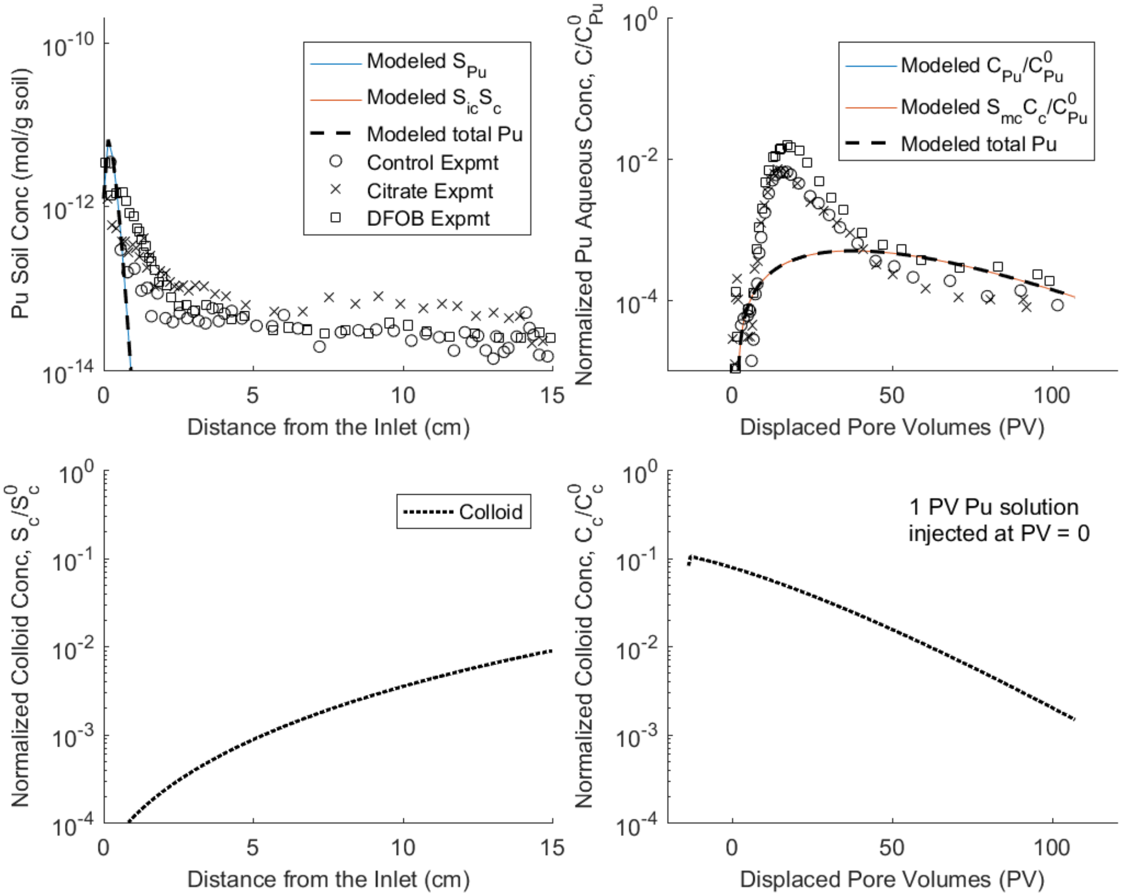

Figure D.31. Plutonium and colloid concentrations were modeled using a one-dimensional colloid-facilitated transport model in HYDRUS. Experimental data from the control, citrate, and DFOB column experiments is shown.
k_{att} = 0.04 min^{-1}; **k_{det} = 1.5 × 10^{-3} min^{-1}**; k_{ac} = 1.0 min^{-1}; k_{dc} = 6.9 × 10^{-5} min^{-1}; K_d = 2000 mL·g^{-1}.

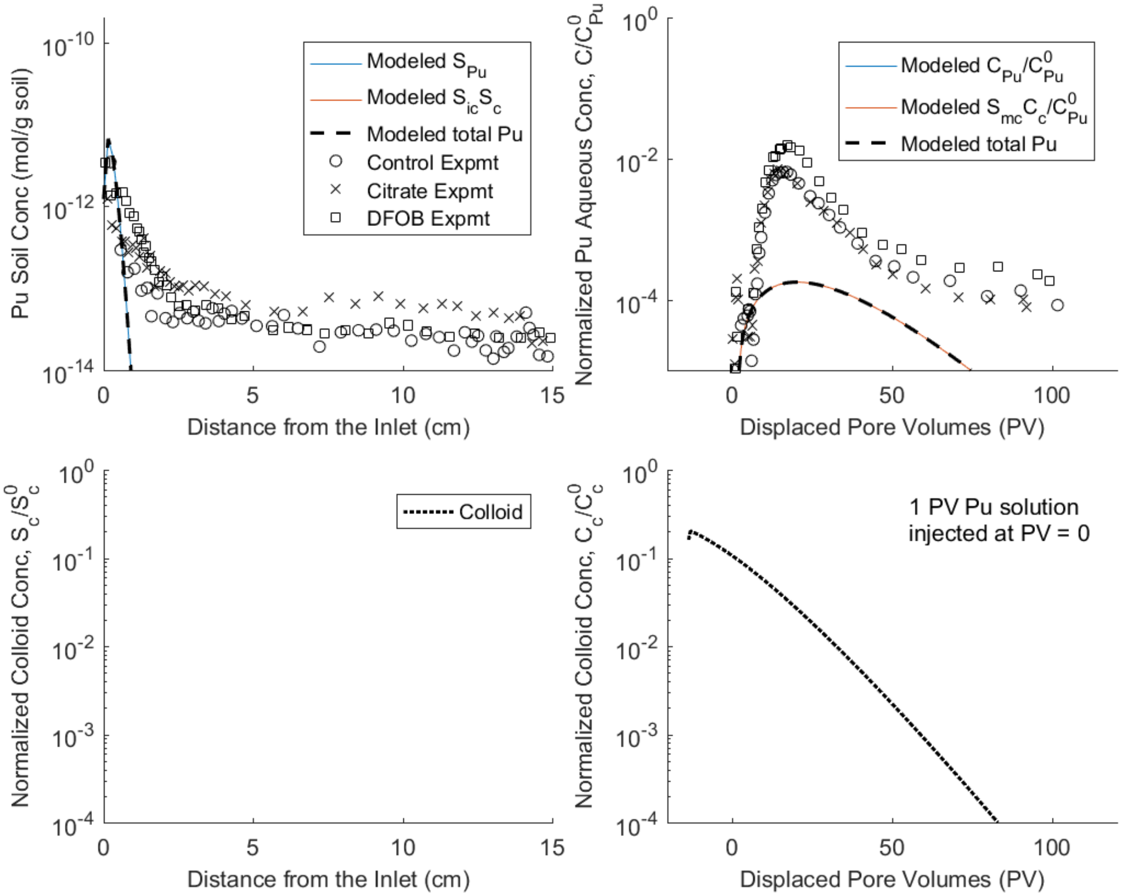

Figure D.32. Plutonium and colloid concentrations were modeled using a one-dimensional colloid-facilitated transport model in HYDRUS. Experimental data from the control, citrate, and DFOB column experiments is shown.
k_{att} = 0.04 min^{-1}; **k_{det} = 3 × 10^{-3} min^{-1}**; k_{ac} = 1.0 min^{-1}; k_{dc} = 6.9 × 10^{-5} min^{-1}; K_d = 2000 mL·g^{-1}.

Effect of Varying Pu Adsorption Rate Constant to Colloids, k_{ac}

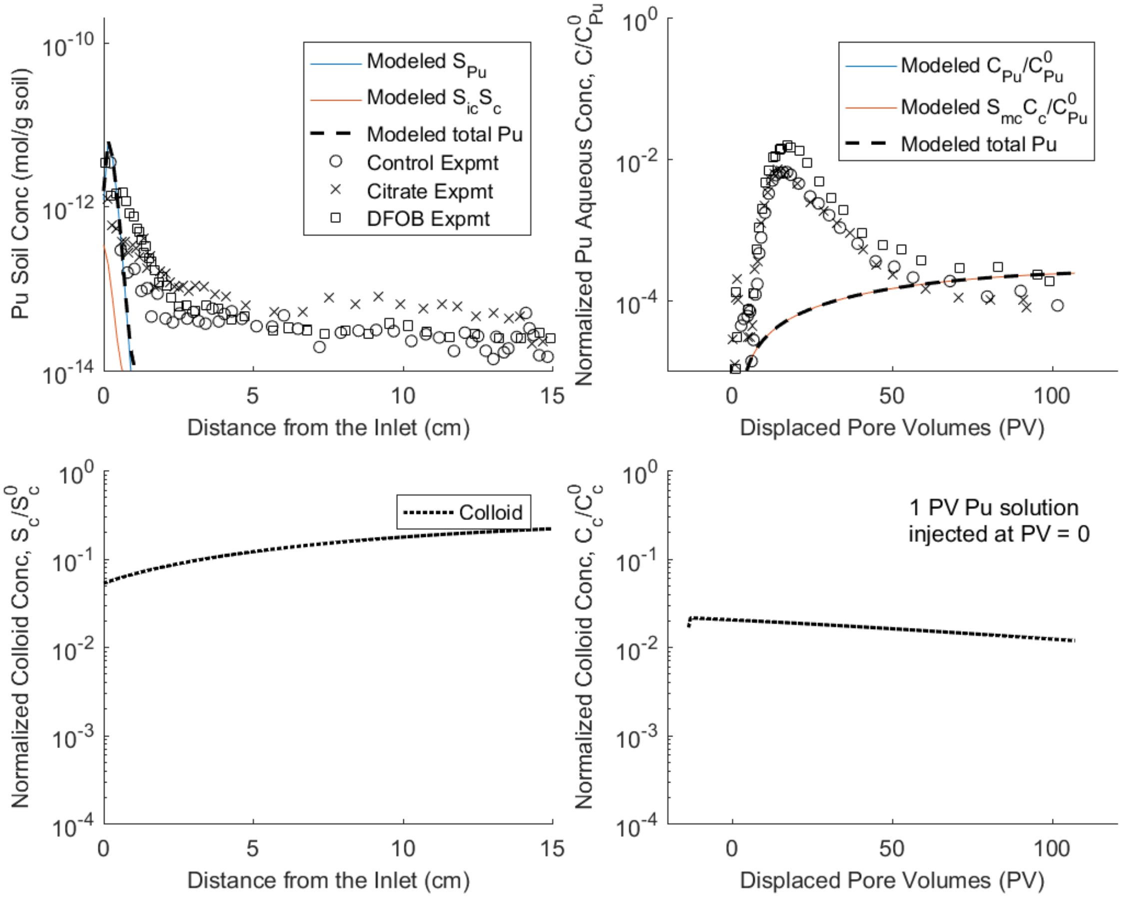

Figure D.33. Plutonium and colloid concentrations were modeled using a one-dimensional colloid-facilitated transport model in HYDRUS. Experimental data from the control, citrate, and DFOB column experiments is shown.
k_{att} = 0.04 min^{-1}; k_{det} = 3 × 10^{-4} min^{-1}; **k_{ac} = 0.3 min^{-1}**; k_{dc} = 6.9 × 10^{-5} min^{-1}; K_d = 2000 mL·g^{-1}.

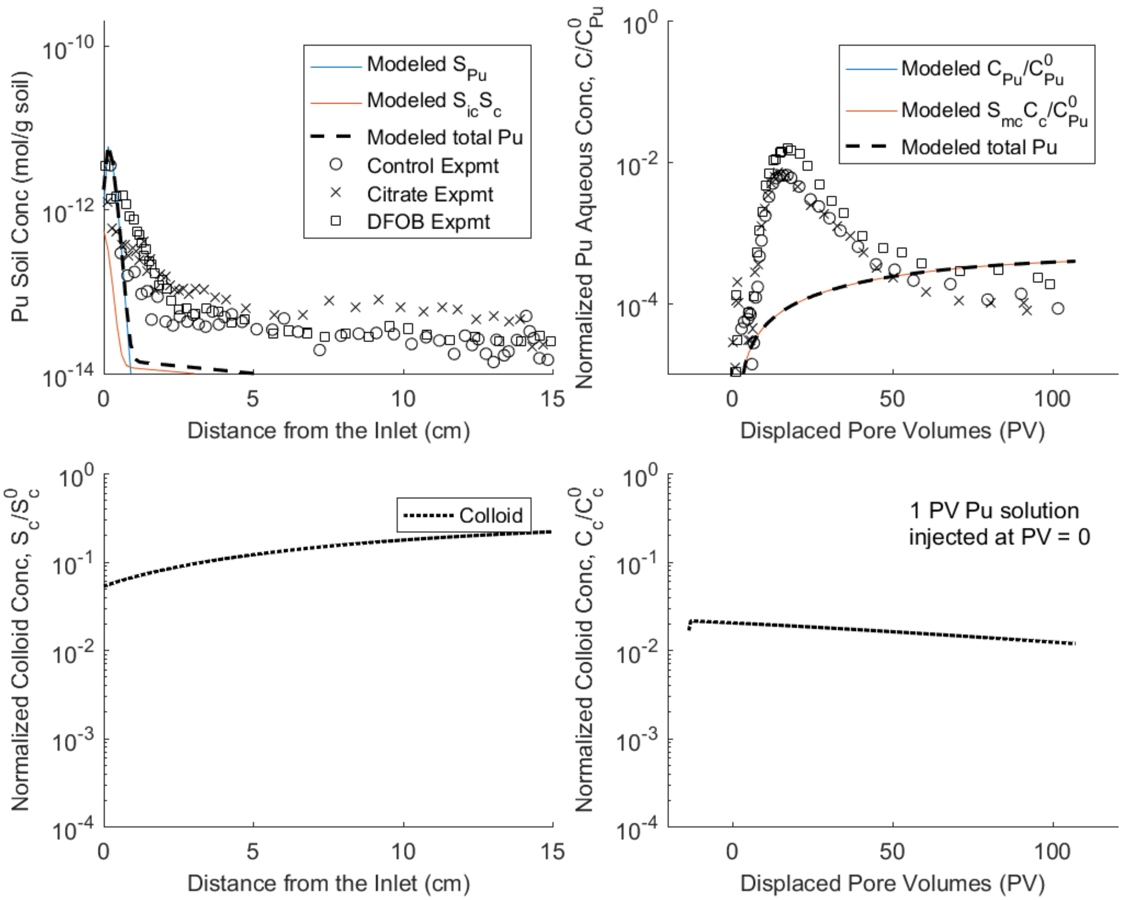

Figure D.34. Plutonium and colloid concentrations were modeled using a one-dimensional colloid-facilitated transport model in HYDRUS. Experimental data from the control, citrate, and DFOB column experiments is shown.
k_{att} = 0.04 min^{-1}; k_{det} = 3 × 10^{-4} min^{-1}; **k_{ac} = 0.5 min^{-1}**; k_{dc} = 6.9 × 10^{-5} min^{-1}; K_d = 2000 mL·g^{-1}.

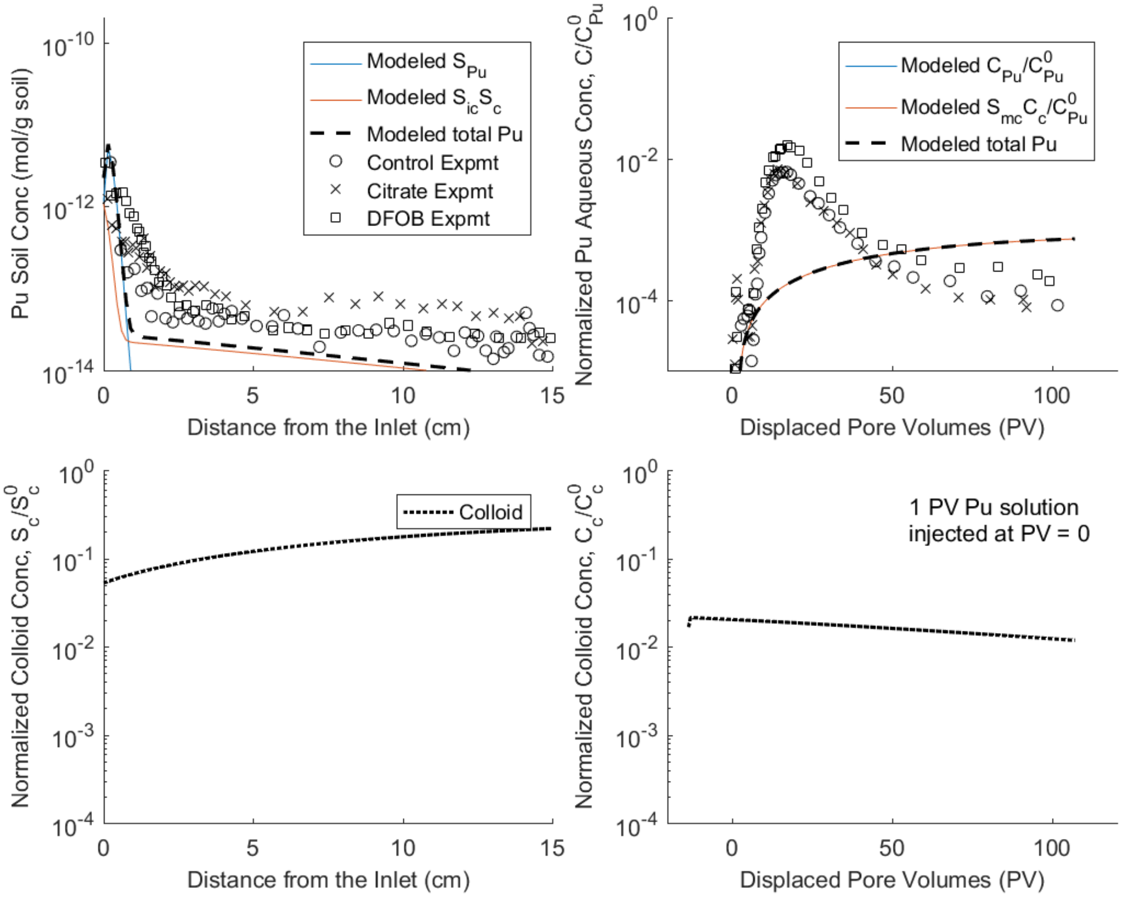

Figure D.35. Plutonium and colloid concentrations were modeled using a one-dimensional colloid-facilitated transport model in HYDRUS. Experimental data from the control, citrate, and DFOB column experiments is shown.
k_{att} = 0.04 min^{-1}; k_{det} = 3 × 10^{-4} min^{-1}; **k_{ac} = 1.0 min^{-1}**; k_{dc} = 6.9 × 10^{-5} min^{-1}; K_d = 2000 mL·g^{-1}.

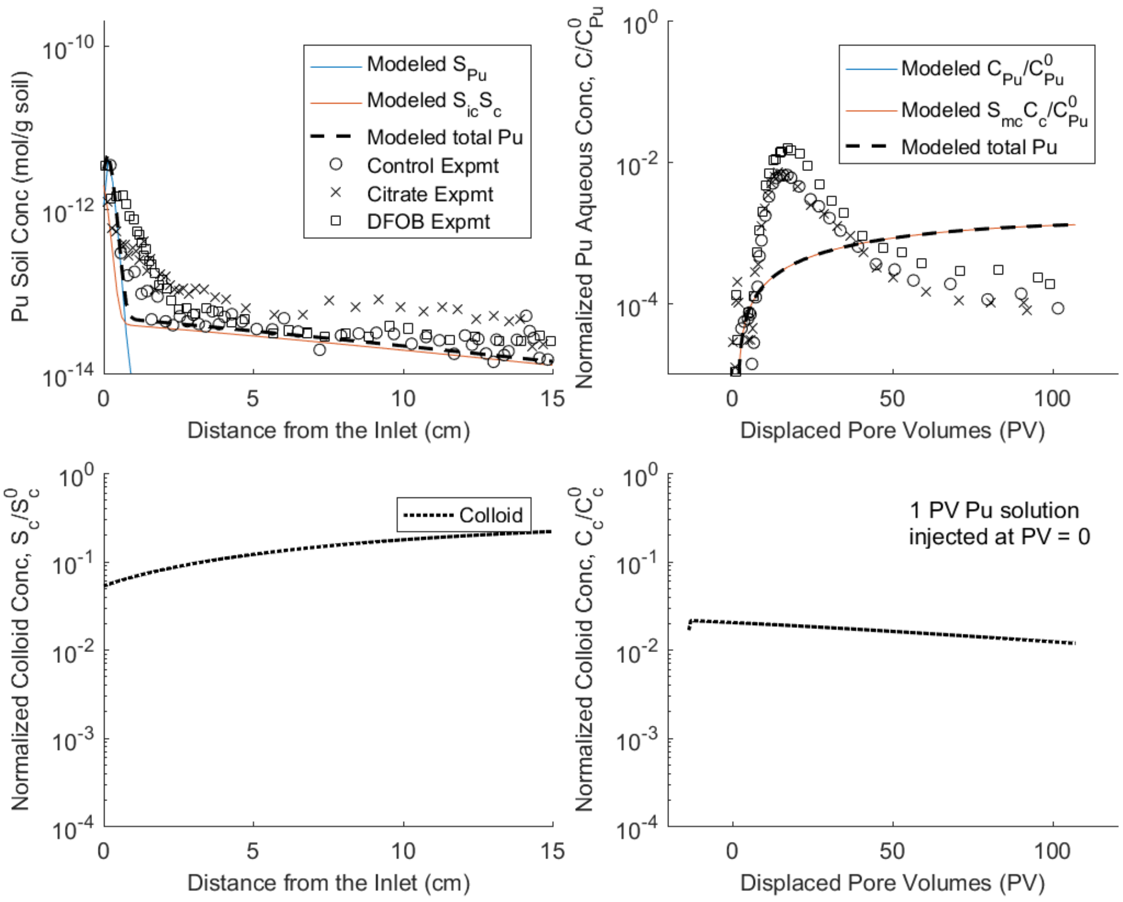

Figure D.36. Plutonium and colloid concentrations were modeled using a one-dimensional colloid-facilitated transport model in HYDRUS. Experimental data from the control, citrate, and DFOB column experiments is shown.
k_{att} = 0.04 min^{-1}; k_{det} = 3 × 10^{-4} min^{-1}; **k_{ac} = 2.0 min^{-1}**; k_{dc} = 6.9 × 10^{-5} min^{-1}; K_d = 2000 mL·g^{-1}.

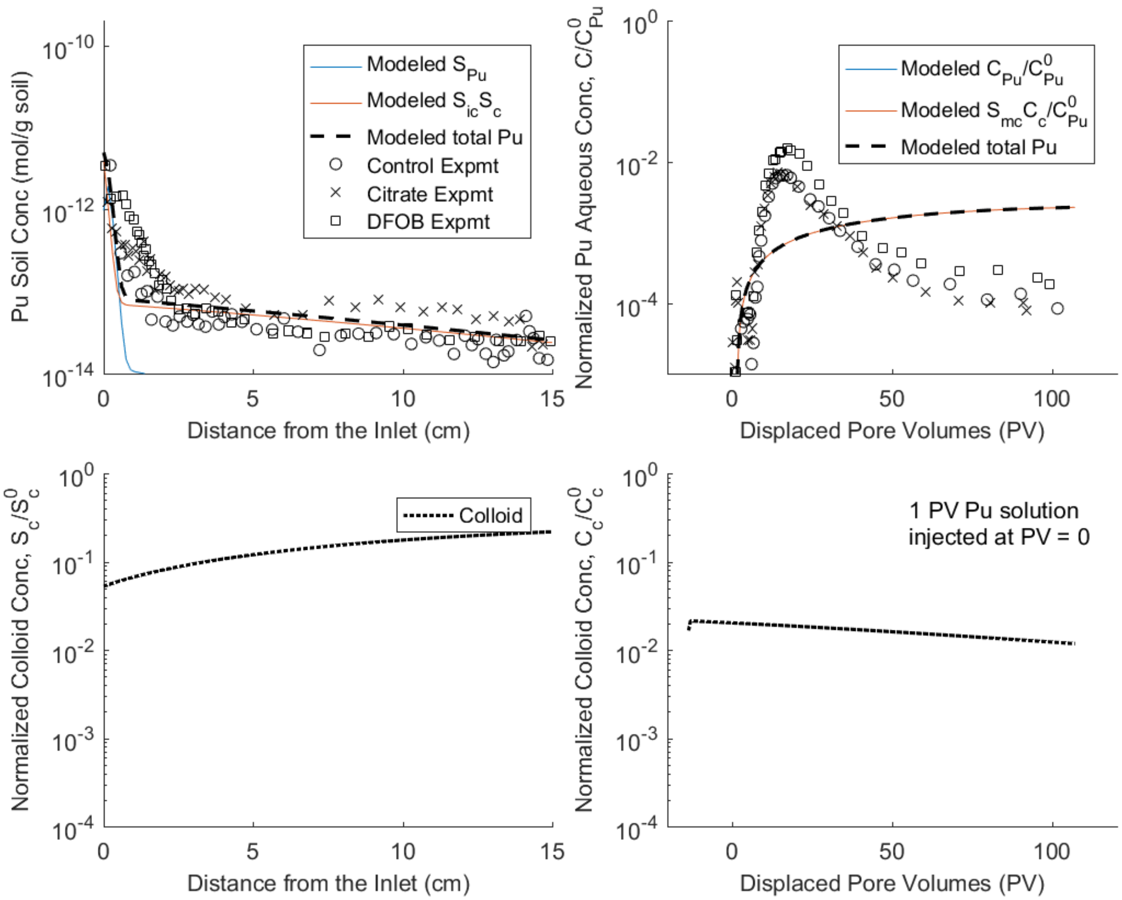

Figure D.37. Plutonium and colloid concentrations were modeled using a one-dimensional colloid-facilitated transport model in HYDRUS. Experimental data from the control, citrate, and DFOB column experiments is shown.
k_{att} = 0.04 min^{-1}; k_{det} = 3 × 10^{-4} min^{-1}; $\mathbf{k_{ac} = 5.0\ min^{-1}}$; k_{dc} = 6.9 × 10^{-5} min^{-1}; K_d = 2000 mL·g^{-1}.

Effect of Varying Pu Desorption Rate Constant from Colloids, k_{dc}

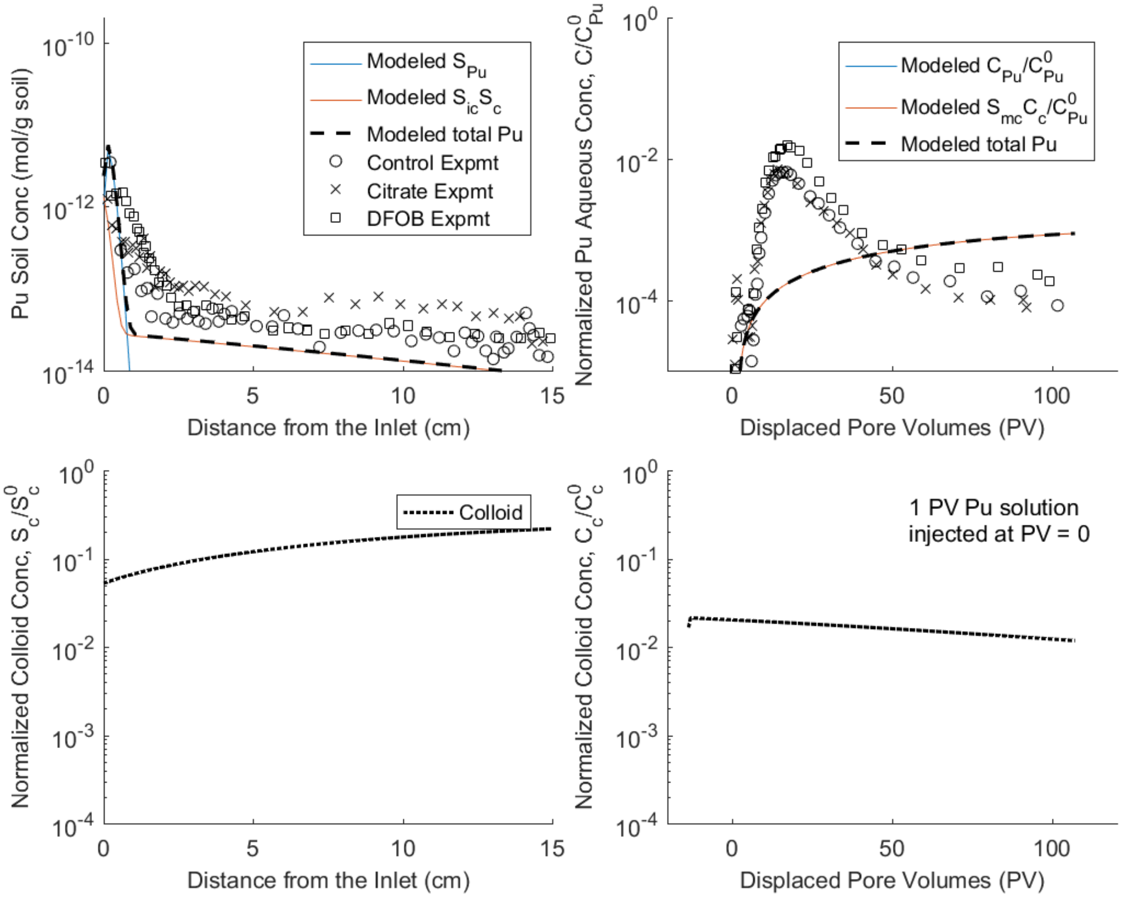

Figure D.38. Plutonium and colloid concentrations were modeled using a one-dimensional colloid-facilitated transport model in HYDRUS. Experimental data from the control, citrate, and DFOB column experiments is shown.
k_{att} = 0.04 min^{-1}; k_{det} = 3 × 10^{-4} min^{-1}; k_{ac} = 1.0 min^{-1}; **k_{dc} = 1 × 10^{-5} min^{-1}**; K_d = 2000 mL·g^{-1}.

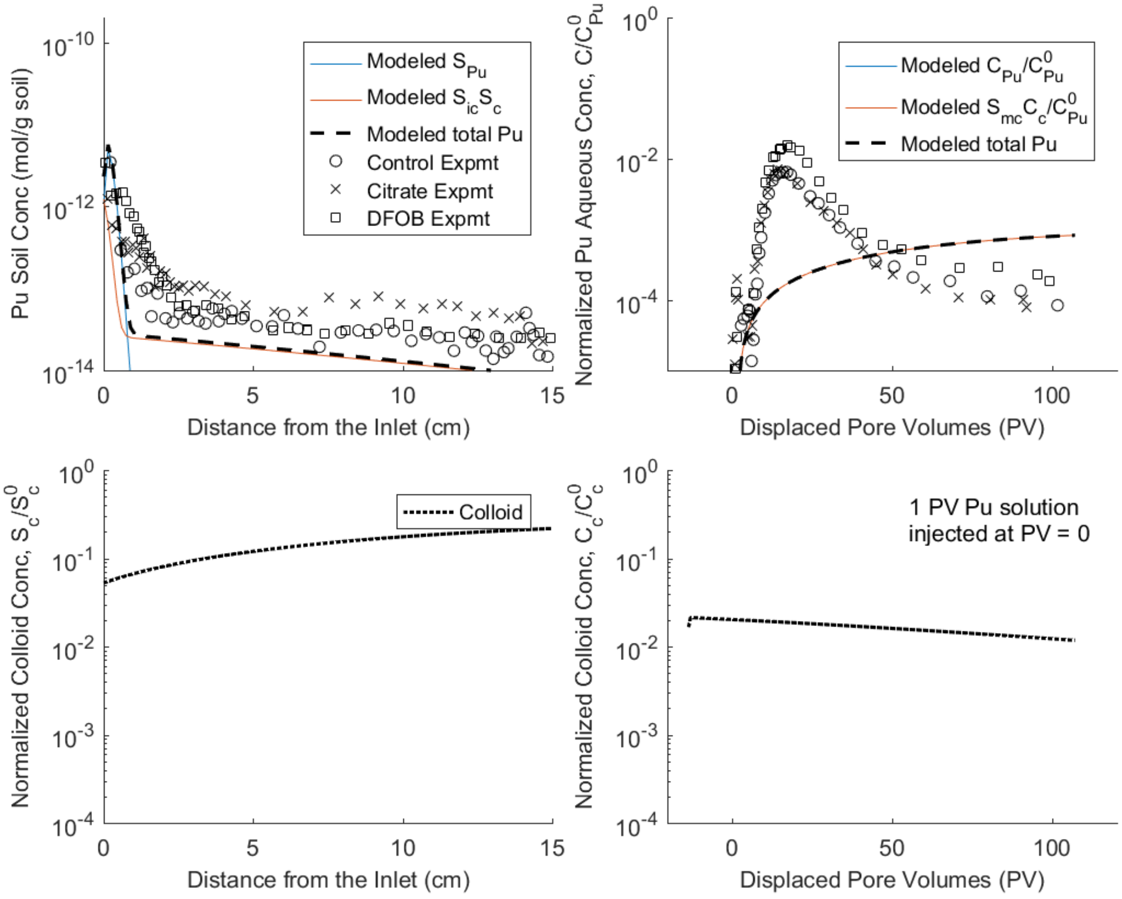

Figure D.39. Plutonium and colloid concentrations were modeled using a one-dimensional colloid-facilitated transport model in HYDRUS. Experimental data from the control, citrate, and DFOB column experiments is shown.
k_{att} = 0.04 min^{-1}; k_{det} = 3 × 10^{-4} min^{-1}; k_{ac} = 1.0 min^{-1}; **k_{dc} = 3 × 10^{-5} min^{-1}**; K_d = 2000 mL·g^{-1}.

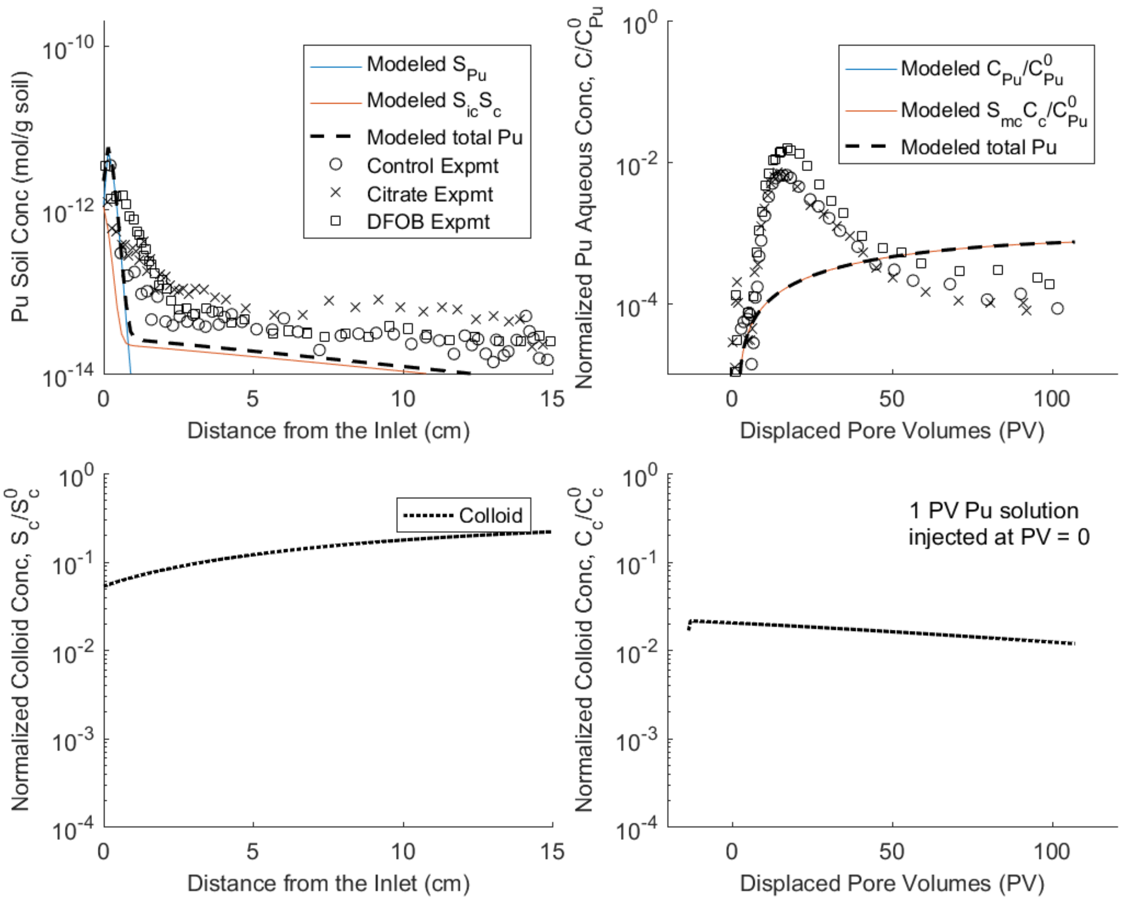

Figure D.40. Plutonium and colloid concentrations were modeled using a one-dimensional colloid-facilitated transport model in HYDRUS. Experimental data from the control, citrate, and DFOB column experiments is shown.
k_{att} = 0.04 min^{-1}; k_{det} = 3 × 10^{-4} min^{-1}; k_{ac} = 1.0 min^{-1}; **k_{dc} = 6.9 × 10^{-5} min^{-1}**; K_d = 2000 mL·g^{-1}.

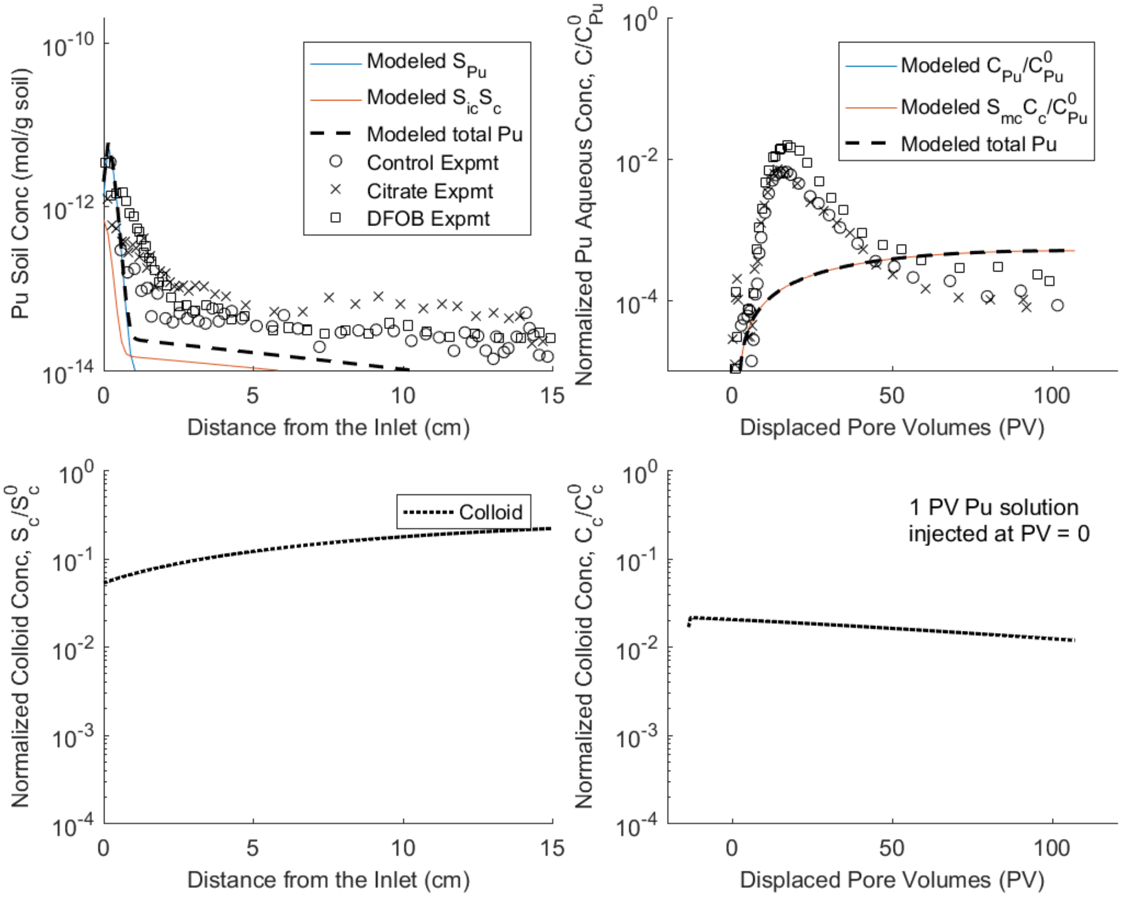

Figure D.41. Plutonium and colloid concentrations were modeled using a one-dimensional colloid-facilitated transport model in HYDRUS. Experimental data from the control, citrate, and DFOB column experiments is shown.
k_{att} = 0.04 min^{-1}; k_{det} = 3 × 10^{-4} min^{-1}; k_{ac} = 1.0 min^{-1}; **k_{dc} = 2 × 10^{-4} min^{-1}**; K_d = 2000 mL·g^{-1}.

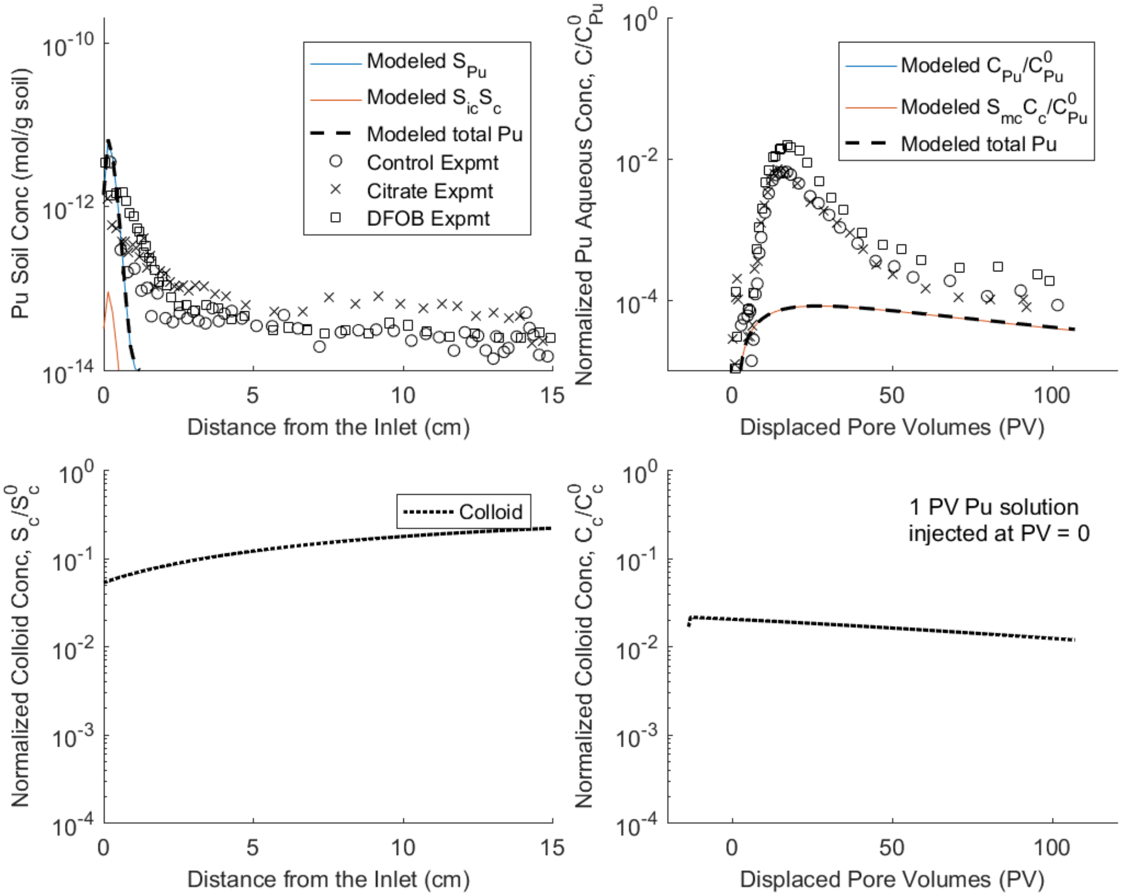

Figure D.42. Plutonium and colloid concentrations were modeled using a one-dimensional colloid-facilitated transport model in HYDRUS. Experimental data from the control, citrate, and DFOB column experiments is shown.
k_{att} = 0.04 min^{-1}; k_{det} = 3×10^{-4} min^{-1}; k_{ac} = 1.0 min^{-1}; **k_{dc} = 2×10^{-3} min^{-1}**; K_d = 2000 $\text{mL}\cdot\text{g}^{-1}$.

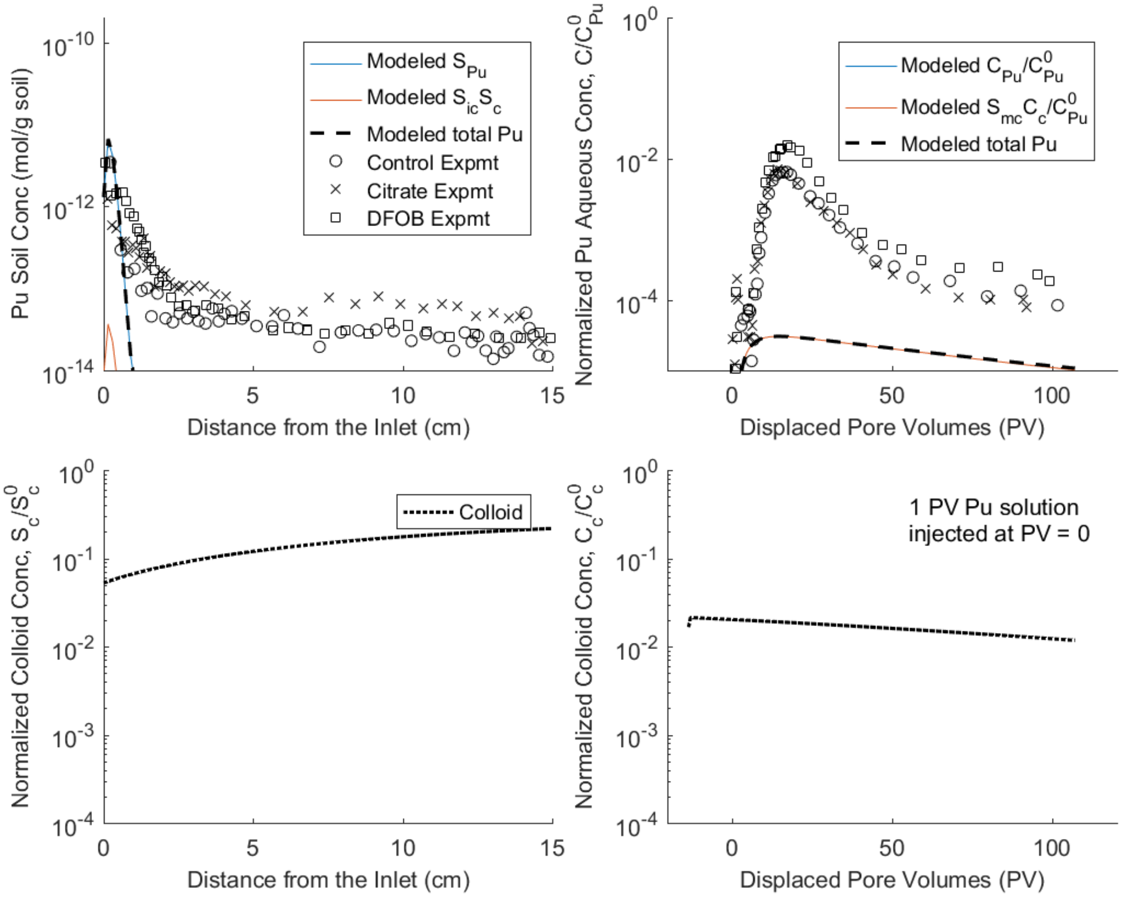

Figure D.43. Plutonium and colloid concentrations were modeled using a one-dimensional colloid-facilitated transport model in HYDRUS. Experimental data from the control, citrate, and DFOB column experiments is shown.
k_{att} = 0.04 min^{-1}; k_{det} = 3 × 10^{-4} min^{-1}; k_{ac} = 1.0 min^{-1}; **k_{dc} = 5 × 10^{-3} min^{-1}**; K_d = 2000 mL·g^{-1}.

Effect of Varying Distribution Coefficient, K_d

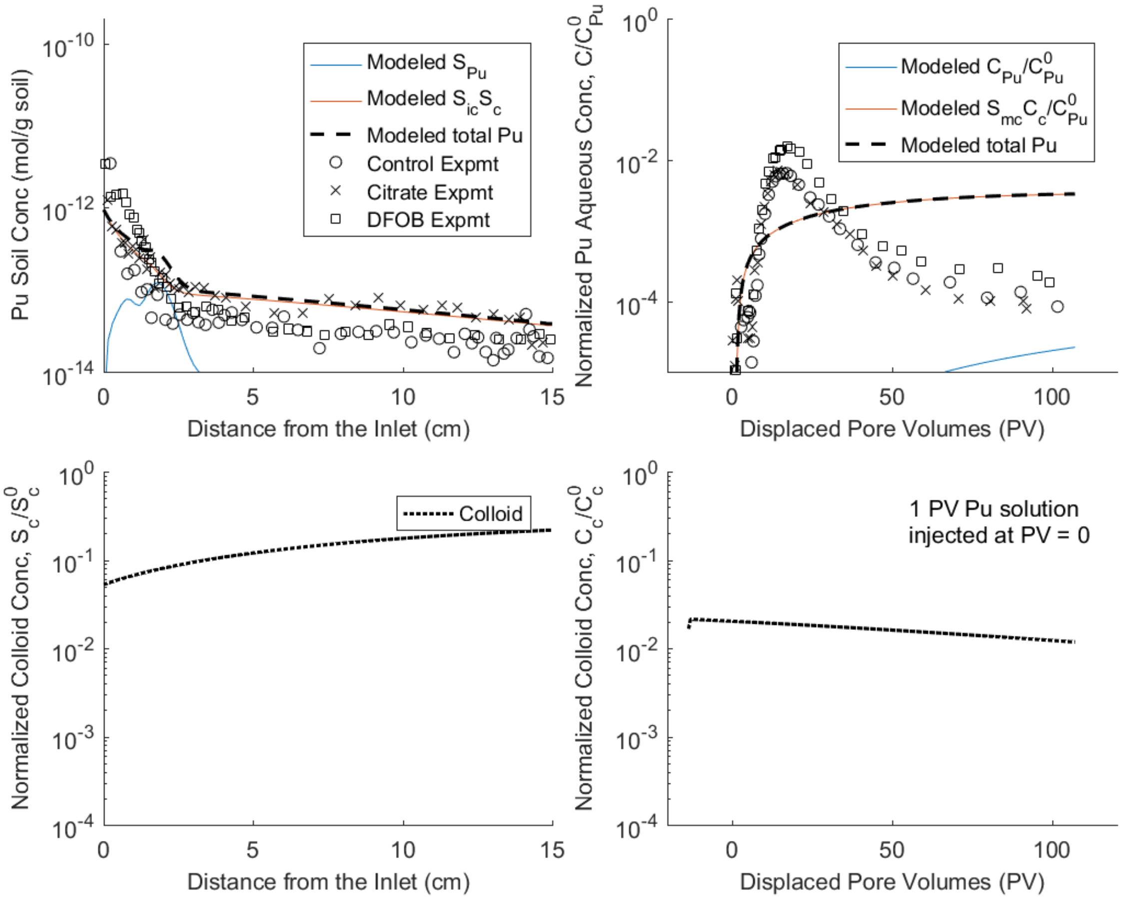

Figure D.44. Plutonium and colloid concentrations were modeled using a one-dimensional colloid-facilitated transport model in HYDRUS. Experimental data from the control, citrate, and DFOB column experiments is shown.
k_{att} = 0.04 min^{-1}; k_{det} = 3 × 10^{-4} min^{-1}; k_{ac} = 1.0 min^{-1}; k_{dc} = 6.9 × 10^{-5} min^{-1}; **K_d = 200 mL·g^{-1}**.

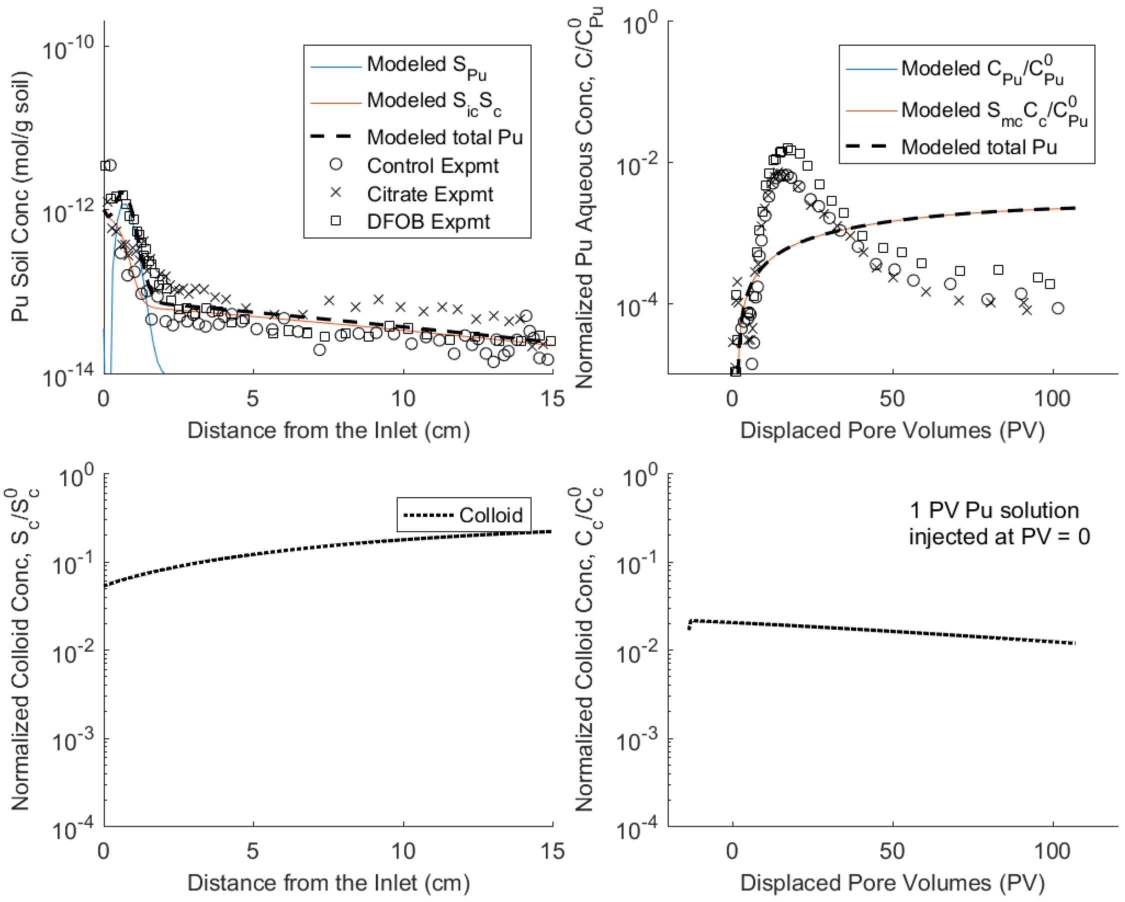

Figure D.45. Plutonium and colloid concentrations were modeled using a one-dimensional colloid-facilitated transport model in HYDRUS. Experimental data from the control, citrate, and DFOB column experiments is shown.
k_{att} = 0.04 min^{-1}; k_{det} = 3 × 10^{-4} min^{-1}; k_{ac} = 1.0 min^{-1}; k_{dc} = 6.9 × 10^{-5} min^{-1}; **K_d = 500 mL·g^{-1}**.

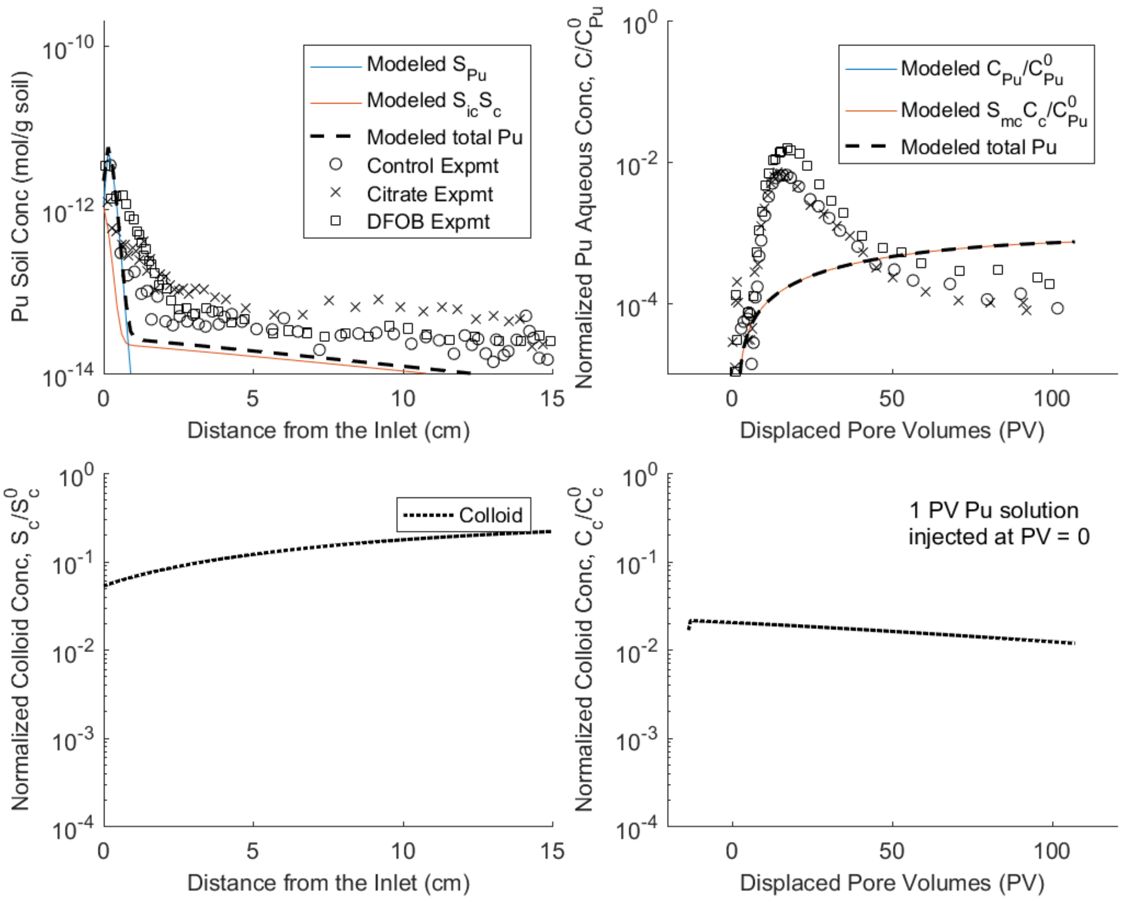

Figure D.46. Plutonium and colloid concentrations were modeled using a one-dimensional colloid-facilitated transport model in HYDRUS. Experimental data from the control, citrate, and DFOB column experiments is shown.
k_{att} = 0.04 min^{-1}; k_{det} = 3 × 10^{-4} min^{-1}; k_{ac} = 1.0 min^{-1}; k_{dc} = 6.9 × 10^{-5} min^{-1}; **K_d = 2000 mL·g^{-1}**.

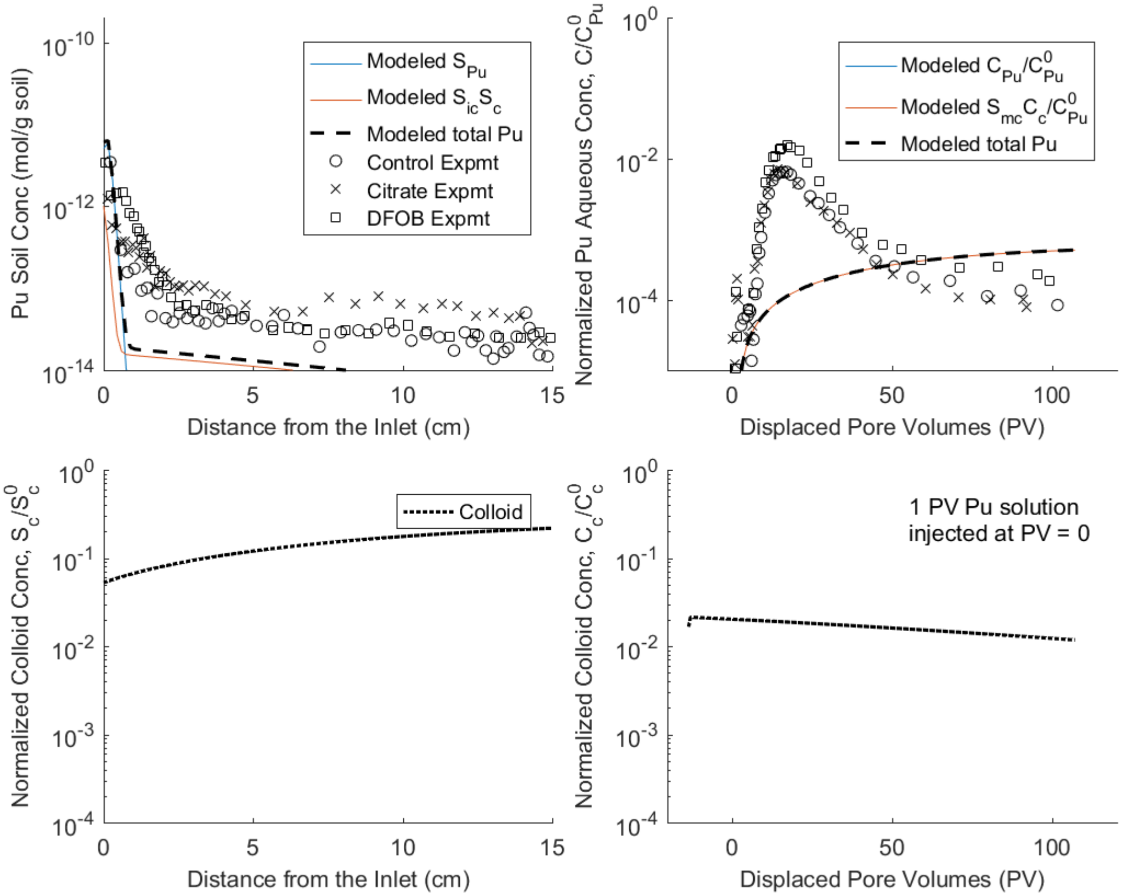

Figure D.47. Plutonium and colloid concentrations were modeled using a one-dimensional colloid-facilitated transport model in HYDRUS. Experimental data from the control, citrate, and DFOB column experiments is shown.
k_{att} = 0.04 min^{-1}; k_{det} = 3 × 10^{-4} min^{-1}; k_{ac} = 1.0 min^{-1}; k_{dc} = 6.9 × 10^{-5} min^{-1}; **K_d = 3000 mL·g^{-1}**.

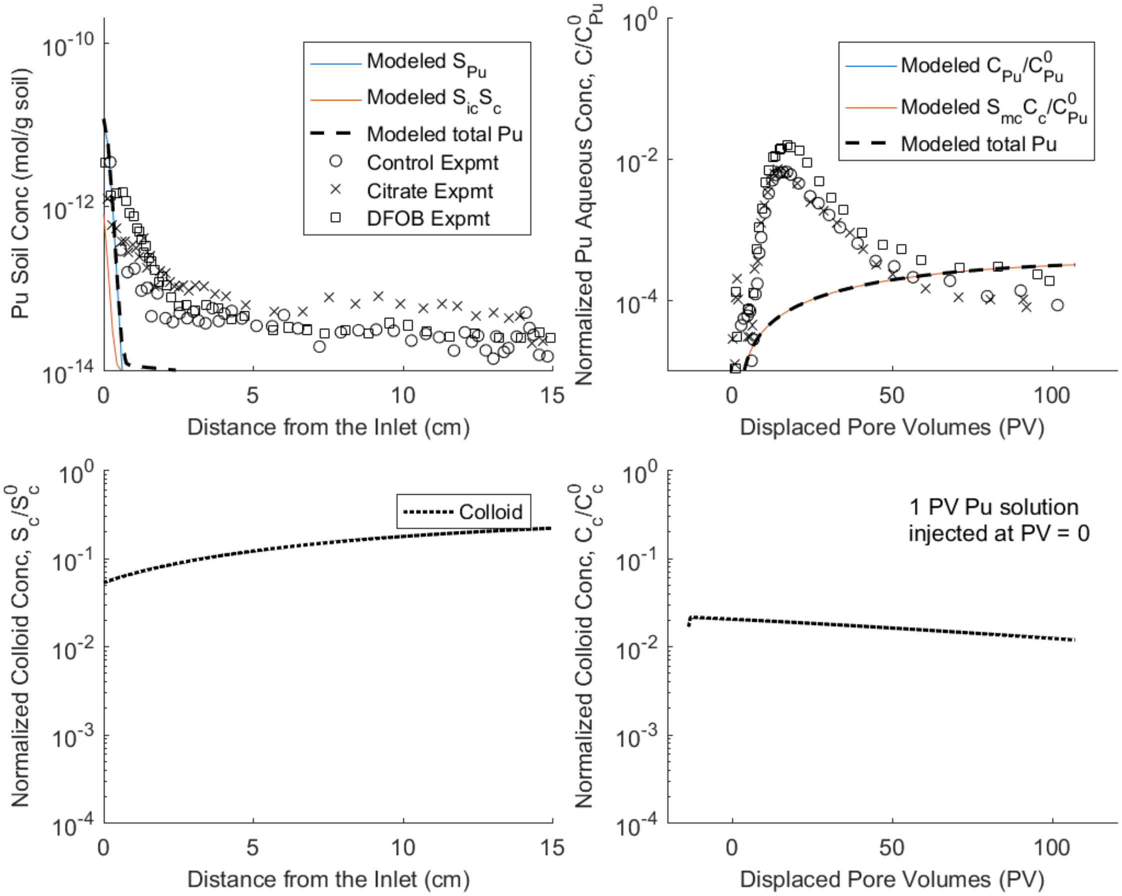

Figure D.48. Plutonium and colloid concentrations were modeled using a one-dimensional colloid-facilitated transport model in HYDRUS. Experimental data from the control, citrate, and DFOB column experiments is shown.
k_{att} = 0.04 min^{-1}; k_{det} = 3 × 10^{-4} min^{-1}; k_{ac} = 1.0 min^{-1}; k_{dc} = 6.9 × 10^{-5} min^{-1}; **K_d = 5000 mL·g^{-1}**.

Ligand-Facilitated Transport

The mathematical formulation for the ligand-facilitated transport model is the similar to that of the colloid-facilitated transport model, and the modeling was also performed using the C-Ride module of Hydrus 1D. The Hydrus input parameters are the same, but their definitions have changed (Table D.6). Instead of colloids, an organic ligand with properties representative of soil organic matter is considered to facilitate Pu transport. Instead of Pu (de)sorption reactions with colloids, complexation and dissociation of Pu with the ligand is considered. Instead of colloid attachment–detachment processes with soil, ligand (de)sorption reactions with soil are considered. The "*k*" parameters are pseudo-first-order rate constants which assume that the concentration of soil sorption sites is much greater than the concentration of ligands, and that the concentration of ligands is much greater than the concentration of Pu.

Table D.6. Additional variables used as inputs for the ligand-facilitated transport model

Variable	Units	Description
k_{att}	min^{-1}	ligand sorption to soil
k_{det}	min^{-1}	ligand desorption from soil
k_{ac}	min^{-1}	formation of Pu–ligand complexes
k_{dc}	min^{-1}	dissociation of Pu–ligand complexes

The key difference from the colloid-facilitated transport model is that reactions are assumed to reach equilibrium instantaneously which reduces the number of adjustable parameters. The complexation of Pu with a model organic ligand can be described by Eqn. D.18, where the stability constant is given by Eqn. D.19. Because constant pH is considered, a conditional stability constant (Eqn. D.20) can be used, and this conditional stability constant can be used to replace k_{ac} and k_{dc} as an adjustable parameter (Eqn. D.21). Similarly, the ligand distribution coefficient, K_d^{ligand}, defined in Eqn. D.22 can be used to replace k_{att} and k_{det} as an adjustable model parameter. However, the values of k_{att}, k_{det}, k_{ac}, and k_{dc} must still be calculated for the Hydrus 1D software input. In order to simulate so-called instantaneous reaction equilibrium, the parameters k_{att}, k_{det}, k_{ac}, and k_{dc} were chosen to be sufficiently large for the reactions to reach equilibrium on timescales similar to the computational time step of Hydrus, while maintaining the relationships with K'_{PuL} and K_d^{ligand} (Eqns. D.23 and D.24).

Published parameter values to use with the ligand-facilitated transport models were limited. Due to the heterogeneous nature of soil and organic matter, it was challenging to estimate the distribution coefficient for the soil organic matter. Sorption profiles for a variety of humic and fulvic acids have been previously measured for goethite, kaolinite, and alumina (Banik et al., 2007; Conroy et al., 2017; Schlautman and Morgan, 1994). Some K_d^{ligand} values calculated from previous studies of organic matter adsorption to minerals are tabulated in Table D.7. Measurements of Pu complexation with organic matter are limited. An approach which considers proton binding sites with discrete pK_a values to describe organic matter has been used for Leonardite humic acid and Suwanee River fulvic acid, standard I to determine Pu complexation stability constants with organic matter (Simpkins, 2011; Zimmerman et al., 2014). An empirical formula has been used previously to calculate the fraction of Pu bound to Suwanee River fulvic acid, standard I (Tinnacher et al., 2015).

$$Pu^{4+} + HL \leftrightarrow PuL^{3+} + H^{+} \tag{D.18}$$

$$K_{PuL} = \frac{[PuL^{3+}][H^{+}]}{[Pu^{4+}]} \tag{D.19}$$

$$K'_{PuL} = \frac{K_{PuL}}{[H^{+}]} = \frac{[PuL^{3+}]}{[Pu^{4+}]} \tag{D.20}$$

$$K'_{PuL} = \frac{S_{mc}C_c}{C_{Pu}} = \frac{k_{ac}}{k_{dc}} \tag{D.21}$$

$$K_d^{ligand} = \frac{k_{att}}{k_{det}} \tag{D.22}$$

$$k_{ac} = k_{dc}K'_{PuL} \tag{D.23}$$

$$k_{att} = k_{det}K_d^{ligand} \tag{D.24}$$

Table D.7. Summary of parameters from literature for modeling ligand-facilitated tranport

Organic Matter Frac. Sorbed	K_d^{ligand} (mL·g^{-1})	K'_{PuL} (-)	pH	Source	Comment
	7700		5	Conroy et al. (2016)	5 mg$_c$/L HA,[a] 3.9 m^2·L^{-1} goethite
	3900		5	Conroy et al. (2016)	5 mg$_c$/L FA,[b] 3.9 m^2·L^{-1} goethite
0.72	660		5	Banik et al. (2007)	20 mg/L HA,[c] 4 g/L kaolinite
0.28	95		5	Banik et al. (2007)	20 mg/L FA,[d] 4 g/L kaolinite
0.95 – 1.0	>4200		5	Schlautman and Morgan (1994)	4 mg/L HA,[e] 0.4 g/L alumina
0.77 – 0.81	830 - 1100		5	Schlautman and Morgan (1994)	4 mg/L FA,[f] 0.4 g/L alumina
		1.3 – 2.6	5	Zimmerman et al. (2014)	Pu(IV), HA,[a] stability constant for discrete protonation site approach [g]
		0.04	4	Tinnacher et al. (2015)	Pu(IV) complexation with FA,[h] extrapolation of empirical equation [i]
		0.003	5	Simpkins (2011)	Pu(IV), FA,[h] stability constants for discrete protonation site approach [j]

[a] Leonardite humic acid

[b] Suwanee River fulvic acid, standard II

[c] Aldrich humic acid

[d] Gorleben fulvic acid

[e] Suwanee River humic acid

[f] Suwanee River fulvic acid

[g] The stability constant for Pu(IV) complexation with humic acid protonation sites (pK$_a$ = 7) was used to calculate the concentration of bound Pu for conditions: 10 to 20 μg$_c$·L^{-1}; 5 × 10^{-10} M Pu(IV); 10 mM NaCl; E_h = 0.3 V; 1.59 × 10^{-3} mol$_{sites}$·g$_c$$^{-1}$

[h] Suwanee River fulvic acid, standard I

[i] Calculation: $K'_{PuL} = 0.1 \times C_c^{0.68}$ with C_c = 0.26 mg$_c$/L estimated from the blank column experiment in this work

[j] The stability constant for Pu(IV) complexation with fulvic acid protonation sites (pK$_a$ = 7) was used to calculate the concentration of bound Pu for conditions: 10 to 20 μg$_c$·L^{-1}; 5 × 10^{-10} M Pu(IV); 10 mM NaCl; E_h = 0.3 V; 1.89 × 10^{-3} mol$_{sites}$·g$_c$$^{-1}$

Results of modeling Ligand-Facilitated Transport

The parameter values determined from literature were of little use for demonstrating the ligand-facilitated transport model. In order to simulate enhanced Pu mobility with the ligand-facilitated transport model, it was necessary to use K'_{PuL} values orders of magnitude greater than those calculated from previous studies of humic and fulvic acid (Table D.8). Although siderophores and organic chelating molecules can form stable Pu complexes capable of competing with the sorption sites on the soil, K'_{PuL} values on the order of 10^4 mL·g^{-1} are unreasonable for typical soil organic matter. Although increasing the K'_{PuL} value increased the proportion of Pu which partitioned to a second, mobile Pu peak at 0.6 cm, adjusting this parameter did not affect the distance of Pu transport in the column.

Table D.8. Parameters for consideration for the ligand-facilitated transport model

Parameter	Units	Literature Range	Range Modeled	Reasonable Fit
K_d^{ligand}	mL·g^{-1}	95 – 7700	150 – 1000	none
K'_{PuL}	-	0.003 – 2.6	0.5 – 17000	none
K_d	mL·g^{-1}	200 – 3000	1000	not varied

The ligand-facilitated transport model produced bimodal distributions of Pu in the soil for K_d^{ligand} values of 200 to 500 mL·g^{-1}, but it was not possible to elute any aqueous Pu (Figs. D.49–D.52). In the model, Pu mobilized by the organic ligand in the soil coincided with the SOM-free solution front. After the passage of the SOM-free solution front, Pu in the first 2 cm of the soil column no longer interacted with the modeled soil organic matter. The rate of passage of the mobile Pu peak in the soil depended on the K_d^{ligand} value. The value of 1000 mL·g^{-1} was considered a practical upper limit to the K_d^{ligand} value, since at greater values, the organic ligand would not mobilize the Pu relative to the unbound Pu.

The mobile Pu was eluted at ≈17 PV which has a corresponding K_d^{ligand} value of 8 mL·g^{-1}. However, the ligand-facilitated transport model did not indicate the enhancement of Pu mobility below the K_d^{ligand} value of 200 mL·g^{-1}. As the K_d^{ligand} value decreased, the mass of SOM which interacted with Pu before being flushed down-gradient decreased. Additionally, increasingly greater values of K'_{PuL} were required by the model in order to partition Pu into the mobile Pu peak. When ligand distribution coefficients below 200 mL·g^{-1} were considered (Fig. D.52), the modeled SOM was flushed down-gradient during conditioning before it contacted Pu. Thus, the ability of the SOM in this model to enhance Pu mobility was limited.

The modeling results demonstrated a lack of fit to the experimental data for an extensive range of parameters. This indicated that the process of ligand-facilitated transport as it was formulated in this model could not explain the Pu distribution observed. The model had several limitations. The model was limited to a single conceptual ligand, whereas real-world soil organic matter contains a plethora of different organic molecules. The model assumed that sorption and complexation reactions were instantaneous, but kinetic effects may have affected Pu transport. The model assumed that organic matter sorption to soil was linear, but the sorption sites were likely extremely heterogeneous.

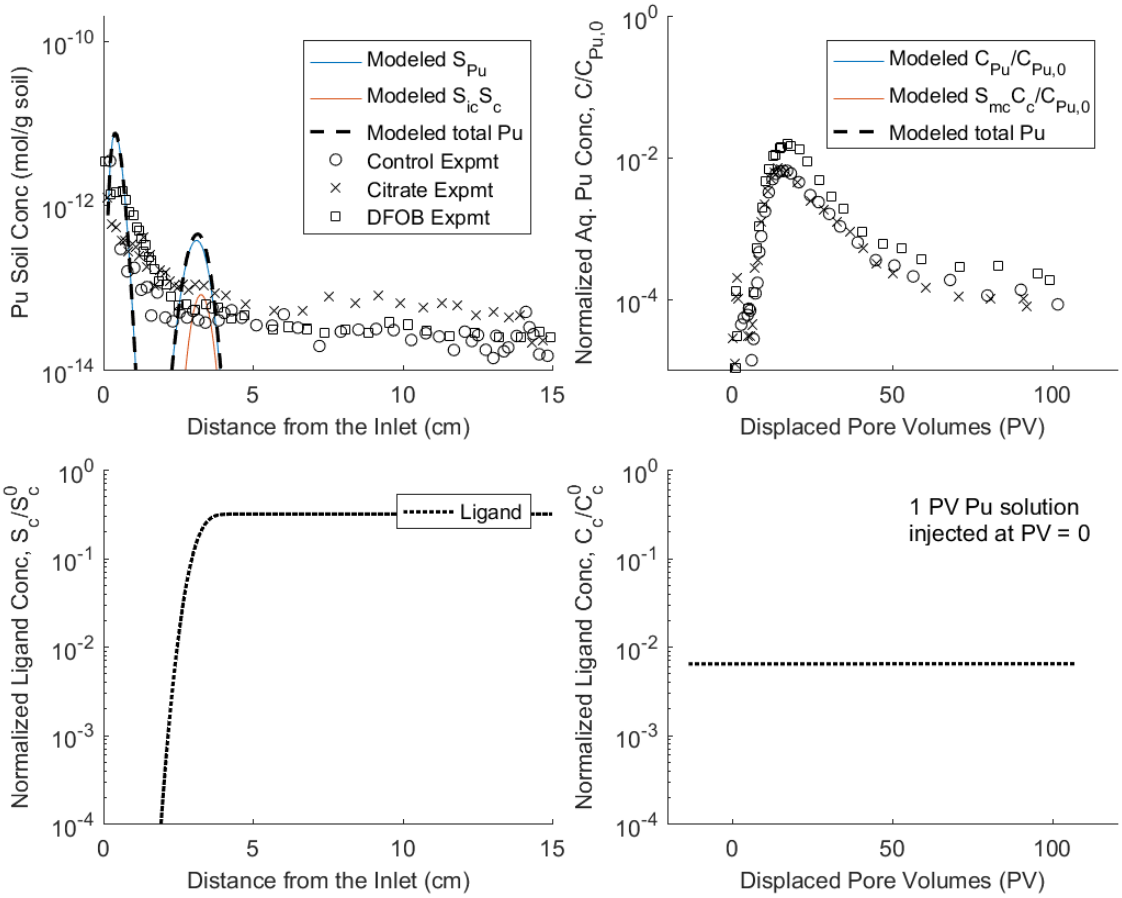

Figure D.49. Plutonium and ligand concentrations were modeled using a one-dimensional ligand-facilitated transport model in HYDRUS. Experimental data from the control, citrate, and DFOB column experiments is shown. K_d^{ligand} = 500 mL·g^{-1}; K'_{PuL} = 1200; K_d = 2000 mL·g^{-1}.

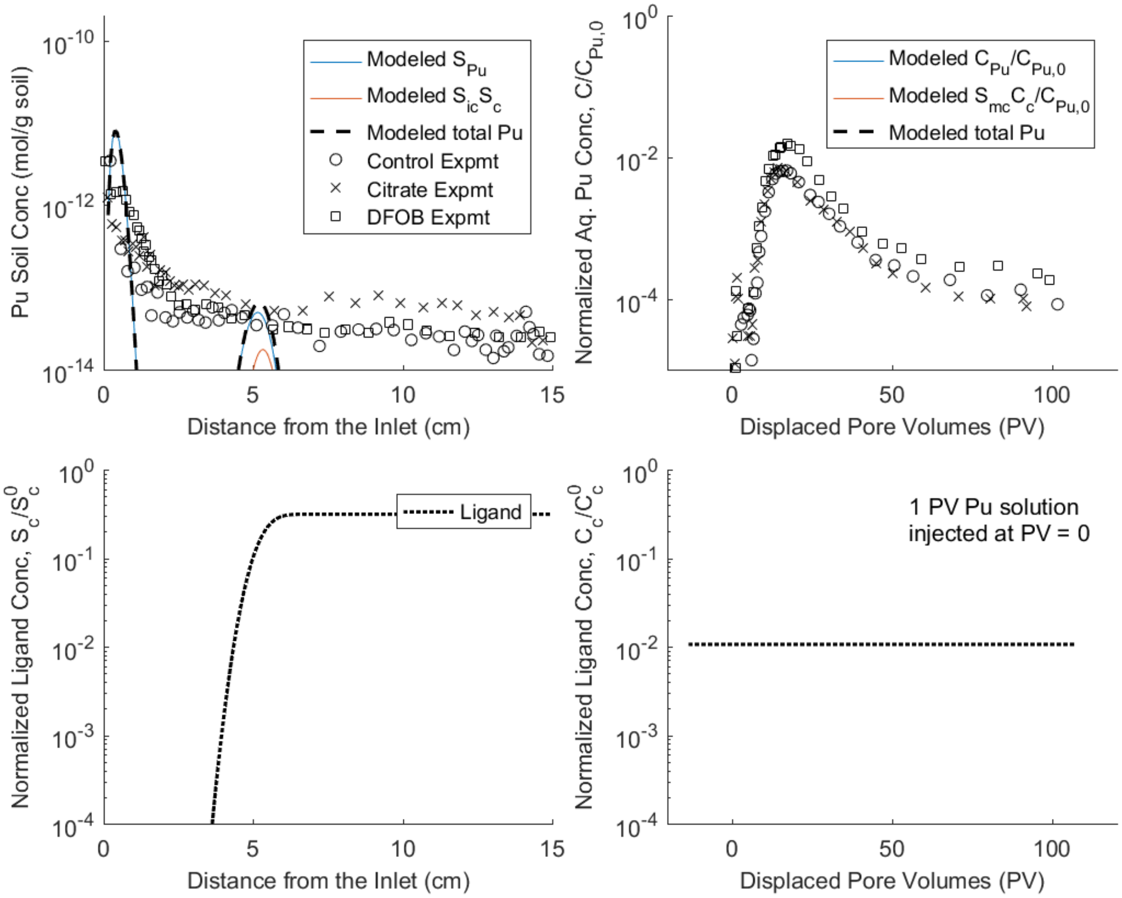

Figure D.50. Plutonium and ligand concentrations were modeled using a one-dimensional ligand-facilitated transport model in HYDRUS. Experimental data from the control, citrate, and DFOB column experiments is shown. K_d^{ligand} = 300 mL·g^{-1}; K'_{PuL} = 2100; K_d = 2000 mL·g^{-1}.

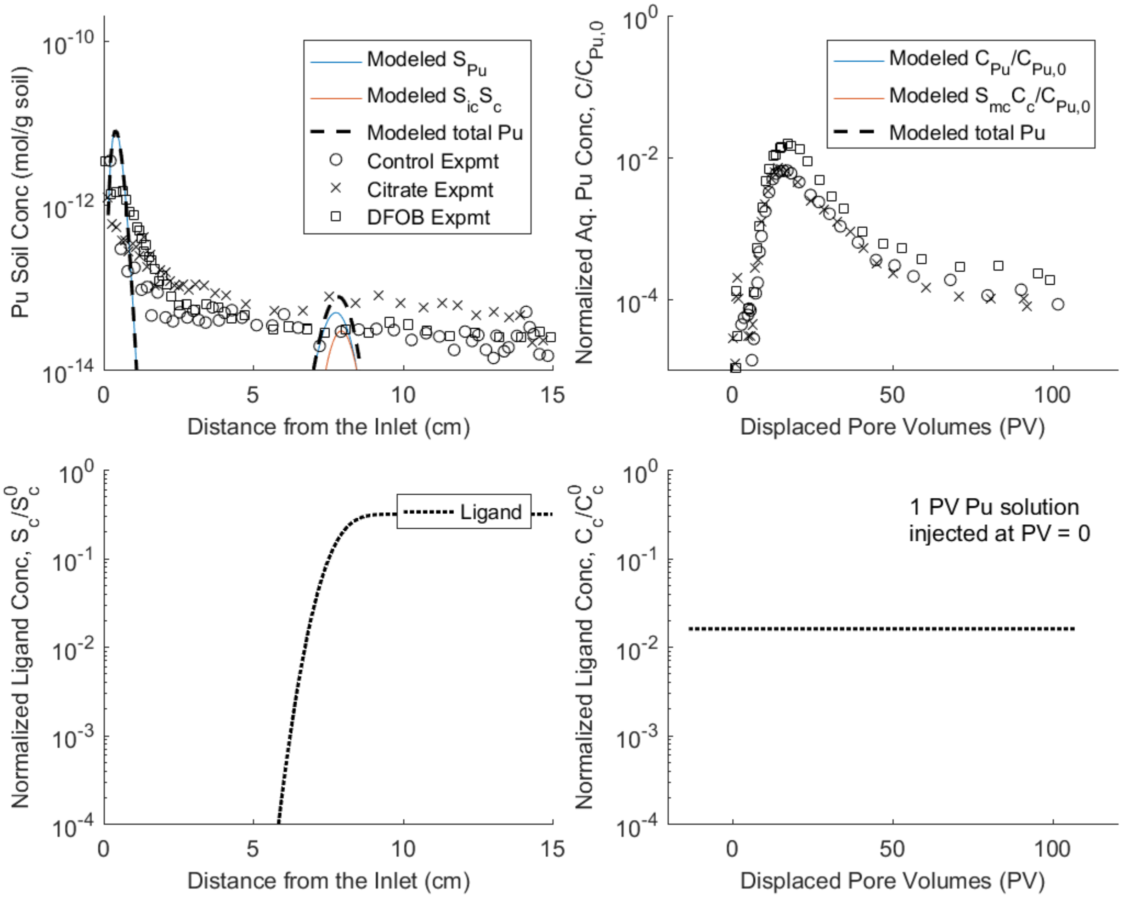

Figure D.51. Plutonium and ligand concentrations were modeled using a one-dimensional ligand-facilitated transport model in HYDRUS. Experimental data from the control, citrate, and DFOB column experiments is shown. K_d^{ligand} = 200 mL·g^{-1}; K'_{PuL} = 3500; K_d = 2000 mL·g^{-1}.

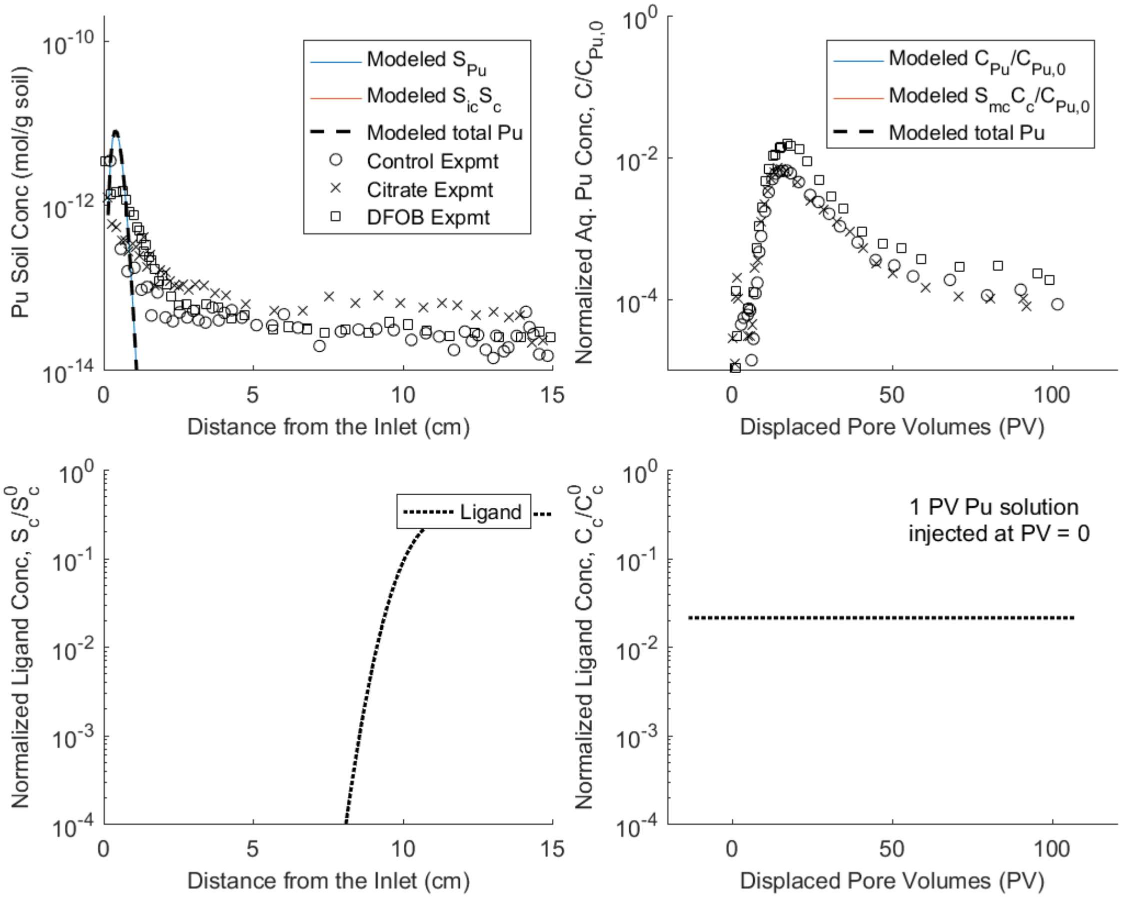

Figure D.52. Plutonium and ligand concentrations were modeled using a one-dimensional ligand-facilitated transport model in HYDRUS. Experimental data from the control, citrate, and DFOB column experiments is shown. K_d^{ligand} = 150 mL·g^{-1}; K'_{PuL} = 17000; K_d = 2000 mL·g^{-1}.

More Hypothetical Processes for Pu Transport in SRS Soil

There are several additional processes involving the organic ligands which potentially affected Pu mobility in the soil. The ligand may have acted synergistically with soil organic matter to enhance the formation of Pu–SOM aqueous complexes. The presence of the ligand may have promoted the formation of mobile colloids by dissolving sand surface coatings or breaking up clay-sized particles. If a mobile form of Pu was generated in the presence of the ligand, then Pu may have been mobilized beyond the bounds of the ligand front. Another possibility is that citrate and DFOB formed organic surface coatings which may have enhanced or diminished Pu sorption. The Langmuir isotherms (Fig. C.3) suggest some surface site saturation is occurring within the ligand front. For the steady-state aqueous ligand concentration of 0.278 mM within the ligand front, 88% or 41% of soil surface sites are estimated to be occupied by citrate or DFOB, respectively. Because these phenomena are limited to the first <1.5 cm of the column, none of these processes can be explicitly ruled out.

Appendix E

Humic Substances Information

Table E.1. Elemental composition as a percentage of mass for Suwanee River Fulvic Acid I standard (SRFA I), Suwanee River Fulvic Acid II standard (SRFA II), and Leonardite Humic Acid standard (HA) (International Humic Substances Society). [a]

	H2O [b]	Ash [c]	C	H	O	N	S	P
SRFA I	8.8	0.46	52.44	4.31	42.2	0.72	0.44	<0.01
SRFA II	16.9	0.58	52.34	4.36	42.98	0.67	0.46	0.004
HA	7.2	2.58	63.81	3.7	31.27	1.23	0.76	<0.01

[a] Elements are the elemental composition in %(w/w) of a dry, ash-free sample.

[b] H_2O content is the %(w/w) of H_2O in the air-equilibrated sample (a function of relative humidity).

[c] Ash is the %(w/w) of inorganic residue in a dry sample.

Table E.2. Acidic functional groups reported in terms of carbon for Suwanee River Fulvic Acid I standard (SRFA I), Suwanee River Fulvic Acid II standard (SRFA II), and Leonardite Humic Acid standard (HA) (International Humic Substances Society).

	Carboxylic [a] (meq/g carbon)	Phenolic [b] (meq/g carbon)	Total (meq/g carbon)
SRFA I	11.44	2.91	14.35
SRFA II	11.17	2.84	14.01
HA	7.46	2.31	9.77

[a] Charge density at pH 8.0

[b] Two times the change in charge density between pH 8.0 and pH 10.0

Table E.3. Acidic functional groups reported in terms of mass for Suwanee River Fulvic Acid I standard (SRFA I), Suwanee River Fulvic Acid II standard (SRFA II), and Leonardite Humic Acid standard (HA). [a]

	Carboxylic (meq/g)	Phenolic (meq/g)	Total (meq/g)
SRFA I	6.00	1.53	7.53
SRFA II	5.85	1.49	7.33
HA	4.76	1.47	6.23

[a] Calculated from carbon content of each material

Table E.4. ^{13}C NMR Estimates of carbon distribution as a percentage of carbon for Suwanee River Fulvic Acid I standard (SRFA I), Suwanee River Fulvic Acid II standard (SRFA II), and Leonardite Humic Acid standard (HA) (International Humic Substances Society).

	Carbonyl	Carboxyl	Aromatic	Acetal	Heteroaliphatic	Aliphatic
SRFA I	7	20	24	5	11	33
SRFA II	5	17	22	6	16	35
HA	8	15	58	4	1	14

Appendix F

Key Terms

aging	aging of a sorbate occurs when a surface process occurring after initial sorption causes a change in sorbate surface state over time which manifests as a decrease in sorbate desorbability with increasing contact time
CV	displaced chamber volumes
DFOB	desferrioxamine B
DOC	dissolved organic carbon
HR-TEM	high resolution tunneling electron microscope
ICP-MS	inductively coupled plasma mass spectrometry
ICPS	ion counts per second, units for raw data collection for inductively coupled plasma mass spectrometry
LA-ICP-MS	laser ablation inductively coupled plasma mass spectrometry
MDC	minimum detectable concentration
nanoSIMS	nano-secondary ionization mass spectrometry
NOL	natural organic ligands
PTFE	polytetrafluoroethylene, commercially known as Teflon
PV	displaced pore volumes
residence time effect	an alternate term for aging which describes a decrease in sorbate desorbability with increasing contact time
site or surface state	may describe a sorption site or a chemical/physical state of a sorbate on the surface. For modeling purposes, different sites are defined operationally based on different kinetic rates.
SOM	soil organic matter
SRS	Savanna River Site, South Carolina, United States
TOC	total organic carbon

REFERENCES

Adamson, A. W.; Gast, A. P. *Physical Chemistry of Surfaces*, 6th ed.; Wiley: New York, 1997.

Ainsworth, C. C.; Gassman, P. L.; Pilon, J. L.; Sluys, V. D.; G, W. Cobalt, Cadmium, and Lead Sorption to Hydrous Iron Oxide: Residence Time Effect. *Soil Sci. Soc. Am. J.* **1994**, *58* (6), 1615–1623.

André, C.; Choppin, G. R. Reduction of Pu(V) by Humic Acid. *Radiochim. Acta* **2000**, *88* (9–11).

Appel, C.; Ma, L. Q.; Dean Rhue, R.; Kennelley, E. Point of Zero Charge Determination in Soils and Minerals via Traditional Methods and Detection of Electroacoustic Mobility. *Geoderma* **2003**, *113* (1–2), 77–93.

Atkinson, R. J.; Posner, A. M.; Quirk, J. P. Adsorption of Potential-Determining Ions at the Ferric Oxide-Aqueous Electrolyte Interface. *J. Phys. Chem.* **1967**, *71*, 550–558.

Backes, C. A.; McLaren, R. G.; Rate, A. W.; Swift, R. S. Kinetics of Cadmium and Cobalt Desorption from Iron and Manganese Oxides. *Soil Sci. Soc. Am. J.* **1995**, *59* (3), 778–785.

Bajo, S.; Gann, C.; Eikenberg, J.; Wyer, L.; Beer, H.; Ruthi, M.; Jaggi, M.; Zumsteg, I. *Separation of Plutonium on the Anion Exchanger BIO-RAD 1-X2 and Its Application to Radiochemical Analysis*; PSI Bericht Nr. 07-05; Paul Scherrer Institut: Villigen, Switzerland, 2007.

Banik, N. L. Speciation of Tetravalent Plutonium in Contact with Humic Substances and Kaolinite under Environmental Conditions. Dissertation, Johannes Gutenberg-University Mainz: Mainz, Germany, 2006.

Banik, N. L.; Buda, R. A.; Bürger, S.; Kratz, J. V.; Trautmann, N. Sorption of Tetravalent Plutonium and Humic Substances onto Kaolinite. *Radiochim. Acta* **2007**, *95* (10), 569–575.

Barrow, N. J.; Brümmer, G. W.; Fischer, L. Rate of Desorption of Eight Heavy Metals from Goethite and Its Implications for Understanding the Pathways for Penetration. *Eur. J. Soil Sci.* **2012**, *63* (3), 389–398.

Bar-Tal, A. F. Analyses of Adsorption Kinetics Using a Stirred-Flow Chamber: I. Theory and Critical Tests. *Soil Sci. Soc. Am. J.* **1990**, *54* (5), 1273.

References (Continued)

Begg, J. D.; Zavarin, M.; Zhao, P.; Tumey, S. J.; Powell, B.; Kersting, A. B. Pu(V) and Pu(IV) Sorption to Montmorillonite. *Environ. Sci. Technol.* **2013**, *47* (10), 5146–5153.

Begg, J. D.; Zavarin, M.; Kersting, A. B. Plutonium Desorption from Mineral Surfaces at Environmental Concentrations of Hydrogen Peroxide. *Environ. Sci. Technol.* **2014**, *48* (11), 6201–6210.

Begg, J. D.; Zavarin, M.; Tumey, S. J.; Kersting, A. B. Plutonium Sorption and Desorption Behavior on Bentonite. *J. Environ. Radioact.* **2015**, *141*, 106–114.

Blinova, O.; Novikov, A.; Perminova, I.; Goryachenkova, T.; Haire, R. Redox Interactions of Pu(V) in Solutions Containing Different Humic Substances. *J. Alloys Compd.* **2007**, *444–445*, 486–490.

Boggs, M. A.; Dai, Z.; Kersting, A. B.; Zavarin, M. Plutonium(IV) Sorption to Montmorillonite in the Presence of Organic Matter. *J. Environ. Radioact.* **2015**, *141*, 90–96.

Bondietti, E. A.; Reynolds, S. A.; Shanks, M. H. Interaction of Pu with Complexing Substances in Soils and Natural Water. In *Transuranium Nuclides in the Environment*; IAEA-SM-199/51; International Atomic Energy Agency: Vienna, 1976; pp 273–287.

Boukhalfa, H.; Reilly, S. D.; Neu, M. P. Complexation of Pu(IV) with the Natural Siderophore Desferrioxamine B and the Redox Properties of Pu(IV)(Siderophore) Complexes. *Inorg. Chem.* **2007**, *46* (3), 1018–1026.

Braithwaite, A.; Richardson, S.; Moyes, L. N.; Livens, F. R.; Bunker, D. J.; Hughes, C. R.; Smith, J. T.; Hilton, J. Sorption Kinetics of Uranium-238 and Neptunium-237 on a Glacial Sediment. *Czech. J. Phys.* **2000**, *50* (2), 265–269.

Bruemmer, G. W.; Gerth, J.; Tiller, K. G. Reaction Kinetics of the Adsorption and Desorption of Nickel, Zinc and Cadmium by Goethite. I. Adsorption and Diffusion of Metals. *J. Soil Sci.* **1988**, *39* (1), 37–52.

Buda, R.; Banik, N. L.; Kratz, J. V.; Trautmann, N. Studies of the Ternary Systems Humic Substances – Kaolinite – Pu(III) and Pu(IV). *Radiochim. Acta* **2008**, *96* (9–11).

Bunn, R. A.; Magelky, R. D.; Ryan, J. N.; Elimelech, M. Mobilization of Natural Colloids from an Iron Oxide-Coated Sand Aquifer: Effect of PH and Ionic Strength. *Environmental Science & Technology* **2002**, *36* (3), 314–322.

References (Continued)

Cantrell, K. J. *Transuranic Contamination in Sediment and Groundwater at the U.S. DOE Hanford Site*; Report PNNL-18640; Pacific Northwest National Laboratory: Richland, WA, 2009.

Carlton, W. H.; Evans, A. G.; Geary, L. A.; Murphy, Jr., C. E.; Pinder, J. E.; Strom, R. N. *Assessment of Plutonium in the Savannah River Site Environment*; Technical Report WSRC-RP-92-879 Rev.1; Westinghouse Savannah River Company, LLC: Aiken, SC, 1992.

Cheah, S.-F.; Kraemer, S. M.; Cervini-Silva, J.; Sposito, G. Steady-State Dissolution Kinetics of Goethite in the Presence of Desferrioxamine B and Oxalate Ligands: Implications for the Microbial Acquisition of Iron. *Chem. Geol.* **2003**, *198* (1–2), 63–75.

Choppin, G.; Bond, A.; Hromadka, P. Redox Speciation of Plutonium. *J. Radioanal. Nucl. Chem.* **1997**, *219* (2), 203–210.

Choppin, G. R. Actinide Speciation in the Environment. *Radiochim. Acta* **2003**, *91* (11–2003), 645–650.

Choppin, G. R. Actinide Speciation in Aquatic Systems. *Mar. Chem.* **2006**, *99* (1–4), 83–92.

Choppin, G. R. Actinide Speciation in the Environment. *J. Radioanal. Nucl. Chem.* **2007**, *273* (3), 695–703.

Choppin, G. R.; Stout, B. E. Actinide Behavior in Natural Waters. *Sci. Total Environ.* **1989**, *83* (3), 203–216.

Clark, D. L.; Hecker, S. S.; Jarvinen, G. D.; Neu, M. P. Plutonium. In *Chemistry of the Actinide and Transactinide Elements*; Springer: Dordrecht, The Netherlands, 2010; Vol. 2, pp 813–1264.

Cleveland, J. *The Chemistry of Plutonium*; American Nuclear Society: La Grange Park, IL, 1979.

Cleveland, J. M.; Rees, T. F. Characterization of Plutonium in Maxey Flats Radioactive Trench Leachates. *Science* **1981**, *212* (4502), 1506–1509.

Cocozza, C.; Tsao, C. C. G.; Cheah, S.-F.; Kraemer, S. M.; Raymond, K. N.; Miano, T. M.; Sposito, G. Temperature Dependence of Goethite Dissolution Promoted by Trihydroxamate Siderophores. *Geochim. Cosmochim. Ac.* **2002**, *66* (3), 431–438.

References (Continued)

Conroy, N. A.; Zavarin, M.; Kersting, A. B.; Powell, B. A. The Effect of Natural Organic Matter on Plutonium Sorption to Goethite. *Environ. Sci. Technol.* **2017**, *51*, 699–708.

Cornell, R. M.; Schwertmann, U. *The Iron Oxides: Structure, Properties, Reactions, Occurrences and Uses,* 2nd ed.; Wiley-VCH: Weinham, 2003.

Cvetkovic, V.; Painter, S.; Turner, D.; Pickett, D.; Bertetti, P. Parameter and Model Sensitivities for Colloid-Facilitated Radionuclide Transport on the Field Scale. *Water Resour. Res.* **2004**, *40* (6).

Demirkanli, D. I.; Molz, F. J.; Kaplan, D. I.; Fjeld, R. A.; Serkiz, S. M. Modeling Long-Term Plutonium Transport in the Savannah River Site Vadose Zone. *Vadose Zone J.* **2007**, *6* (2), 344.

Denham, M.; Kastner, J. R.; Jerome, K. M.; Santo Domingo, J.; Looney, B. B.; Franck, M. M. *Effects of Fenton's Reagent on Aquifer Geochemistry and Microbiology at the A/M Area, Savannah River Site*; Technical Report WSRC-TR-99-00428; Westinghouse Savannah River Company, LLC: Aiken, SC, 1999.

Dzombak, D. A.; Morel, F. M. *Surface Complexation Modeling: Hydrous Ferric Oxide*; Wiley New York, 1990; Vol. 393.

Eick, M. J.; Peak, J. D.; Brady, P. V.; Pesek, J. D. Kinetics of Lead Adsorption/Desorption on Goethite: Residence Time Effect. *Soil Sci.* **1999**, *164* (1), 28–39.

Emerson, H. P. Experimental Evidence for Colloid-Facilitated Transport of Plutonium. Dissertation, Clemson University: Clemson, SC, 2014.

Felmy, A. R.; Cantrell, K. J.; Conradson, S. D. Plutonium Contamination Issues in Hanford Soils and Sediments: Discharges from the Z-Plant (PFP) Complex. *Phys. Chem. Deep Earth* **2010**, *35* (6–8), 292–297.

Fischer, L.; Muhlen, E. Z.; Brümmer, G. W.; Niehus, H. Atomic Force Microscopy (AFM) Investigations of the Surface Topography of a Multidomain Porous Goethite. *Eur. J. Soil Sci.* **1996**, *47* (3), 329–334.

Fjeld, R. .; Serkiz, S. .; McGinnis, P. .; Elci, A.; Kaplan, D. I. Evaluation of a Conceptual Model for the Subsurface Transport of Plutonium Involving Surface Mediated Reduction of Pu(V) to Pu(IV). *J. Contam. Hydrol.* **2003**, *67* (1–4), 79–94.

Fjeld, R. A.; DeVol, T. A.; Goff, R. W.; Blevins, M. D.; Brown, D. D.; Ince, S. M.; Elzerman, A. W. Characterization of the Mobilities of Selected Actinides and

References (Continued)

Fission/Activation Products in Laboratory Columns Containing Subsurface Material from the Snake River Plain. *Nucl. Technol.* **2001**, *135* (2), 92–108.

Flury, M.; Qiu, H. Modeling Colloid-Facilitated Contaminant Transport in the Vadose Zone. *Vadose Zone Journal* **2008**, *7* (2), 682.

Foti, S. C.; Freiling, E. C. The Determination of the Oxidation States of Tracer Uranium, Neptunium and Plutonium in Aqueous Media. *Talanta* **1964**, *11* (3), 385–392.

Fox, M. A.; Whitesell, J. K. *Organic Chemistry*; Jones and Bartlett Publishers: Sudbury, MA, 2004.

Garman, S. M.; Eick, M. J.; Beck, M. Desorption Kinetics of Lead from Goethite: Effect of Residence Time and Mixing. *Soil Sci.* **2007**, *172* (3), 177–188.

van Genuchten, M. T.; Simunek, J. Integrated Modeling of Vadose Zone Flow and Transport Processes. In *Proc. Unsaturated Zone Modeling: Progress, Challenges and Applications*; Wageningen UR Frontis Series; Kluwer Academic Publishers: Dordrecht, The Netherlands, 2004; Vol. 6, pp 37–69.

Glover, L. J.; Eick, M. J.; Brady, P. V. Desorption Kinetics of Cadmium^{2+} and Lead^{2+} from Goethite: Influence of Time and Organic Acids. *Soil Sci. Soc. Am. J.* **2002**, *66* (3), 797–804.

Guillaumont, R.; Fanghänel, T.; Fuger, J.; Grenthe, I.; Neck, V.; Palmer, D. A.; Rand, M. H. *Update on the Chemical Thermodynamics of Uranium, Neptunium, Plutoniuim, Americium and Technicium*; Mompean, F. J., Illemassene, M., Domenech-Orti, C., Ben Said, K., Eds.; Chemical Thermodynamics Series; North Holland ElsevierScience B. V.: Amsterdam, 2003; Vol. 5.

Haack, E. A.; Johnston, C. T.; Maurice, P. A. Mechanisms of Siderophore Sorption to Smectite and Siderophore-Enhanced Release of Structural Fe^{3+}. *Geochim. Cosmochim. Ac.* **2008**, *72* (14), 3381–3397.

Haliena, B.; Zheng, H.; Melson, N.; Kaplan, D. I.; Barnett, M. O. Decreased Salinity and Actinide Mobility: Colloid-Facilitated Transport or PH Change? *Environmental Science & Technology* **2016**, *50* (2), 625–632.

Hamilton-Taylor, J.; Kelly, M.; Mudge, S.; Bradshaw, K. Rapid Remobilisation of Plutonium from Estuarine Sediments. *J. Environ. Radioact.* **1987**, *5* (6), 409–423.

Hetrick, C. S.; Martin, D. K. *Radioactive Releases at the Savannah River Site 1954-1988*; Report WSRC-RP-737; Westinghouse Savannah River Company: Aiken, SC, 1990.

References (Continued)

Hu, Y.-J.; Kestrel Schwaiger, L.; Booth, C. H.; Kukkadapu, R. K.; Cristiano, E.; Kaplan, D.; Nitsche, H. Molecular Interactions of Plutonium(VI) with Synthetic Manganese-Substituted Goethite. *Radiochim. Acta* **2010**, *98* (9–11), 655–663.

International Humic Substances Society. Acidic Functional Groups of IHSS Samples http://www.humicsubstances.org/acidity.html (accessed Jul 12, 2016).

Jin, M.; Delshad, M.; Dwarakanath, V.; McKinney, D. C.; Pope, G. A.; Sepehrnoori, K.; Tilburg, C. E.; Jackson, R. E. Partitioning Tracer Test for Detection, Estimation, and Remediation Performance Assessment of Subsurface Nonaqueous Phase Liquids. *Water Resour. Res.* **1995**, *31* (5), 1201–1211.

Kaplan, D. I.; Serkiz, S. M.; Fjeld, R. A.; Coates, J. T. *Influence of PH and Oxidation State on Plutonium Mobility Through and SRS Sediment*; Technical Report WSRC-TR-2001-00472, Rev. 0; Westinghouse Savannah River Company: Aiken, SC, 2001.

Keberle, H. The Biochemistry of Desferrioxamine and Its Relation to Iron Metabolism. *Ann. NY Acad. Sci.* **1964**, *119* (2), 758–768.

Keeney-Kennicutt, W. L.; Morse, J. W. The Redox Chemistry of Pu(V)O_2^+ Interaction with Common Mineral Surfaces in Dilute Solutions and Seawater. *Geochim. Cosmochim. Ac.* **1985**, *49* (12), 2577–2588.

Kersting, A. B.; Efurd, D. W.; Finnegan, D. L.; Rokop, D. J.; Smith, D. K.; Thompson, J. L. Migration of Plutonium in Ground Water at the Nevada Test Site. *Nature* **1999**, *397*, 56–59.

Kim, C. S.; Lentini, C. J.; Waychunas, G. A. Associations between Iron Oxyhydroxide Nanoparticle Growth and Metal Adsorption/Structural Incorporation. In *Adsorption of Metals by Geomedia II: Variables, Mechanisms, and Model Applications*; Bernett, M. O., Kent, D., Eds.; Developments in Earth and Environmental Sciences; Elsevier, 2007; Vol. 7, pp 153–185.

Kirsch, R.; Fellhauer, D.; Altmaier, M.; Neck, V.; Rossberg, A.; Fanghänel, T.; Charlet, L.; Scheinost, A. C. Oxidation State and Local Structure of Plutonium Reacted with Magnetite, Mackinawite, and Chukanovite. *Environ. Sci. Technol.* **2011**, *45* (17), 7267–7274.

Knopp, R.; Neck, V.; Kim, J. Solubility, Hydrolysis and Colloid Formation of Plutonium(IV). *Radiochim. Acta* **1999**, *86* (3–4), 101–108.

Kobashi, A.; Choppin, G.; Morse, J. A Study of Techniques for Separating Plutonium in Different Oxidation States. *Radiochim. Acta* **1988**, *43*, 211–215.

References (Continued)

Kraemer, S. M.; Cheah, S.-F.; Zapf, R.; Xu, J.; Raymond, K. N.; Sposito, G. Effect of Hydroxamate Siderophores on Fe Release and Pb(II) Adsorption by Goethite. *Geochim. Cosmochim. Ac.* **1999**, *63* (19–20), 3003–3008.

Kraemer, S. M.; Xu, J.; Raymond, K. N.; Sposito, G. Adsorption of Pb(II) and Eu(III) by Oxide Minerals in the Presence of Natural and Synthetic Hydroxamate Siderophores. *Environ. Sci. Technol.* **2002**, *36* (6), 1287–1291.

Kraemer, S. M. Iron Oxide Dissolution and Solubility in the Presence of Siderophores. *Aquat. Sci.* **2004**, *66* (1), 3–18.

Kubicki, J. D.; Schroeter, L. M.; Itoh, M. J.; Nguyen, B. N.; Apitz, S. E. Attenuated Total Reflectance Fourier-Transform Infrared Spectroscopy of Carboxylic Acids Adsorbed onto Mineral Surfaces. *Geochim. Cosmochim. Ac.* **1999**, *63* (18), 2709–2725.

Lackovic, K.; Johnson, B. B.; Angove, M. J.; Wells, J. D. Modeling the Adsorption of Citric Acid onto Muloorina Illite and Related Clay Minerals. *Journal of Colloid and Interface Science* **2003**, *267* (1), 49–59.

Lehmann, R. G.; Harter, R. D. Assessment of Copper-Soil Bond Strength by Desorption Kinetics. *Soil Sci. Soc. Am. J.* **1984**, *48* (4), 769.

Li, D.; Kaplan, D. I.; Roberts, K. A.; Seaman, J. C. Mobile Colloid Generation Induced by a Cementitious Plume: Mineral Surface-Charge Controls on Mobilization. *Environmental Science & Technology* **2012**, *46* (5), 2755–2763.

Lu, N.; Triay, I. R.; Cotter, C. R.; Kitten, H. D.; Bentley, J. *Reversibility of Sorption of Plutonium-239 onto Colloids of Hematite, Goethite, Smectite, and Silica: A Milestone Final Report of YMP*; Technical Report LA-UR-98-3057; Los Alamos National Laboratory: Los Alamos, NM, 1998a.

Lu, N.; Cotter, C. R.; Kitten, H. D.; Bentley, J.; Triay, I. R. Reversibility of Sorption of Plutonium-239 onto Hematite and Goethite Colloids. *Radiochim. Acta* **1998b**, *83* (4), 167–173.

Lu, N.; Conca, J.; Parker, G. R.; Leonard, P. A.; Moore, B.; Strietelmeier, B.; Triay, I. R. *Adsorption of Actinides onto Colloids as a Function of Time, Temperature, Ionic Strength, and Colloid Concentration*; Technical Report LA-UR-00-5121; Los Alamos National Laboratory: Los Alamos, NM, 2000.

Lu, N.; Reimus, P. W.; Parker, G. R.; Conca, J. L.; Triay, I. R. Sorption Kinetics and Impact of Temperature, Ionic Strength and Colloid Concentration on the

Adsorption of Plutonium-239 by Inorganic Colloids. *Radiochim. Acta* **2003**, *91* (12–2003), 713–720.

Marsac, R.; Banik, N. L.; Lützenkirchen, J.; Buda, R. A.; Kratz, J. V.; Marquardt, C. M. Modeling Plutonium Sorption to Kaolinite: Accounting for Redox Equilibria and the Stability of Surface Species. *Chemical Geology* **2015**, *400*, 1–10.

Marty, R. C.; Bennett, D.; Thullen, P. Mechanism of Plutonium Transport in a Shallow Aquifer in Mortandad Canyon, Los Alamos National Laboratory, New Mexico. *Environ. Sci. Technol.* **1997**, *31* (7), 2020–2027.

McGinnis, P. L. Evaluation of a Plutonium Subsurface Transport Model Involving Reduction of Plutonium (V) to Plutonium (IV) on Soil Surfaces. Thesis, Clemson University: Clemson, SC, 2000.

Montgomery, D.; Barber, K.; Edayilam, N.; Oqujiuba, K.; Young, S.; Biotidara, T.; Gathers, A.; Danjaji, M.; Tharayil, N.; Martinez, N.; et al. The Influence of Citrate and Oxalate on 99 Tc VII , Cs, Np V and U VI Sorption to a Savannah River Site Soil. *Journal of Environmental Radioactivity* **2017**, *172*, 130–142.

Morse, J. W.; Choppin, G. R. Laboratory Studies of Plutonium in Marine Systems. *Mar. Chem.* **1986**, *20* (1), 73–89.

Neck, V.; Altmaier, M.; Seibert, A.; Yun, J. I.; Marquardt, C. M.; Fanghänel, T. Solubility and Redox Reactions of Pu(IV) Hydrous Oxide: Evidence for the Formation of PuO_{2+x}(s, Hyd). *Radiochim. Acta* **2007**, *95* (4).

Neck, V.; Kim, J. I. Solubility and Hydrolysis of Tetravelent Actinides. *Radiochim. Acta* **2001**, *88* (1), 1–16.

Neff, D.; Dillmann, P.; Bellot-Gurlet, L.; Beranger, G. Corrosion of Iron Archaeological Artefacts in Soil: Characterisation of the Corrosion System. *Corros. Sci.* **2005**, *47* (2), 515–535.

Neu, M.; Hoffman, D.; Roberts, K.; Nitsche, H.; Silva, R. J. Comparison of Chemical Extractions and Laser Photoacoustic-Spectroscopy for the Determination of Plutonium Species in Near-Neutral Carbonate Solutions. *Radiochim. Acta* **1994**, *66*, 251–258.

Neubauer, U.; Nowack, B.; Furrer, G.; Schulin, R. Heavy Metal Sorption on Clay Minerals Affected by the Siderophore Desferrioxamine B. *Environ. Sci. Technol.* **2000**, *34* (13), 2749–2755.

References (Continued)

Nitsche, H.; Lee, S. C.; Gatti, R. C. Determination of Plutonium Oxidation States at Trace Levels Pertinent to Nuclear Waste Disposal. *J. Radioanal. Nucl. Chem.* **1988**, *124* (1), 171–185.

Nitsche, H.; Edelstein, N. M. Solubilities and Speciation of Selected Transuranium Ions. A Comparison of a Non-Complexing Solution with a Groundwater from the Nevada Tuff Site. *Radiochim. Acta* **1985**, *39*, 23–33.

Novikov, A. P.; Kalmykov, S. N.; Utsunomiya, S.; Ewing, R. C.; Horreard, F.; Merkulov, A.; Clark, S. B.; Tkachev, V. V.; Myasoedov, B. F. Colloid Transport of Plutonium in the Far-Field of the Mayak Production Association, Russia. *Science* **2006**, *314* (5799), 638–641.

Ohnuki, T.; Yoshida, T.; Ozaki, T.; Kozai, N.; Sakamoto, F.; Nankawa, T.; Suzuki, Y.; Francis, A. J. Chemical Speciation and Association of Plutonium with Bacteria, Kaolinite Clay, and Their Mixture. *Environmental Science & Technology* **2007**, *41* (9), 3134–3139.

Orlandini, K. A.; Penrose, W. R.; Nelson, D. M. Pu(V) as the Stable Form of Oxidized Plutonium in Natural Waters. *Mar. Chem.* **1986**, *18* (1), 49–57.

Painter, S.; Cvetkovic, V.; Pickett, D.; Turner, D. R. Significance of Kinetics for Sorption on Inorganic Colloids: Modeling and Experiment Interpretation Issues. *Environ. Sci. Technol.* **2002**, *36* (24), 5369–5375.

Pang, L.; Šimůnek, J. Evaluation of Bacteria-Facilitated Cadmium Transport in Gravel Columns Using the HYDRUS Colloid-Facilitated Solute Transport Model: BACTERIA-FACILITATED Cd TRANSPORT IN GRAVEL COLUMNS. *Water Resour. Res.* **2006**, *42* (12), n/a-n/a.

Penrose, W. R.; Metta, D. N.; Hylko, J. M.; Rinckel, L. A. The Reduction of Plutonium(V) by Aquatic Sediments. *J. Environ. Radioact.* **1987**, *5* (3), 169–184.

Penrose, W. R.; Polzer, W. L.; Essington, E. H.; Nelson, D. M.; Orlandini, K. A. Mobility of Plutonium and Americium through a Shallow Aquifer in a Semiarid Region. *Environ. Sci. Technol.* **1990**, *24* (2), 228–234.

Philippini, V.; Naveau, A.; Catalette, H.; Leclercq, S. Sorption of Silicon on Magnetite and Other Corrosion Products of Iron. *J. Nucl. Mater.* **2006**, *348* (1–2), 60–69.

Powell, B. A.; Fjeld, R. A.; Coates, J. T.; Kaplan, D. I.; Serkiz, S. M. *Plutonium Oxidation State Geochemistry in SRS Subsurface Environment (U)*; Technical Report WSRC-TR-2003-00035, Rev. 0; Westinghouse Savannah River Company, LLC: Aiken, SC, 2002.

References (Continued)

Powell, B. A.; Fjeld, R. A.; Kaplan, D. I.; Coates, J. T.; Serkiz, S. M. Pu(V)O_2^+ Adsorption and Reduction by Synthetic Magnetite (Fe_3O_4). *Environ. Sci. Technol.* **2004**, *38* (22), 6016–6024.

Powell, B. A.; Fjeld, R. A.; Kaplan, D. I.; Coates, J. T.; Serkiz, S. M. Pu(V)O_2^+ Adsorption and Reduction by Synthetic Hematite and Goethite. *Environ. Sci. Technol.* **2005**, *39* (7), 2107–2114.

Powell, B. A.; Duff, M. C.; Kaplan, D. I.; Fjeld, R. A.; Neville, M.; Hunter, D. B.; Bertsch, P. M.; Coates, J. T.; Eng, P.; Rivers, M. L.; et al. Plutonium Oxidation and Subsequent Reduction by Mn(IV) Minerals in Yucca Mountain Tuff. *Environ. Sci. Technol.* **2006**, *40* (11), 3508–3514.

Powell, B. A.; Kersting, A.; Zavarin, M.; Zhao, P. *Development of a Composite Non-Electrostatic Surface Complexation Model Describing Plutonium Sorption to Aluminosilicates*; Technical Report LLNL-TR-408276; Lawrence Livermore National Laboratory: Livermore, CA, 2011.

Powell, B. A.; Kaplan, D. I.; Serkiz, S. M.; Coates, J. T.; Fjeld, R. A. Pu(V) Transport through Savannah River Site Soils - an Evaluation of a Conceptual Model of Surface- Mediated Reduction to Pu (IV). *J. Environ. Radioact.* **2014**, *131*, 47–56.

Powell, P. E.; Cline, G. R.; Reid, C. P. P.; Szaniszlo, P. J. Occurrence of Hydroxamate Siderophore Iron Chelators in Soils. *Nature* **1980**, *287* (5785), 833–834.

Prout, W. E. Adsorption of Radioactive Wastes by Savannah River Plant Soil. *Soil Sci.* **1958**, *86*, 13–17.

Rai, D.; Sern, R. J.; Swanson, J. L. Solution Species of Plutonium in the Environment. *J. Environ. Qual.* **1980**, *9* (3), 417–420.

Rai, D. Solubility Product of Pu(IV) Hydrous Oxide and Equilibrium Constants of Pu(IV)/Pu(V), Pu(IV)/Pu(VI), and Pu(V)/Pu(VI) Couples. *Radiochim. Acta* **1984**, *35* (2), 97–106.

Rai, D.; Moore, D. A.; Felmy, A. R.; Choppin, G. R.; Moore, R. C. Thermodynamics of the $PuO_2^+ – Na^+ – OH^- – Cl^- – ClO_4^- – H_2O$ System: Use of NpO_2^+ Pitzer Parameters for PuO_2^+. *Radiochim. Acta* **2001**, *89* (8/2001).

Romanchuk, A. Y.; Kalmykov, S. N.; Aliev, R. A. Plutonium Sorption onto Hematite Colloids at Femto- and Nanomolar Concentrations. *Radiochim. Acta* **2011**, *99* (3), 137–144.

Romanchuk, A. Y.; Kalmykov, S. N.; Egorov, A. V.; Zubavichus, Y. V.; Shiryaev, A. A.; Batuk, O. N.; Conradson, S. D.; Pankratov, D. A.; Presnyakov, I. A. Formation of

References (Continued)

Crystalline $PuO_{2+x} \cdot NH_2O$ Nanoparticles upon Sorption of Pu(V,VI) onto Hematite. *Geochim. Cosmochim. Ac.* **2013**, *121*, 29–40.

Ryan, J. N.; Elimelech, M. Colloid Mobilization and Transport in Groundwater. *Colloids Surf., A* **1996**, *107*, 1–56.

Ryan, J. N.; Gschwend, P. M. Colloid Mobilization in Two Atlantic Coastal Plain Aquifers: Field Studies. *Water Resour. Res.* **1990**, *26* (2), 307–322.

Ryan, J. N.; Gschwend, P. M. Effects of Ionic Strencth and Flow Rate on Colloid Release: Relateing Kinetics to Intersurface Potential Energy. *J. Colloid Interface Sci.* **1994a**, *164*, 21–34.

Ryan, J. N.; Gschwend, P. M. Effect of Solution Chemistry on Clay Colloid Release from an Iron Oxide-Coated Aquifer Sand. *Environ. Sci. Technol.* **1994b**, *28*, 1717–1726.

Saiers, J. E.; Hornberger, G. M. The Role of Colloidal Kaolinite in the Transport of Cesium through Laboratory Sand Columns. *Water Resources Research* **1996**, *32* (1), 33–41.

Sanchez, A. L.; Murray, J. W.; Sibley, T. H. The Adsorption of Plutonium IV and V on Goethite. *Geochim. Cosmochim. Ac.* **1985**, *49* (11), 2297–2307.

Santschi, P. H.; Roberts, K. A.; Guo, L. Organic Nature of Colloidal Actinides Transported in Surface Water Environments. *Environ. Sci. Technol.* **2002**, *36* (17), 3711–3719.

Schlautman, M.; Morgan, J. Adsorption of Aquatic Humic Substances on Colloidal-Size Aluminum Oxide Particles: Influence of Solution Chemistry. *Geochim. Cosmochim. Ac.* **1994**, *58* (20), 4293–4303.

Schwertmann, U. The Influence of Aluminum on Iron Oxides: IX. Dissolution of Al-Goethites in 6 M HCl. *Clay Miner.* **1984**, *19* (1), 9–19.

Schwertmann, U.; Cornell, R. M. *Iron Oxides in the Laboratory: Preparation and Characterization*; VCH: Weinheim; New York, 1991.

Schwertmann, U.; Taylor, R. M. Iron Oxides. In *Minerals in Soil Environments*; Soil Science Society of America: Madison, WI, 1989; pp 379–438.

Seaman, J. C.; Bertsch, P. M.; Kaplan, D. I. Spatial and Temporal Variability in Colloid Dispersion as a Function of Groundwater Injection Rate within Atlantic Coastal Plain Sediments. *Vadose Zone Journal* **2007**, *6* (2), 363.

References (Continued)

Selim, H. M.; Amacher, M. C. Sorption and Release of Heavy Metals in Soils: Nonlinear Kinetics. In *Heavy Metals Release in Soils*; Lewis Publishers: Boca Raton, FL, 2001; pp 1–29.

Seyfried, M. S.; Sparks, D. L.; Bar-Tal, A.; Feigenbaum, S. Kinetics of Calcium Magnesium Exchange on Soil Using a Stirred-Flow Reaction Chamber. *Soil Sci. Soc. Am. J.* **1989**, *53* (2), 406–410.

Shaughnessy, D. A.; Nitsche, H.; Booth, C. H.; Shuh, D. K.; Waychunas, G. A.; Wilson, R. E.; Gill, H.; Cantrell, K. J.; Serne, R. J. Molecular Interfacial Reactions between Pu(VI) and Manganese Oxide Minerals Manganite and Hausmannite. *Environ. Sci. Technol.* **2003**, *37* (15), 3367–3374.

Siebner-Freibach, H.; Hadar, Y.; Chen, Y. Interaction of Iron Chelating Agents with Clay Minerals. *Soil Sci. Soc. Am. J.* **2004**, *68* (2), 470.

Siebner-Freibach, H.; Hadar, Y.; Yariv, S.; Lapides, I.; Chen, Y. Thermospectroscopic Study of the Adsorption Mechanism of the Hydroxamic Siderophore Ferrioxamine B by Calcium Montmorillonite. *J. Agric. Food Chem.* **2006**, *54* (4), 1399–1408.

Silva, R. J.; Nitsche, H. Actinide Environmental Chemistry. *Radiochim. Acta* **1995**, *70/71*, 377–396.

Simpkins, L. A. Influence of Natural Organic Matter on Plutonium Sorption to Gibbsite. Master's Thesis, Clemson University: Clemson, SC, 2011.

Šimůnek, J.; He, C.; Pang, L.; Bradford, S. A. Colloid-Facilitated Solute Transport in Variably Saturated Porous Media. *Vadose Zone Journal* **2006**, *5* (3), 1035.

Šimůnek, J. Mass Units for Colloid Facilitated Transport (C-Ride). *PC-Progress Discussion Forums*, 2017.

Šimůnek, J.; van Genuchten, M. T. *The C-Ride Module for HYDRUS-1D Simulating One-Dimensional Colloid-Facilitated Solute Transport in Variably-Saturated Porous Media, Version 1.0*; PC Progress: Prague, Czech Republic, 2015.

Sing, K. S. W.; Everett, D. H.; Haul, R. A. W.; Moscou, L.; Pierotti, R. A.; Rouquerol, J.; Siemieniewska, T. Reporting Physisorption Data for Gas/Solid Systems with Special Reference to the Determination of Surface Area and Porosity (Recomendations 1984). *Pure & Appl. Chem.* **1985**, *57* (4), 603–619.

Skopp, J.; McCallister, D. Chemical Kinetics from a Thin Disk Flow System: Theory. *Soil Sci. Soc. Am. J.* **1986**, *50*, 617–623.

References (Continued)

Smith, D. K.; Finnegan, D. L.; Bowen, S. M. An Inventory of Long-Lived Radionuclides Residual from Underground Nuclear Testing at the Nevada Test Site, 1951–1992. *J. Environ. Radioact.* **2003**, *67* (1), 35–51.

Sparks, D. L. Kinetics and Mechanisms of Chemical Reactions at the Soil Mineral/Water Interface. In *Soil Physical Chemistry*; CRC Press: Boca Raton, FL, 1998; pp 135–191.

Sparks, D. L. New Frontiers in Elucidating the Kinetics and Mechanisms of Metal and Oxyanion Sorption at the Soil Mineral/Water Interface. *J. Plant Nutr. Soil Sci.* **2000**, *163* (6), 563–570.

Sposito, G. *The Chemistry of Soils*, 2nd ed.; Oxford University Press, Inc.: New York, 2008.

Stumm, W.; Morgan, J. J. *Aquatic Chemistry : Chemical Equilibria and Rates in Natural Waters*; Wiley: New York, 1996.

Tinnacher, R. M.; Zavarin, M.; Powell, B. A.; Kersting, A. B. Kinetics of Neptunium(V) Sorption and Desorption on Goethite: An Experimental and Modeling Study. *Geochim. Cosmochim. Ac.* **2011**, *75* (21), 6584–6599.

Tinnacher, R. M.; Begg, J. D.; Mason, H.; Ranville, J.; Powell, B. A.; Wong, J. C.; Kersting, A. B.; Zavarin, M. Effect of Fulvic Acid Surface Coatings on Plutonium Sorption and Desorption Kinetics on Goethite. *Environ. Sci. Technol.* **2015**, *49* (5), 2776–2785.

Triay, I. R.; Cotter, C. R.; Kraus, S. M.; Huddleston, M. H.; Chipera, S. J.; Bish, D. L. *Radionuclide Sorption in Yucca Mountain Tuffs with J-13 Well Water: Neptunium, Uranium, and Plutonium. Yucca Mountain Site Characterization Program Milestone 3338*; Report LA-12956-MS; Los Alamos National Laboratory: Los Alamos, NM, 1996.

Visintin, A. Mathematical Models of Hysteresis. In *The Science of Hysteresis*; Academic Press: Oxford, 2006; Vol. 1, pp 1–123.

Wang, D.; Jin, Y.; Jaisi, D. P. Effect of Size-Selective Retention on the Cotransport of Hydroxyapatite and Goethite Nanoparticles in Saturated Porous Media. *Environmental Science & Technology* **2015**, *49* (14), 8461–8470.

Wateau, F.; Berthelin, J. Microbial Dissolution of Iron and Aluminum from Soil Minerals: Efficiency and Specificity of Hydroxamate Siderophores Compared to Aliphatic Acids. *Eur. J. Soil Biol.* **1994**, *30* (1), 1–9.

References (Continued)

Wong, J. C.; Zavarin, M.; Begg, J. D.; Kersting, A. B.; Powell, B. A. Effect of Equilibration Time on Pu Desorption from Goethite. *Radiochim. Acta* **2015**, *103* (10), 695–705.

Zhao, P.; Zavarin, M.; Leif, R. N.; Powell, B. A.; Singleton, M. J.; Lindvall, R. E.; Kersting, A. B. Mobilization of Actinides by Dissolved Organic Compounds at the Nevada Test Site. *Appl. Geochem.* **2011**, *26* (3), 308–318.

Zimmerman, T.; Zavarin, M.; Powell, B. A. Influence of Humic Acid on Plutonium Sorption to Gibbsite: Determination of Pu-Humic Acid Complexation Constants and Ternary Sorption Studies. *Radiochim. Acta* **2014**, *102* (7).